Naval Research Laboratory

Washington, DC 20375-5320

NRL/MR/7230--16-9667

Ssang Yong 2014 Remote Sensing Experiment

Charles M. Bachmann

Rochester Institute of Technology
Rochester, New York

Andrei Abelev

Marine Physics Branch
Marine Geosciences Division

M. Todd Bounds
C. Reid Nichols

Marine Information Resources Corp.
Ellicott City, Maryland

Robert A. Fusina
Rong-Rong Li

Coastal and Ocean Remote Sensing Branch
Remote Sensing Division

Robert Kremens
Gary Difrancesco

Rochester Institute of Technology
Rochester, New York

Michael Vermillion

Marine Physics Branch
Marine Geosciences Division

Gordon Mattis

South Carolina Research Authority
Charleston, South Carolina

Kevin B. Edwards
Jaime Estrada

Office of Naval Research
Alington, Virginia

May 25, 2016

REPORT DOCUMENTATION PAGE

Form Approved
OMB No. 0704-0188

1. REPORT DATE *(DD-MM-YYYY)*
25-05-2016

2. REPORT TYPE
Memorandum Report

3. DATES COVERED *(From - To)*
April 2014 – September 2015

4. TITLE AND SUBTITLE
Ssang Yong 2014 Remote Sensing Experiment

5a. CONTRACT NUMBER

5b. GRANT NUMBER

5c. PROGRAM ELEMENT NUMBER

5d. PROJECT NUMBER

5e. TASK NUMBER

5f. WORK UNIT NUMBER
72-9824-04

6. AUTHOR(S)
Charles M. Bachmann,*[1] Andrei Abelev, M. Todd Bounds,[2] C. Reid Nichols,[2]
Robert A. Fusina, Rong-Rong Li, Robert Kremens,[1] Gary Difrancesco,[1]
Michael Vermillion, Gordon Mattis,[3] Kevin B. Edwards,[4] and Jaime Estrada[4]

7. PERFORMING ORGANIZATION NAME(S) AND ADDRESS(ES)
Naval Research Laboratory
4555 Overlook Avenue, SW
Washington, DC 20375-5320

Marine Information Resources Corporation
Ellicott City, MD

South Carolina Research Authority
Charleston, SC (support to Marine Corps Forces Pacific Experimentation Center, Camp Smith, HI)

8. PERFORMING ORGANIZATION REPORT NUMBER
NRL/MR/7230--16-9667

9. SPONSORING / MONITORING AGENCY NAME(S) AND ADDRESS(ES)
Office of Naval Research
One Liberty Center
875 N. Randolph Street, Suite 1425
Arlington, VA 22203-1995

10. SPONSOR / MONITOR'S ACRONYM(S)
ONR

11. SPONSOR / MONITOR'S REPORT NUMBER(S)

12. DISTRIBUTION / AVAILABILITY STATEMENT

Approved for public release; distribution is unlimited.

13. SUPPLEMENTARY NOTES
*Formerly at NRL.
[1]Rochester Institute of Technology, 54 Lomb Memorial Drive, Rochester, NY 14623-5604
[2]Marine Information Resources Corporation, Ellicott City, MD 21042
[3]South Carolina Research Authority, Charleston, SC, support to Marine Corps Forces Pacific Experimentation Center, Camp Smith, HI 96861
[4]Office of Naval Research, ONR Reservist Program, Arlington, VA

14. ABSTRACT

This report documents data collected in the North Gyeongsang province of the Republic of Korea (ROK) during the Ssang Yong 2014 (SY14) remote sensing experiment. The collection of calibration and validation data occurred in April 2014, immediately after Exercise Ssang Yong 2014, an annual combined exercise conducted by the Navy and Marine Corps with the ROK. This report describes key instrumentation and ensuing collected data used in the construction of libraries and models required to produce trafficability and bathymetric products from spectral remote sensing imagery. This remote sensing experiment provided data for the development of planning products that could be used in support of future exercises. These data have supported the development of databases, models, and procedures to rapidly process imagery to support a range of missions from natural disaster relief to amphibious landings. The resultant imagery-derived products are based on foundational data that have been collected during this experiment and previous efforts from various other types of coasts.

15. SUBJECT TERMS
Hyperspectral Trafficability Remote sensing

16. SECURITY CLASSIFICATION OF: a. REPORT	b. ABSTRACT	c. THIS PAGE	17. LIMITATION OF ABSTRACT	18. NUMBER OF PAGES	19a. NAME OF RESPONSIBLE PERSON
Unclassified Unlimited	Unclassified Unlimited	Unclassified Unlimited	Unclassified Unlimited	280	Robert Fusina
					19b. TELEPHONE NUMBER *(include area code)* (202) 767-9429

Standard Form 298 (Rev. 8-98)
Prescribed by ANSI Std. Z39.18

TABLE OF CONTENTS

LIST OF FIGURES

LIST OF TABLES

ABBREVIATIONS AND ACRONYMS

ASD	Analytical Spectral Devices
C	Celsius
CBR	California Bearing Ratio
CTD	Conductivity, Temperature, and Depth
DCP	Dynamic Cone Penetrometer
Cal/Val	Calibration/Validation
ESRI	Environmental Systems Research Institute
GIS	Geographic Information System
GPS	Ground Positioning System
GSD	Ground Sample Distance
HAE	Height Above Ellipsoid
JPEG	Joint Photographic Experts Group
LPA	Littoral Penetration Area
LPP	Littoral Penetration Point
LPS	Littoral Penetration Site
LWD	Light Weight Deflectometer
MARFORPAC	Marine Corps Forces Pacific
MCIA	Marine Corps Intelligence Activity
MEB	Marine Expeditionary Brigade
MEC	MARFORPAC Experimentation Center
MEF	Marine Expeditionary Force
MEU	Marine Expeditionary Unit
MSI	Multispectral Imagery
NGA	National Geospatial-Intelligence Agency
NIMA	National Imagery and Mapping Agency
NOAA	National Oceanic and Atmospheric Administration
NRL	Naval Research Laboratory
ONR	Office of Naval Research
P	Pressure
PACOM	Pacific Command
PI	Principle Investigator
PSU	Practical Salinity Unit
QA	Quality Assurance
QC	Quality Control
SY'14	Ssang Yong 2014
TS	Temperature/Salinity
WV2	WorldView-2

EXECUTIVE SUMMARY

The Rochester Institute of Technology (RIT), the US Naval Research Laboratory (NRL), Marine Information Resources Corporation (MIRC), the South Carolina Research Authority (SCRA), and the Office of Naval Research (ONR) developed look up tables for estimating trafficability and bathymetry from spectral remote sensing imagery in littoral regions during a recent experiment conducted on the eastern coast of the Republic of Korea (ROK). This rocky coast experiment builds on a series of earlier experiments and demonstrations by NRL and MIRC at barrier island coasts along Virginia's eastern shore [1]-[4]; along the Pearl River in Mississippi, coral coasts along Kaneohe Bay on Oahu, Hawaii [5], [6], Guam [7], and Tinian [7]; volcanic coasts on Pagan Island [7] in the Commonwealth of the Northern Mariana Islands; and mangrove coasts located in Queensland, Australia [8]. The present effort also builds on a recent two-year project conducted jointly by NRL, Australia Defence Science and Technology Organisation (DSTO), and MIRC under the auspices of the Office of the Under Secretary of Defense Coalition Warfare Program [9]. The present experiment expands the scope of applicability of models developed in these past efforts [10] by developing the requisite spectral and geotechnical data for a new coast type.

Specifically, this memorandum report documents data that were collected during a remote sensing campaign conducted in April 2014 in the North Gyeongsang province along the east coast of the Republic of Korea (ROK). The collection of calibration and validation data occurred immediately after Exercise Ssang Yong 2014, an annual combined exercise conducted by Navy and Marine Corps forces with the ROK to strengthen interoperability and working relationships across the range of military operations from disaster relief to complex, expeditionary operations. This report describes key instrumentation and ensuing collected data used in the construction of libraries and models required to produce trafficability and bathymetric products from spectral remote sensing imagery (e.g., space-borne spectrometers, dynamic cone penetrometers, light weight deflectometers, sediment corers, field spectrometers, water level gages, and sonar).

Information provided in this report characterizes numerous environmental factors that impact naval expeditionary warfare along the east coast of South Korea; these factors were common to the experimental sites where calibration and validation data were collected by the team. Included are meteorological measurements (e.g., air temperature, barometric pressure, wind speed and direction), oceanographic measurements (e.g., water level fluctuations), geotechnical measurements (e.g., grain size distributions, beach slope, and California Bearing Ratio), and optical measurements (spectral libraries, including their angular dependence). These data were used with imagery to create innovative military planning products such as trafficability

maps. Dogu Beach [1], one of the experiment sites, is located within Yeongil Bay and is the location for ROK Marine Amphibious Assault Vehicle training

The three experiment sites, Dogu, Doksuk-ri, and Hwajin-ri beaches, were all used during Exercise Ssang Yong 2014. This remote sensing experiment provided data for the development of planning products that could be used in support of future exercises. These data have supported the development of databases, models, and procedures to rapidly process imagery to support a range of missions from natural disaster relief to amphibious landings. The resultant imagery-derived products are based on foundational data that have been collected during this experiment and previous efforts from various other types of coasts.

[1] LABELLING: Some confusion can be encountered from different spellings of locations that occur on various types of publications. For example, *Dogu Beach* is spelled *Dogue Beach* or *Doku Beach*. Another example involves the mixed use of language, for example *Yeongil Bay* may also be represented as *Yeongil Man*. Attempts were made to use authoritative labeling by adopting labels used by the National Geospatial-Intelligence Agency data. It is also possible to come across names that are recognized differently by various nations (e.g. East Sea/Sea of Japan). In this case, we have chosen to use East Sea.

1.0 Introduction

This Ssang Yong 2014 (SY'14) remote sensing experiment follows directly from a series of remote sensing campaigns [1]-[10] that were planned and executed across a variety of Atlantic and Pacific coasts. Data and information from these previous projects account for littoral processes occurring in Virginia, Mississippi, Hawaii, Guam, Commonwealth of the Northern Mariana Islands, and Australia and are representative of certain coast types that are found in littoral regions, worldwide. Project geodatabases include calibration and validation (Cal/Val) data (e.g., shallow water bathymetry, side scan sonar, water levels, wind speed and direction, bearing strength, grain size distributions, littoral spectra, vegetation density) and multisource overhead imagery (e.g., LiDAR, hyperspectral and multispectral, thermal). Airborne imagery from the Compact Airborne Spectral Imager (CASI) and Hyperspectral Mapper (HyMap) has been used to create innovative imagery-derived products such as trafficability maps and bathymetric charts [1]-[3]. Products from these experiments highlight environmental factors from riverine, drowned-river valley, mangrove, Barrier Island, and coral type coasts that impact amphibious operations.

The data and information from these types of coastal projects are paramount to developing spectral libraries and models that provide updated littoral situational awareness. Continued archiving of these data will prove valuable in the development of a hierarchical coastal classification system [11], [12] that is envisioned to support initial planning for surface warfare, special warfare, mine warfare, and amphibious warfare. Extracting these related littoral variables from satellites such as WorldView-2 (WV2), the imagery data source used in the present effort, supports rapid environmental characterization. Relationships developed by linking these data together supports mission planning by delivering information that enhances capability, flexibility, and mobility in the littorals.

In general, researchers with the ability to query and pull geospatial information from a variety of sources build an initial geodatabase that supports development of the science plan. The geodatabase is updated with Cal/Val data, imagery, and other research results during the experiment. The resultant geodatabase provides the common reference for the development of a variety of products that support decision-making in the dynamic littorals. Project geodatabases [6] and complementary data reports are critical for establishing physical relationships among parameters that promote environmental characterization and the development of rapid baseline information that supports the military decision making process. This enhanced maritime domain awareness improves the capability of Amphibious Readiness Groups and Marine Expeditionary Units charged with protection of sea and air routes, ports, coastal airfields, and critical facilities.

Today's warfighters utilize Geographic Information System (GIS) tools to build products from digital nautical charts, topographic maps, and imagery. In fact, imagery management and exploitation is a core part in amphibious planning. Commercial imagery such as WV2 allows the geospatial analyst to update any baseline information and produce meta-products that serve as decision aids. Baseline data and updated information, when stored in a GIS and categorized by coast type, provide the basis for new products that directly influence navigation ashore, selection

Manuscript approved December 10, 2015.

of littoral penetration points, selection of cushion landing zones, as well as identification of exits off the beach and acceptable corridors for maneuver to landing force objectives.

This project focused on the use of archival data, recently collected data common to the rocky east coast of South Korea, and WV2 imagery to develop trafficability products that support concepts such as Ship-to-Objective Maneuver. Collected data were used to classify beaches and their ability to carry traffic. Trafficability is defined as the ability to move people and/or equipment through a region [1] and is determined by the combined effect of geotechnical factors characterizing the area, including bearing and shear strength, grain size, moisture content, and sediment type, among other things. Research used imagery and Cal/Val data to assess these interrelated geotechnical variables and other factors found along the beaches. For example, the same beach could have different structural characteristics due to man-made structures or varying moisture content owing to natural drainage patterns. Deriving the trafficability of a surface from WV2 images reduces the need for *in situ* geotechnical data collection, a time- and labor-intensive task providing results for only a limited number of locations. Imagery products can cover entire sections of coast in order to support decisions such as the selection of optimal landing sites.

Geospatial information can be combined to build products that aid naval expeditionary forces to obtain a dominant presence in coastal regions that are associated with high temporal and spatial variability, especially along the various rocky and sandy shores that are found along the ROK's 2,413 km long coastline [13], [14]. Available maps, images, and background information can be combined to show favorable maneuver areas, e.g., lowlands that are the product of mountain erosion, especially along the rocky east coast. This research project demonstrates the use of commercial remote sensing in the development of tactical Geospatial Intelligence (GEOINT) by producing trafficability maps from high-resolution reflectance spectra. Imagery was collected at several coastal locations near Pohang on the border of the East Sea. Using information and relationships pertinent to the ROK east coast supports the rapid production of trafficability maps.

A glossary of terms is provided in Appendix A. Definitions of words are restricted to elements that are pertinent to the Marine Corps Planning Process, coastal remote sensing, and GIS.

2.0 Background Information

This research took place along the southeastern region of the Korean Peninsula near Pohang that is influenced by the East Sea and Strait of Korea. South Korea has a temperate climate with four distinct seasons. Winters are usually long, cold, and dry. Summers are generally short, hot, and humid. Spring and autumn are pleasant but short in duration. Mean temperature and precipitation during April in Pohang is 19° C and 77 mm, respectfully. A Moderate Resolution Imaging Spectroradiometer (MODIS) image depicting a record snowfall on January 3, 2010 is provided in Figure 2-1. Snow days, on average, occur two times in January and February, and

once in March. Climate data indicate nine rainy days occur on average in April. The trend is for partly cloudy conditions during April, which is when data were collected for this project.

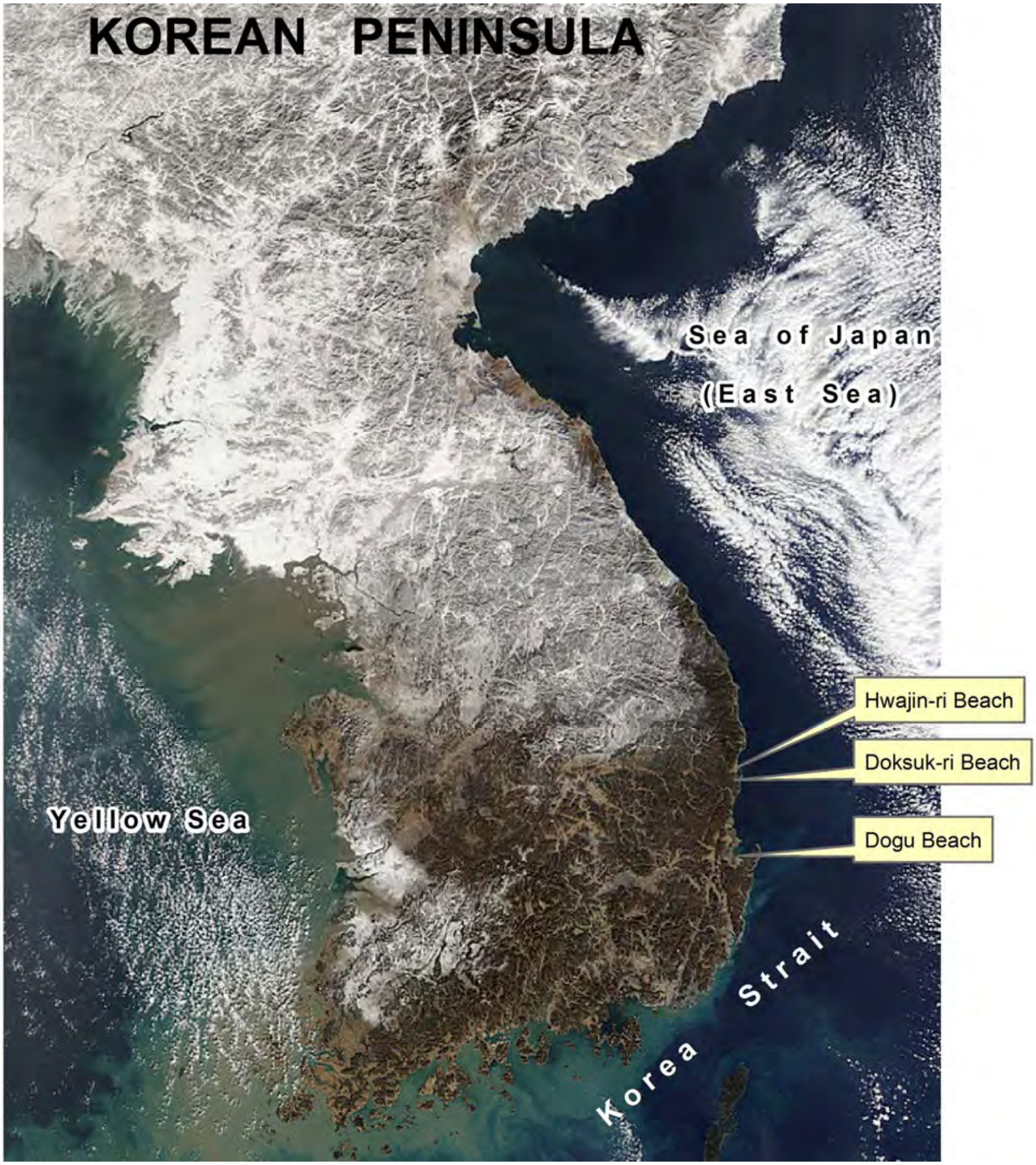

Figure 2-1. Snow covered Korea in January 3, 2010. (Obtained online from http://rapidfire.sci.gsfc.nasa.gov/subsets/?subset=FAS_Korea.2010003.terra.1km). Geophysical parameters describing the Earth's surface (land and ocean) and atmosphere (including clouds) can be derived from MODIS imagery.

Three landing beaches were selected along narrow littoral plains extending along the east coast near Pohang. The beach sands are composed of pulverized, weathered rock along with some fragments of shells and other biogenic material that are built up and eroded by the waves and as sediment transported by the Hyeongsan River and near shore currents. The Hyeongsan River flows for 62 km from Doseo-myeon to the East Sea. Mean annual discharge of 18.3 m^3/sec (1966 ~ present) at Pohang has been reported [15].

Our literature search contributed to the collection of relevant geospatial information that would identify the location of obstacles such as isolated rocks and rocky cliffs that impact amphibious operations [16]. Efforts were made to obtain the geospatial information that is listed in Table 2-1. Littoral Planning Charts, intended for planning, amphibious operations, and non-combatant evacuations, were received from the III Marine Expeditionary Force (III MEF) on 4 April 2014. The Littoral Planning Charts were at a scale of 1:50,000 and portrayed both topographic and maritime features (see Section 6, Geodatabase for SY'14 for file locations of information that has been archived within the database). Extracts from the Littoral Planning Charts are provided in Figure 2-1 to depict landing beaches which were used during SY'14. Other key print and electronic resource findings are described in the annotated bibliography found in Appendix B.

Table 2-1. Littoral Planning Charts Loaded into SsangYong2014.gdb File Geodatabase.

Title	Scale	(Edition)–Series-Sheet-Version	NGA Ref No. / SY'14 Geodatabase ID	Preparer / Printer
Ivo Pohang	1:50,000	(1)-SY14 LIT 50K-A001-(N/A)	(N/A) / 130031	3D MEB G-2 / 3D MEB G-2
Yeongdeok	1:50,000	(3-KAMC)-L754-3518-I	L754X35181 / 35181	ROK / NGA
Pohang	1:50,000	(2-KAMC)-L754-3518-II	L754X35182 / 35182	ROK / NIMA
Pulguk-Sa	1:50,000	(2-KAMC)-L754-4017-I	L754X40171 / 40171	ROK / NIMA
Yongdok	1:50,000	(001)-N/A	LPCXX803470 / 803470	NGA / NGA
Kuryongp'o	1:50,000	(2-KAMC)-L754-4117-IV	L754X41174 / 41174	ROK / ROK
Yongil-Man	1:50,000	(001)-N/A	LPCXX806902 / 806902	NGA / NGA
Hunghae	1:50,000	(001)-N/A	LPCXX806967 / 806967	NGA / NGA

Figure 2-2 shows a view of Dogu Beach and the associated breakwater harbor in Pohang. Dogu Beach was one of three sites studied during the experiment. Formal transects were defined in the Science Plan where samples were collected to characterize the center, left, and right flanks of the beach used during amphibious training exercises. Imagery also illustrates that the new harbor at Pohang was built on reclaimed land. Such modifications impact land drainage, a critical factor, along with terrain and relief, for amphibious planning.

Figure 2-2. Dogu Beach and Pohang Harbor.

ROK Marines routinely train with amphibious assault vehicles at Dogu Beach. Pohang stands at the entrance of the shallow Hyeongsan River at the west end of the Yeongil bay. Pohang includes two harbors — Guhang (old harbor) and Shinhang (new harbor). A factor important for small boat operations (e.g., bridge boats) includes waves, currents, tides and the location of ramps to launch and recover. Sailing directions provided general climate and navigation information to complement the Littoral Planning Charts. Information regarding hazards and contact information to identify the location of boat ramps at two different seaports was obtained for each of the landing beaches [17]. For example, during April, northeast winds tend to cause heavy swell making it difficult for small vessels to enter the harbor. Boat launches were located in the port facility near the mouth of the Hyeongsan River and in a breakwater harbor (Longitude: 129.383491 Latitude: 36.031070) (see Figure 2-3).

Figure 2-3. Pohang Port Facility. The boat ramp was used to deploy a RHIB that was essential to deploy water level gages, buoys, and to complete very shallow water hydrographic surveys.

Data such as maps, charts, and images providing spatially referenced information about the study area were added to the project geodatabase. Other information such as weather observations and tidal predictions with temporal tags arranged in a coherent structure and formatted to support measurement, mapping, monitoring, modeling, spatial reasoning applications, and trafficability assessments were also added to the project geodatabase. This baseline data provides a geospatial framework for the addition of hydrographic survey data, geotechnical measurements, optical measurements, and WV2 imagery. These data are also important for data quality control. The project geodatabase, which is described in Section 6, is integral to the development of initial planning products such as trafficability maps.

Climatological data were obtained from the Korea Meteorological Administration (KMA) and the U.S. Library of Congress [18], [19]. The KMA collection is from the years 1981 through 2010 [18]. It should be noted that amphibious landings during Exercise Ssang Yong actually occurred during March 2014 and the remote sensing experiment occurred during April 2014. Climatic data from KMA, for example, shows average temperature in March of 7.9º C and 13.8º

C for April [18]. The table also includes climate information on maximum, minimum and surface temperatures, precipitation levels, humidity, pressures, fog, and hours of sunshine [18]. Relevant climatic data are provided in Appendix C. Additional information from the Library of Congress website shows the ROK has four distinct seasons, is influenced more by the Asian continental air masses (cold) than the air over the Pacific Ocean (warm) and tends to experience three typhoons a year [19] during the months from June to September.

3.0 Quality Assurance / Quality Control

The research team focused significant effort on the collection of high quality data for the production of amphibious decision aid products. The Principal Investigator (PI) from Rochester Institute of Technology (RIT) in synchronization with collaborators established written procedures for the quality control (QC) of calibration and validation data through an initial science plan (for example QC Considerations and checklists see Appendix D).

The collection of high quality littoral data requires sustained quality assurance (QA) and QC practices to ensure credibility and value to military planners and operators. QA is partly determined by the selection of appropriate hardware that is sufficiently accurate and reliable to produce high-quality littoral data. QA also requires well-documented procedures for note taking; sensor calibration; calibration checks and/or *in situ* verification, including post-deployment calibration; proper deployment considerations, such as measures for corrosion control and anti-fouling; reliable data communications; adequate maintenance intervals; and implementation of a robust QC process. Post-deployment calibration (instrument verification after recovery) and maintenance issues are outside of the scope of this data report.

Following data collection, QC involves taking steps that support the delivery of high quality data and requires both automation and human intervention. QC practices include many different procedures that assess accuracy in file naming conventions, data format, verify data checksum counts, ensure timely arrival of data, apply threshold checks (minimum/maximum rate of change), neighbor checks, climatology checks, model comparisons, signal/noise ratios, and generation of data flags, most of which are described in detail in this document. Field notes and photo-documentation were essential to support many QC tasks.

The process of ensuring data quality is not always straightforward. QA/QC procedures may be specific to an organization, sensor technology or even to a particular manufacturer’s model, so the establishment of a methodology that is applicable to every sensor remains challenging. Our approach involved using industry standard procedures and familiarization training prior to deployment. The following companies produce sensors that were used during the experiment:

Table 3-1. Industry standard sensors used during Ssang Yong 2014 Remote Sensing Experiment.

Manufacturer	Description	Sensor
Kessler DCP	Instruments to measure California Bearing Ratio and soil bearing strength.	Dynamic Cone Penetrometer
USACE Static Cone Penetrometer	Measures shear strength with depth to 18”, Cone Index	Force sensor (calibrated proving-ring)
Onset/HOBO	Data logging devices to measure environmental parameters.	U30-NRC Weather Station and U20 Water Level Data Logger
PANalytical Boulder (formerly ASD Inc.)	Laboratory-quality *in situ* field hyperspectral measurements with equivalent illumination and viewing geometry for accurate correlation to satellite and aircraft sensor data.	FieldSpec 3/4
Seafloor Systems	Portable hydrographic survey equipment.	HydroLite-TM
Trimble	GNSS Survey and Positioning Systems	R-8 2 GNSS RTK and PRO-XH
Zorn	Dynamic plate bearing test systems for measuring the bearing capacity (deflection) of subgrade/subsoils and unbound base layers.	Light Weight Deflectometer
This is a partial list describing key instruments and sensors used for the development of imagery-derived amphibious planning projects. Their use is defined in technical manuals, American Society for Testing and Materials (ASTM) standards, and by organizations such as the International Hydrographic Office and the World Meteorological Organization.		

The type of sensor system collecting the data and the system processing and transmitting the measurements can affect which QC procedures are used. *In situ* systems such as the HOBO data logger with sufficient on-board processing power within the sensor may process the original (raw) data. Other sensors measuring water temperature, salinity, and barometric pressure may be required to produce derived products, such as time series of water level fluctuations.

Sensors can be deployed in several ways. Stationary sensor deployments are on fixed platforms or moorings where there is minimal horizontal or vertical movement. Mobile platforms

such as the SonarMite MILSpec™ were fixed to the RHIB. Sensors deployed on mobile platforms such as gliders require attention to proper QA procedures both before and after the deployment. One might need to confirm location or distance measurements for a transducer, antenna, or pressure sensor at the end of a deployment. In some cases, moorings in a training area could be hit by amphibious craft and dragged from their original deployment locations.

To conduct real time QC on observations, the first prerequisite is to understand the science and context within which the measurements are taken. For example, background knowledge on littoral deployment sites is critical, especially since sensors can be deployed numerous ways and under a variety of conditions. In this study, background information on waves, tides, and shallow water processes were considered during the literature search phase and ensuing scientific planning phases of the remote sensing experiment. While each sensor provides vastly different products, QC techniques can be applied broadly. Examples include the proper selection of thresholds (e.g., cloud cover, winds, precipitation, water levels, and swells) for the east coast of Korea during April, a check for temporal data spikes, and conformation of mooring locations on recovery since moorings were located in proximity to boat lanes. Human involvement is therefore important to ensure that solid scientific principles are applied to data evaluation to ensure that good data are not discarded and bad data are not distributed or included in analysis.

Data are evaluated using QC tests, and the results of those tests are recorded by inserting flags in the data files. Scientists may incorporate additional flags for inclusion in metadata records to further assist with troubleshooting. For example, an observation may fall outside of established thresholds and be flagged as having failed. For example, if data such as temperature exceeds an upper limit, a ”failed high” flag may indicate that the values were higher than the expected range. Such detailed flags primarily support follow-on scientific analyses.

A successful QC effort is highly dependent upon selection of the proper thresholds, which should not be determined arbitrarily but should be based on historical knowledge or statistics derived from more recently acquired data. Such data should be collected by advance parties.

The QA effort, which complements the science plan, ensures that end data products suitable for use during the MCPP are of high value. This work also ensures that the geodatabase can be used by the remote sensing and mapping community to update official products such as littoral planning charts.

The following two subsections suggest ways to ensure QA by using specific procedures and techniques. Operators should document the processes they use to perform QA. Additionally, details of QA for sensors associated with specific observations should be captured and made available to data consumers as part of the accompanying metadata (e.g., sensor calibration date, sensor service history).

Sensor Comparison:

An effective QA effort continuously strives to ensure that end data products are of high value and to prove they are free of error. Operators should seek out partnering opportunities to inter-compare systems by co-locating differing sensors. For example, this project benefits from the dual use of bottom-mounted water level gages and moored GPS buoys. Agreement of multiple

systems provides a robust observation, while disagreement may offer a measure of data uncertainty. If possible, operators should retain an alternate sensor or technology from a second vendor for similar in-house checks.

QA Levels for Best Practices:

A wide variety of techniques are used by researchers to assure that sensors are properly calibrated and operating within specifications. While all researchers must conduct some form of validation, there is no need to force instrument operators to adhere to one single method. A balance exists between available resources, level of proficiency of the instrument operator, and target data reproducibility requirements. The various techniques span a range of validation levels and form a natural hierarchy that can be used to establish levels of certification for instrument operators. For this experiment, instrument operators participated in familiarization training during March 2014 at Rochester Institute of Technology (RIT).

4.0 Field Experiment

The data collection phase of SY'14 included three scientists from Rochester Institute of Technology (RIT), four scientists from the Naval Research Laboratory (NRL), two scientists from Marine Information Resources Corporation (MIRC), two US Navy Reservists, and one engineer from the South Carolina Research Authority (SCRA). Primary equipment used for data collection included the Goniometer at Rochester Institute of Technology (GRIT) (which incorporates a field spectrometer), light weight deflectometers, dynamic cone penetrometers, sand cone field density apparatus, a meteorological station; Global Positioning System (GPS) base stations, multiple GPS units, ground-based LiDAR, cameras, and a microscope. Key components of Data Quality Assurance (DQA) were (a) pre-deployment training at RIT, (b) development of a Science Plan by the PI, (c) use of standardized procedures for data collection, and (d) completion of descriptive field notes and photo-documentation. Key elements of DQA were discussed in Section 3.0. The collection of quality controlled Cal/Val data was useful for the development of trafficability maps.

Trafficability is determined most significantly by measuring strength, composition, grain sizes, moisture content, and density of soils. Composition of soil at a beach consists of sediments (sand, silt, clay) and biological materials (e.g. shells, algae, coral fragments). The specific minerals found in sediments depend strongly on the coast type as do the biological components. Grain size distributions are determined, generally by geologic history, the prevailing wave spectrum, and the size of particulates that are transferred to the beach, whether rolling down the slope of a hill or mountain, settling at high tide, or brought by human interaction. On the beach, higher waves bring smaller grains toward the sea leaving coarser grains further back on the beach. Finer sands on a beach generally cause a gentler slope due lower strength characteristics (internal friction) relative to the coarser, e.g. gravel, cobble type material. The source of moisture content in beach sands stems from multiple sources: the ocean waves reaching the sands, rivers and streams running through the beach to the sea, rain, and human interaction (e.g. irrigation runoff or beach nourishment).

Most beaches are composed of sediments that are derived from the erosion or weathering of soil and rocks. Waves and currents rework the accumulated beach sediments, smoothing the shape of beach materials and sorting them by size, shape, and density. Further, seafloor sediments may be referred to by origin as either terrigenous (land-derived) or pelagic (ocean derived). Terrigenous sediments may include gravels, sands, silts, and clays. They are formed on or adjacent to land and are transported by currents, wind, icebergs, or by man during beach nourishment or reclamation projects. Pelagic sediments include abyssal clays, siliceous oozes, and calcareous oozes. These sediments are formed in the sea and are composed of clays or skeletal material from plants or animals.

Dogu, Doksuk-ri, and Hwajin-ri Beaches are all located in the North Gyeongsang province of South Korea along the east coast. In reference to Pohang Town Hall, Dogu Beach is located approximately seven kilometers east, Doksuk-ri Beach 23 kilometers north, and Hwajin-ri Beach 25 kilometers north.

The Cal/Val phase of SY'14 was carried out from 14-25 April 2014. Ground and sea truth data were taken consisting of *in situ* spectral, geotechnical, and bathymetric measurements were taken to understand relationships between the bearing strength, beach profiles, and their corresponding surface spectral reflectance. All data were archived into a project geodatabase.

4.1 Site Characteristics

Specific study locations during the SY'14 Experiment are provided in Figure 4-1. The sites are located in the greater Pohang area.

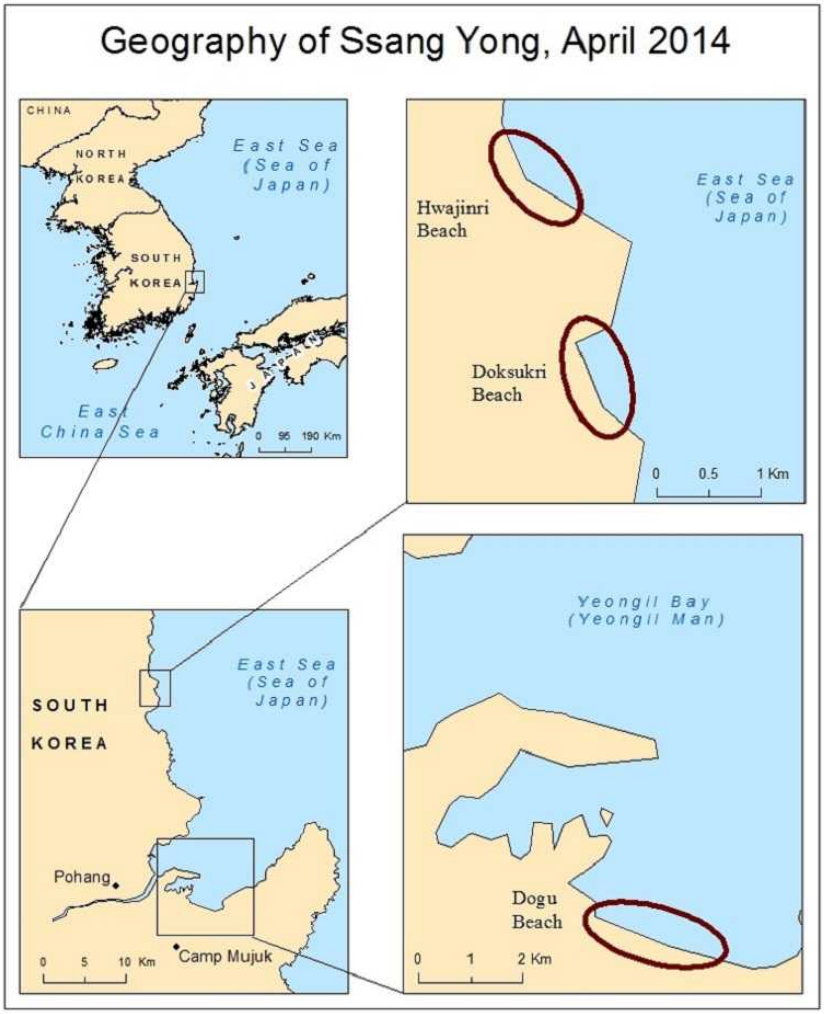

Figure 4-1. Location of Study Areas during the Ssang Yong 2014 Remote Sensing Experiment.

Knowing key biological and physical aspects of a particular coast can help predict the types of obstacles to expect when approached. The east coast of Korea (rocky coast) in the past rose slowly resulting in hills, mountains (Taebaek), and headlands along the coast [20]. Weathering processes, micro-tidal ranges, and waves contribute to the terraces and sandy beaches, unlike the west coast that has macro-tidal ranges and extensive mudflats [20]. Some of the sediments at the beach locations near Pohang receive continuous deposition from rivers and small streamlets emptying into the East Sea.

The Hyeongsan River flows from Doseo-myeon, Ulju-gun in Ulsan to the East Sea via Yeongil Bay, covering a distance of about 62 km. Development along the river includes the port of Pohang and the POSCO steel mill. Yeongil Bay is considered to be one of Korea's most industrialized regions and is contaminated by persistent organic pollutants [21]. Yeongil Bay is also considered one of the most contaminated coastal areas in South Korea [21]. Marine debris

on the beaches ranged in size from small broken plastic particles and intact Styrofoam floats to abandoned small vessels.

Dogu Beach (see Figure 4-2), a landing beach for exercises and ongoing training, was a primary study site located along Yeongil Bay (Yeongil Man), which is directly connected to the East Sea. Dogu Beach trends southeast from the Naeng streamlet to Hweol Dong. Seaweed is in abundance at Dogu Beach along with various trash items including old plastic and Styrofoam buoys and galley trash (vegetables) from nearby merchant vessels, all found strewn along the beach during the experiment.

Figure 4-2. Dogu Beach transects. Five potential transects were selected from visual inspection of Google Earth imagery from February 2013 prior to the start of the field experiment.

Doksuk-ri Beach and Hwajin-ri Beach are also used for military training and are approximately 25 kilometers north of Dogu Beach (see Figure 4-1). Hwajin-ri has some large boulders and a rock formation along its approximate 1.6 km length.

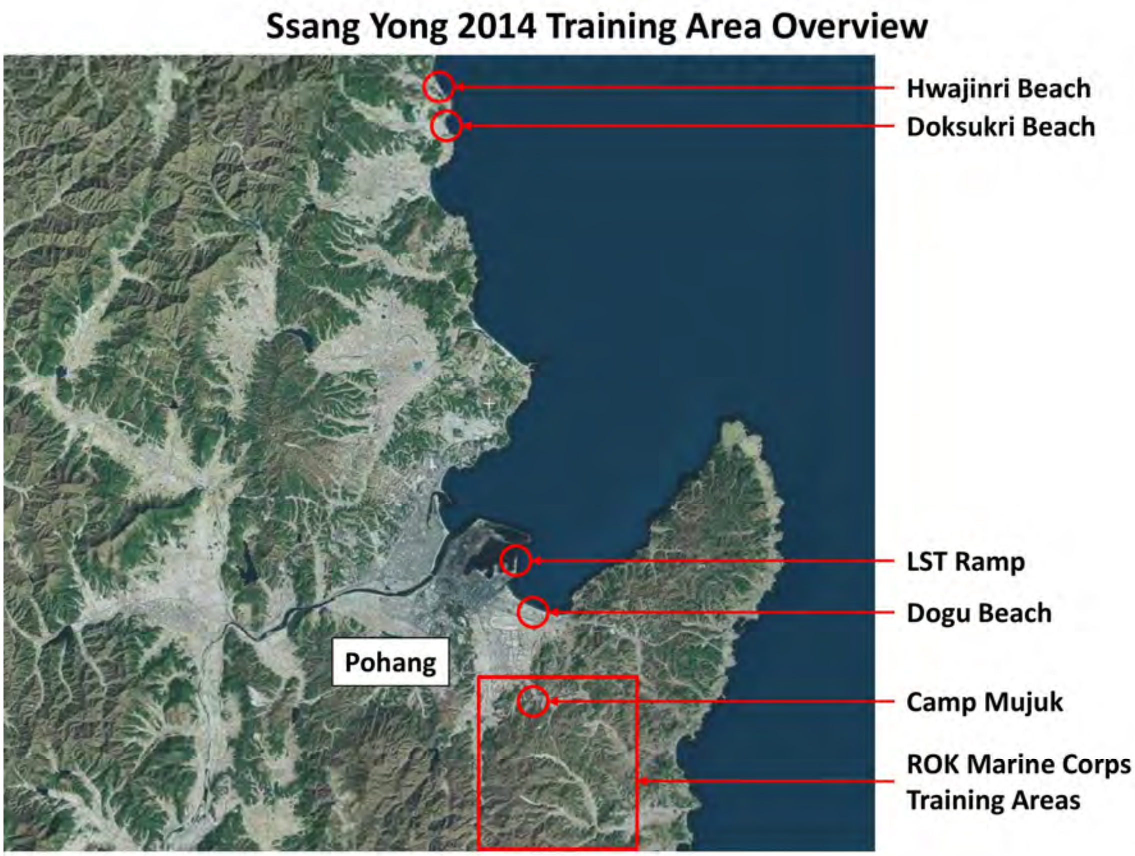

Figure 4-3. Overview of Training Area Ssang Yong 2014.

Unlike Dogu and Hwajin-ri Beaches, Doksuk-ri Beach is steeper and characterized by an abundance of pebbles and cobbles. Variations in beach composition were characterized through an analysis of standard quadrats, using a one meter cutout from a tarp (see Figure 4-4); these quadrats are linked to GPS points and photos within the project geodatabase. Table 4-1 characterizes landing beach morphodynamics and dimensions (length and width), such as geographical position. (For more information on the quadrats used during the experiment see Appendix E). More detailed sediment characterization methods (grain-size analysis) give further insight into the composition of the beach materials.

Figure 4-4. One Meter Cutout. Doksuk-ri Beach. Coordinates and a photograph were taken for each flag in this image and placed into the project geodatabase to support beach characterizations.

Table 4-1. General beach shapes and geometries. Lengths include the landing area from left to right flank.

Name	Shape	Length and width	Geographic Position
Dogu	Straight	979 m, 68 m	In Yeongil Bay
Hwajin-ri	Straight	283.6 m, 89.6 m	Faces ocean (East Sea)
Doksuk-ri	Concave	810 m, 52.8 m	Faces ocean (East Sea)

4.1 Satellite Imagery

WV2 is a high spectral resolution multispectral satellite that was launched in October 2009. The satellite is in a sun-synchronous 100-minute orbit around the earth, at an altitude of 770 km

[22]. The sensor is a push broom style imager, collecting one row of an image at a time using linear detector arrays [23]. WV2 has the ability to image 785,000 square kilometers a day and averages a revisit time of 1.1 days [22]. This short refresh rate makes WV2 a valuable asset to provide updated littoral information for amphibious planning. WV2 provides eight bands across the reflective solar wavelength region of 400 – 1040 nm. The spectral coverage of the WV2 imagery is depicted in Table 4-2.

WV2 imagery was collected on three particular days during the experiment to make example products for amphibious planning. However, cloud free observations were made only during one of the three days. Clear imagery for the two northern beaches Doksuk-ri and Hwajin-ri were of sufficient quality to be used for developing products. In this project, the WV2 imagery was used to predict trafficability of the study sites. These products can be used to determine the feasibility of using WV2 to support maneuver and construction of military roads and expeditionary airfields. Additional imagery such as Landsat and WV2 from the months immediately following the exercise has also been collected and is being evaluated for potential use in future projects. Landsat-8 images were collected from the USGS website that occurred during 14Apr2014 while the experiment was being conducted. QuickLooks of images that were used in this project appear in Appendix F.

Some additional imagery was collected in September 2014 and has been archived in the file geodatabase, e.g., Landsat-8 and Landsat-5 images. Landsat imagery may be used for base maps and change detection, but does not have fine enough resolution for this project's focus on trafficability analysis.

Table 4-2. Spectral configuration of WorldView-2.

Band	Spectral Range
Coastal:	400 – 450 nm
Blue:	450 – 510 nm
Green:	510 – 580 nm
Yellow:	585 – 625 nm
Red:	630 – 690 nm
Red Edge:	690 – 770 nm
Near-IR1:	770 – 895 nm
Near-IR2:	860 – 1040 nm
Additional details on the WorldView-2 satellite may be accessed online at URL: http://www.digitalglobe.com.	

WorldView-3 (WV3), which was launched on 13 Aug 2014, should be considered as a valuable resource for future experiments. WV3 has a higher resolution and a faster revisit time (less than 24 hours) than WV2. These aspects of WV3 will enhance the capability to derive updated littoral situational awareness products from multispectral space-borne sensors.

4.2 Calibration/Validation Data

Cal/Val data for SY'14 were collected and include spectral, meteorological, geotechnical, and hydrographic measurements. Photographs, ground control points, and field notes document Cal/Val data collection for QA and QC. Data collection locations were chosen by the PI and are documented in the Science Plan. Planned sampling positions along field transects were chosen in order to observe the natural variability of beach characteristics. Once on site, the team adjusted site positions based on the local conditions encountered in order to follow this same principle and ensure that the typical variability found on these beaches was appropriately sampled. At each of these sample locations, spectral and geotechnical data were collected to determine spectral signatures and their associated geotechnical properties.

At each sampling location, ground control points were taken to provide coordinates for referencing the sample position into the project geodatabase and to assist with the processing of the field data. Many static points and roving GPS points were collected. The static GPS positions included equipment positions and orientations of instruments (especially the goniometer). The roving GPS measurements were used to develop beach contours and to outline specific littoral features (e.g. streamlets and other natural as well as man-made objects). Stations where goniometer spectra and coincident geotechnical measurements were taken are all associated with GPS data, field notes, and photographs.

Instrumentation needed to collect data required for trafficability analysis includes spectrometers, lightweight deflectometers, static and dynamic cone penetrometers, and a field density sand cone. The portable field spectrometers are used to collect field spectra in support of remote sensing image analysis from hyperspectral and multispectral imaging sensors, although in this specific experiment and demonstration only multispectral commercial satellite imagery was made available (i.e., several WV2 images). Spectral signatures of the beaches and tidal areas were collected in two ways, one using nadir-only measurements with a field spectrometer as had been done in the past in [1], [2], [4]-[8], and also with GRIT, which measures the angular variation of the spectral signature, sampling over the hemisphere of possible observation geometries as had also been done in the past during three earlier campaigns using the Goniometer for Outdoor Portable Hyperspectral Earth Reflectance (GOPHER) (one campaign at the VCR in 2011 [24], [25] and two in Queensland, Australia in 2012 and 2013 under the CWP THEMAS program [9]). The lightweight deflectometer (LWD) measures the dynamic deflection modulus (elastic response of the surface) by dropping a weight onto an accelerometer embedded in a base plate, which simulates the response of the surface to vehicle traffic. Field measurements of sediment density were also acquired using a standard sand cone apparatus following ASTM standard procedures. The dynamic cone penetrometer (DCP) determines the sediment strength properties by measuring penetration into soil at fixed kinetic energy input (weight drop on anvil). Shear strength and SoilCone Index (CI) were determined using a USACE Static Cone Penetrometer. Soil sampling was also conducted and some analyses were completed at Camp Mujuk to determine soil moisture content as well as grain size profiles. The use of geotechnical instruments in conjunction with hyperspectral signature measurements fostered the accurate characterization of SY'14 beaches and follows procedures developed over many of our past experiments [1], [2], [4]-[12], [24], [25].

In situ measurement data for characterization of beach composition included:

a. Multi-angular hyperspectral reflectance measurements taken using an ASD FieldSpec 4 spectrometer/goniometer (GRIT) developed at the Rochester Institute of Technology.
b. Dynamic modulus measurements taken using a Zorn ZFG2000 Light Drop Weight Tester, a type of Light Weight Deflectometer (LWD).
c. Sediment strength measurements taken with a Kessler Dynamic Cone Penetrometer (DCP).
d. Shear strength measurements taken with a Static Cone Penetrometer.
e. Positions of soil sites collected taken using a Trimble® Geo-XH GPS unit and R-8 unit.
f. Profile survey of beach gradient collected using a Trimble R-8 GPS unit mounted on a wheel.
g. Beach topography collected using a SICK Laser-Measurement-System-200 Ground-based LiDAR scanner.

In situ measurement data for characterization of shallow water characteristics included:

a. Bathymetric measurements taken with an Ohmex® SonarMite MILSpec™ Echo Sounder.
b. Water level measurements taken using a Trimble R-8 Kinematic GPS receiver mounted on a PVC frame buoy.
c. Water depth and temperature measurements taken with bottom-mounted HOBO U20 Titanium water level pressure gauges.
d. Meteorological measurements taken with a HOBO U-30 Weather Station.

5.0 Visualization

From 14-25 April 2014, the RIT led team carried out the *in situ* segment of the data collection experiment on Dogu, Doksuk-ri, and Hwajin-ri beaches. Teams were formed to collect an assortment of different data types: spectral, geotechnical, spatial, atmospheric, and oceanic. Field notes, along with photographs were taken to provide metadata for the experiment and can be viewed within the project geodatabase in sub-directories of the "Attribute_Data" directory.

Data collections also included meteorological and oceanographic measurements that will be used to remove effects that result from scattering and absorption in the atmosphere and from reflection at the sea surface from the measured spectral radiances recorded by the spectral sensors. Since radiative transfer across wind-blown water surfaces is more complex and difficult to describe quantitatively than transfer within the water column, these environmental observations are imperative for follow-on numerical modeling tasks. Refinement of imagery post-processing through careful application of calibration and atmospheric correction procedures results in improved bathymetric retrievals and estimates of soil properties such as bearing strength for trafficability analysis. Atmospheric correction is a critical image processing step that results in determining the best values for remotely sensed littoral features and remains one of the most challenging aspects of the QA/QC process.

Reflectance of the objects recorded by the WV2 satellite may be affected by atmospheric absorption and scattering, sensor-target illumination geometry, and sensor calibration. We deployed weather stations and collected spectral validation data from deployed standard reference panels on the ground to assess and correct calibration as needed. We also collected other types of calibration/validation data such as ground control points, which are used to assess the accuracy of georectification. The weather station installed at Camp Mujuk and other resources such as space-based ozone measurements from NASA provided data useful for atmospheric correction. The weather station provided meteorological information for the times when imagery was collected. In addition, atmospheric pressure variation was removed from bottom-mounted pressure gage observations to obtain water level fluctuations. The resulting time series were used to tide synchronize imagery.

5.1 Spectral Collection

A reference station spectrometer was used during all spectral data collections to collect white reference plaque data (see Figure 5-1); the plaque is made from a material known as Spectralon™, a widely used calibration standard. The data from the reference station spectrometer is later used to radiometrically adjust the reflectance measurements taken by the hyperspectral GRIT and the rover nadir spectral measurements that also were taken with a second spectrometer unit during the experiment. The data allows the continuous readings to monitor and record variations in the downwelling solar irradiance, which occurs due to changes in the amount of atmospheric scattering and absorption during spectrometer measurements. Using this reference station spectrometer data from the white standard helps to mitigate the effects of variations in solar illumination during spectrometer measurement cycles, and follow a process that we developed and described in [26] for using the recorded output of two spectrometers recording simultaneously. The method was developed originally for two nadir looking spectrometers, one looking continuously at a white Spectralon® reference plaque, while the other spectrometer alternately measured from a white Spectralon reference plaque and the sample of interest. However, the method has been adapted to work with goniometer data such as that obtained from GOPHER [24], [25] and GRIT in the present experiment. (See more information on the spectral data collected in Appendix G).

Figure 5-1. Reference station spectrometer. Used to continuously monitor a White Reference standard made of Spectralon® during spectral sampling by the hyperspectral GRIT to characterize the angular dependence of the spectral response and a second rover spectrometer used for nadir-only spectral measurements.

5.1.1 Portable/Handheld Spectral Data

A field spectrometer was used during expected WV2 imagery collection days to record spectral reference data from calibration panels for later atmospheric corrections of imagery (see Figure 5-2). The collection from the field spectrometer consisted of alternating between white plaque (Spectralon) data and the different colored calibration panels.

Figure 5-2. Calibration Panels. (Top) Calibration Panels at Hwajin-ri Beach during WorldView-2 imagery acquisition; (bottom) portable ASD field spectrometer rover unit acquiring radiance samples from the white calibration panel during the Worldivew-2 imagery collection overpass.

5.1.2 Multi-Angular Spectral Data

GRIT collects a spectral collecting range of (350-2500 nm), and is track mounted on a quarter-arc for zenith travel and has a full azimuth rotation ability (see Figure 5-3). GRIT is used to measure the bi-directional reflectance distribution function (BRDF). BRDF can be understood as the spectral reflectance as a function of sun-target-sensor angle, and allows for easier distinction of landscape properties based on this angular dependence of the spectral reflectance. GRIT provides spectral data for a designated point from all azimuth and zenith angles, creating a complete spectral library for future reference and analysis. In particular it supports the more accurate characterization of the surface and terrain for off-nadir remote sensing imaging geometries. The goniometer collected white plaque reference data prior to and after full collection soil spectra at a site location (see Figure 5-4). In addition, GRIT spectral BRDF collected during the WV2 overpass and imagery collection can be used in conjunction with the nadir spectrometer measurements taken from the reference panels to improve calibration of the WV2 imagery data.

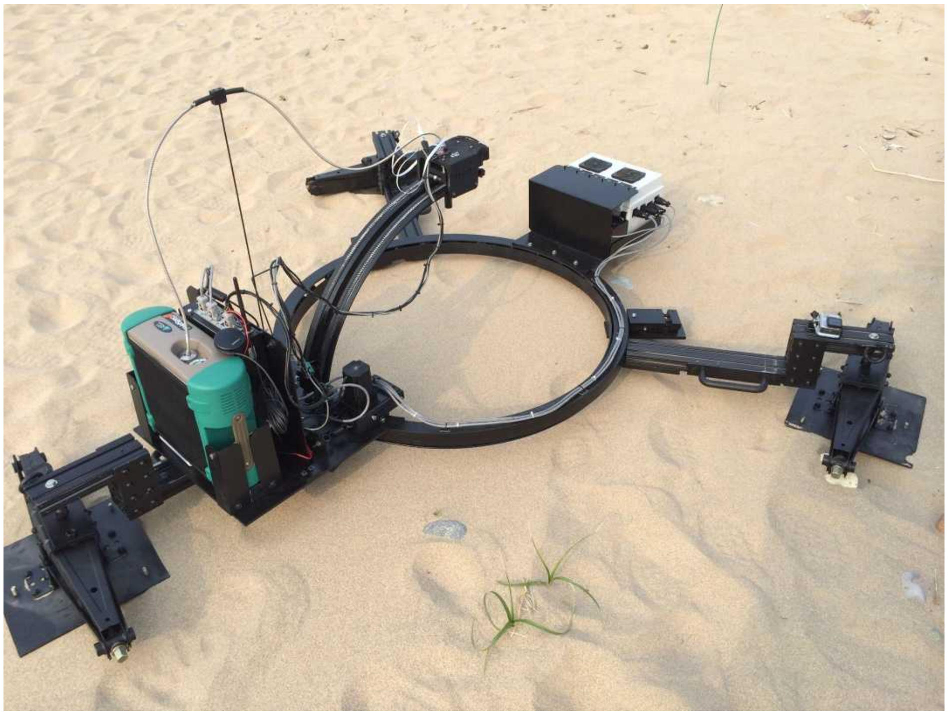

Figure 5-3. The GRIT hyperspectral goniometer at Dogu Beach.

Figure 5-4. The GRIT (hyperspectral goniometer) with White Reference Plaque. Used in calibration just prior to sediment spectral sampling.

5.2 Geotechnical Collection

A comprehensive geotechnical investigation was conducted at each survey site to assess the surface trafficability. Following the conclusion of the optical (non-destructive) tests at each site, a series of geotechnical tests and then sampling followed, as close as possible to the optically measured location. First, time sensitive samples were taken for subsequent lab determination of soil moisture content. These were properly sealed to prevent any moisture loss prior to the lab measurements at end of each field day. Then a series of tests followed, including static penetrometer (SCP), dynamic penetrometer (DCP), Light-Weight Deflectometer (LWD), field density using cone (sand-replacement technique). It was not necessary to conduct other tests (e.g. vane shear test) as the sediments encountered at all the sites did not include cohesive (clayey) types, where these tests would be informative. Extensive bulk sampling then followed, with the samples, properly sealed, taken to the laboratory, set up at Camp Mujuk.

Once in the laboratory, samples were processed, including moisture content measurement and oven drying, according to the standard ASTM procedures. Several laboratory tests were then conducted on the oven-dried and processed samples, including grain size analysis by dry sieving, minimum and maximum density tests (allowing for calculations of relative density values), and specific gravity tests by water pycnometer. Again, all tests were conducted according to the ASTM procedures for geotechnical testing of soils. All geotechnical data are archived in the project geodatabase.

5.2.1 Sediment Shear Strength

Shear strength tests conducted included Static Cone Penetrometer – a standard tool used for mobility estimates, yielding CI – cone index of the sediment, a Dynamic Cone Penetrometer (DCP) which is useful in profiling to a deeper depth than that achievable with a static cone, especially in harder, more dense granular materials and may also be correlated with a California Bearing Ratio (CBR) – a widely used index measure of soil compaction or strength. Finally, plate-drop tests were conducted using a LWD, which simulates subgrade deformation under vehicular load by measuring the displacement under a calibrated dynamic plate impact. Results of the SCP and DCP tests are given in Appendix R and results of the LWD tests are reproduced in Appendix S. These appendixes also provide additional details on data processing and derived soil parameters for each test.

The SCP was pushed into the soil at a constant rate (see Figure 5-5), while recording the force (or pressure) during this continuous soil failure. Two different configurations of the SCP were used, one with a $0.2 in^2$ projected cone area and one with the $0.5 in^2$. The smaller cone allows reaching deeper into the soil strata in harder soils, while the larger cone provides a higher resolution of measurements, important in softer surficial layers. Both cone tests were performed at all the sampling sites. Cone Index can then be calculated as a function of depth from each cone type – a primary measure of soil trafficability, as noted above. In some soils, remolding may significantly degrade soil strength, resulting in continually reduced terrain mobility with every successive vehicle pass. In these cases, a remolding test may be conducted, measuring just such strength degradation (Army FM5-430-00-1). We did not, however, encounter any soils on any of the beaches surveyed that warranted these remolding tests. In these cases, the cone index

measured is equivalent to the Rated Cone Index (RCI) as no strength degradation upon remolding occurs.

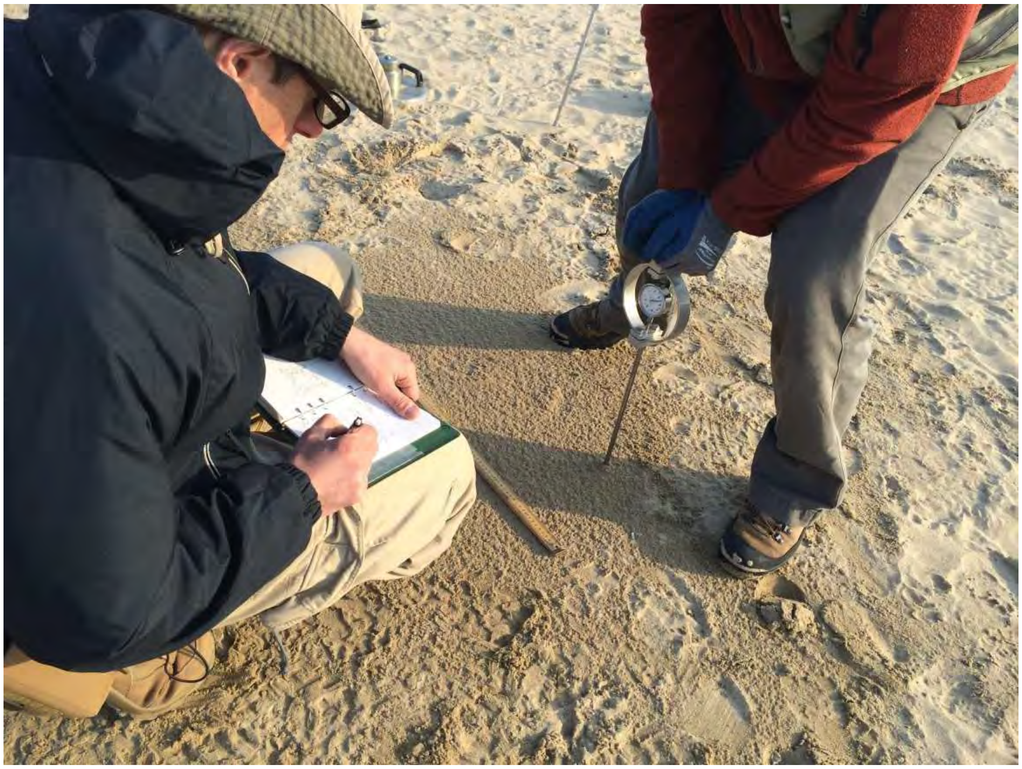

Figure 5-5. Static Cone Penetrometer.

Dynamic Cone Penetrometer (DCP) is an alternative method of determining the sediment shear strength as a function of depth (see Figure 5-6). The specific instrument used for these measurements is a Kessler Dynamic Cone Penetrometer, which consists of either a 4kg or 8kg weight attached to a rod with a steel drive rod and cone attached to the end. In all cases during the SY14 experiments, only the 4kg weight was used. While more labor-intensive, it provides a higher resolution of strength measurements with depth, especially important in softer surficial materials, important for trafficability estimates. The heavier weight may be more appropriate to the harder strata, e.g. compacted road gravel subgrades. During testing, the weight is repeatedly dropped on the anvil of the drive rod, delivering a calibrated impulse, and with each blow, the distance that the cone advances into the soil is recorded. This record is translated into a measure of shear strength as a function of depth using a standard index known as the California Bearing Ratio (CBR), a commonly used measure of sediment compaction or strength. CBR is a ratio of the load required to reach a certain depth at the sampling site, relative to the "standard load" required to reach the same depth in a standard crushed rock material (California limestone). Details of the data processing and test results are given in Appendix R.

Figure 5-6. Dynamic Cone Penetrometer.

5.2.2 Dynamic Deflection Modulus and Bearing Strength

The Zorn ZFG2000 Light Drop Weight Tester is known as a Lightweight Deflectometer (LWD). The LWD provides a measurement of the dynamic deflection modulus of the soil. This modulus represents the elastic response of the sediment to an impulse loading, and is used in civil engineering applications as a complimentary measure of soil strength and relative density, which allows estimating bearing capacity and trafficability properties (Figure 5-7).

Figure 5-7. Light Weight Deflectometer. The standard weight is free falling toward the anvil, generating a calibrated impulse loading on the plate and the sediment beneath.

The Zorn LWD consists of an accelerometer embedded in a steel plate of diameter 300mm, and a mountable rod with a 10kg weight that is repeatedly dropped on the base plate/accelerometer assembly. Three pulses are normally performed and the measured data is stored on the device for subsequent unloading. The memory card records the deflection of the plate on the ground in response to the dropping of the 10kg weight from a known reference height, as a function of time. These curves are used to estimate the dynamic deflection modulus (Evd) in MN/m^2. These calculations allow for estimating the CBR, a measure of sediment bearing capacity and thus a trafficability estimate. The details of the calculations and the LWD data are given in Appendix S.

5.2.3 Field Density Measurements

Field density measurements were conducted using an American Society for Testing and Materials (ASTM D1556-07) standard sand cone apparatus shown in Figure 5-8. The instrument consists of a canister with calibrated sand of known density and a standard plate with a hole for soil sample excavation. First, a base plate is placed on the sediment surface and a sample is excavated from the hole to a desired depth (normally 2-3" but as shallow as 1" is possible). This excavated material is collected for subsequent weight and moisture content measurements. Then, a canister with the calibrated sand is placed over the hole and the sand is dispensed filling the hole and the dispensing cone. Weight differences of the canister before and after sand deposition (and prior device and sand calibration) allows for calculating the volume of the excavated hole, which together with the excavated sample mass measurement, gives the wet field density result. Laboratory measurements of moisture content of the collected sample allows for calculating the dry field density of the soil, subsequently. Details of the calculations and the results for all the stations tested are given in Appendix T.

Figure 5-8. Sand cone density apparatus. Canister with calibrated sand is placed over the excavated hole (and a standard base plate) for determination of the wet field density of soil. Dry density is calculated after the laboratory measurement of the field moisture content.

5.2.4 Laboratory Geotechnical Measurements

The laboratory phase of geotechnical analysis included the following standard tests: moisture content, specific gravity, grain size distributions, minimum, and maximum density tests. These

tests were conducted in accordance with the appropriate ASTM standards and were used for sediment classification according to the Unified Soil Classification System (USCS, ASTM D2487), as well as calculation of relative density. Relative density is of particular interest in soil trafficability estimates from remote hyperspectral measurements (of granular materials) as was shown in an NRL seminal publication on phase-angle dependency of reflectance on relative density in complex coastal sediments [29].

5.2.5 Sediment Moisture Content

The procedure to determine the soil moisture content (ASTM D2216) first involved collecting sediment samples at site locations and storing them in double zip lock bags to prevent any moisture loss before accurate lab measurements can be made. At the end of each day, the samples were transported to Camp Mujuk, weighed in their original wet state, and then re-weighed after drying in a standard drying oven (Figure 5-9) at an ASTM – prescribed temperature of 110°C overnight. ASMT allows for a lower temperature drying, when a large amount of organic material (e.g. peat) is present in samples. No such cases were encountered in any sampling locations, and thus, the standard drying temperature was used. The ratio of the weight of water to that of the dry soil sample, expressed in percent, is the standard geotechnical (gravimetric) moisture content measure. Complete set of results is given in Appendix U.

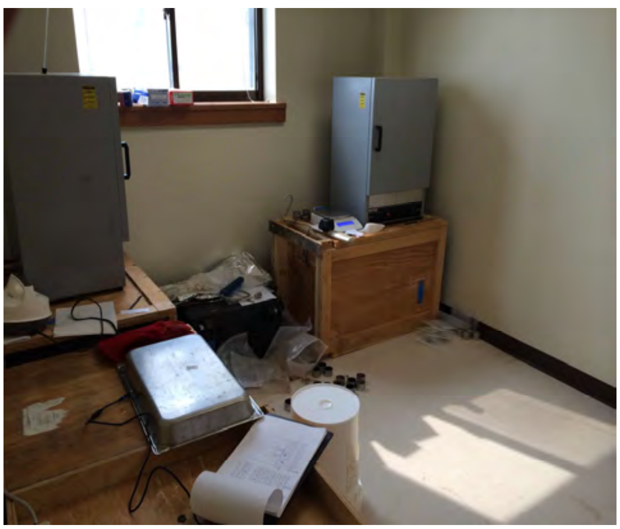

Figure 5-9. Drying ovens used in field laboratory established by the team on site at Camp Mujuk.

5.2.6 Sediment Grain Size and Soil Classification

The standard grain-size analysis test (ASTM D422 and D6913) was used to determine the relative proportions of different grain sizes as they are distributed among certain size ranges. A Humboldt H4325 mechanical sieve shaker (Figure 5-10) was used in the tests. Following such mechanical separation, the mass of each sieve with the soil retaining on it was determined on a precision scale. Then, the total percentage of material passing each sieve was calculated. Each fraction was then placed on a sheet of paper and photographed for future reference.

Figure 5-10. Soil Analysis. (Left) Mechanical sieve shakers and (middle and right) sieves used for grain size distribution analysis in the field laboratory established by the team at Camp Mujuk.

After the complete grain-size analysis, the soils were classified according to the Unified Soil Classification System (USCS, ASTM D2487). The procedure included determination of grain-size curve parameters, such as the coefficient of uniformity and the coefficient of curvature. No plasticity tests were necessary in any of the samples collected and thus, these data were sufficient to provide the final determination of the soil class. For more detail on the USCS procedure and the grain-size and classification data for all the samples, see Appendix U.

5.2.7 Specific Gravity

Determination of the specific gravity, or grain density, of materials was performed using a water pycnometer (Figure 5-11) method (see ASTM D854). All but two of the samples collected had grain size that allowed for this method of measurements. The samples dominated by coarse gravel and cobbles (stations DK1-4 and DK-1-5) were not tested. The procedure involves using a premeasured amount of soil from the sample before funneling into a water pycnometer, adding de-aired water to the fill line, then weighing and recording the temperature. ASTM D854 provides guidance on computing the weighted average specific gravity for those samples containing both coarse and fine materials. Additional information and test results are given in Appendix V.

Figure 5-11. Water pycnometer. Used to determine specific gravity for finer sediments in our laboratory testing at Camp Mujuk.

5.2.8 Minimum, Maximum, and relative density

In addition to measuring the field density and in case of granular sediments (sand and non-plastic silts), a further investigation into the degree of packing of the grains is useful in that it yields additional parameters, which could be related to sediment strength and, therefore, trafficability estimates. These are useful measures to correlate with data as derived from the remote sensing measurements [29]. The sediments therefore can be tested to obtain limiting values for their ability to density, as expressed by the Minimum and Maximum Density that these specific sediments can attain. All soils sampled in the field (except for the two stations at Doksuk-ri beach with large cobbles) were tested for these two values of density limits using the pour and the air-pluviation techniques (ASTM D7481-09, D4254-83, and Creswell et al., 1999), best representing the natural sediment formation processes. Once determined, the present state of granular compaction as expressed via the Field Density results, may be represented by Relative Density as follows:

$$D_d = \frac{\rho_{dmax}(\rho_d - \rho_{dmin})}{\rho_d(\rho_{dmax} - \rho_{dmin})} \times 100,$$

where:
ρ_d is field dry density
ρ_{dmin} is minimum dry density
ρ_{dmax} is maximum dry density

D_d is expressed in percentage. Additional details and data are given in Appendix W.

5.3 Spatial Collection

Trimble GPS units were used to determine the precise location of test sites, and to calculate beach gradient at the various landing beaches. These data were used to support imagery analysis that resulted in accurate trafficability maps. Elevation products such as beach profiles were integrated with very shallow water hydrographic surveys. Beach gradients are necessary for the planning of surf zone breaching, as it is a limiting factor for the maneuverability of some types of amphibious vehicles.

5.3.1 GPS Position Data Collection

GPS positions for all stations were collected with a Trimble Geo-XH and R-8 GPS unit capable of sub-decimeter accuracy. GPS coordinates were recorded at all positions where the goniometer and geotechnical measurements were collected. These data are critical make accurate retrievals from imagery. The GPS position for calibration panels where recorded. The location of calibration panels (Camp Mujuk and Hwajin-ri) supports improved processing of the WV2 data by comparison with ground measurements of known spectral response at the calibration panels. In addition, GPS positions of site natural features, man-made features, and deployed calibration panels serve as fiducials for ensuring accuracy in georectification, key for development of WV2 planning products. Figure 5-12 shows one of two GPS base stations deployed by the field team during the experiment. One base station was deployed at Camp Mujuk, while a second was positioned by the team at a nearby ROK military base near the Dogu landing beach. The base stations both included Trimble 5700 GPS receivers and Zephyr dual frequency geodetic antennas.

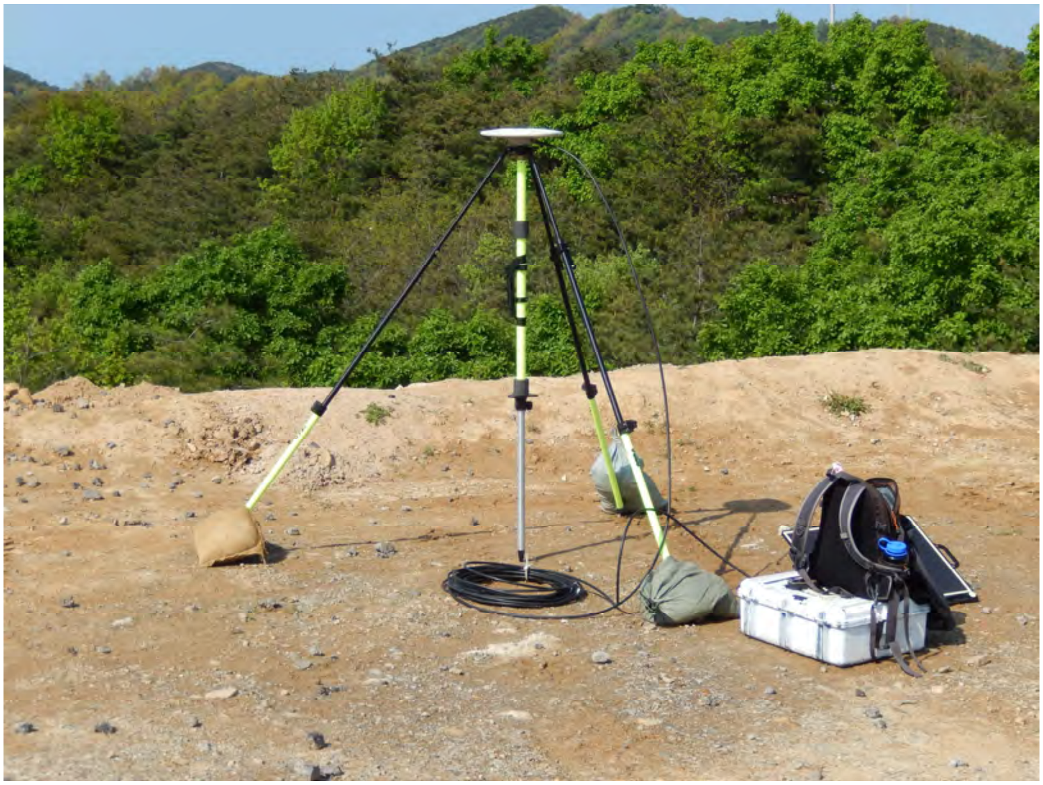

Figure 5-12. GPS base station deployed at Camp Mujuk by the field team.

5.3.2 Digital Elevation Data Collection with Ground-Based LiDAR

A LiDAR (SICK Laser-Measurement-System-200) scanner and a Trimble GPS unit, along with two Kinematic GPS (KGPS) base stations to ensure high accuracy, were used to determine beach profiles for the three beaches surveyed. Past studies in Australia used Trimble terrestrial LiDAR and kinematic GPS to determine beach profiles see [27].

The GPS profile data were collected using two units: a stationary base station, which used an altitude and position reference point, and a mobile rover unit. The base stations were kept on a tripod in the same location while the wheel-mounted rover was used to survey the beach to determine beach profiles. As described above, the base stations were set up at Camp Mujuk and Dogu beach.

LiDAR measures the time it takes infrared light to leave the sensor and return when reflected from an object (see Figure 5-13). The LiDAR data were used to create high quality digital elevation models (DEMs). The maximum usable range is approximately 50 m for the SICK Laser-Measurement-System-200 used in this experiment. The degree of azimuthal rotation during scans is adjustable between 0 and 180 degrees. The maximum azimuthal range was used for all scans. Fiducials were placed into the landscape for each scan, and GPS coordinates were obtained for each fiducial along with the position of the LiDAR unit and its' height from the ground to the base plate the sensor is mounted to. Fiducials used were of two types: (1) any

distinct object lying on the beach that would be recognized in a scan and (2) a series of Styrofoam balls brought by the field team and deployed at positions where the GPS coordinates were also recorded by the field team. The individual scans may be merged/overlapped using the fiducials as common reference points. For more information on LiDAR data see Appendix H.

Figure 5-13. LiDAR Capturing Data at Dogu Beach.

5.4 Atmospheric Properties

Since reflectance of the objects recorded by the WV2 satellite may be affected by atmospheric absorption and scattering, sensor-target illumination geometry, and sensor calibration, we deployed a weather station; collected ground based spectral data from known positions and standard reference panels, and very shallow water Cal/Val data. For example, the weather station (see Figure 5-14) installed at Camp Mujuk and online maps of ozone obtained from NASA provide useful information for atmospheric correction. The weather station provided meteorological information, such as relative humidity, for the times when imagery was collected. Data collected from the Camp Mujuk weather station are provided in Appendix I along with summary plots of u (east) - and v (north) - wind components. Normally the team also uses a hand-held sun photometer to measure aerosol optical depth; however, the photometer malfunctioned and was not usable during the experiment.

Figure 5-14. Meteorological Station. Camp Mujuk.

In order to support atmospheric correction of imagery, ozone data were collected from NOAA (2014). Daily average Dobson Units and additional information on ozone values are provided in Appendix J.

5.5 Oceanographic Properties

Geotechnical information on beaches and shallow water is not easily found in historic databases and national data archives. Some geotechnical information from past hydrographic and bathymetric surveys may be found on products such as Digital Bathymetric Data Base Variable Resolution (DBDB-V), which may be obtained from the U.S. Naval Oceanographic Office (NAVOCEANO).

During boat operations, hydrographic data were collected by deploying three pressure gages, one at each beach study site, two water level buoys with kinematic GPS (for reference to the ellipsoid), and one HydroLite™ echo sounder. One water level buoy was deployed off Dogu Beach and the other at Hwajin-ri Beach, both with accompanying bottom-mounted pressure gages. A Rigid Hull Inflatable Boat (RHIB) (Figure 5-15) was launched from a ramp on the Hyeongsan River in order to deploy the water level buoy and the pressure gage in very shallow water off of Dogu Beach on April 14, 2014. The RHIB was launched from a ramp just east of Josa-ri to deploy the third pressure gage, which was moored off Hwajin-ri Beach. This ramp was also used to deploy a bottom-mounted pressure gage and water level buoy off Doksuk-ri Beach. The three pressure gages collected pressure and temperature data. Each buoy was deployed with a GPS antenna in order to collect precise location and water level data. The HydroLite assembly includes an integrated GPS antennae and fathometer to measure near shore bathymetry. Bathymetric measurements were taken at all three beaches. On 17, 20, and 24 April 2014, the water level buoys were serviced, which included downloading data and changing batteries. The buoy and bottom-mounted pressure gages were recovered on the 25 April 2014.

Figure 5-15. RHIB with Water Level Buoy on the Bow during battery change over.

5.6 Bathymetry Survey

The HydroLite™ measures water-depth data from an Ohmex SonarMite BT shallow-water echo sounder (the BT means the SonarMite is equipped with Bluetooth connectivity) (see Figure 5-16). The HydroLite has been designed to survey depths that range from 0.3 m to 75 m. Unlike fish-finders that use wide beams and average-water-depth data, the SonarMite uses a narrow beam to provide independent “6 Hz pings” that define the water bottom in greater detail.

The specially designed transducer and specialized software that includes filtering helps to overcome error sources such as pitch and roll. Mapping-grade horizontal positions are provided by the Trimble GPS. The data logger used was the Trimble Recon, which ran the Pocket PC version of the SonarMite Program from Ohmex. Bluetooth technology provides connectivity between the transducer and GPS. The GPS and sounding data were downloaded to a laptop located at Camp Mujuk at the end of each survey day.

Figure 5-16. Wireless HydroLite-TM™ used for Bathymetric Survey.

The GPS positioning antenna was mounted 61 cm above the transducer to keep the operator's body and boat structures from interfering with satellite reception. The mounting minimized turbulence generated around or in front of the transducer when moving. The transducer was mounted directly below the positioning antenna. The location was forward of propeller turbulence. The transducer was always submerged and did not touch the seafloor or any obstacles.

The speed of sound traveling through water is directly proportional to the density of the water. Therefore, primary parameters affecting density are

- Turbidity - the amount of suspended sediment.
- Salinity - The amount of dissolved salt in the seawater.
- Temperature - The temperature of the water sample.
- Pressure - Sum of water depth and barometric pressure.

The SonarMite default Speed of Sound in Water setting was used. Future post processing cold use the temperatures recorded by the water level gages. The default value was 1500 m/s, which is an average value for saltwater. The difference in sound velocity between warm fresh water and cold salt water is about +/-30 m/s, which represents a change of depth of +/-2%. This error can be compared to the very shallow water survey areas. For a depth of 10m an error in sound velocity could cause a difference up to 20cm.

Depths indicated on the Littoral Planning Charts for the study areas were referenced to Mean Sea Level (MSL). These are therefore the average depths to be expected under average conditions for purposes of amphibious planning. We therefore subtracted tide data from the HydroLite soundings to obtain depths reckoned to MSL.

Very shallow water bathymetric maps are included in Appendix K.

5.6.1 Water Level Collection

Water level fluctuations were recorded by two moored water level buoys, each containing a Trimble model R-8 kinematic GPS unit to record water level height above the ellipsoid (HAE) (see Figure 5-17). Data downloads were conducted every few days during boat operations (see Figure 5-18). The boat team also deployed three submerged HOBO U20 Titanium pressure gauges. All moored instruments were deployed on 14 April 2014 and collected on 25 April 2014. Gauges were placed 30 cm above the sea floor. Each gage was wire tied to a long rod that was fastened to a five and one half inch steel wheel rim that was used to anchor the assembly to the seafloor (see Figure 5-19). The water level gauges record pressure data that was corrected by subtracting atmospheric pressure changes that were measured by the meteorological station. MSL water levels above the ellipsoid are provided in Table 5-1. Tide predictions were collected for the month of April 2014 and may be viewed in Appendix L.

Figure 5-17. Water level buoy. Kinematic GPS unit being prepared in the black case mounted in the center.

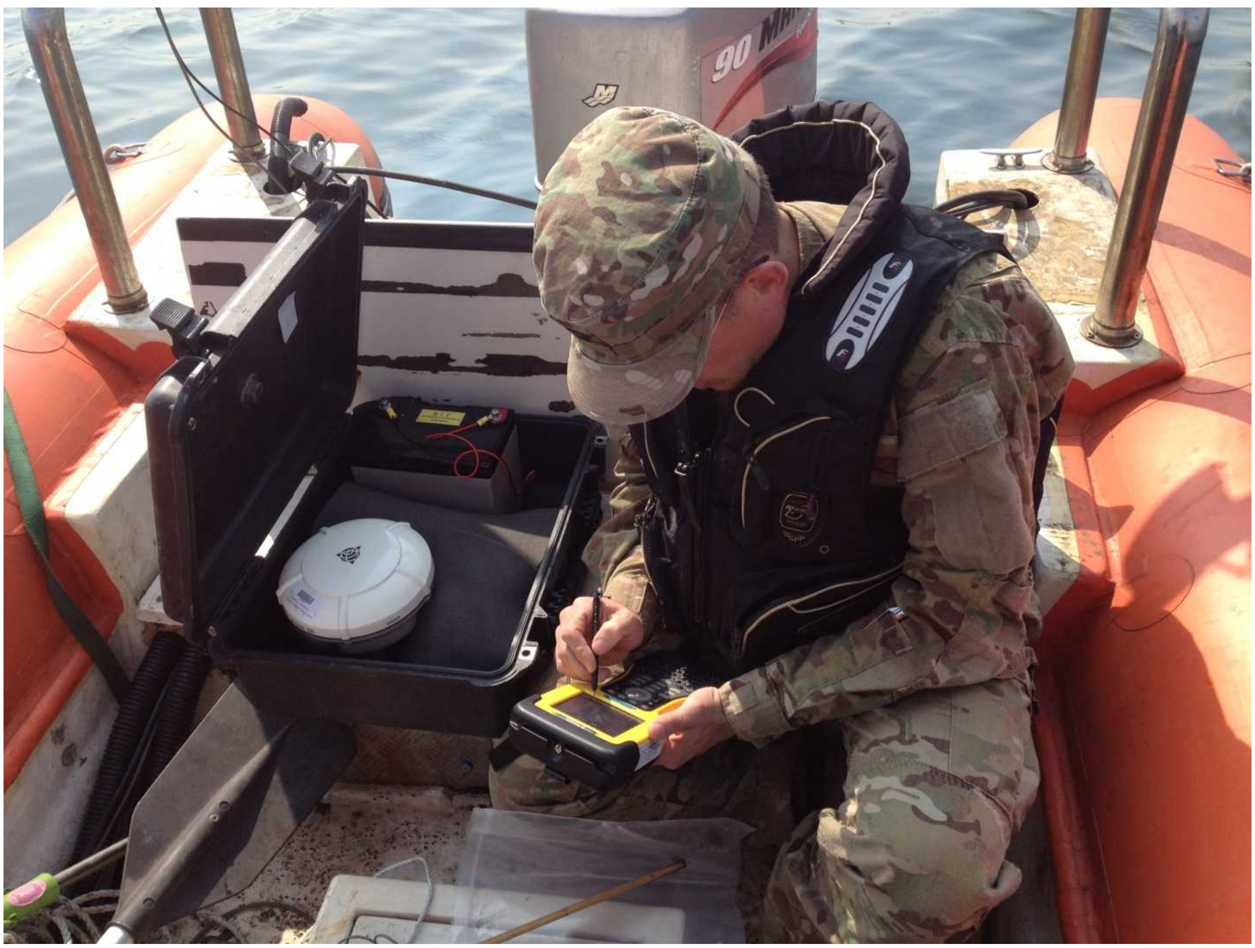

Figure 5-18. Data Download from Buoy Mounted GPS Unit.

Figure 5-19. Rims used to anchor water level gauges. Pressure gauges were fixed to the vertical rods to be 30 cm above the sea floor.

The buoy was constructed by RIT from a frame of PVC piping. The unit was located inside a watertight plastic container. Buoy water level time series can be used to tide synchronize the collected spectral imagery [28]. For example, it was determined from buoy data the WV2 image collected on 25 April 2014 is during high tide at 34cm above mean sea level. (See Appendix M for more information on water level buoy data).

The water loggers started recording data every thirty seconds on 14 April 2014 at 0700 and ended on 21 April 2014. Temperature from the sensors and salinity records from Park (2009) were used to process this data (Additional information and graphs of the water level data are provided in Appendix N).

6.0 Geodatabase for Ssang Yong 2014

The main **Ssang Yong 2014 Geodatabase** directory (Figure 6-1) includes the Environment Systems Research Institute's (ESRI) folder with the .gdb extension. Other important project information outside the file geodatabase and depicted in Figure 6-1 is the Excel Workbook (Data.xlsx), and an ESRI ArcMap document with filename SsangYong2014.mxd.

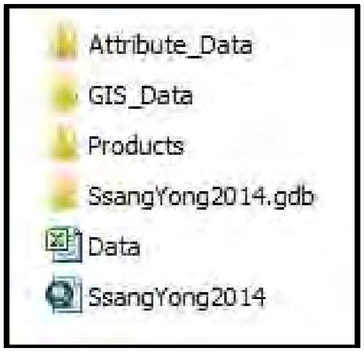

Figure 6-1. Schematic of the directory, Ssang Yong 2014 Geodatabase.

Links have been created within the map document and will be broken if certain files or folders are moved from their current location. It is suggested that files and folders be copied then created in a new working location with the originals left in their current directories, unless the links are understood and remade after displacement. Current links are within the Attribute_Data\Photographs directory, Products\Data_Report directory, and with the Data Excel Workbook. The links are used within the map document for ease of access within the ArcMap interface. ArcMap and ArcCatalog are part of ESRI's ArcGIS suite and were used to create, edit, and analyze files within the geodatabase. ArcMap was used to create the map document.

The first three sub-directories (Attribute_Data, GIS_Data, and Products) each contain original data such as photos, map documents, TINs, and the data report. The Attribute_Data sub-directory contains all data collected for the experiment. This includes sensor data collected on the ground, information found online, satellite imagery, notes, and data processed after the experiment. Geographic coordinate data that were not able to be placed into the file geodatabase but are linked and viewed within the map document along with other map documents can be found within the GIS_Data sub-directory. The data report and any images created are in the Products sub-directory. The Data.xlsx Excel Workbook holds all processed data from the field. For a more detailed look into the contents of the geodatabase and user instructions see Appendix O.

An ArcGIS map document was created to view all data that were linked to coordinates and placed into the project geodatabase. For user guidelines to maneuver around the geodatabase see Appendix P.

More than 2000 handheld photographs were taken during the SY'14 field experiment. Many (e.g. Figure 6-2, which was taken at Hwajin-ri beach) were stamped with GPS coordinates (e.g., 36º 14' 58.119N Latitude, 129º 22' 32.7 East Longitude) in the properties section of each image. Most importantly, for specific images at sites where geotechnical data and spectra were collected see Appendix Q. These photos document instrument orientations and complement stored metadata. Some of the images may be used to make a panoramic image of the landing beaches or as a base where other data layers may be displayed (e.g. LiDAR or bathymetric data). Many of these photographs have been used in other progress and project reports. All photographs were placed in the directory Ssang Yong 2014\Attribute_Data\Photographs and geotagged photographs can be found within the map document when opened with ArcMap.

Ninety seven exercise photographs were downloaded from the Defense Video and Imagery Distribution System (see www.dvidshub.net) for Exercise Ssang Yong 2014. Some of these representative photographs were also stored in the Ssang Yong Geodatabase (Ssang Yong 2014\Attribute_Data\Miscellaneous\SY'14_Exercise_Photos_dvidshub.net). Selected images highlight beach features and trafficability conditions for amphibious craft and vehicles that were launched from the sea, navigated through very shallow water regions, breached the surf zone, and maneuvered to inland landing force objectives (see Figure 6-3).

Figure 6-2. Photo with GPS coordinates attached

Figure 6-3. Left: Dogu Beach. Right: Doksuk-ri Beach. Both during Ssang Yong 2014.

7.0 Trafficability Products

In this section, some results of the applying the HITT (Hyper-spectral Imagery Trafficability Tool, [10]) to WV2 multi-spectral data are given. This tool can be used in correlations with any of the several geotechnical parameters describing soil strength, as relevant to trafficability estimates. Most commonly, the soil subgrade modulus has been used as a parameter of choice, as determined by the LWD. This is due to the fact that the accumulated spectral-to-geotechnical correlation tables are richest for this parameter – encompassing larger datasets related to more coast types and coastal sediment types. The richness of these empirical datasets improves the overall predictions of sediment geotechnical properties across the HSI/MSI imagery. Alternatively, other relevant measures of soil strength, e.g. the Cone Index (CI) can also be processed using HITT. These databases are somewhat smaller in size (and coast/sediment type coverage) but may be more directly applicable for end-users in direct interpretation and amphibious mission planning.

Several examples of the products are shown in the figures below. The products are displayed as surficial Cone Index values, with masking of those areas that are either open water, or other features that failed to produce a reasonable spectral match within the set spectral distance parameter.

Hwajin-ri Beach:

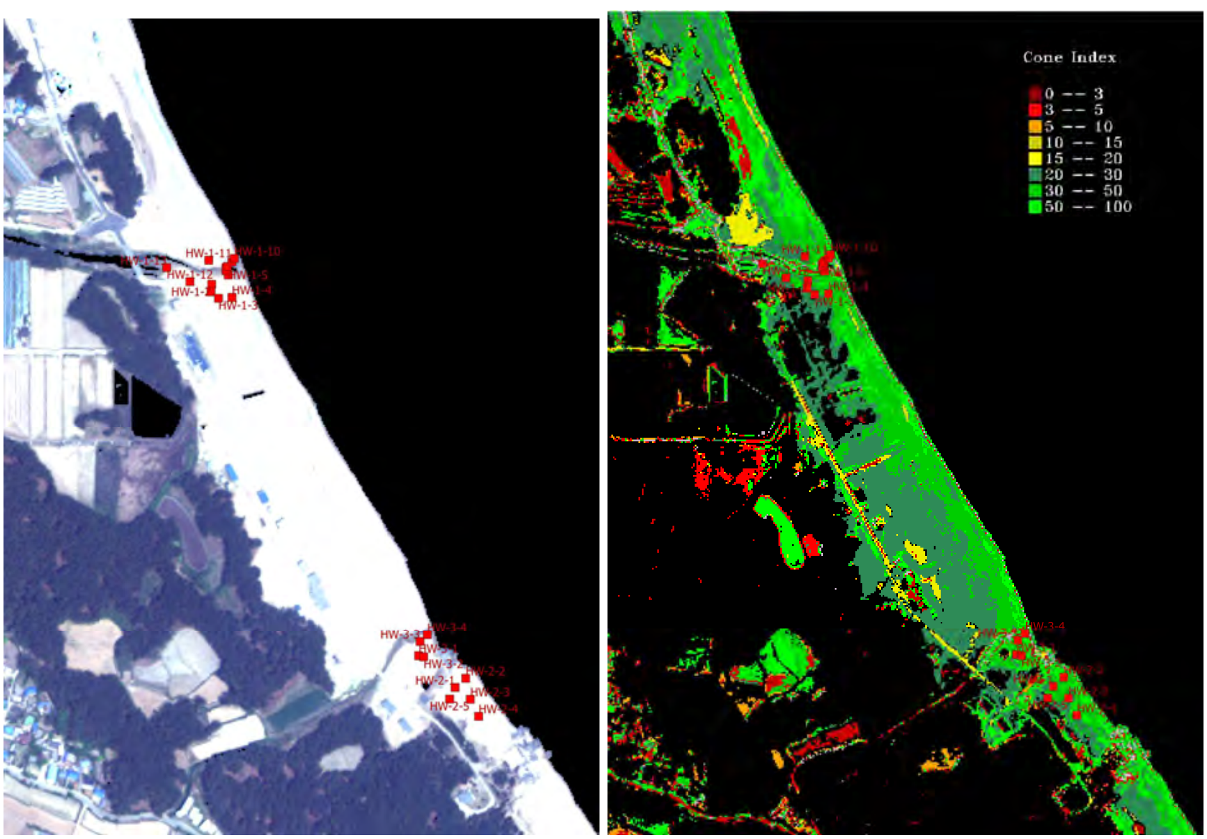

Figure 7-1 Hwajin-ri beach. WV2 Multi-spectral image (shown as RGB) taken on April 25, 2014 on left with locations of ground sampling stations occupied during the ground campaign. Right – HITT calculated best match for surface Cone Index values.

Doksuk-ri beach

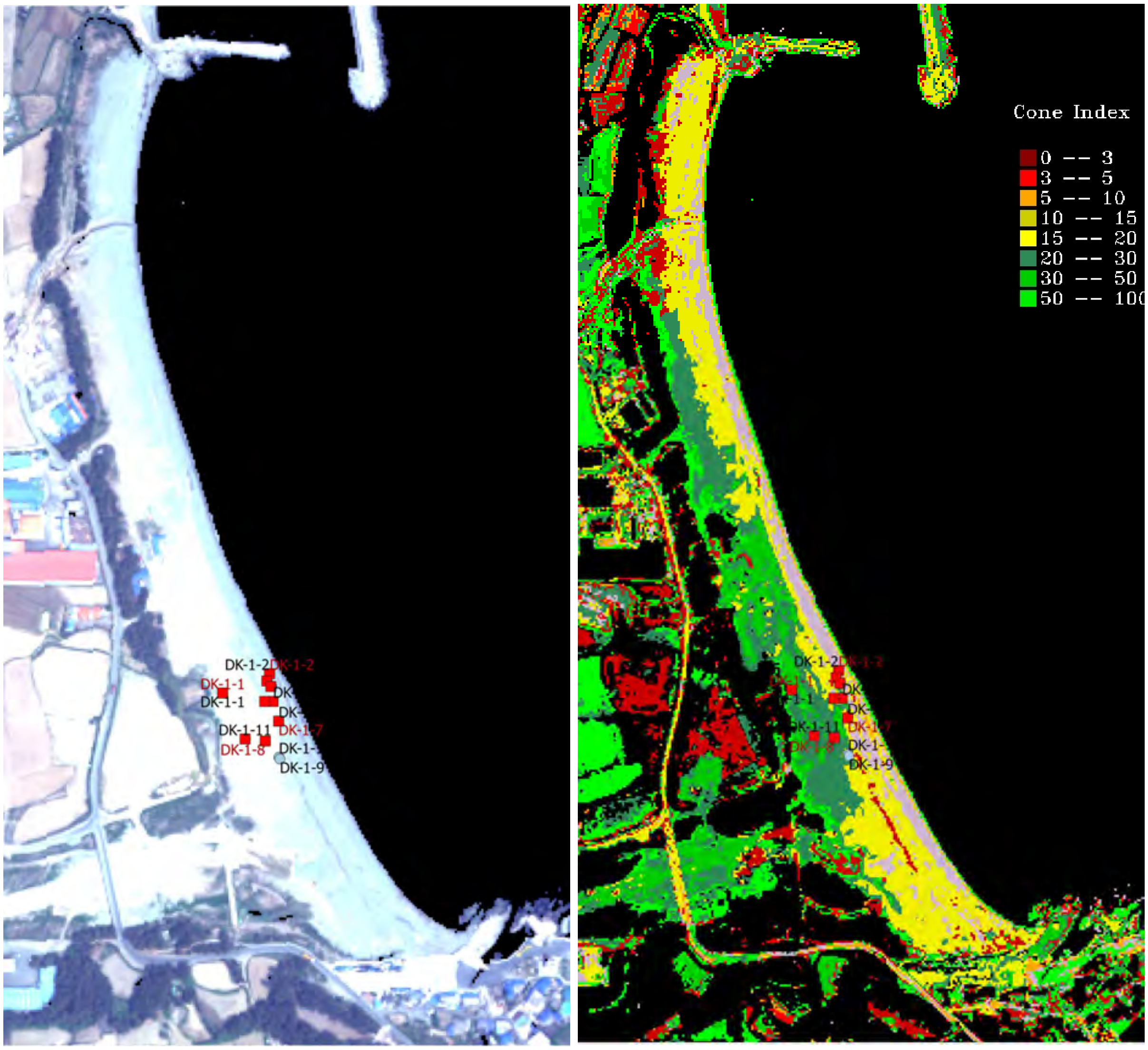

Figure 7-2 Doksuk-ri beach. WV2 Multi-spectral image (shown as RGB) taken on April 25, 2014 on left with locations of ground sampling stations occupied during the ground campaign. Right – HITT calculated best match for surface Cone Index values. Areas of no spectral match are indicated in grey (near the water line)

Dogu Beach:

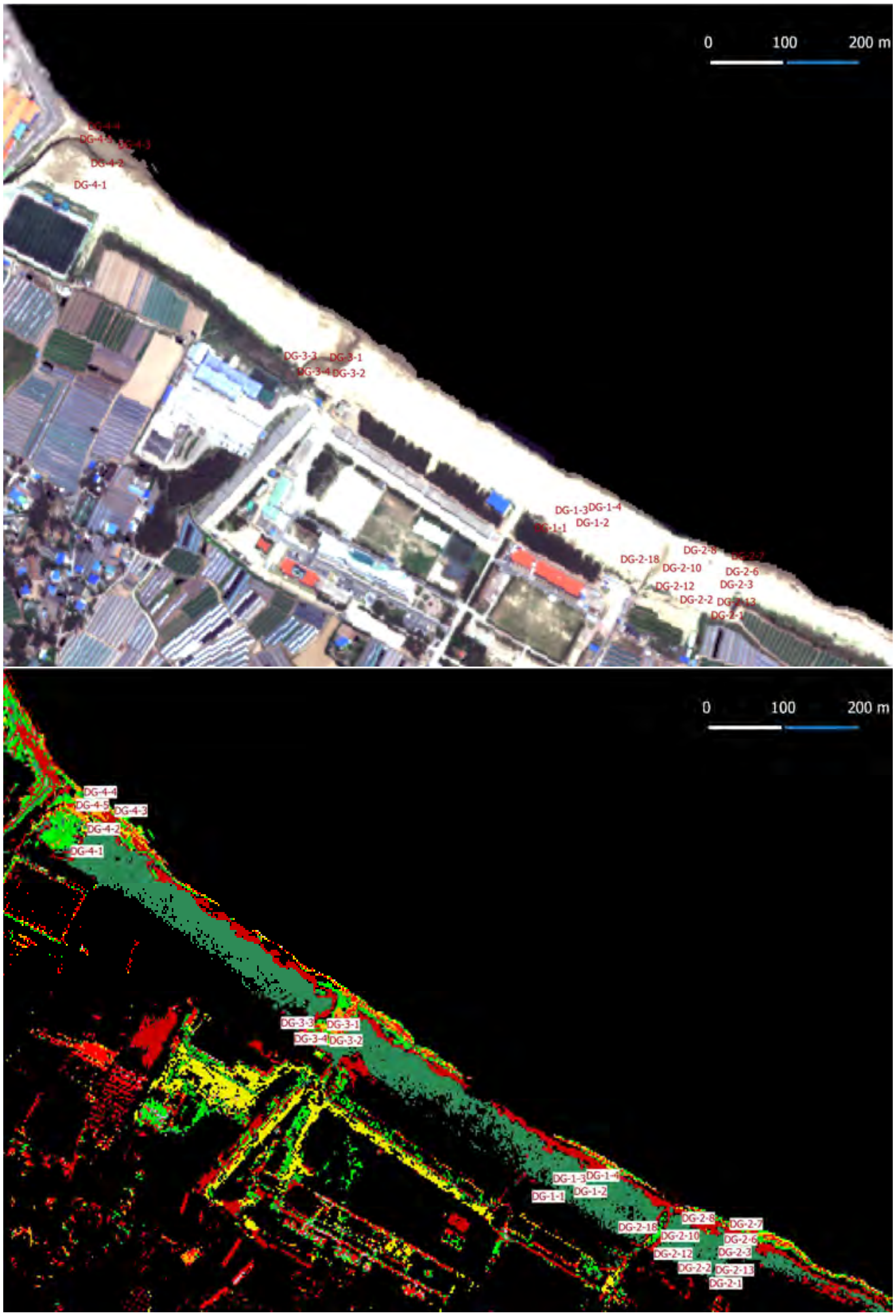

Figure 7-3 Dogu beach. WV2 Multi-spectral image (shown as RGB) taken on May 9, 2014 (top) with locations of ground sampling stations occupied during the ground campaign. HITT calculated best match for surface Cone Index values (bottom).

8.0 Acknowledgements

This remote sensing experiment would not have been possible without support from the Office of Naval Research. Various administrative and logistics personnel from ONR, RIT, MIRC, and the NRL completed time-critical tasks that were instrumental in project success. Their efforts contributed to the collection of high quality data from the east coast of the Republic of Korea. The National Geospatial-Intelligence Agency was very responsive in providing commercial imagery without which the project would not have been successful. Special thanks go to III MEF Science Advisor Katherine Mangum who supported this project from its inception, and to the staff at Camp Mujuk who provided critical lab space and materials while the field team was on site.

9.0 References

[1] Bachmann, C. M., C. R. Nichols, M. J. Montes, R. Li, P. K. Woodward, R. A. Fusina, W. Chen, V. Mishra, W. Kim, J. Monty, K. McIlhany, K. Kessler, D. Korwan, D. Miller, E. Bennert, G. Smith, D. Gillis, J. Sellars, C. Parrish, A. Weidemann, W. Goode, A. Schwarzschild, and B. Truitt, 2009. "Airborne Remote Sensing of Trafficability in the Coastal Zone," NRL Review, Washington, D.C.: Naval Research Laboratory, pages 223-228, http://www.dtic.mil/dtic/tr/fulltext/u2/a525045.pdf.

[2] Bachmann, C. M., C. R. Nichols, M. Montes, R. Li, P. Woodward, R. A. Fusina, W. Chen, V. Mishra, W. Kim, J. Monty, K. McIlhany, K. Kessler, D. Korwan, D. Miller, E. Bennert, G. Smith, D. Gillis, J. Sellers, C. Parrish, A. Schwarzschild, B. Truitt, 2010. "Retrieval of Substrate Bearing Strength from Hyperspectral Imagery During the Virginia Coast Reserve (VCR '07) Multi-Sensor Campaign," *Marine Geodesy, 33(2-3): 101-116,* doi: 10.1080/01490419.2010.492278.

[3] Bachmann, C. M., M. J. Montes, R. A. Fusina, C. Parrish, J. Sellars, A. Weidemann, W. Goode, C. R. Nichols, P. Woodward, K. McIlhany, V. Hill, R. Zimmerman, D. Korwan, B Truitt, A. Schwarzschild, "Bathymetry Retrieval from Hyperspectral Imagery in the Very Shallow Water Limit: a Case Study from the 2007 Virginia Coast Reserve (VCR '07) Multi-sensor Campaign," 2010. *Marine Geodesy, 33:53-75,* doi: 10.1080/01490410903534333

[4] Bachmann, C. M., R. A. Fusina, M. J. Montes, et al, 2012. "Virginia Coast Reserve 2007 Remote Sensing Experiment," NRL Memorandum Report, NRL/MR/7230—12-9402, March 9, 2012, 169 pages, http://www.dtic.mil/docs/citations/ADA559955.

[5] Bachmann, C. M., R. A. Fusina, M. J. Montes, R. Li, C. R. Nichols, J. C. Fry, E. Hallenborg, C. E. Parrish, and J. Sellars. 2012a. "Hawaii-Hyperspectral Airborne Remote Sensing (HIHARES) Experiment," NRL Memorandum Report, NRL/MR/7230—12-9403, Washington, D.C.: Naval Research Laboratory, 117 pages, http://www.dtic.mil/dtic/tr/fulltext/u2/a559833.pdf.

[6] Fusina, R. A, J. C. Fry, C. R. Nichols, C. M. Bachmann, R. Li, J. Sellars, C. Parrish, M. J. Montes, C. Gross, S. A. White, K. Lee, and C. A. Jones, Geodatabase Development to Support

Hyperspectral Imagery Exploitation. In Proceedings of the IEEE International Geoscience & Remote Sensing Symposium, Honolulu, Hawaii, July 25-30, 2010e,

[7] Bachmann, C. M., R. A. Fusina, M. J. Montes, R. Li, C. Gross, J. C. Fry, C. R. Nichols, D. F. Ezrine, W. D. Miller, C. Jones, K. Lee, J. Wende and C. McConnon, 2012c. “Mariana Islands–Hyperspectral Airborne Remote Environmental Sensing Experiment 2010,” NRL Memorandum Report NRL/MR/7230—12-9405, Washington, D.C.: Naval Research Laboratory, 487 pages, http://www.dtic.mil/docs/citations/ADA559525.

[8] Bachmann, C. M., R. A. Fusina, M. J. Montes, R. Li, C. Gross, C. R. Nichols, J. C. Fry, C. Parrish, J. Sellars, S. White, C. Jones, and K. Lee, 2012b. “Talisman-Saber 2009 Remote Sensing Experiment,” NRL Memorandum Report NRL/MR/7230—9404, Washington, D.C.: Naval Research Laboratory, 173 pages, http://www.dtic.mil/docs/citations/ADA559586.

[9] Bachmann, C. M., R. J. Hughes, A. Abelev, E. van Roggen, C. R. Nichols, G. Mattis, R. A. Fusina, R.-R. Li, K. Z. Doctor, M. J. Montes, W. Philpot, D. Gray, S. Carr, S. Kharabash, A. Brady, G. Smith, J. Gardner, D. Korwan, W. D. Miller, C. Snow, M. Vermillion, G. rick, Z. Peterson, R. Winter, J. Vrbanich, J. Eggleton, G. Mason, B. Gates, A. Hammond, J. Junek, K. Burel, G. Christie, (in pre-publication review). “Tools for Hyperspectral Exploitation from Multi-Angular Spectra (THEMAS): May 2012 and June 2013 Experiments,” NRL Memorandum Report, in pre-publication review.

[10] Bachmann, C. M., M. J. Montes, R. A. Fusina, 2012. “NRL Hyperspectral Imagery Trafficability Tool (HITT): Software and Spectral-Geotechnical Look-up Tables for Estimation and Mapping of Soil Bearing Strength from Hyperspectral Imagery,” NRL Memorandum Report, NRL/MR/7230—12-9365, September 28, 2012, 51 pages, available online: http://www.dtic.mil/docs/citations/ADA569187.

[11] Bachmann, C. M., C. R. Nichols, M. J. Montes, R. A. Fusina, J. C. Fry, R. Li, D. Gray, D. Korwan, C. Parrish, J. Sellars, S. A. White, J. Woolard, K. Lee, C. McConnon, and J. Wende, 2010c. Coastal Characterization from Hyperspectral Imagery, In Optical Remote Sensing of the Environment, OSA Technical Digest (CD) (Optical Society of America, 2010), paper OMD2, pp. 138-141.

[12] Bachmann, C. M., C. R. Nichols, M. J. Montes, R. A. Fusina, R.-R. Li, C. Gross, J. Fry, C. Parrish, J. Sellars, S. A. White, C. A. Jones, K. Lee, “Coastal Characterization from Hyperspectral Imagery: An Intercomparison of Retrieval Properties from Three Coast Types,” Proc. IGARSS 2010, Honolulu, HI, pp. 138-141.

[13] Nichols, C.R., P.T. Brennan, S.J. Cento, K.R. Dedrick, and G.H. Tuell. Adapting an Enhanced Multiple Database Integration and Update Capability to Support Coastal Operations, in Proceedings of the MTS/IEEE Oceans 2001 Annual Conference, Honolulu, HI, November 2001, 9 pp.

[14] Nichols, C.R., D. Lamb, T. Donato, and X.-H. Yan, 2004. Oceanographic Information Collection and Data Availability for the Han River Estuary, NRL Memorandum Report, NRL/MR/7205—04-8837, Naval Research Laboratory, Washington, D.C.

[15] Chikamori, H., L. Heng and T. Daniell, (ed.) 2012. Catalogue of Rivers for Southeast Asia and the Pacific. Volume VI, UNESCO Jakarta Office, Available online. URL: http://flood.dpri.kyoto-u.ac.jp/ihp_rsc/riverCatalogue/. Accessed on April 4, 2014.

[16] MCIA, Generic Intelligence Requirements Handbook, Quantico, VA: Marine Corps Intelligence Activity, 1995.

[17] NGA, (Enroute) Sailing Directions, Coasts of Korea and China, Pub 157, Springfield, VA: National Geospatial-Intelligence Agency

[18] Pohang Climate. Korea Meteorological Administration. Accessed on 11Jun14. http://www.kma.go.kr/weather/climate/average_30years.jsp?yy_st=2011&stn=138&norm=M&obs=0&x=21&y=10

[19] Library of Congress Federal Research Division, South Korea: A Country Study (Area Handbook Series), 4th Edition, Washington, DC: United States Government Printing, 1992. Available online. URL: http://lcweb2.loc.gov/frd/cs/krtoc.html. Accessed on April 2, 2014.

[20] Bird, E. C. F., Schwartz, Maurice L, 1985. “The World’s Coastline”, Van Nostrand Reinhold Company Inc. ISBN 0-442-21116-3. 833-836.

[21] Khim, Seong Jong, Villeneuve, Daniel L., et al. 2005. “Dioxin-like and Estrogenic Compounds and Activities Associated with Marine Sediment from Yeongil Bay, Korea.”

[22] Digital Globe Inc. 2014. Digital Globe. [ONLINE] Available at: http://www.digitalglobe.com/ [Accessed 05 June 14]

[23] Updike & Comp, 2010. Radiometric Use of World-View-2 Imagery. https://www.digitalglobe.com/sites/default/files/Radiometric_Use_of_WorldView-2_Imagery%20%281%29.pdf

[24] Bachmann, C. M., D. Gray, A. Abelev, W. Philpot, et al, 2012, “Linking goniometer measurements to hyperspectral and multi-sensor imagery for retrieval of beach properties and coastal characterization,” Proc. Of SPIE, Vol. 8390, pages 83901D-1 – 82901D-9, April 2012.

[25] Bachmann, C. M., A. Abelev, W. Philpot, K. Z. Doctor, M. J. Montes, R. Fusina, Rong-Rong Li, E. van Roggen, 2014. “Retrieval of Sand Density from Hyperspectral BRDF,” Proc. Of SPIE, Vol 9088, http://dx.doi.org/10.1117/12.2050682.

[26] Bachmann, C. M., M. J. Montes, C. Parrish, R. A. Fusina, C. R. Nichols, R-R. Li, E. Hallenborg, C. A. Jones, K. Lee, J. Sellars, S. A. White, J. C. Fry, submitted. “A dual-

spectrometer approach to reflectance measurements under sub---optimal sky conditions," *Optics Express*, Vol. 20, No. 8, pp. 8959---8973, April 9, 2012d, doi: 10.1364/OE.20.008959.

[27] van Roggen, E. M. and C. R. Nichols, Beach Profile Changes at Freshwater Beach in Queensland, Australia, in Nichols, C. R. and R. G. Williams (Eds.). 2013. Proceedings of Ocean Waves Workshop. New Orleans, LA: University of New Orleans. Available online. URL: http://scholarworks.uno.edu/oceanwaves/2013.

[28] Bachmann, C. M., C. R. Nichols, and J. D. Sellars, Field Expedient Water Level Measurements to Support the Exploitation of Hyperspectral Imagery, in Nichols, C. R. and R. G. Williams (Eds.). 2011. Proceedings of Ocean Waves Workshop. New Orleans, LA: University of New Orleans. Available online.
URL: http://scholarworks.uno.edu/oceanwaves/2011/Session3/5/3.

[29] Bachmann, Charles M., William Philpot, Andrei Abelev, and Dan Korwan. (2014) "Phase Angle Dependence of Sand Density Observable in Hyperspectral Reflectance." Remote Sensing of Environment 150 (July): 53–65. doi:10.1016/j.rse.2014.03.024.

APPENDIX A

Glossary

Introduction

This Data Report contains several terms whose meanings are critical for follow-on investigations or for amphibious planning. These terms are listed below to ensure that the meanings are easily related to the development of imagery-derived amphibious planning tools.

Accuracy –The degree of conformity of a measure to a standard or true value.

All-Source Intelligence – Intelligence products and/or organizations and activities that incorporate all sources of information, including, most frequently, human resources intelligence, imagery intelligence, measurement and signature intelligence, signals intelligence, and open source data, in the production of finished intelligence. (see Joint Publication 1-02)

Alongshore – Parallel to and near the shoreline; longshore

Bathymetry – The measurement of water depths in oceans, seas, and lakes; also information derived from such measurements.

Beach – The zone of unconsolidated material that extends landward from the low water line to the place where there is marked change in material or physiographic form, or to the line of permanent vegetation (usually the effective limit of storm waves). The seaward limit of a beach--unless otherwise specified--is the mean low water line.

Beach Profile – A cross section of elevations from the dune or sea wall and extending across the foreshore and into the nearshore. The shape of the beach profile determines how the coast responds to storms, the manner in which waves break as surf, and what part of the beach is useable for landing craft.

Clay – A fine grained, plastic, sediment with a typical grain size less than 0.004 mm.

Data Record - A data record is one or more messages that form a coherent, logical, and complete observation.

Dissemination - The timely distribution of information and/or intelligence in the most suitable form to those who need it.

Dobson Unit - A Dobson unit is a unit of measurement for a trace gas in the atmosphere widely used for ozone.

Engineer Reconnaissance - The gathering of specific, detailed, technical information required by supporting engineer forces in order to prepare for and accomplish assigned missions.

Foreshore - The beach face, the portion of the shore extending from the low-water line up to the limit of wave uprush at high tide.

Geospatial Intelligence (GEOINT) - Intelligence derived from the exploitation and analysis of imagery and geospatial information that describes, assesses, and visually depicts physical features and geographically referenced activities on the Earth.

Geographic Information System (GIS) **–** A system of spatially referenced information, including software to acquire, store, manipulate, analyze, and display spatial data. This remote sensing experiment included the collection of map extracts, images, time series data, spectra, and qualitative data.

Goniometer – An instrument used for measuring geometric angles.

Gradient - A measure of slope in meters of rise or fall per meter of horizontal distance.

Grain Size Analysis - The process of determining grain-size distribution (see ASTM D 653).

Headland – A land mass having a considerable elevation. The rugged east coast of South Korea faces the East Sea. Sandy beaches are located between the headlands.

Hinterland - The region lying inland from the coast

Inshore Area - The water area adjacent to a land mass in which the proximity and contour of the bottom or the nearby coastline influence and limit the effectiveness of deep-water assets and systems. This area normally extends seaward to a fixed distance established by the area commander as necessary to protect assets located in ports, harbors, approaches, amphibious objective areas, choke points, straits, and roadsteads from surface and subsurface threats.

Kuroshio Current - The Kuroshio (Black Stream) begins where the North Equatorial Current approaches the Philippines and continues northward east of Taiwan. It then crosses a ridge between Kyushu and the Okinawa Islands and forms the East China Sea meander, and proceeds through the Tokara Strait, after which it takes a sharp turn to the north. The Kuroshio turns east and separates from the coast at about 35ºN. The Kuroshio Current is part of the overall wind-driven subtropical gyre circulation cell that exists in the North Pacific.

Littoral - In naval operations, that portion of the world's land masses adjacent to the oceans within direct control of and vulnerable to the striking power of sea-based forces.

Liquifaction - The process of transforming any solid from a solid state to a liquid state, usually as a result of increased pore pressure and reduced shearing resistance (see ASTM D 653).

Longshore Current - A current located in the surf zone, moving generally parallel to the shoreline, generated by waves that are approaching at an angle with the shoreline.

Macro-Tidal – Tidal ranges greater than 4 m.

Mean Sea Level (MSL) - The average height of the surface of the sea for all stages of the tide; used as a reference for elevations.

Meso-Tidal - Tidal range between 2 m and 4 m.

Micro-Tidal – Tidal range less than 2 m.

Mud - A fluid-to-plastic mixture of finely divided particles of solid material and water.

Nearshore - The zone which extends from the swash zone to the position marking the start of the offshore zone, typically at water depths of the order of 20 m.

Particle Size - In dealing with sediments and sedimentary rocks it is necessary to apply precise dimensions to terms such as clay, sand, pebble, cobble, etc.

Pebbles - Beach material usually well-rounded and between about 4 mm to 64 mm diameter

Permeability - The property of bulk materials such as sand which permit the movement of water through its pores or interstitial spaces.

Photomosaic - An assemblage of photographs, each of which shows part of a region, put together in such a way that each point in the region appears once and only once in the assemblage, and scale variation is minimized.

Quality Assurance (QA) - A planned and systematic pattern of all actions necessary to provide confidence that adequate technical requirements are established, that products and services conform to those requirements, and that satisfactory performance is achieved.

Quality Control (QC) - QC involves follow-on steps that support the delivery of high quality data and requires both automation and human intervention.

Real Time - Real time means that: data are delivered without delay for immediate use; time series extends only backwards in time, where the next data points are not available; and there may be delays ranging from a few seconds to a few hours or even days, depending upon the variable.

Revetment - A facing of stone, concrete, etc., to protect an embankment, or shore structure, against erosion by wave action or currents. Along the East Coast of South Korea there were many revetments, including the retaining wall found Hwanji-ri beach.

Riprap – Armor stones used for revetment, toe protection for bluffs, or structures exposed to wave action.

Run-Up – The rush of water up a structure or beach on the breaking of a wave.

Sand - Sediment particles, often largely composed of quartz, with a diameter of between 0.062 mm and 2 mm, generally classified as fine, medium, coarse or very coarse. Beach sand may sometimes be composed of organic sediments such as calcareous reef debris or shell fragments.

Sediment - Particles derived from rocks or biological materials that have been transported by a fluid.

Silt - Sediment particles with a grain size between 0.004 mm and 0.062 mm, i.e. coarser than clay particles but finer than sand (See ASTM D 653).

Situational Awareness (SA) - Knowledge and understanding of the current situation that promote timely, relevant, and accurate assessment of friendly, enemy, and other operations within the battlespace in order to facilitate decisionmaking. An informational perspective and skill that fosters an ability to determine quickly the context and relevance of events that are unfolding.

Slope - The degree of inclination to the horizontal. Usually slope is expressed as a ratio (e.g., 1:25, which indicates one unit rise in 25 units of horizontal distance). It may also be represented as a decimal fraction (e.g., 0.04).

Soil - A layer of weathered, unconsolidated material on top of bed rock; often also defined as containing organic matter and being capable of supporting plant growth.

Tide Tables – Tables which give daily predictions of the times and heights of the tide. These predictions are usually supplemented by tidal differences and constants by means of which additional predictions can be obtained for numerous other places.

Trafficability - The ability of the terrain to support the movement of vehicles and people.

Wetlands - Lands whose saturation with water is the dominant factor determining the nature of soild development and the types of plant and animal communities that live in the soil and on its surface.

APPENDIX B

Annotated Bibliography

Introduction

Relevant information that supports the development of planning products for Exercise Ssang Yong 2014 can be found in the following print and non-print resources. With each citation there are descriptive and evaluative comments that describe the utility of this material to the development of amphibious planning products from historical information, *in-situ* data, imagery, and numerical model output. Annotations provide future researchers or amphibious planners with the relevance of the resources, many of which resulted in foundational information for this remote sensing experiment.

Print Resources

Bachmann, C. M., C. R. Nichols, M.J. Montes, R.-R. Li, P.K. Woodward, R.A. Fusina, W. Chen, V. Mishra, W. Kim, J. Monty, K. McIlhany, K. Kessler, D. Korwan, D. Miller, E. Bennert, G. Smith, D. Gillis, J. Sellars, C. Parrish, A. Weidemann, W. Goode, A. Schwarzschild, and B. Truitt, 2009, Airborne Remote Sensing of Trafficability in the Coastal Zone. NRL Review, Washington, D.C.: Naval Research Laboratory, pages 223-228.

A summary article describing Office of Naval Research and National Geospatial-Intelligence Agency sponsored research at the Virginia Coast Reserve describing preliminary efforts to derive bathymetric retrievals and trafficability maps from hyperspectral imaging along a barrier island coast.

Bachmann, C.M., M.J. Montes, R.A. Fusina, C. Parrish, J. Sellars, A. Weidemann, W. Goode, C.R. Nichols, P. Woodward, K. McIlhany, V. Hill, R. Zimmerman, D. Korwan, B. Truitt, and A. Schwarzschild, 2010, Bathymetry Retrieval from Hyperspectral Imagery in the Very Shallow Water Limit: A Case Study from the 2007 Virginia Coast Reserve (VCR'07) Multi-Sensor Campaign, Marine Geodesy, Volume 33, Issue 1, pages 53 – 75.

A well reviewed and frequently cited refereed journal article describing a validated approach to extracting bathymetric information from hyperspectral imagery. Discussions focus on a scientific model that uses near infra-red (NIR) reflectance to retrieve bathymetry in very shallow water.

Bachmann, Charles M.; C. Reid Nichols; Marcos J. Montes; Rong-Rong Li; Patrick Woodward; Robert A. Fusina; Wei Chen; Vimal Mishra; Wonkook Kim; James Monty; Kevin Mcilhany; Ken Kessler; Daniel Korwan; W. David Miller; Ellen Bennert; Geoff Smith; David Gillis; Jon Sellars; Christopher Parrish; Arthur Schwarzschild; Barry Truitt, 2010, Retrieval of Substrate Bearing Strength from Hyperspectral Imagery During the Virginia Coast Reserve (VCR'07) Multi-Sensor Campaign. Marine Geodesy. Volume 33, Issue 2-3, pp 101-116.

A well reviewed and frequently cited refereed journal article describing a method to use airborne hyperspectral imagery to derive trafficability maps with a spectral-geotechnical lookup table. A spectrum-matching and look-up-table methodology is commonly used to exploit spectral region imagery.

Bachmann, C. M., R.A. Fusina, M. J. Montes, R-R Li, C.R. Nichols, J.C. Fry, E. Hallenborg, C.E. Parrish, and J. Sellars. 2012, Hawaii-Hyperspectral Airborne Remote Sensing (HIHARES) Experiment. NRL Memorandum Report, NRL/MR/7230—12-9403, Washington, D.C.: Naval Research Laboratory.

This Naval Research Laboratory report describes data collected during the Hyperspectral Airborne Remote Environmental Sensing experiment which was conducted at Marine Corps Base Hawaii and Marine Corps Training Area—Bellows from January 21 to February 6, 2009. This report describes the collection, processing, and analysis of imagery from the HyVista Hyperspectral Mapper (HyMap™). Calibration and validation data were archived in a geodatabase that was used to help characterize coralline coastal features in the vicinity of Käne‘ohe Bay, which is sited on the west side of Mökapu Peninsula and a low-lying coastal terrace abutting the steep eastern side of the Ko‘olau Range. Data were used to assess trafficability along a variety of geologically different beaches. Examples included low lying narrow beaches, those associates with seawalls, ramps, and dredged channels, and some isolated beaches composed of rocky mud, small mangrove forests, and shallow deltas of sediments deposited from the nearby mountains.

Bachmann, C. M., R.A. Fusina, M.J. Montes, R-R Li, C. Gross, C.R. Nichols, J.C. Fry, C. Parrish, J. Sellars, S. White, C. Jones, and K. Lee, 2012. Talisman-Saber 2009 Remote Sensing Experiment, NRL Memorandum Report NRL/MR/7230—9404, Washington, D.C.: Naval Research Laboratory.

This Naval Research Laboratory report describes data collected at the Shoalwater Bay Training Area (SWBTA) located in Australia from May 18 to 29, 2009. It describes the collection, processing, and analysis of imagery from the HyVista Hyperspectral Mapper (HyMap™). Calibration and validation data were archived in a geodatabase that was used to help characterize mangrove coastal features common to the Capricorn coast of Queensland. Data were used to assess trafficability along beaches inside of Shoalwater Bay and beaches facing the Coral Sea. Bathymetric charts and trafficability maps were provided to military planners during Exercise Talisman-Saber 2009, which was conducted primarily in Australia and surrounding waters from July 13 to 16, 2009.

Bachmann, C.M., R.A. Fusina, M.J. Montes, R-R Li, C. Gross, J.C. Fry, C.R. Nichols, D.F. Ezrine, W.D. Miller, C. Jones, K. Lee, J. Wende and C. McConnon, 2012. Mariana Islands–Hyperspectral Airborne Remote Environmental Sensing Experiment 2010, NRL

Memorandum Report NRL/MR/7230—12-9405, Washington, D.C.: Naval Research Laboratory.

This Naval Research Laboratory report describes data collected in the Mariana Islands from February through March 2010. It describes the collection, processing, and analysis of imagery from the HyVista Hyperspectral Mapper (HyMap™). Models were developed to facilitate rapid processing of hyperspectral imagery (HSI), generating shallow water bathymetric charts and the production of trafficability maps. Research focused on spectral and geotechnical library development, bathymetry, and location of World War II remnant hazards on Pagan, Tinian, and Guam. Ground control data collected during the remote sensing experiment were provided to personnel assigned to Marine Corps Forces Pacific for use in building digital elevation models and maps for remote areas such as Pagan, a volcanic island in the Commonwealth of the Northern Mariana Islands. Surveyed calibration panels, World War II relics, and underwater panels were also used in developing anomaly detection algorithms. Several of the narrow beaches that were surveyed were actual landing beaches used by Marines during Operation Forager occurring between June and November, 1944.

Bird, E. C. F., Schwartz, Maurice L, 1985. "The World's Coastline", Van Nostrand Reinhold Company Inc. ISBN 0-442-21116-3.

This general reference was used to identify geographic and geological characteristics common to the southeast coast of the Republic of Korea. The locations and importance of rivers flowing from the Taebaek Mountains were discussed as well as Yeongil Bay. Geological information includes descriptions of cliffs, rocky shorelines, and sandy beaches with patches of cobbles and larger pebbles that come from the nearby hills and mountains.

MCIA, Generic Intelligence Requirements Handbook (GIRH), MCIA-1540-002-95, Quantico, VA: Marine Corps Intelligence Activity, 1995

This reference provides a listing of information requirements for amphibious operations. In particular are factors of interest for terrain and hydrographic analysis. Examples include port characteristics, transportation networks, beach composition, winds, visibility, waves, tides, currents, and astronomical data.

Electronic Resources

Chikamori, H., L. Heng, and T. Daniell, 2012. Catalogue of Rivers for Southeast Asia and the Pacific, Volume V1, UNESCO Jakarta Office, Available online, URL: http://flood.dpri.kyoto-u.ac.jp/ihp_rsc/riverCatalogue/, Accessed on July 14, 2014.

This catalog provides general hydrometeorological data that were gathered from various and often diverse sources. Of particular interest to this project was information on the Hyeongsan river which flows through the south-eastern part of Gyeongbuk province. The Dukdong Dam

located along this river is important to meeting agricultural water demand and municipal water supply for Gyeongju and Pohang.

CIA, The World Factbook 2013-14. Washington, DC: Central Intelligence Agency, 2013 . Available online. URL: https://www.cia.gov/library/publications/the-world-factbook/index.html. Accessed on June 6, 2014.

The World Factbook provides information on the history, people, government, economy, geography, communications, transportation, military, and transnational issues for 267 world entities. For South Korea, we found general geographic, climate, and maritime information for the Republic of Korea.

Korean Coast Guard. Available online. URL: http://www.kcg.go.kr/global/index.jsp. Accessed on June 6, 2014.

This web site provides information on Korean Coast Guard activities relevant to monitoring and surveillance of marine pollution and prevention of hazardous spills. A Coast Guard Station is located in Pohang.

Korea Hydrographic and Oceanographic Administrations (KHOA) Home Page, Available online. URL: http://www.khoa.go.kr/. Accessed on June 6, 2014

This website provide access to tide predictions and local meteorological and oceanographic data from the North-East Asian Regional Global Ocean Observing System (NEAR-GOOS). Available information included sea surface temperature, salinity, currents, waves, sea-level, dissolved oxygen, nutrients, and other hydrographic elements.

Korea Meteorological Administration. Available online. URL: http://web.kma.go.kr/eng/index.jsp, Accessed on June 6, 2014.

Climatic and weather information was obtained from the Korea Meteorological Administration (KMA). Information from this website is derived from approximately 100 weather stations including 10 radar, 4 upper-air observation stations, and Automatic Weather Stations (AWS). The below image and time series highlights the passage of a weather system that was moving offshore on April 20, 2014. Cloud cover from this weather system impacted the quality of WorldView-2 imagery collects scheduled for April 17th.

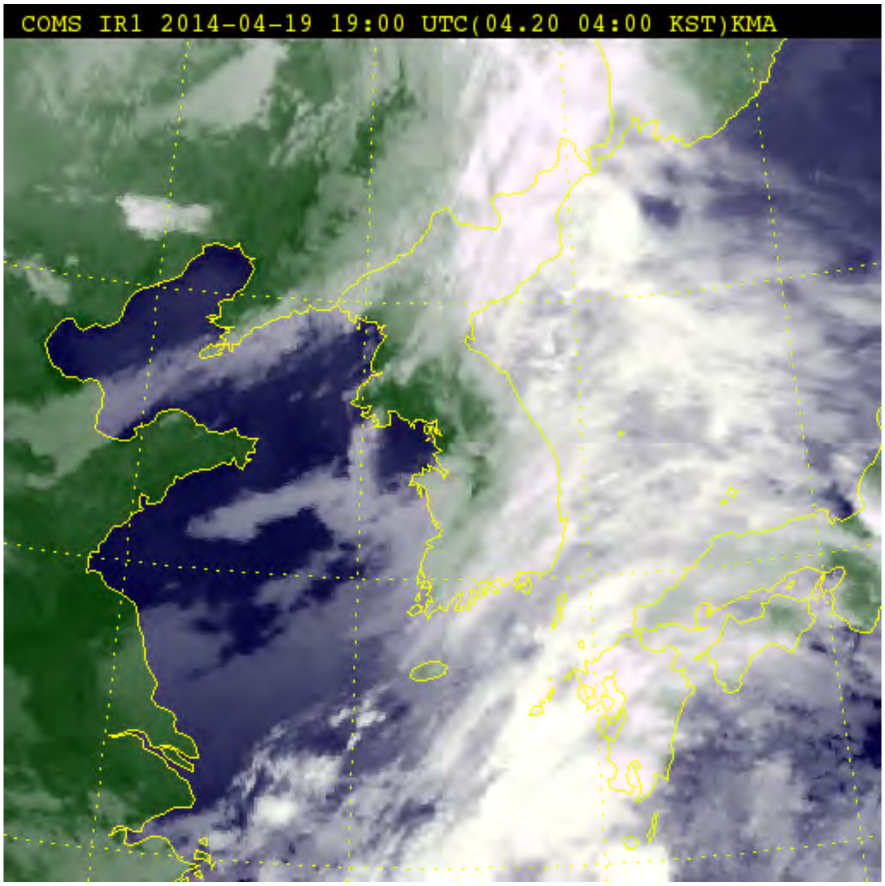

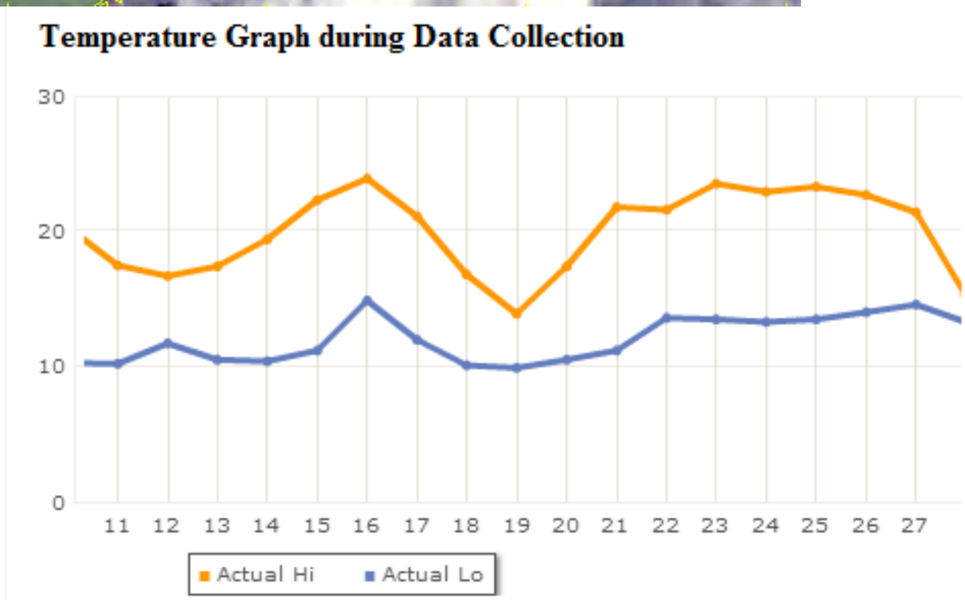

Figure C-1. Weather data from KMA. Top Panel. Imagery from COMS, the first multi-purpose geostationary satellite for Korea. This image shows passage of a cold front on April 20, 2014. Bottom Panel. Time series of air temperatures (ºC) for Pohang, South Korea during the experiment.

Library of Congress Federal Research Division, South Korea: A Country Study (Area Handbook Series), 4th Edition, Washington, DC: United States Government Printing, 1992. Available online. URL: http://lcweb2.loc.gov/frd/cs/krtoc.html. Accessed on April 2, 2014.

This Web site contains the online versions of books previously published (1988-98) in hard copy by the Federal Research Division of the Library of Congress under the Country Studies/Area Handbook Program sponsored by the U.S. Department of the Army. This country study presents a description and analysis of the historical setting and the social, economic, political, and national security systems and institutions of South Korea.

NGA, 2013a. Pacific Ocean and Southeast Asia, Sailing Directions (Planning Guide), Publication 120, 10th Edition, Springfield, VA: National Geospatial-Intelligence Agency, Available online, URL: http://msi.nga.mil/MSISiteContent/StaticFiles/NAV_PUBS/SD/Pub120/Pub120bk.pdf. Accessed on June 6, 2014.

Publication 120 included relevant physical, industrial, navigational and regulatory information about the greater Pohang area. Of particular importance was information on fishing nets located within the approaches to landing beaches, especially Doksukri and Hwajinri.

NGA, 2013b. Coasts of Korea and China, (Enroute) Sailing Directions, Pub. 157, Springfield, Virginia: National Geospatial-Intelligence Agency Available online. URL: http://msi.nga.mil/MSISiteContent/StaticFiles/NAV_PUBS/SD/Pub157/Pub157bk.pdf. Accessed on June 6, 2014.

Publication 157 provided detailed maritime approach information for Pohang to include information about the temperate climate, coastal weather, currents, tides and the names of relevant nautical charts.

NGA, 2014, World Port Index, Pub. 150. 23rd Edition, Springfield, VA: National Geospatial-Intelligence Agency. Available online. URL: http://msi.nga.mil/MSISiteContent/StaticFiles/NAV_PUBS/WPI/Pub150bk.pdf. Accessed on July 14, 2014

Publication 150 provides the locations and physical characteristics of, and the facilities and services offered by major ports and terminals world-wide (approximately 3700 entries), in a tabular format. Entries are organized geographically, in accordance with the diagrams located in the front of the publication. Pohang Port is Index Number 60410.

OMI Ozone Time Series Data. Global Monitoring Division, National Oceanic and Atmospheric Administration. Available Online. URL: http://www.esrl.noaa.gov/gmd/grad/neubrew/OmiDataTimeSeries.jsp. Accessed on June 6, 2014.

NOAA provides global ozone concentrations from the Ozone Monitoring Instrument at a spatial resolution of 36 x 48 km. Information is also provided on air quality components such as NO_2, SO_2, BrO, OClO, and aerosol characteristics.

Ozone and UV Monitoring, Environment Canada. Available online. URL: http://exp-studies.tor.ec.gc.ca/clf2/e/main.html. Accessed on May 7, 2014.

Maps and tables describing the ozone layer are provided by Environment Canada, Science and Technology Branch, Atmospheric Science and Technology Directorate, Air Quality Research Division. Maps of ozone concentrations are provided that merge ground-based measurements and specialized sensors on satellites, such as the Total Ozone Mapping Spectrometer (TOMS), the Stratospheric Aerosol and Gas Experiment and the Solar Backscatter Ultra Violet spectrometer. These data are of potential value for atmospheric correction of WorldView-2 imagery.

Padwick, Deskevich, Pacifici, & Smallwood, 2010. WorldView-2 pan-sharpening, American Society for Photogrammetry and Remote Sensing, Available online. URL: http://www.asprs.org/a/publications/proceedings/sandiego2010/sandiego10/Padwick.pdf. Accessed on July 14, 2014.

This proceedings article describes the utility of combining the lower resolution color pixels with the higher resolution panchromatic pixels to produce high resolution WorldView-2 color imagery.

Park, Jooh-Moh, Chong-Min Park, Tsugio Park. 2009. Ecology Study on the Vitex rotundifolia communities in Korea. Journal of Japanese Society of Coastal Forest. 17-23. Available online. URL: http://jscf.jp/Journal_PDF/JSCF08(1)/JSCF8(1)17-23E.pdf. Accessed on April 2, 2014.

This paper describes characteristics of Monk's pepper (*Vitex rotundifolia*), a deciduous broad-leafed shrub native to seashores throughout the Pacific. This woody perennial plant typically grows approximately 1 m in height. The research investigated the plant's habitats, e.g., it's mean altitude (3 to 10m) and the mean gradient (up to15°). The study included beaches in Hwajinri and the impact of military patrol roads and fences.

Port of Pohang, Available online. URL: http://pohang.mltm.go.kr. Accessed on June 6, 2014.

This website provides geo-coordinates for key navigational locations and instructions for use of the Vessel Traffic Service. It provided information relevant to radio broadcasting when there are special weather reports or other restrictions for safe navigation of vessels. A rigid-hulled inflatable boat, (RHIB) was deployed from a boat ramp at the Port of Pohang to access Dogu Beach. High waves prevented RHIB survey and buoy maintenance operations on April 20, 2014.

APPENDIX C

Climatological Data

Introduction

The Korea Meteorological Administration has archived climatological data from 1981 through 2010 for the area of Pohang, South Korea (see www.kma.go.kr). Information relevant to this remote sensing study includes average temperature, surface temperature, average humidity, wind speed, average daily fog duration, mean monthly sunshine, precipitation, sea level pressure, and average vapor pressure. This climatological information is saved in the project geodatabase as a spreadsheet (see Attribute_Data\Atmospheric\Climate Data). Other meteorological data are found in Appendix I.

Table 1. Climatological Data for Pohang, South Korea.

Climate Data for Pohang (1981-2010)												
Month	Jan	Feb	Mar	Apr	May	Jun	Jul	Aug	Sep	Oct	Nov	Dec
Average Temperature (ºC)	1.8	3.8	7.9	13.8	18.2	18.4	24.9	25.7	18.5	16.6	10.3	4.4
Surface Temperature (ºC)	1.5	4.2	9.4	16.5	21.8	25.3	27.9	29.0	19.4	17.7	9.9	3.5
Average Humidity (%)	49.1	51.8	57.0	57.9	64.6	73.9	78.7	78.8	75.9	65.5	57.6	51.0
Wind Speed (m/s)	3.0	2.9	3.0	3.0	2.8	2.5	2.6	2.7	2.7	2.6	2.6	2.8
Average Daily Fog Duration (hours)	0.14	0.18	0.45	1.55	1.16	5.52	2.67	2.36	0.46	0.30	0.71	0.11
Monthly Sunshine (hours)	188.7	176.4	189.9	214.0	223.9	183.7	161.1	170.3	154.5	193.7	182.8	190.4
Precipita-tion (mm)	36.5	40.8	60.9	68.9	85.2	141.6	203.2	227.4	177.1	43.7	41.1	25.7
Sea Level Pressure (hPa)	1023.1	1021.8	1019.3	1015.4	1011.9	1008.8	1007.7	1009.3	1014.2	1018.9	1022.0	1023.3
Average Vapor Pressure (hPa)	3.7	4.4	6.2	9.0	13.1	18.6	9.7	26.0	19.7	12.6	7.6	4.6
Source data for this table was obtained at Korea Meteorological Administration website: http://www.kma.go.kr												

APPENDIX D

Quality Assurance / Quality Control Lists

Introduction

Data Quality Assurance (DQA) was considered before any data collection took place, during data collection in Pohang, South Korea, and during data processing. A variety of DQA considerations for SY'14 were discussed during science planning and included the following Quality Control (QC) procedures:

- Pre-deployment calibrations on sensors, especially field spectrometers
- *In-situ* comparison before recovery, and post-deployment calibrations when appropriate
- Periodic calibration of back-up instruments
- Taking photographs and recording manual notes
- Recording all actions related to sensor's calibration, cleaning, deployment, etc.
- Monitoring battery voltage and watching for unexpected fluctuations
- Timekeeping

During instrument selection, the following factors were considered:

- Selection of a reliable and supportive manufacturer and appropriate models, especially items such as the DCP which is used by the US Marine Corps and the SonarMite which is used by the US Army.
- Operating ranges for Pohang, e.g., some instruments don't operate satisfactorily in the littoral environment.
- Consideration of resolution/precision required to develop imagery-derived planning products.
- Sampling frequency to ensure that environmental factors are adequately measured.
- Setting up instrument reporting frequency to support follow-on data processing and production.
- Tracking time, e.g., response time of the sensor, sensor lag, clock rift, etc.
- Ability to make instrument checks such as visual inspections for defects, bio-fouling, etc.
- Planning for power management such as scheduling power checks, battery changes, etc.
- Standardizing sensor clock to a reference such as local or GPS time

Considerations included review of specifications in order to

- Determine expected accuracy
- Compare sensors in their ability to meet data and information requirements.
- Determine if the sensor meets those specifications
- Determine whether scientific results are good enough (fit for purpose, i.e., data are adequate for nominal use as preliminary data)

In general collaborators were encouraged to

- Document serial numbers and model ID from the supplier for their instruments.
- Generate useful inventory lists and checklist to ensure instruments and components are operationally ready.
- Keep inventory records, opcheck dates, and calibration information with instruments.
- Responsible parties were expected to plot their own calibration constants or deviations from a standard to determine if the sensor has a drift in one direction or another.

An example Pre-Deployment Checklist is provided below:

□ Familiarize yourself with instruction manuals.

□ Establish, use, and submit (with a reference and version #) a documented sensor preparation procedure (protocol). Should include cleaning sensor according to the manufacturer's procedures.

□ Calibrate sensor against an accepted standard and document (with a reference and version #).

□ Compare the sensor with an identical, calibrated sensor measuring the same parameter in the same area (in a calibration lab).

□ View calibration specifications with a critical eye (don't presume the calibration is infallible). Execute detailed review of calibrated data.

□ Check the sensor history for past calibrations, including a plot over time of deviations from the standard for each (this will help identify trends such a progressively poorer performance). Control chart calibrations.

□ Check the sensor history for past repairs, maintenance, and calibration.

□ Consider storing and handling requirements before shipping.

□ How does the instrument respond to factors such as heat, cold, vibration, sand, and salt?

□ Provide detailed documentation on operational checks and operations.

□ Record operator/user experiences with this sensor after reading the manual.

□ Search the literature for information on your particular sensor(s) to see what experiences other researchers may have had with the sensor(s).

□ Establish and use a formal pre-deployment checklist.

□ Ensure that instrument operators are well-trained or practiced. Use a visual tracking system for training to identify those operators who are highly trained and then pair them with inexperienced personnel. Have a data quality review chain.

Deployment Checklist:

□ Clean instruments.

□ Inventory components.

□ Verify sensor serial numbers.

□ Deploy and co-locate multiple sensors (attention to interference if too close).

□ Perform visual inspection; take photos if possible (verify position of sensors, connectors, fouling, and cable problems).

□ Verify instrument function at deployment site prior to site departure. Allot sufficient time for temperature equilibration.

□ Monitor sensors for issues (freezing, fouling, collisions with vessels).

□ Automate processing so you can monitor the initial deployment and confirm the sensor is working while still on-site.

□ Specify date/time for all recorded events.

□ Check software to ensure that the sensor configuration and calibration coefficients are correct. Also check sampling rates and other timed events, like wiping and time averaging.

□ Visually inspect data stream to ensure reasonable values.

□ Conduct intercomparison test with handheld instrument.

□ Note weather conditions and members of field crew.

Post-deployment Checklist:

□ Take pictures of recovered sensor for use in metadata.

□ Check to make sure all clocks agree or, if they do not agree, record all times and compare with GPS time.

□ Post-calibrate sensor and document before and after cleaning readings.

□ Perform *in-situ* side by side check using another sensor.

□ Provide a mechanism for feedback on possible data problems and/or sensor diagnostics.

□ Clean and store the sensor properly or redeploy.

□Visually inspect physical state of instrument.

□ Verify sensor performance by:

  □ Checking nearby stations;

  □ Making historical data comparisons (e.g., long-term time-series plots, which are particularly useful for identifying long-term bio-fouling or calibration drift.)

□ Ensure all parts are inventoried prior to packing.

Table D-1. Common Tests for Quality Control.

Test Type	Explanation
Minimum or Maximum Exceeded	Data point exceeds sensor or operator-selected min/max.
Climatology Test	Test that data point falls within seasonal expectations.
Spike Test	Data point *n*-1 exceeds a selected threshold relative to adjacent data points.
Rate of Change Test	Excessive rise/fall test. This test inspects the time series for a time rate of change that exceeds a threshold value
Flat Line Test	Invariant value.

APPENDIX E

Quadrats

Table of Contents

List of Figures

List of Tables

Introduction

Once on the beach, the science team determined a need to estimate the distribution of beach materials. A one meter square was cut out of a tarp for use as a quadrat (Figure E-1) to estimate the size distribution of beach materials (e.g., sands, gravel, and cobbles). Photographs and GPS points were taken of each quadrat location. The GPS location was taken at the center of the $1m^2$ quadrat. Six locations were recorded at Doksuk-ri Beach and three at Hwajin-ri Beach (see Table E-1).

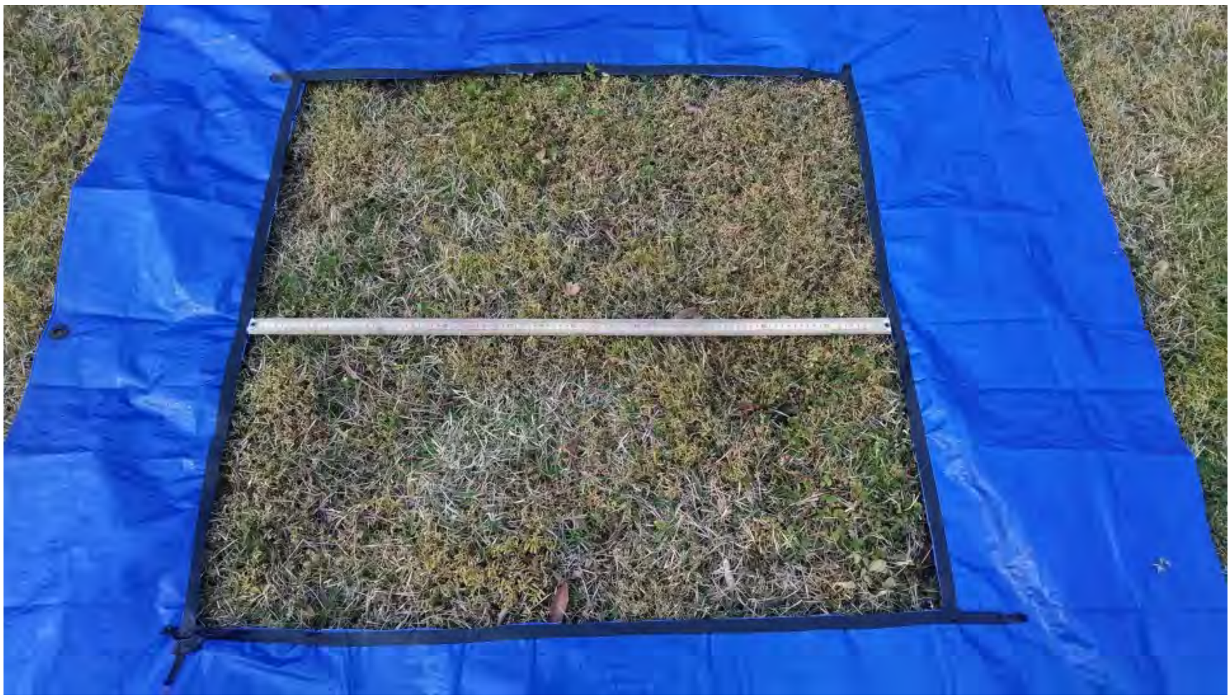

Figure E- 1. One meter cut-out used to characterize beaches. The quadrat is suitable for sampling larger diameter beach materials such as gravel (4.75 - 75mm) and cobble (75-300mm), ASTM Standard D2487.

Table E-1. Photographs taken of quadrats deployed on the beach. The top three rows are from Hwajin-ri Beach. The bottom six rows are from Doksuk-ri Beach. Percentages are provided for grain sizes that are less than 4.75 mm which consists of sands (75µm – 4.75mm), silts (2 - 75µm), and clays (< 2µm).

Photograph of Quadrat	Highlighted Location of Quadrat	Latitude	Longitude
	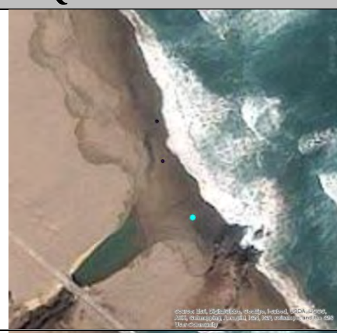	36.245496 N	129.378284 E
		Coverage of Grains Smaller Than Gravel Size (4.75mm) within Quadrat	
		85% smaller than gravel size	
	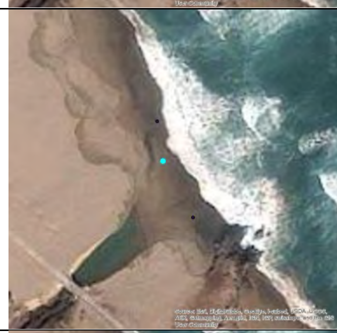	36.245746 N	129.378121 E
		18.5% smaller than gravel size	
	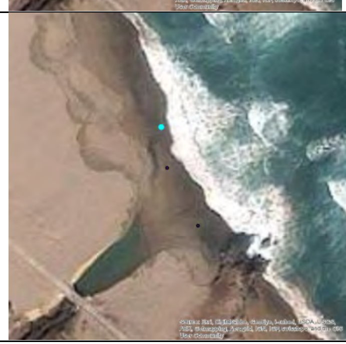	36.245922 N	129.378091 E
		89.6% smaller than gravel size	

Photograph of Quadrat	Highlighted Location of Quadrat	Latitude	Longitude
		36.226928 N	129.382122 E
		Coverage of Grains Smaller Than Gravel Size (4.75mm) within Quadrat	
		0% smaller than gravel size	
	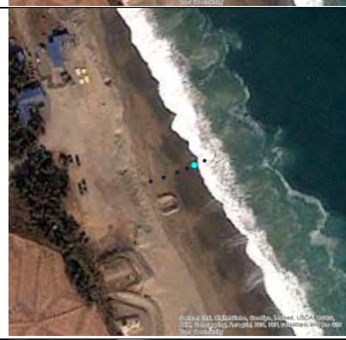	36.226903 N	129.382052 E
		0 % smaller than gravel size	
	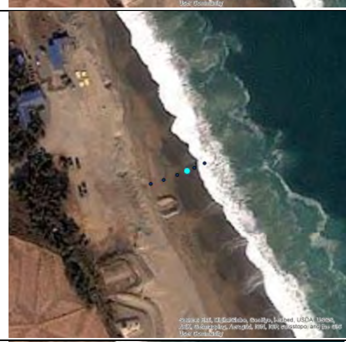	36.226886 N	129.382004 E
		0 % smaller than gravel size	
	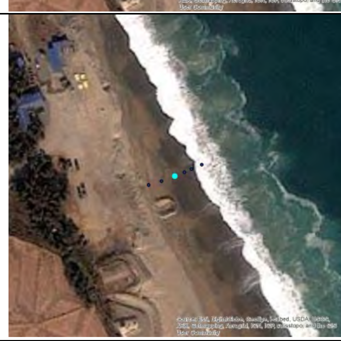	36.226865 N	129.381939 E
		94% smaller than gravel size	
	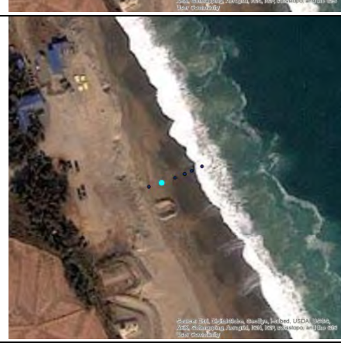	36.226838 N	129.381849 E
		60% smaller than gravel size	

Photograph of Quadrat	**Highlighted Location of Quadrat**	**Latitude**	**Longitude**
		36.226816 N	129.381763 E
		Coverage of Grains Smaller Than Gravel Size (4.75mm) within Quadrat	
		55% smaller than gravel size	

Methods

The first three photographs (Hwajin-ri Beach) were analyzed within the ArcMap environment and the remaining in an ENVI environment. In ArcMap, polygons were drawn over the area covered by larger grains (> 4.75mm) (see Table E-2, center image) or sandy areas depending on which was apparently a smaller area to draw. Once the polygons were finished a measured area was determined from all polygons and divided by the entire area within the quadrat to provide a percentage of grains smaller than 4.75mm. The percentages of the remaining photographs were determined in a similar method (software instead of the human eye) but used an automatic feature extraction in ENVI which determines differences in texture and spectra to determine feature separations.

Table E- 1. Example of Percentage Extraction of Grains Smaller than 4.75mm.

Third photograph from Table E-1	Polygons drawn over all grains larger than 4.75mm	Polygon drawn over entire area within quadrat
		

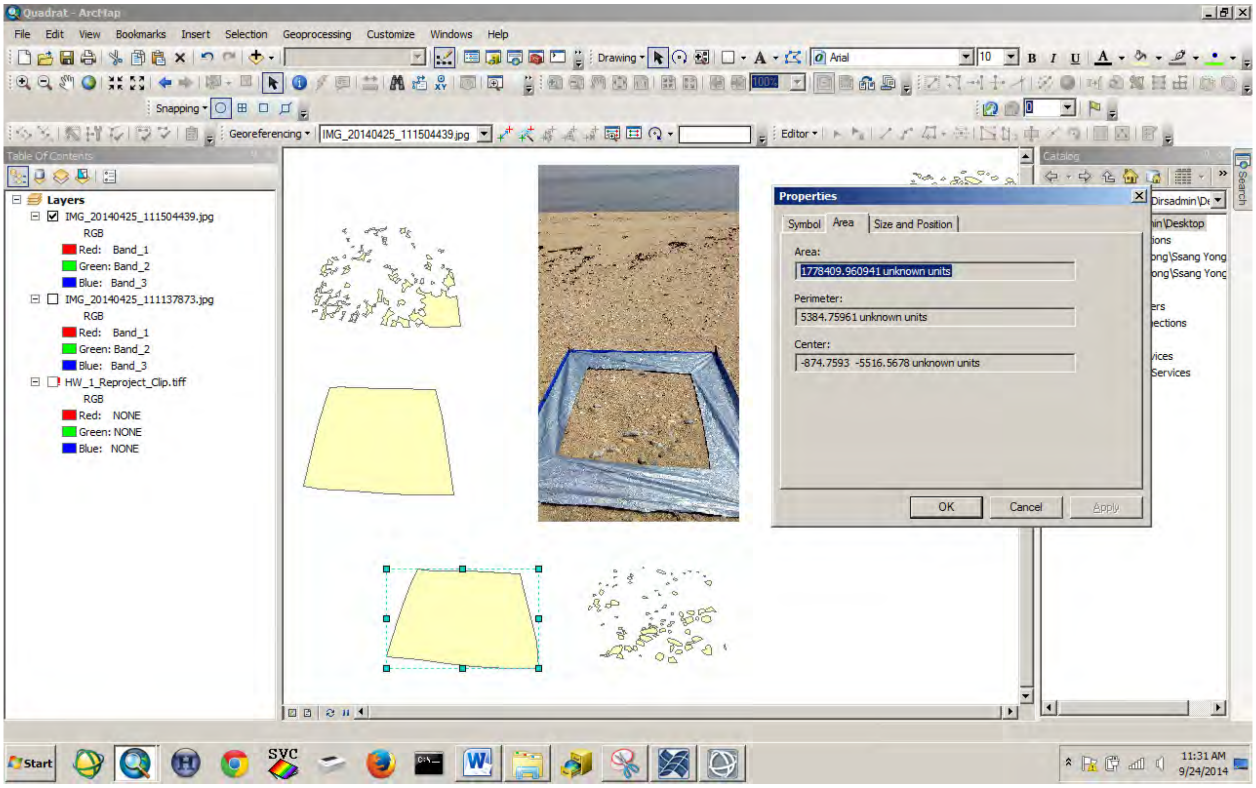

Figure E- 2. Polygon area measurement of surface within quadrat.

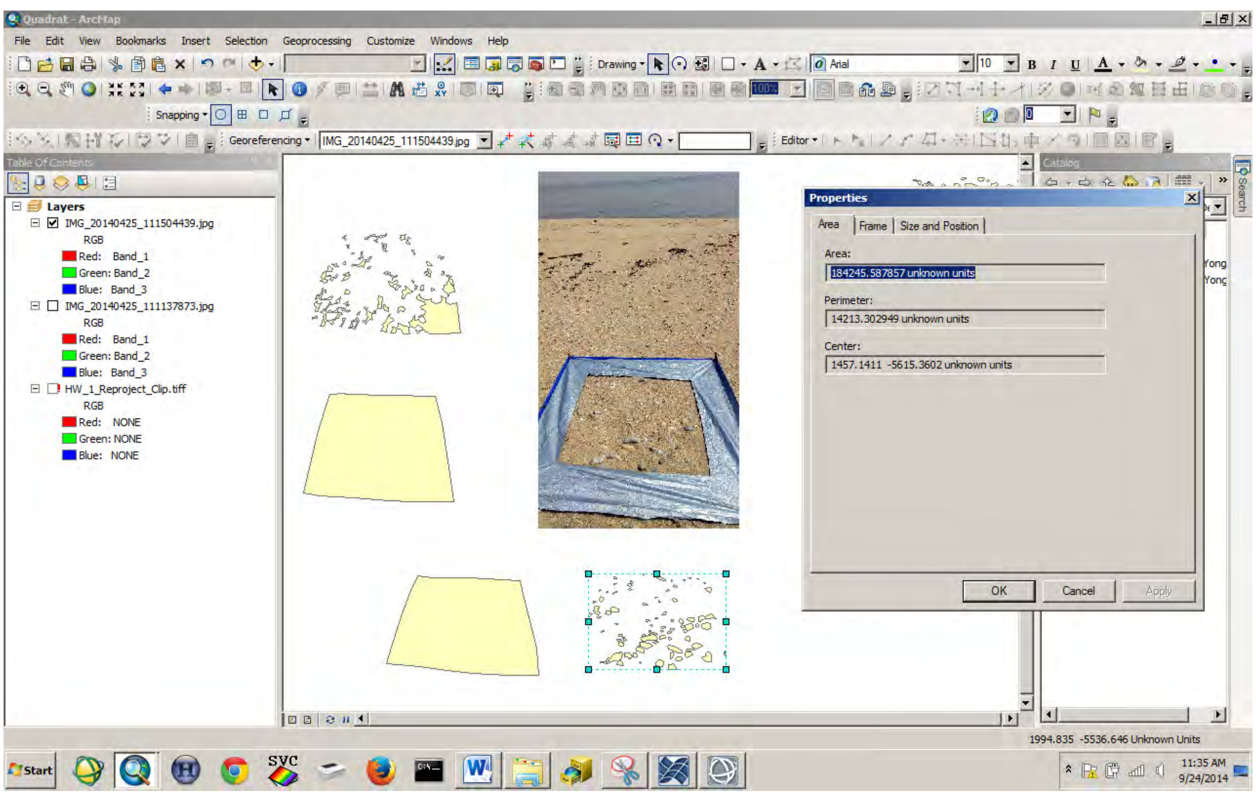

Figure E- 3. Polygon area measurement of larger grains on surface.

APPENDIX F

QuickLooks

Introduction

Relevant imagery of the study area was collected from USGS (Landsat 5, 8), Digital Globe (WorldView-2), and Nasa's Terra Satellite (Moderate Resolution Imaging Spectroradiometer or MODIS) and archived in the project geodatabase. These images are useful to build base maps, reference maps, and extracting features such as waterlines, creating vector models, and showing variation in the amount of beach that is available for maneuver during different phases of the tide. Change detection can also be used to identify variability in wetlands, shoreline retreat rates (erosion), and the growth of distal bars (accretion). The waterline is the land-sea boundary at time of imaging. For extracting the Mean High Water Line or shoreline from imagery, a tidal model must be referenced to surveyed positions with good elevation accuracy. All images were georeferenced to the World Geodetic System 1984 (WGS 84) datum in the project geodatabase.

For convenience, quick looks of imagery are provided for preview in Table F-1. Imagery that has been used in the remote sensing study are listed as imagery thumbnails, source of the image along with date and time, the general area covered by the image, and the filename used within the project geodatabase. General differences in Landsat-8 andWorldView-2 sensor characteristics are provided in Table F-2.

Table F- 1. QuickLooks of imagery that have been archived in the Project Geodatabase.

Thumbnail	Source	Area	File Name
	MODIS (Nasa's Terra Satellite), 03Jan2010	Snow Covered Korea	Snow_Covered_Korea
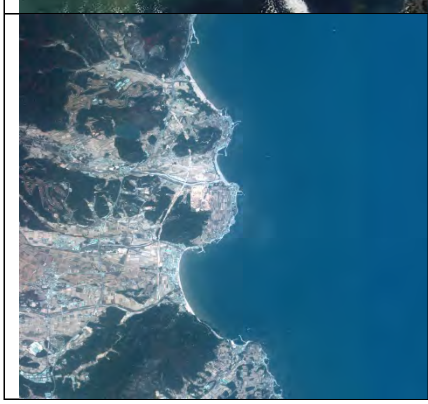	WorldView-2, 25Apr2014 02:39	Northern Beaches used during the Ssang Yong 2014 Experiment.	WV2_25Apr2014_023915_UTC

	WorldView-2, 09May2014 02:23:51	Dogu Beach; Pohang port facility; POSCO, and Yeongil Bay.	14MAY09022351-M1BS-500119110010_01_P001-BROWSE
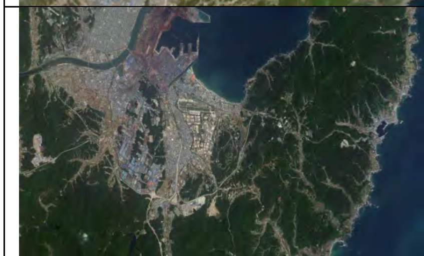	WorldView-2, 19May2014 02:54:22	Dogu Beach; Pohang port; POSCO; and Yeongil Bay.	14MAY19025422-M1BS-500123114010_01_P001-BROWSE
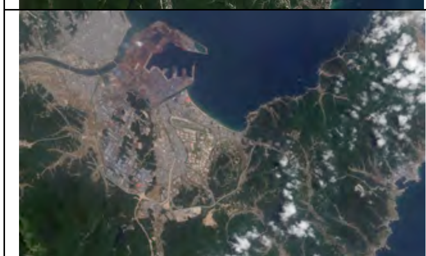	WorldView-2, 22May2014 02:44:25	Dogu Beach; Pohang port; POSCO; and Yeongil Bay.	14MAY22024425-M1BS-500123677010_01_P001-BROWSE
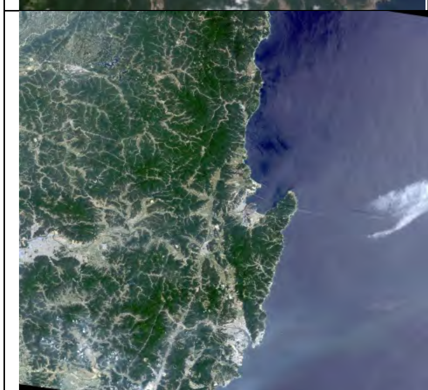	Landsat-5 22Jun2010 01:49	ROK east coast including study areas for 2014 Ssang Yong remote sensing experiment.	LT51140352010173HAJ01_B1_Com
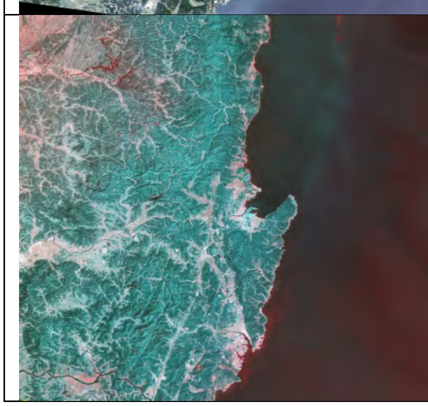	Landsat-8 imagery, 14Apr2014 01:59	ROK east coast including study areas for 2014 Ssang Yong remote sensing experiment.	LC81140352014104LGN00_B1_Com

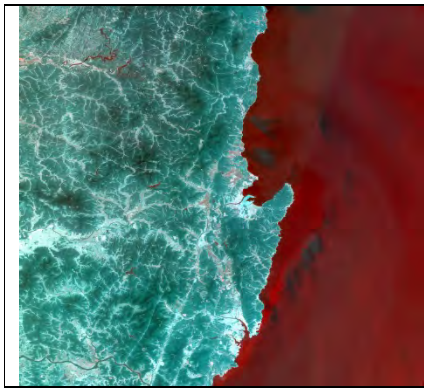	Landsat-8 Imagery, 16May2014 01:59	ROK east coast including study areas for 2014 Ssang Yong remote sensing experiment.	LC81140352014136LGN00_B1_Com

Table F-2. General characteristic for WorldView-2 and Landsat 8.

WorldView-2		**Landsat 8**	
Band	Spectral Range	Band	Spectral Range
Coastal:	400 – 450 nm	Coastal aerosol:	430 – 450 nm
Blue:	450 – 510 nm	Blue:	450 – 510 nm
Green:	510 – 580 nm	Green:	530 – 590 nm
Yellow:	585 – 625 nm		
Red:	630 – 690 nm	Red:	640 – 670 nm
Red Edge:	690 – 770 nm		
Near-IR1:	770 – 895 nm	Near Infrared:	850 – 880 nm
Near-IR2:	860 – 1040 nm		
		SWIR 1:	1570 – 1650 nm
		SWIR 2:	2110 – 2290 nm
		Cirrus:	1360 – 1380 nm
Panchromatic:	450 - 800	Panchromatic:	500 – 680 nm
		Thermal Infrared 1:	10600 – 11190 nm
		Thermal Infrared 2:	11500 - 12510
Multispectral Resolution	1.85 Meter	Multispectral Resolution:	30 Meters
Panchromatic Resolution:	0.46 Meter	Panchromatic Resolution:	15 Meters
		Thermal Resolution:	100 Meters
Re-Visit Time:	1.1 Days	Re-Visit Time:	16 Days
Additional details on the WorldView-2 satellite may be accessed online at URL: http://www.digitalglobe.com.		Additional details on the Landsat 8 satellite may be accessed online at URL: http://landsat.usgs.gov.	

APPENDIX G

Site Spectra

Introduction

Field spectrometers provide ground truth for comparison with measurements taken from remote sensing. The spectra were measured with three Analytical Spectral Devices (ASD) full-range spectrometers. One ASD spectrometer was mounted on a goniometer, the Goniometer of the Rochester Institute of Technology (GRIT) which measures reflectance at multiple zenith and azimuth angles (BRDF). Another was mounted on a fixed tripod and used to collect information about variations in downwelling irradiance: this spectrometer recorded the reflected solar radiance from a white Spectralon reference, during both goniometer collections and nadir-only spectral collections measured with a third ASD spectrometer at each site location and the calibration panels. The data in this appendix are reported for each type of data: nadir-only spectra and GRIT angular-dependent BRDF spectra.

For the nadir-looking spectra collected at site locations, spectra were edited to eliminate spectral regions with very high water vapor absorption. Edited bands were from 1.35 um to 1.44 μm, 1.79 μm to 1.95 μm, and 2.45 μm to 2.5 μm. For the nadir-looking spectra, one exception was at site DG-2-8, which exhibits SWIR noise between 1.95-2.03 μm. If used in further processing nadir spectrum DG-2-8 bands in this region should be treated as bad-bands. The most-obvious differences among the nadir spectra appear in the SWIR where mineral absorption features are strongest. This results from the variations in materials found on beaches and tidal flats at the field experiment venues. In some instances, distinct absorption features or also appear in the visible and near infra-red (VNIR), however, for sediments in this spectral region, differences among spectra often appear as general changes in the shape of the spectra.

In this document, the bi-directional reflectance distribution function (BRDF) spectra are portrayed as a set. Normally, before use, they are also reprocessed to take account of variations in illumination over the BRDF hemispherical scan. This process uses a second ASD spectrometer, which was mounted on a tripod and recorded radiance from a white reference Spectralon panel throughout the BRDF scan cycle (Figure G-1). The BRDF plots also include spectra with instrument self-shading: before use with imagery, these self-shaded spectra are also normally removed from further consideration.

BRDF spectra exhibit the additional variations due to the effects both of geometric factors related to the phase angle (angle formed by the sun, ground, and sensor, with vertex at the ground point) as well as the underlying differences in density, grain size distributions, and surface roughness (Figure G-2), which are known from physical radiative transfer theory to effect the angular distribution seen in BRDF spectra. The GRIT ASD spectrometer was a new generation ASD FR4, and for this instrument, the bad bands covered a somewhat narrower spectral range between 1.342-1.390 μm, 1.808-1.923 μm, and 2.477-2.500 μm. BRDF data provide important information that describe variations in phase angle geometry that can occur depending on the specifics of how imagery is collected, for example, off-nadir viewing geometries. Even in conventional measurements from an aircraft, the phase angle across the field of view in the across-track direction can often vary significantly, and the angular structure of the BRDF can vary significantly and is wavelength-dependent (Figure G-3). These variations are captured in the BRDF reflectance spectra portrayed in this appendix. Similarly, the BRDF contains information about the underlying density, grain size distribution, and surface roughness

all of which impact the angular distributions seen in these spectra. Thus repeat-pass imaging along different headings or at different times of day along the same heading can take advantage of this information to infer additional information about the geophysical parameters of the scene.

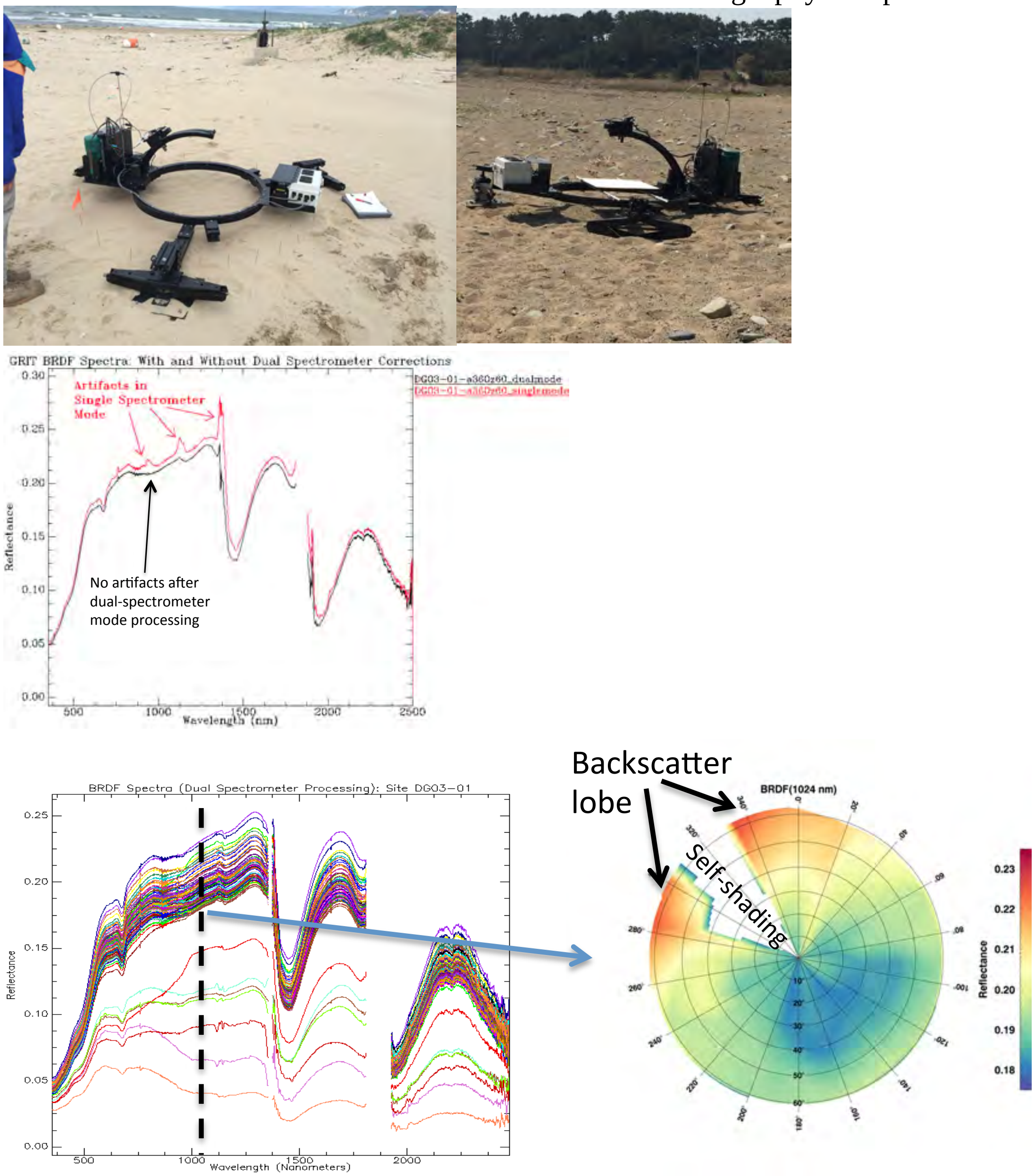

Figure G-1. GRIT hyperspectral goniometer at SY'14 beach sites during our April 2014 field data collection. (Top, Left) GRIT recording reflected radiance from the beach surface; (top, right) GRIT recording calibration measurements of radiance from a Spectralon™ white reference standard. (Middle, left) During GRIT BRDF scan and calibration cycles, a second spectrometer records the down-welling radiance reflected by a white Spectralon™ reference, allowing correction for variations in illumination using a dual-spectrometer method previously developed by us (Bachmann, Montes, etal, Optics Express, http://dx.doi.org/10.1364/OE.20.008959) ; (middle, right) spectral quality improves using dual mode spectrometer processing of GRIT BRDF data, which mitigates effects of variations in illumination that cause data artifacts (red line); these artifacts are removed in the dual-spectrometer GRIT spectrum (black line). (Bottom, left) Example GRIT BRDF spectral measurements. (Bottom, right) BRDF for a specific wavelength rendered as a polar angular plot to portray the angular distribution of the reflected light.

The next two sections portray the nadir-only reflectance spectra, and the GRIT BRDF (angular dependent) reflectance spectra. For the GRIT BRDF reflectance spectra, reflectance was recorded every 20 degrees in azimuth from 0 to 360 degrees, and every 15 degrees in zenith from 0 to 60 degrees. Each scan consisted of 95 reflectance measurements over the hemisphere defined by these azimuth and zenith angle ranges.

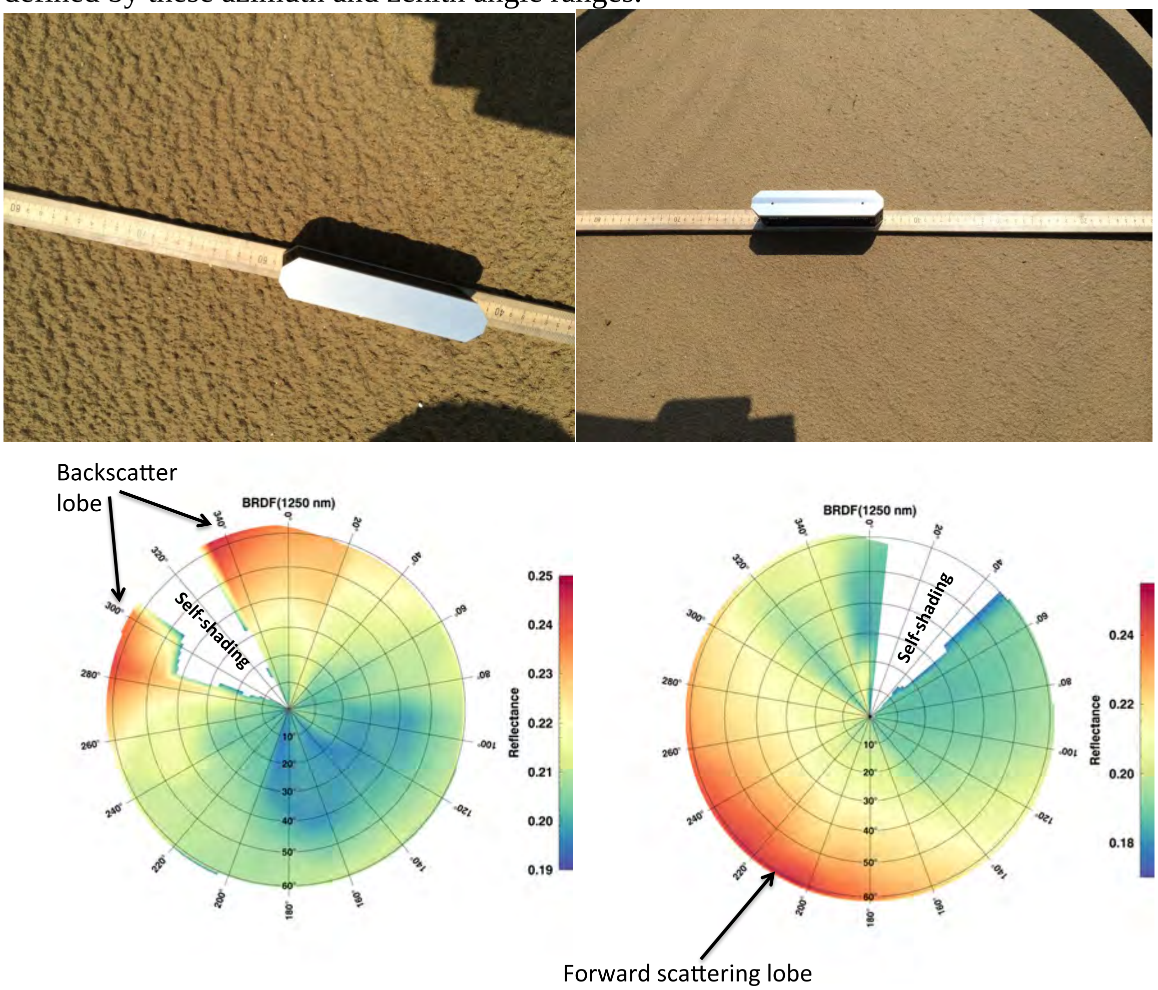

Figure G-2. (Top) Photos of two sites at Dogu Beach with similar composition and moisture content (31.9% and 34.6%), but significant differences in surface roughness. The surface roughness has a significant impact on the shape of the GRIT BRDF: (bottom) with the rough beach surface (left) producing a significant backscatter peak, while the smooth beach surface (right) produced the opposite result with a significant forward scattering peak but no backscatter peak. Shown: the BRDF plots for the two sites for a wavelength of 1250 nm.

GRIT contains an on-board IMU, which automatically records the roll, pitch, of the sensor on the zenith arc to ensure an accurate reading of sensor look direction. Once the instrument is leveled, the IMU records the pose of the sensor during the BRDF reflectance scan. The IMU also provides feedback when leveling the instrument prior to the start of each scan. The roll and pitch readings of the IMU were accurate to within a couple of degrees. Although the IMU recorded heading (absolute azimuthal direction), during this campaign, the recorded heading was deemed unreliable, and two alternative methods were used to ensure absolute bearing was recorded: an

approximate compass heading was recorded for each azimuth, and a marking pin was placed in the sediment at each azimuth position and later recorded with high-precision differential GPS (the more accurate of the two methods).

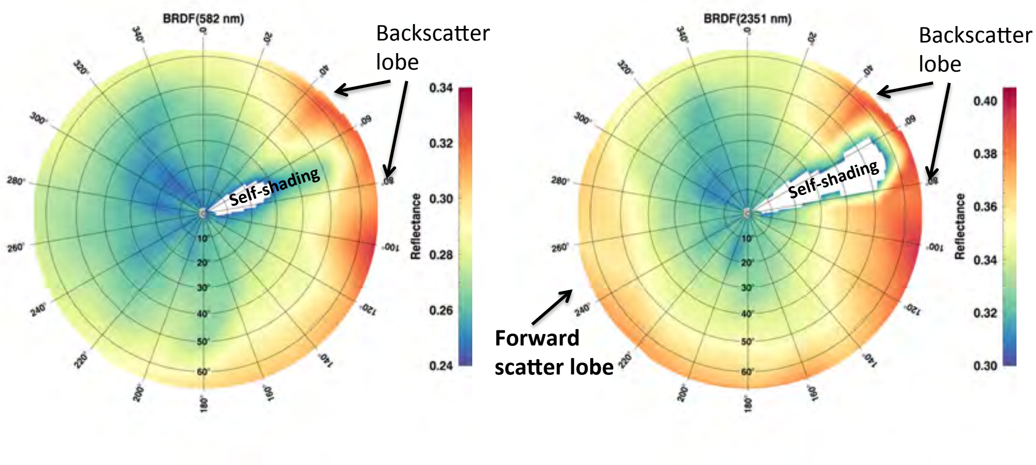

Figure G-3. BRDF examples from a site on Hwajin-ri Beach (HW02-03) show variations that occur in BRDF structure with wavelength. (Top) BRDF at 582 nm (in the green part of the spectrum); (bottom) BRDF at 2351 nm (in the SWIR). At 582 nm, backscatter dominates, while at 2351 nm, there is also a significant forward scattering lobe.

Nadir Reflectance Spectra

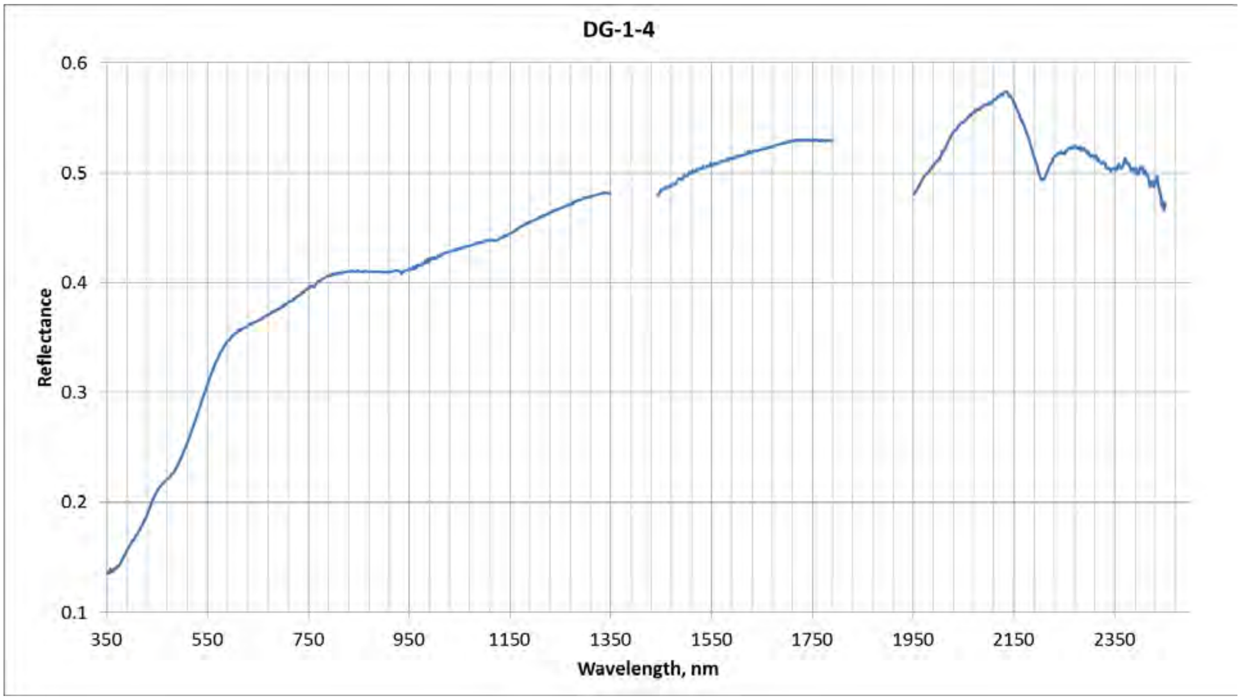

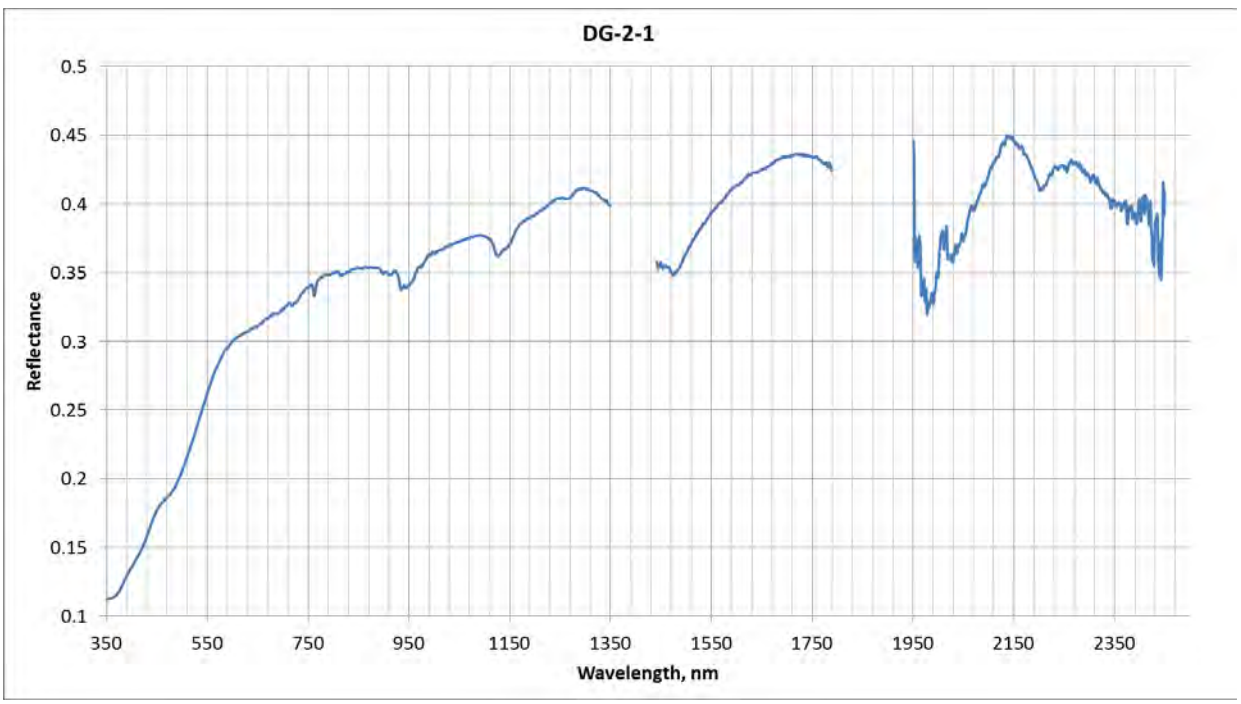

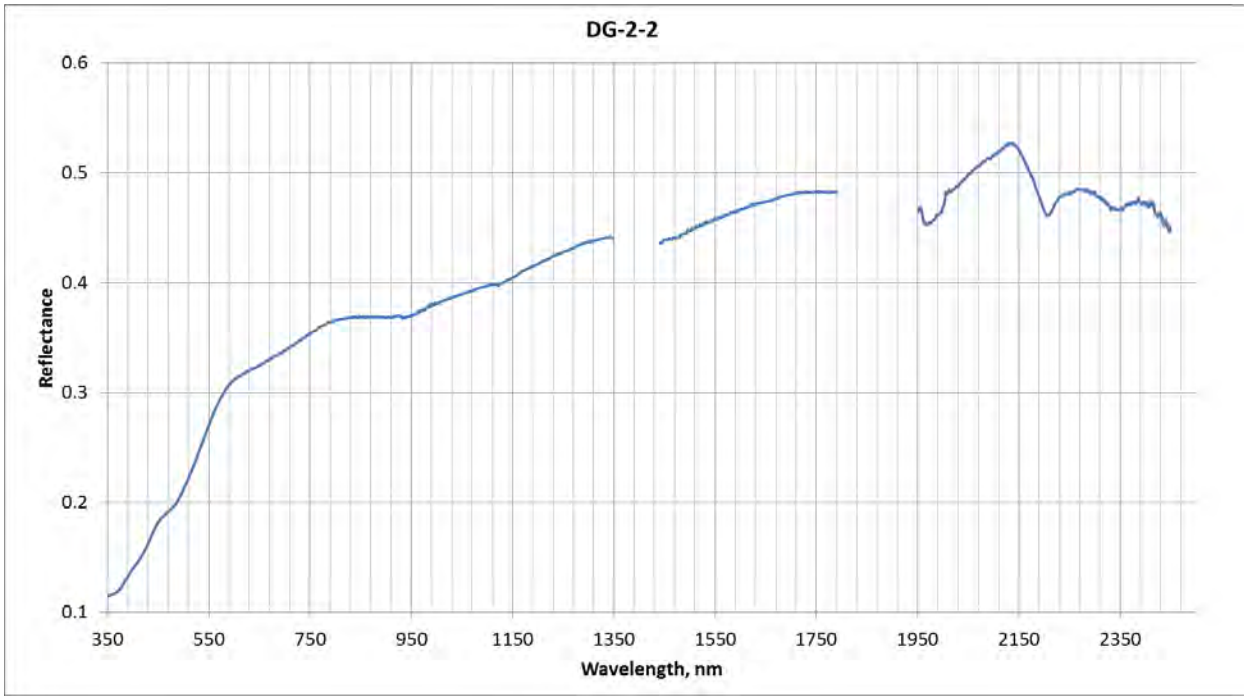
DG-2-2
0.6
0.5
0.4
0.3
0.2
0.1
Reflectance
350
550
750
950
1150
1350
1550
1750
1950
2150
2350
Wavelength, nm

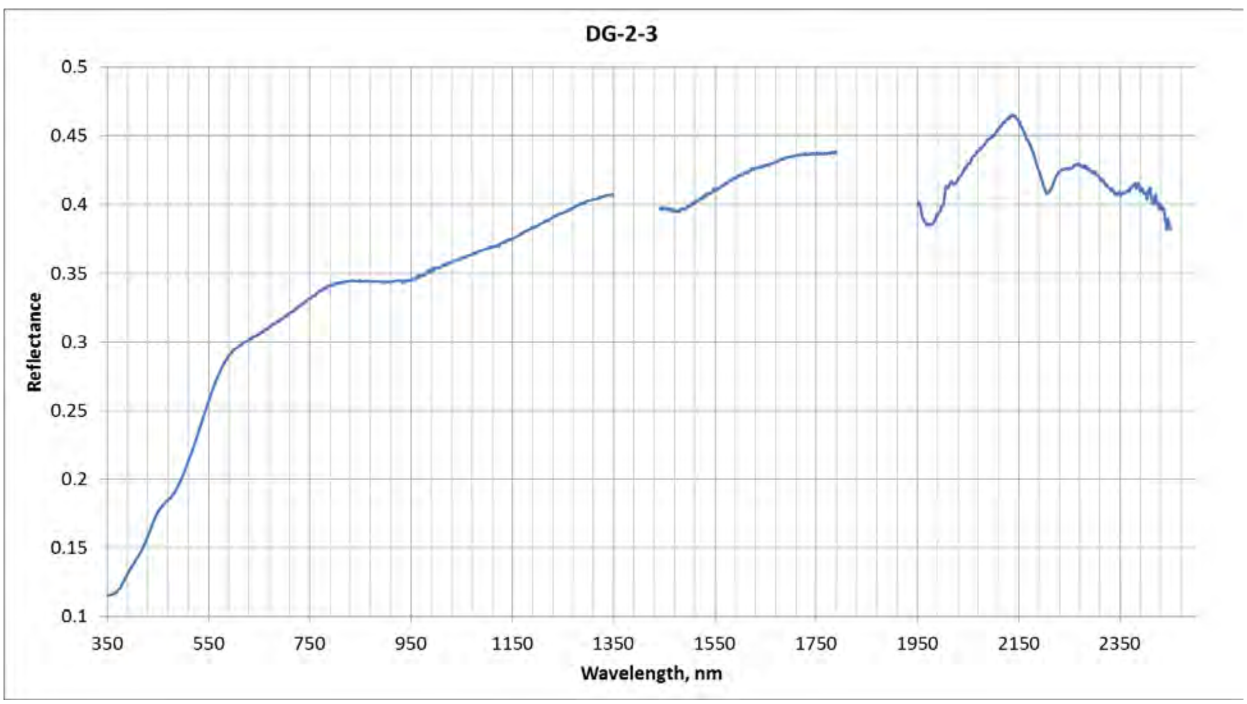
DG-2-3
0.5
0.45
0.4
0.35
0.3
0.25
0.2
0.15
0.1
Reflectance
350
550
750
950
1150
1350
1550
1750
1950
2150
2350
Wavelength, nm

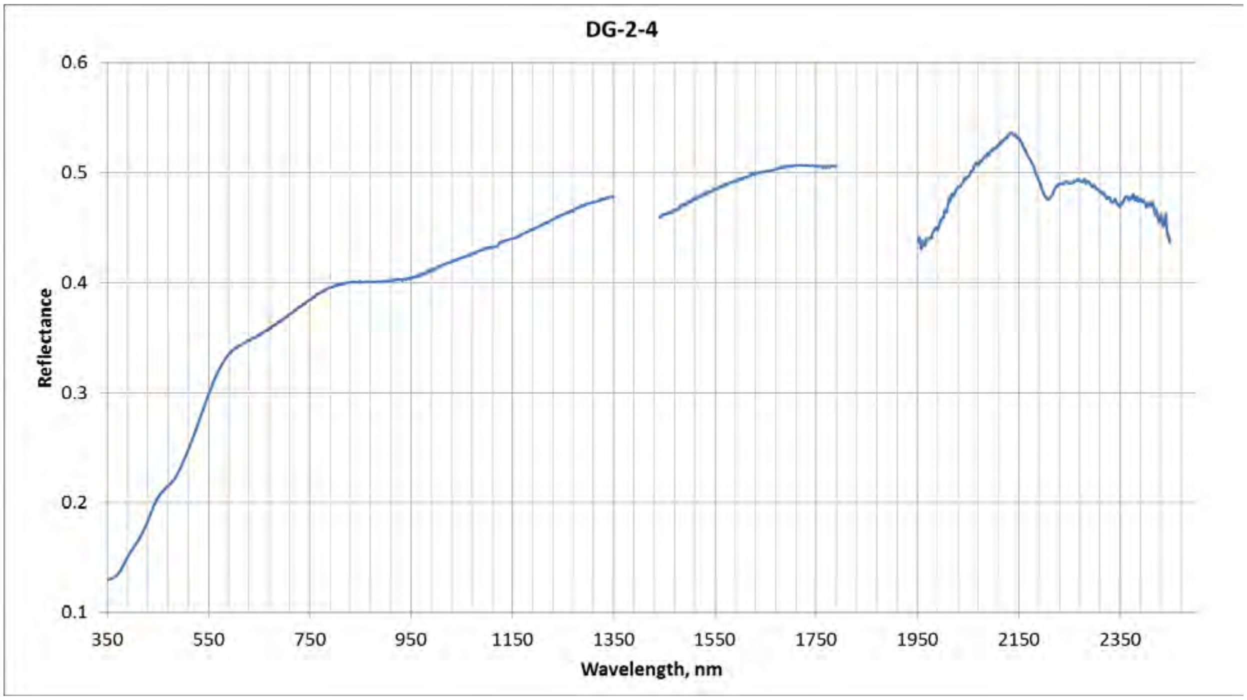

DG-2-4
0.6
0.5
0.4
0.3
0.2
0.1
Reflectance
350
550
750
950
1150
1350
1550
1750
1950
2150
2350
Wavelength, nm

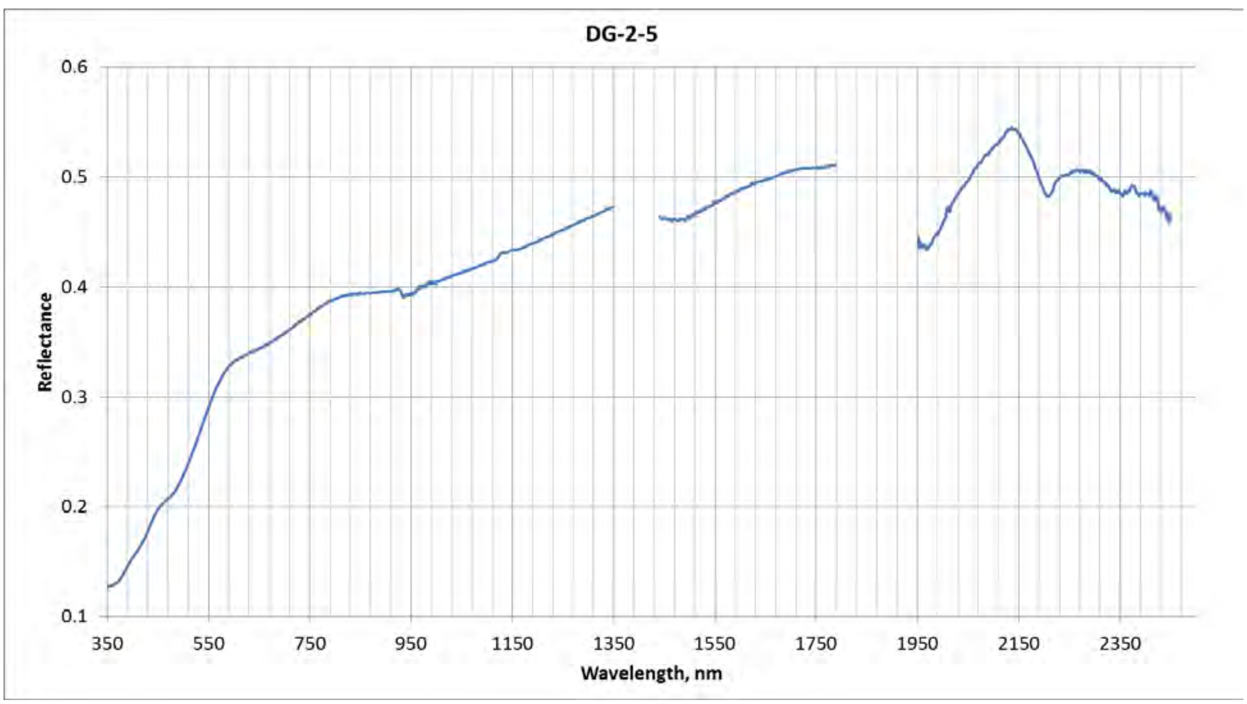

DG-2-5
0.6
0.5
0.4
0.3
0.2
0.1
Reflectance
350
550
750
950
1150
1350
1550
1750
1950
2150
2350
Wavelength, nm

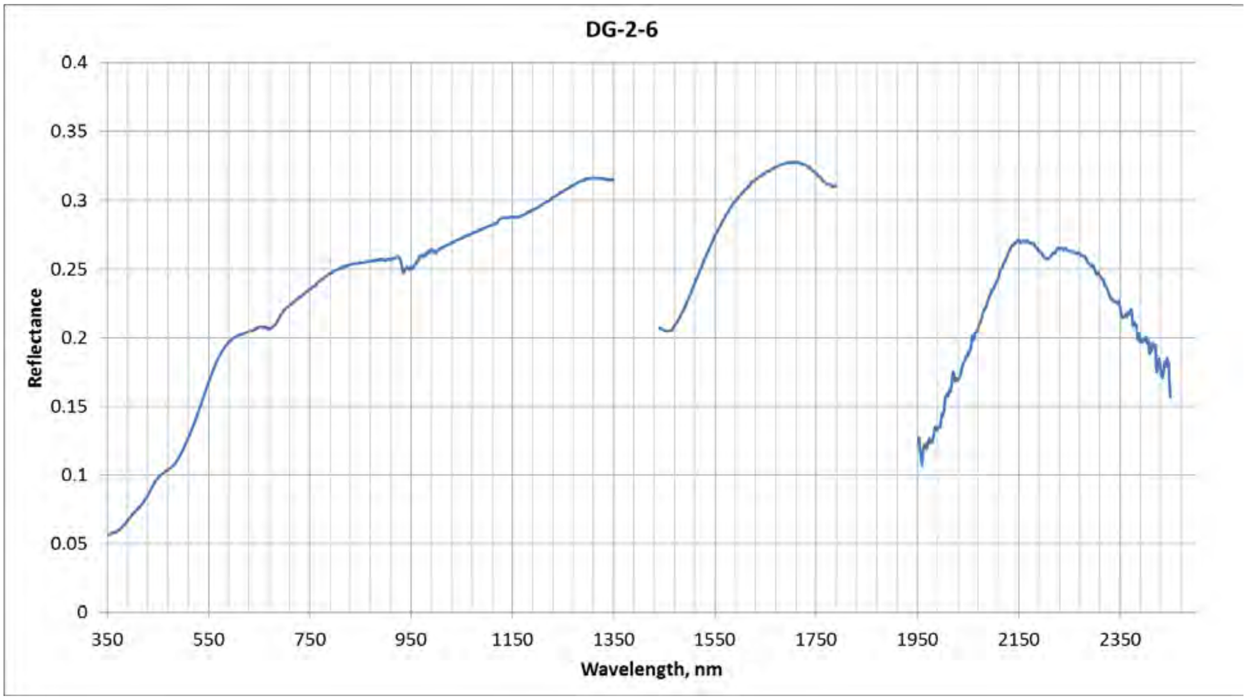
DG-2-6
0.4
0.35
0.3
0.25
0.2
0.15
0.1
0.05
0
Reflectance
350
550
750
950
1150
1350
1550
1750
1950
2150
2350
Wavelength, nm

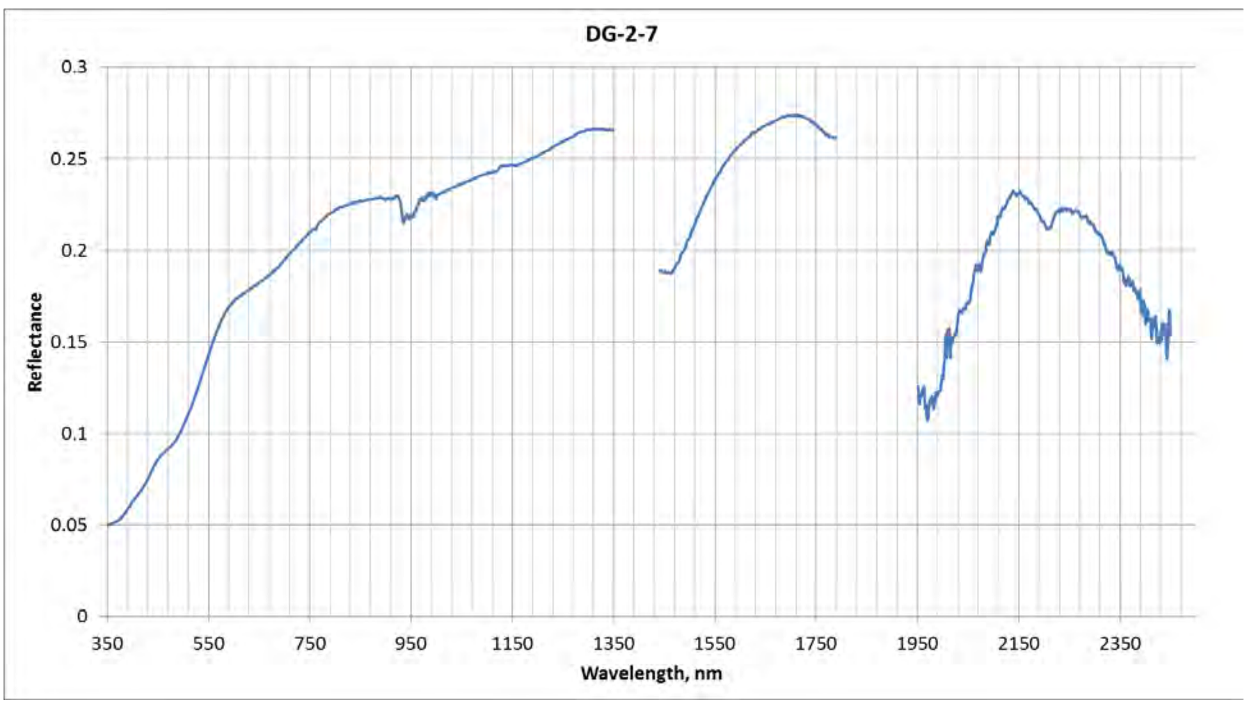
DG-2-7
0.3
0.25
0.2
0.15
0.1
0.05
0
Reflectance
350
550
750
950
1150
1350
1550
1750
1950
2150
2350
Wavelength, nm

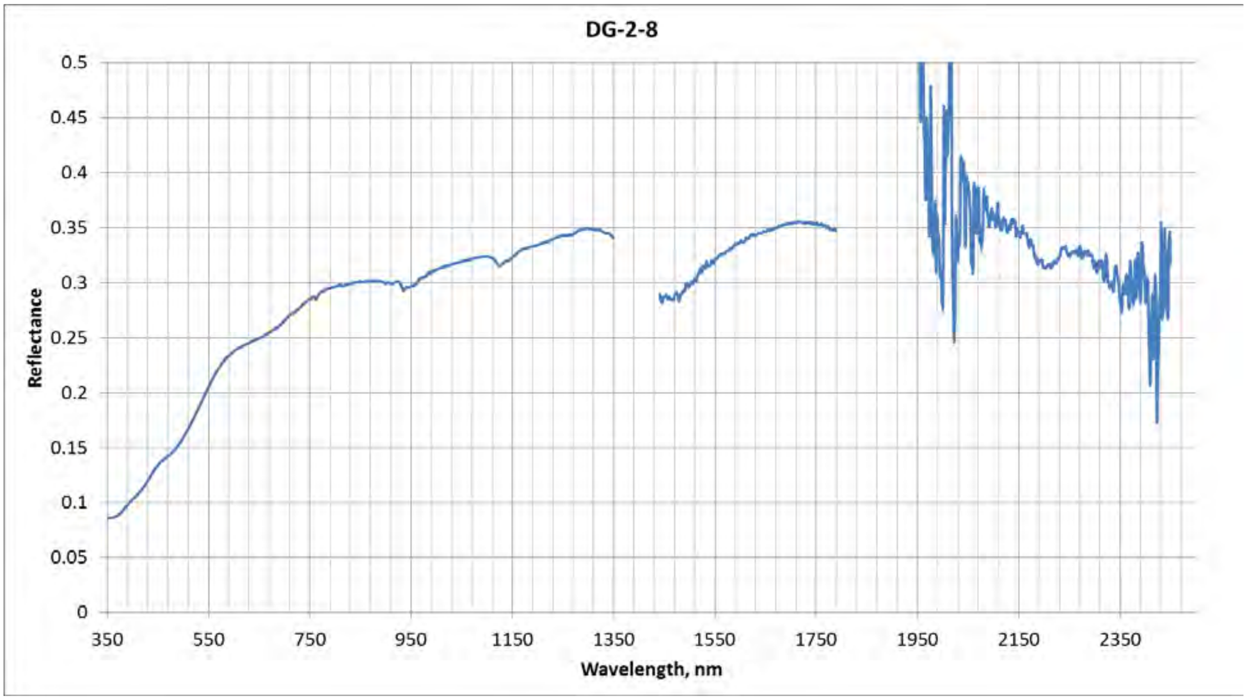
DG-2-8
Reflectance
Wavelength, nm
0.5
0.45
0.4
0.35
0.3
0.25
0.2
0.15
0.1
0.05
0
350
550
750
950
1150
1350
1550
1750
1950
2150
2350

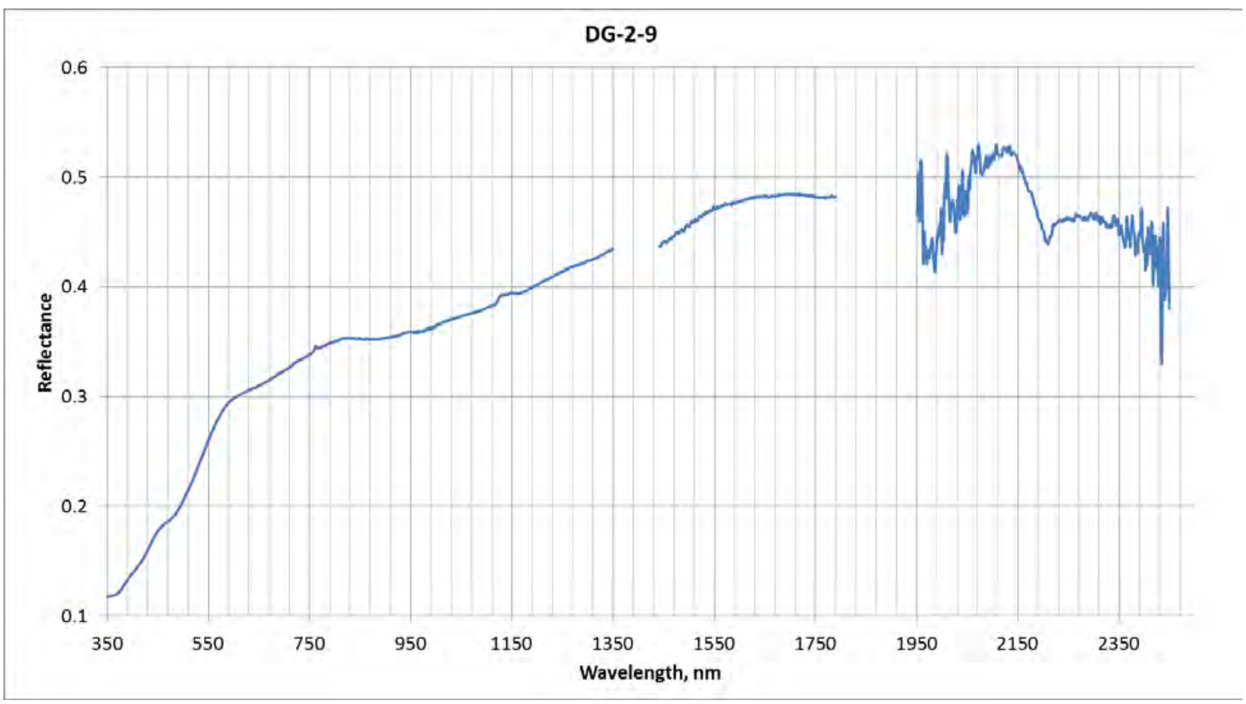
DG-2-9
Reflectance
Wavelength, nm
0.6
0.5
0.4
0.3
0.2
0.1
350
550
750
950
1150
1350
1550
1750
1950
2150
2350

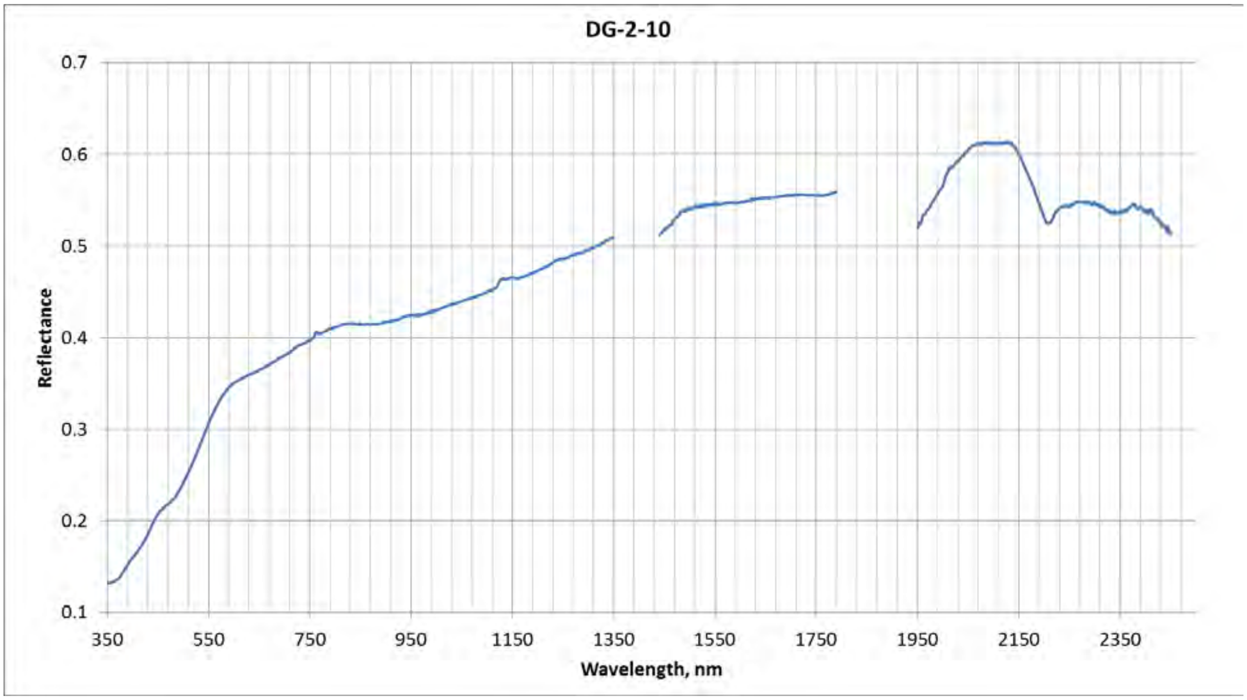
DG-2-10
Reflectance
Wavelength, nm
0.7
0.6
0.5
0.4
0.3
0.2
0.1
350
550
750
950
1150
1350
1550
1750
1950
2150
2350

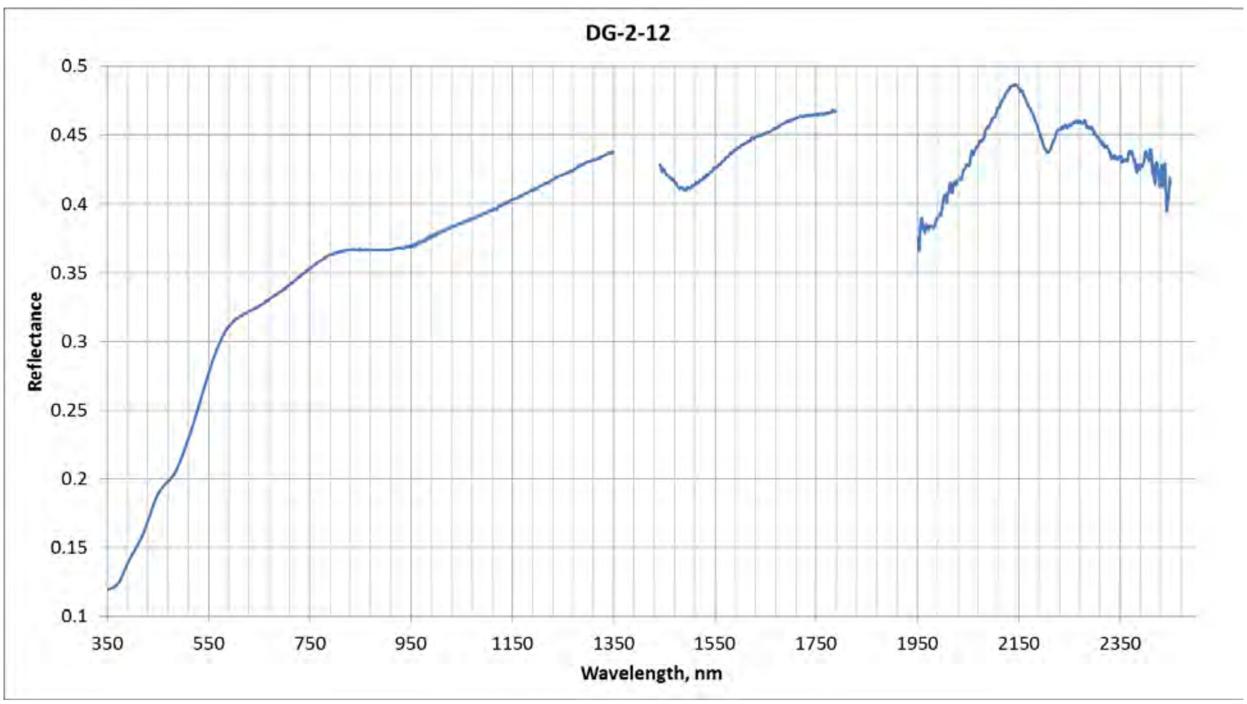
DG-2-12
Reflectance
Wavelength, nm
0.5
0.45
0.4
0.35
0.3
0.25
0.2
0.15
0.1
350
550
750
950
1150
1350
1550
1750
1950
2150
2350

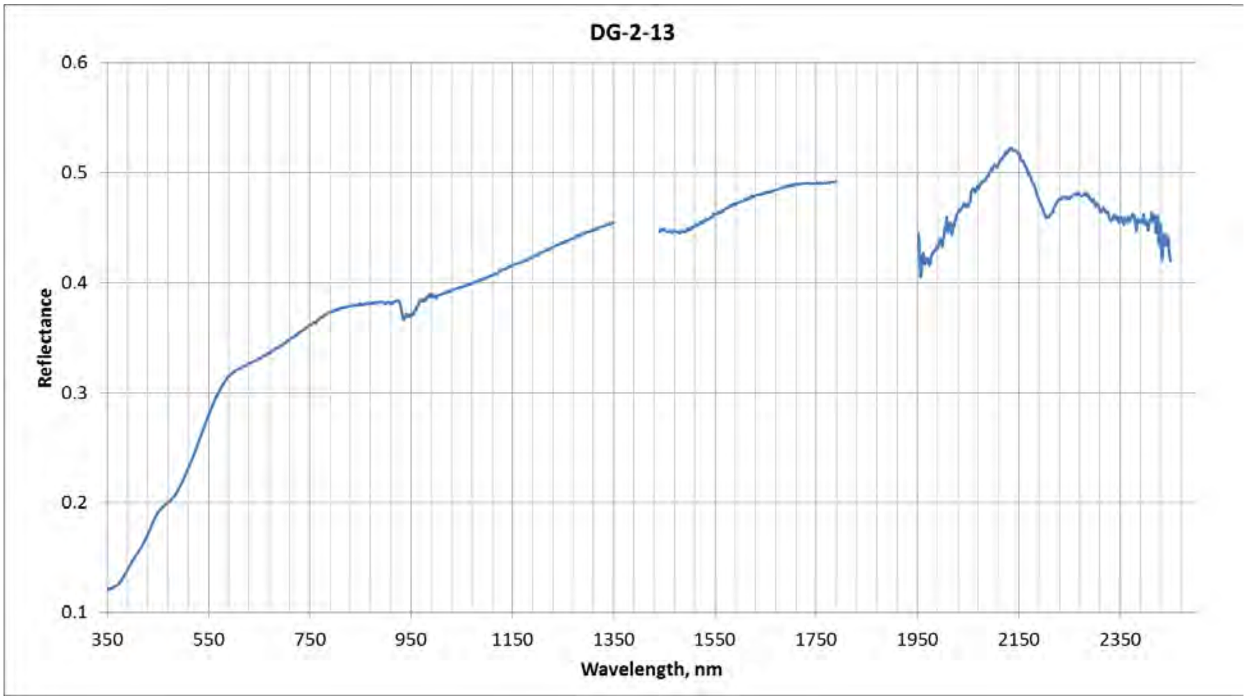
DG-2-13
Reflectance
Wavelength, nm
0.1
0.2
0.3
0.4
0.5
0.6
350
550
750
950
1150
1350
1550
1750
1950
2150
2350

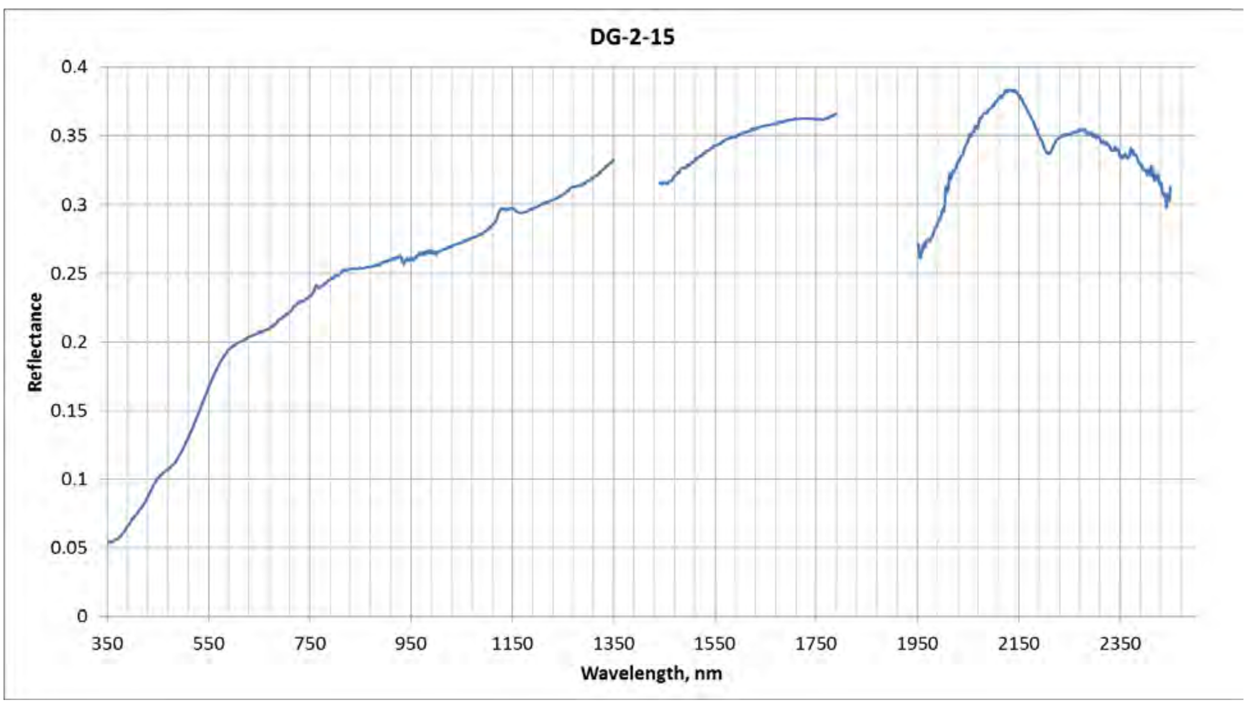
DG-2-15
Reflectance
Wavelength, nm
0
0.05
0.1
0.15
0.2
0.25
0.3
0.35
0.4
350
550
750
950
1150
1350
1550
1750
1950
2150
2350

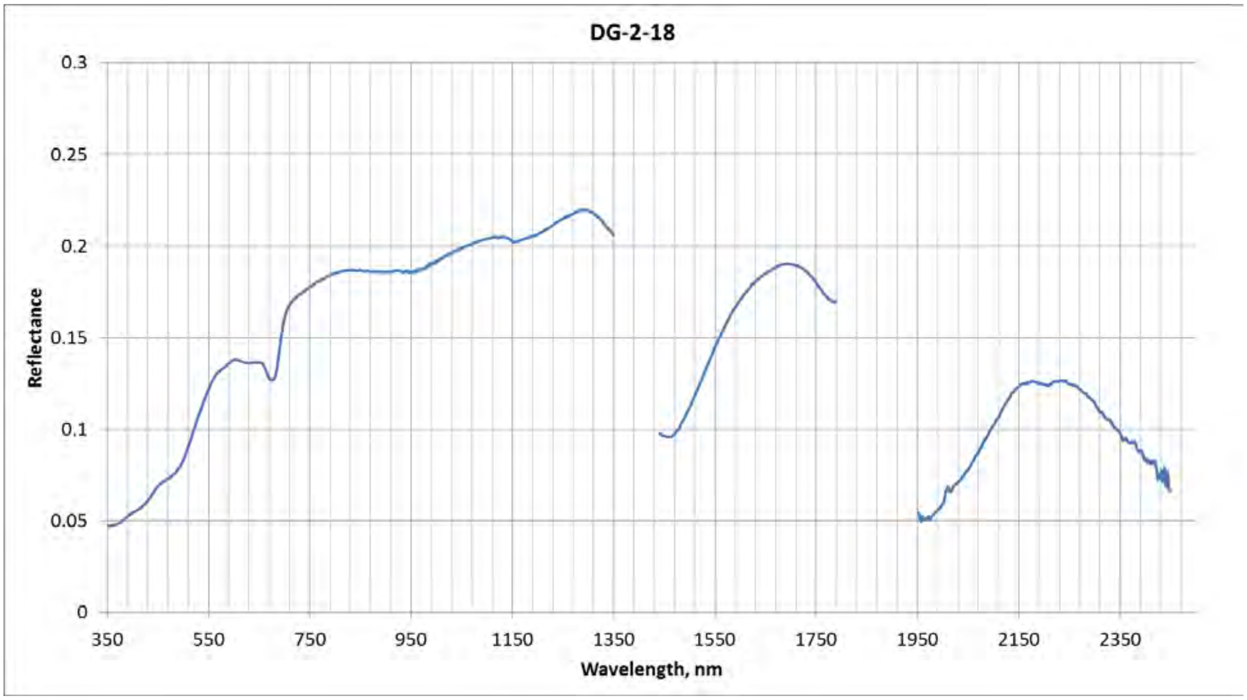
DG-2-18
Reflectance
Wavelength, nm
0.3
0.25
0.2
0.15
0.1
0.05
0
350
550
750
950
1150
1350
1550
1750
1950
2150
2350

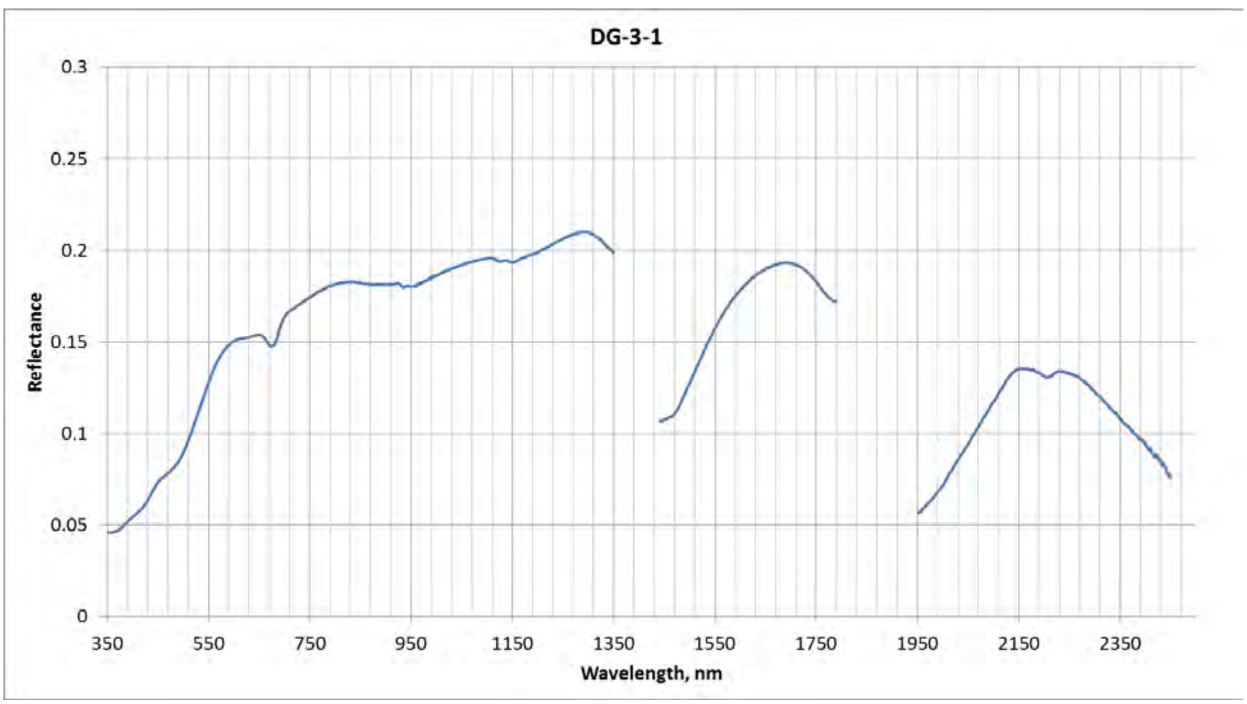
DG-3-1
Reflectance
Wavelength, nm
0.3
0.25
0.2
0.15
0.1
0.05
0
350
550
750
950
1150
1350
1550
1750
1950
2150
2350


DG-3-2
Reflectance
0.3
0.25
0.2
0.15
0.1
0.05
0
350
550
750
950
1150
1350
1550
1750
1950
2150
2350
Wavelength, nm

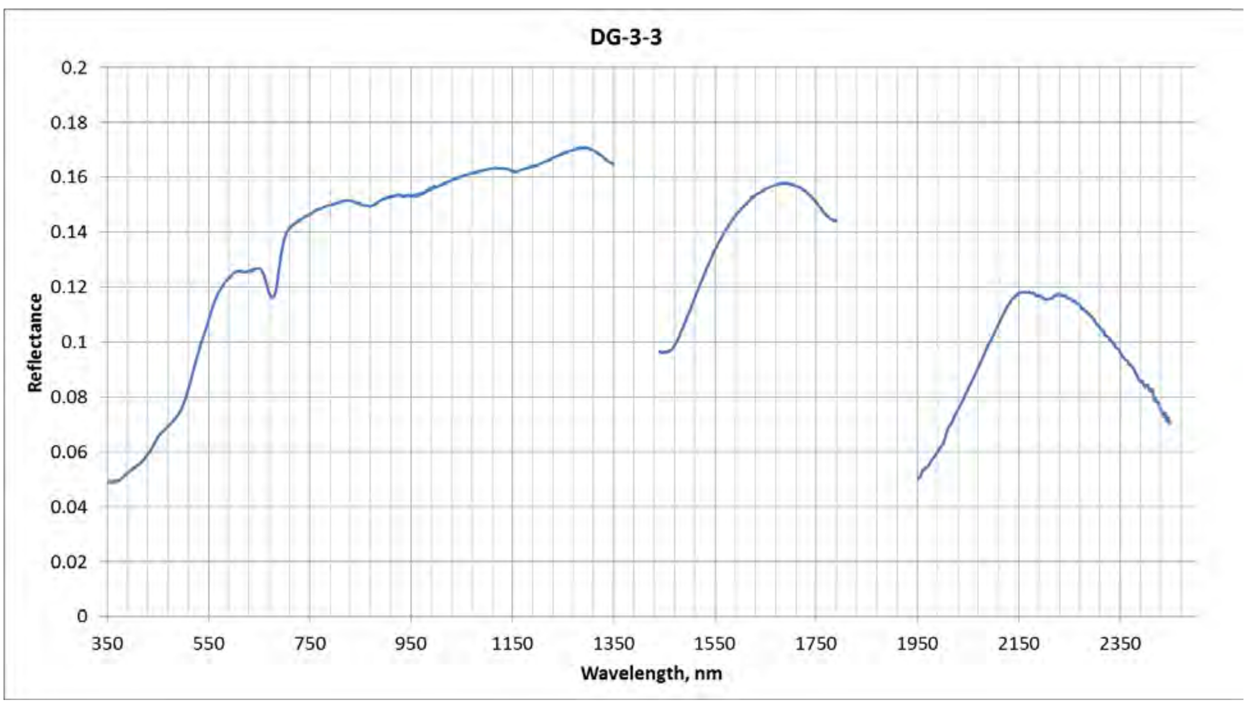
DG-3-3
Reflectance
0.2
0.18
0.16
0.14
0.12
0.1
0.08
0.06
0.04
0.02
0
350
550
750
950
1150
1350
1550
1750
1950
2150
2350
Wavelength, nm

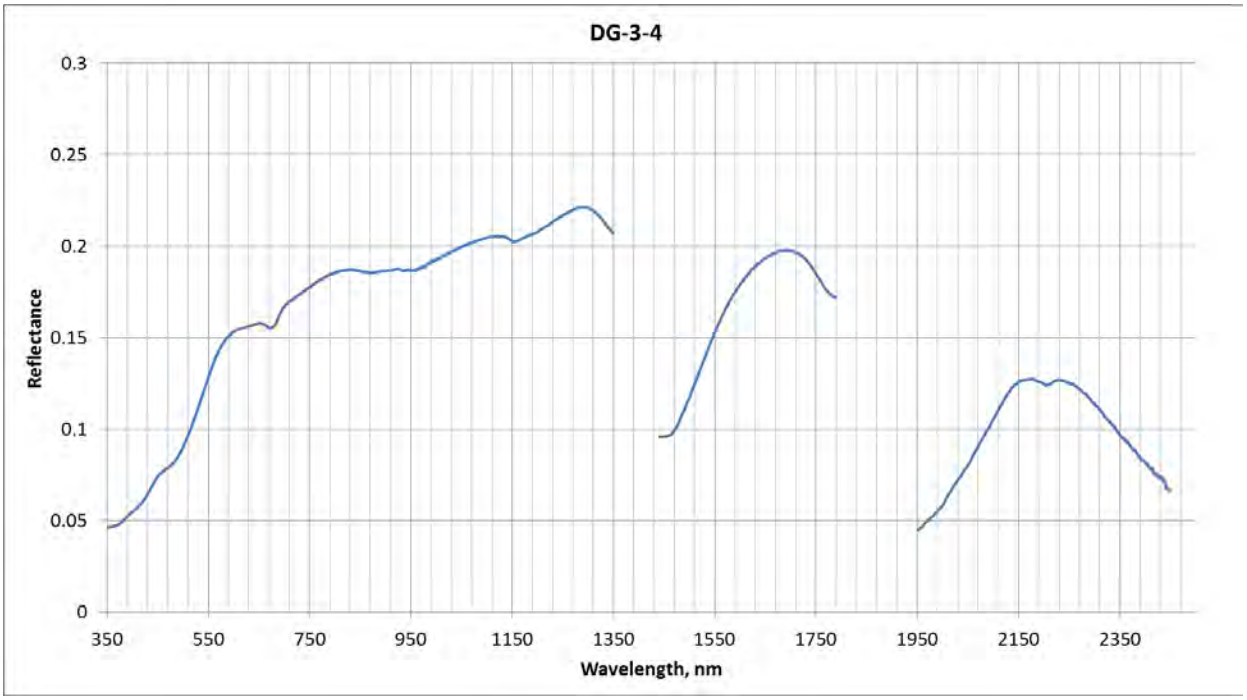
DG-3-4
Reflectance
Wavelength, nm
0.3
0.25
0.2
0.15
0.1
0.05
0
350 550 750 950 1150 1350 1550 1750 1950 2150 2350

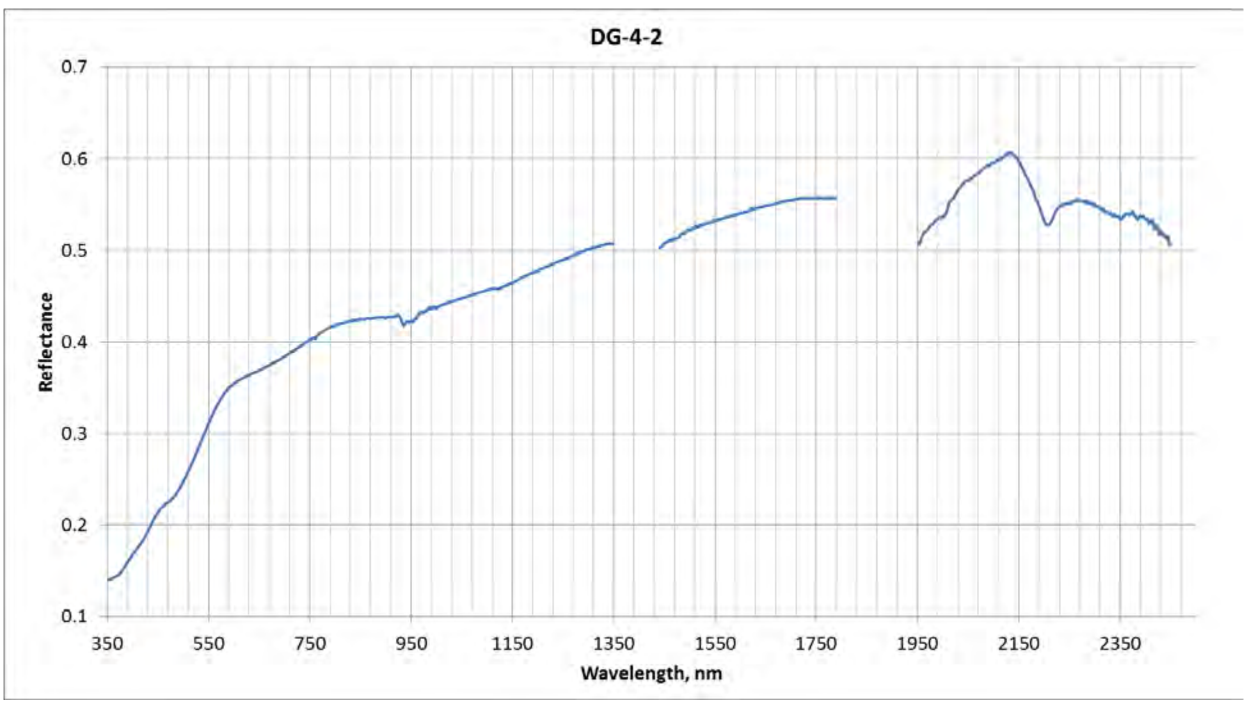
DG-4-2
Reflectance
Wavelength, nm
0.7
0.6
0.5
0.4
0.3
0.2
0.1
350 550 750 950 1150 1350 1550 1750 1950 2150 2350

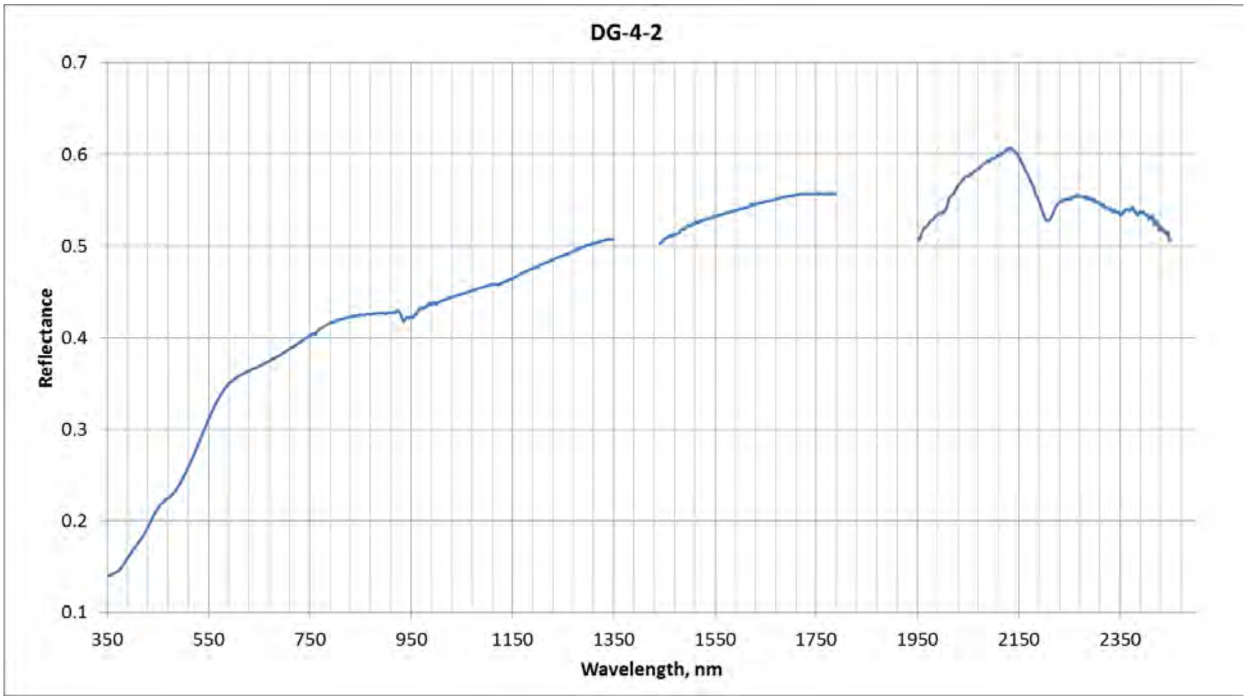
DG-4-2
Reflectance
0.7
0.6
0.5
0.4
0.3
0.2
0.1
350
550
750
950
1150
1350
1550
1750
1950
2150
2350
Wavelength, nm

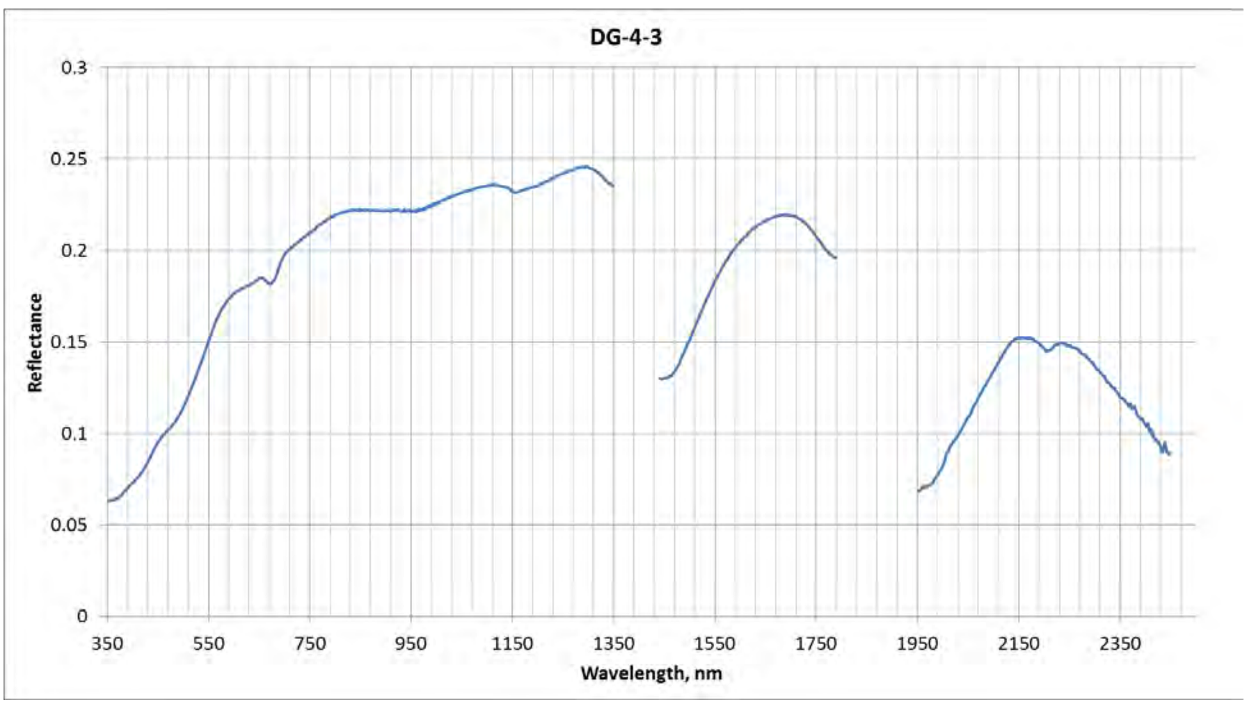
DG-4-3
Reflectance
0.3
0.25
0.2
0.15
0.1
0.05
0
350
550
750
950
1150
1350
1550
1750
1950
2150
2350
Wavelength, nm

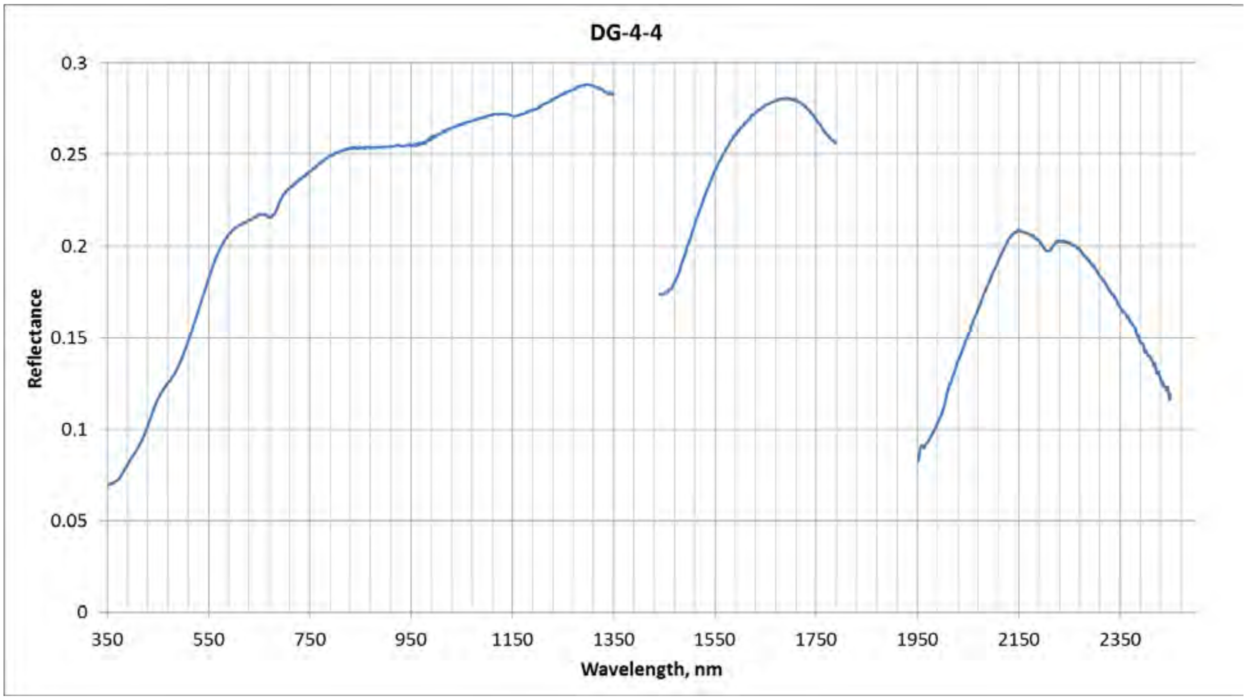
DG-4-4
Reflectance
Wavelength, nm
0.3
0.25
0.2
0.15
0.1
0.05
0
350
550
750
950
1150
1350
1550
1750
1950
2150
2350

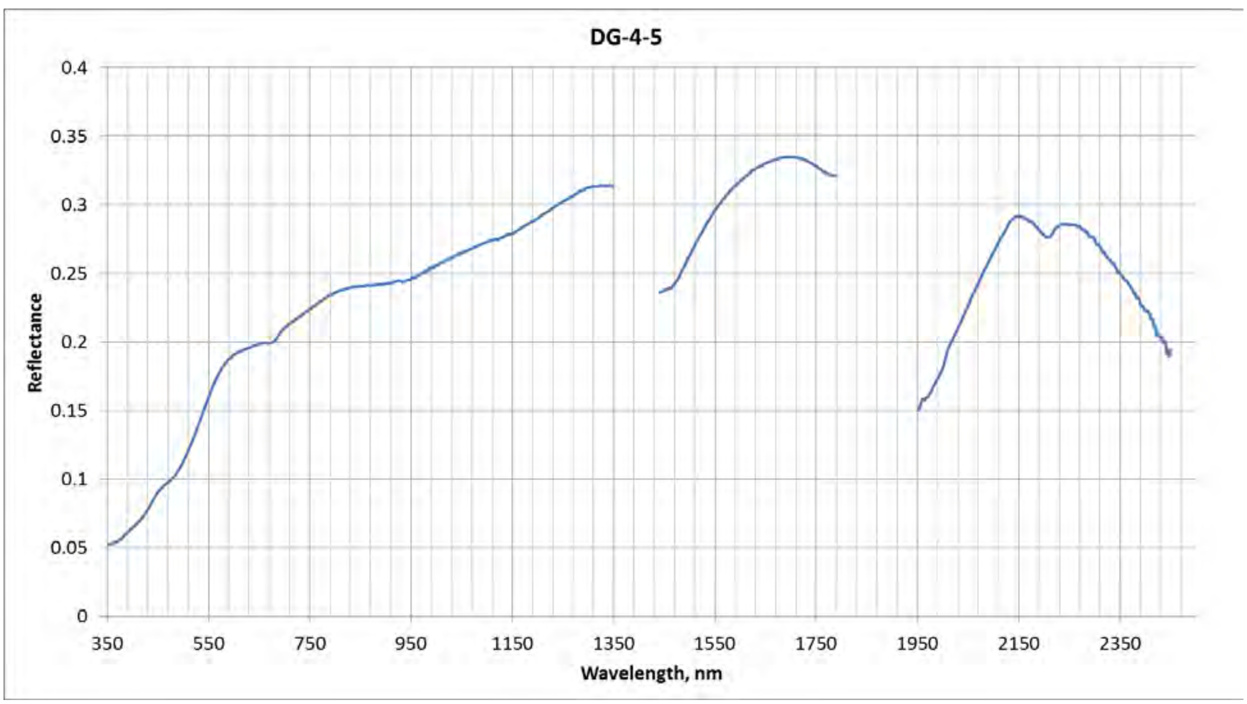
DG-4-5
Reflectance
Wavelength, nm
0.4
0.35
0.3
0.25
0.2
0.15
0.1
0.05
0
350
550
750
950
1150
1350
1550
1750
1950
2150
2350

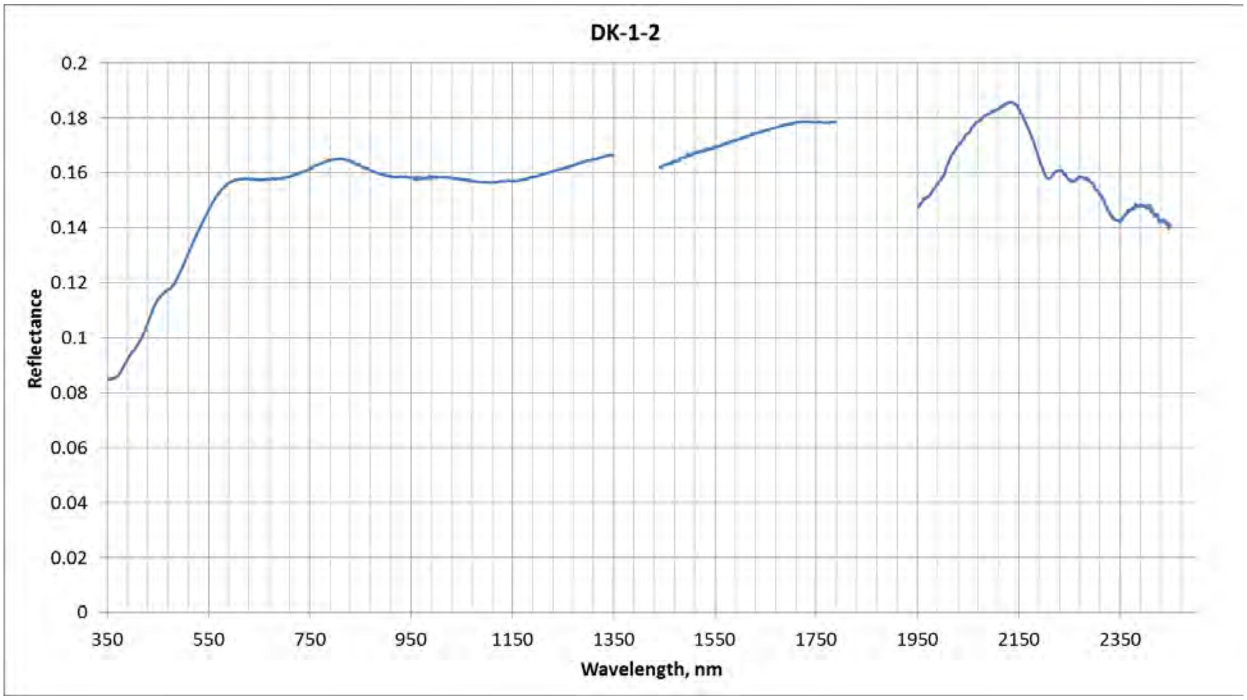

DK-1-2
Reflectance
0.2
0.18
0.16
0.14
0.12
0.1
0.08
0.06
0.04
0.02
0
350
550
750
950
1150
1350
1550
1750
1950
2150
2350
Wavelength, nm

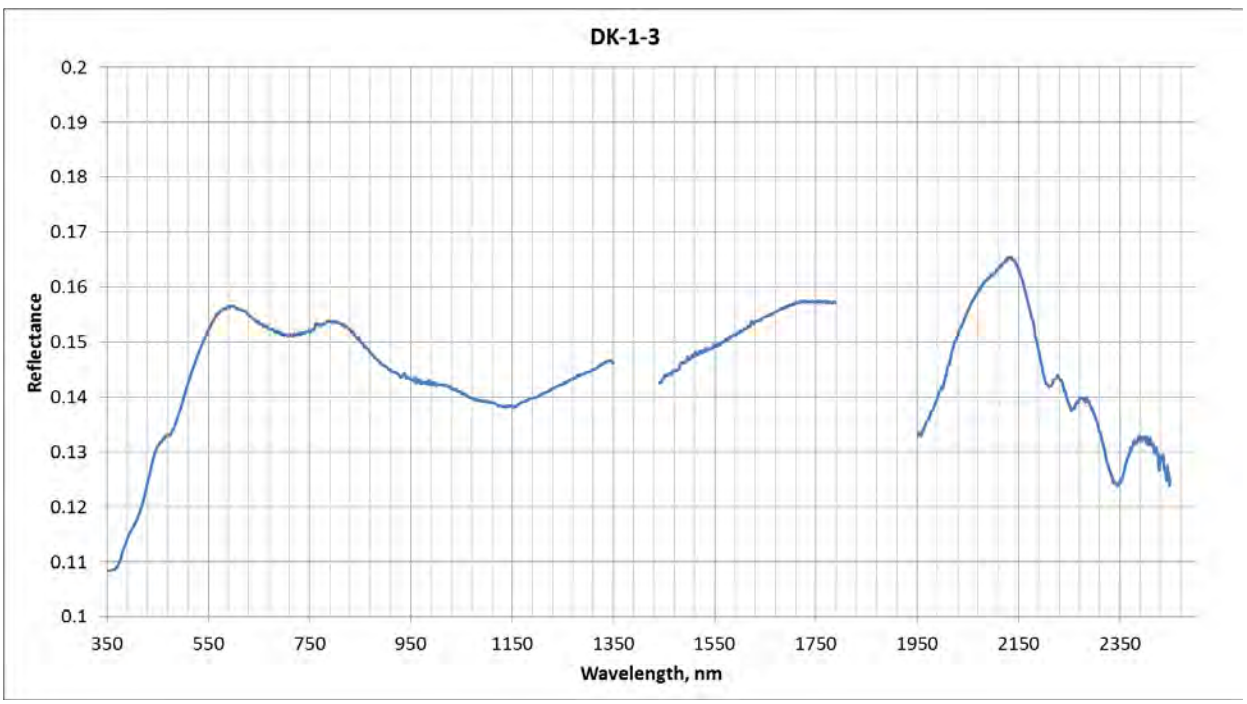

DK-1-3
Reflectance
0.2
0.19
0.18
0.17
0.16
0.15
0.14
0.13
0.12
0.11
0.1
350
550
750
950
1150
1350
1550
1750
1950
2150
2350
Wavelength, nm

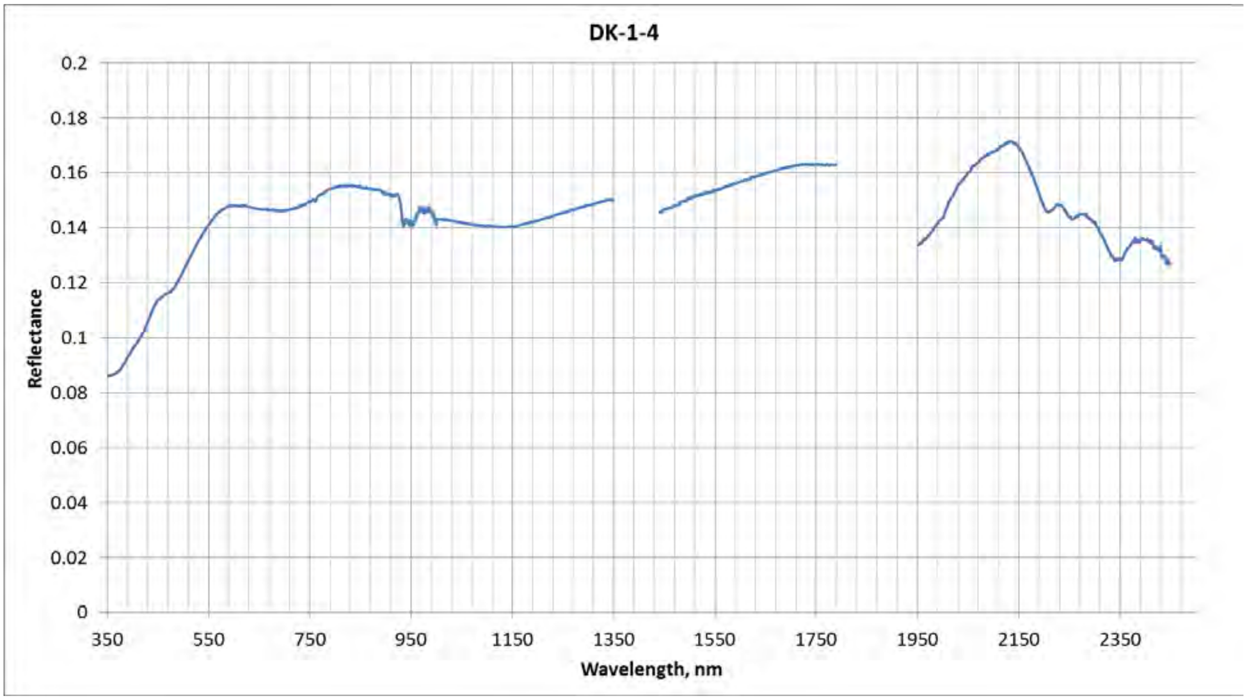
DK-1-4
Reflectance
Wavelength, nm
0.2
0.18
0.16
0.14
0.12
0.1
0.08
0.06
0.04
0.02
0
350
550
750
950
1150
1350
1550
1750
1950
2150
2350

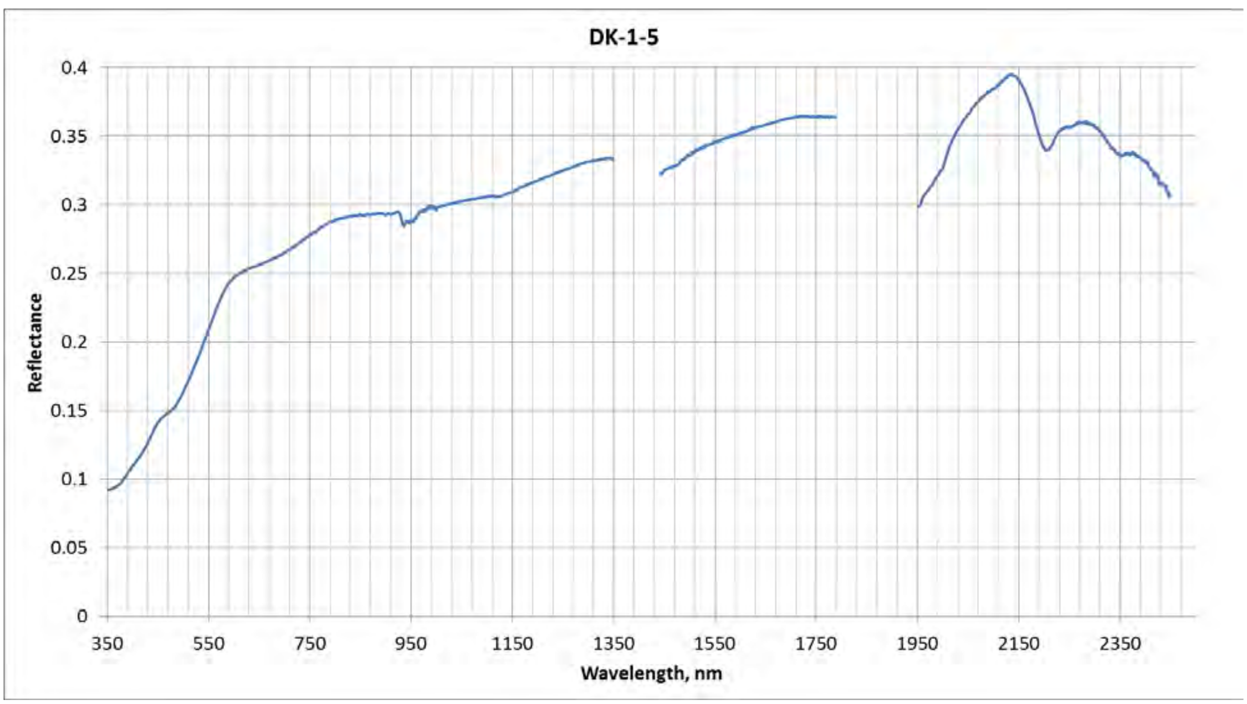
DK-1-5
Reflectance
Wavelength, nm
0.4
0.35
0.3
0.25
0.2
0.15
0.1
0.05
0
350
550
750
950
1150
1350
1550
1750
1950
2150
2350

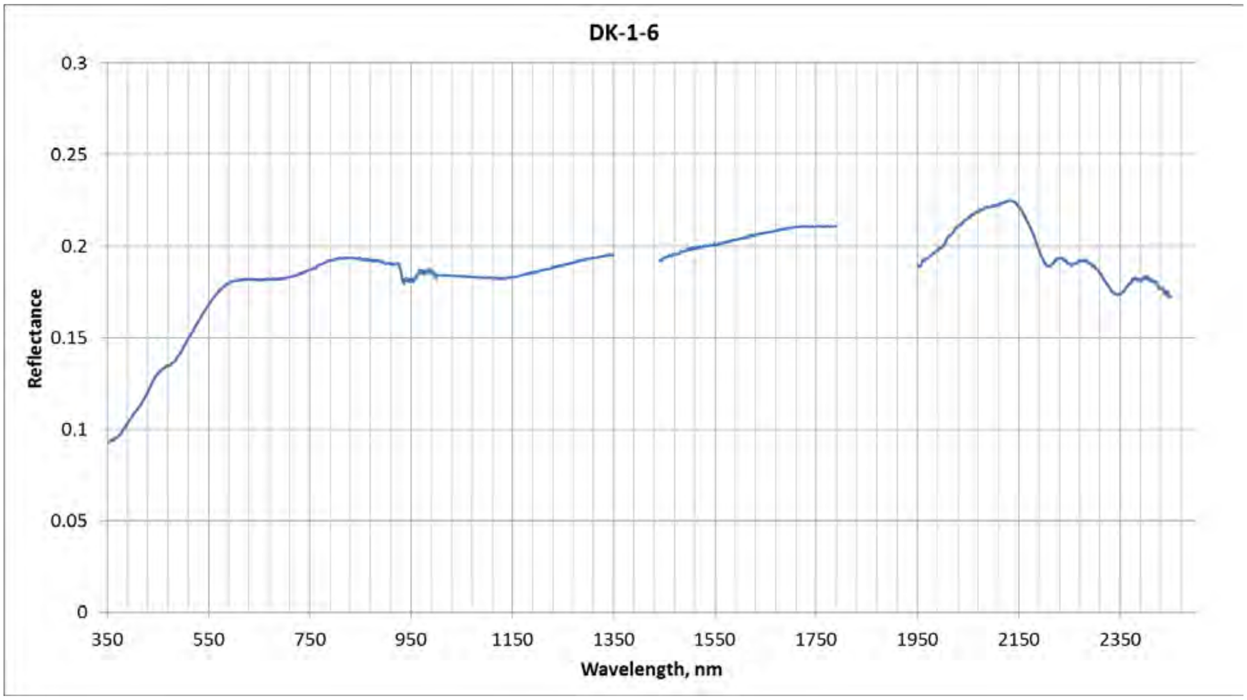
DK-1-6
Reflectance
0.3
0.25
0.2
0.15
0.1
0.05
0
350
550
750
950
1150
1350
1550
1750
1950
2150
2350
Wavelength, nm

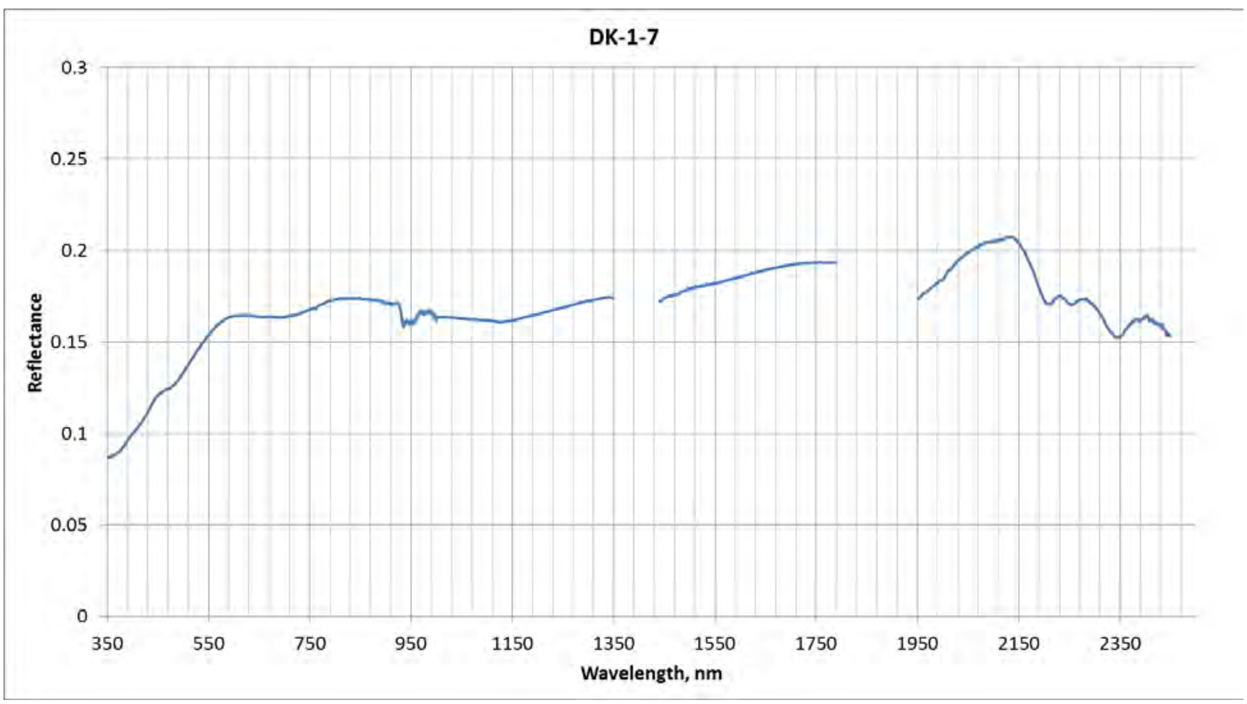
DK-1-7
Reflectance
0.3
0.25
0.2
0.15
0.1
0.05
0
350
550
750
950
1150
1350
1550
1750
1950
2150
2350
Wavelength, nm

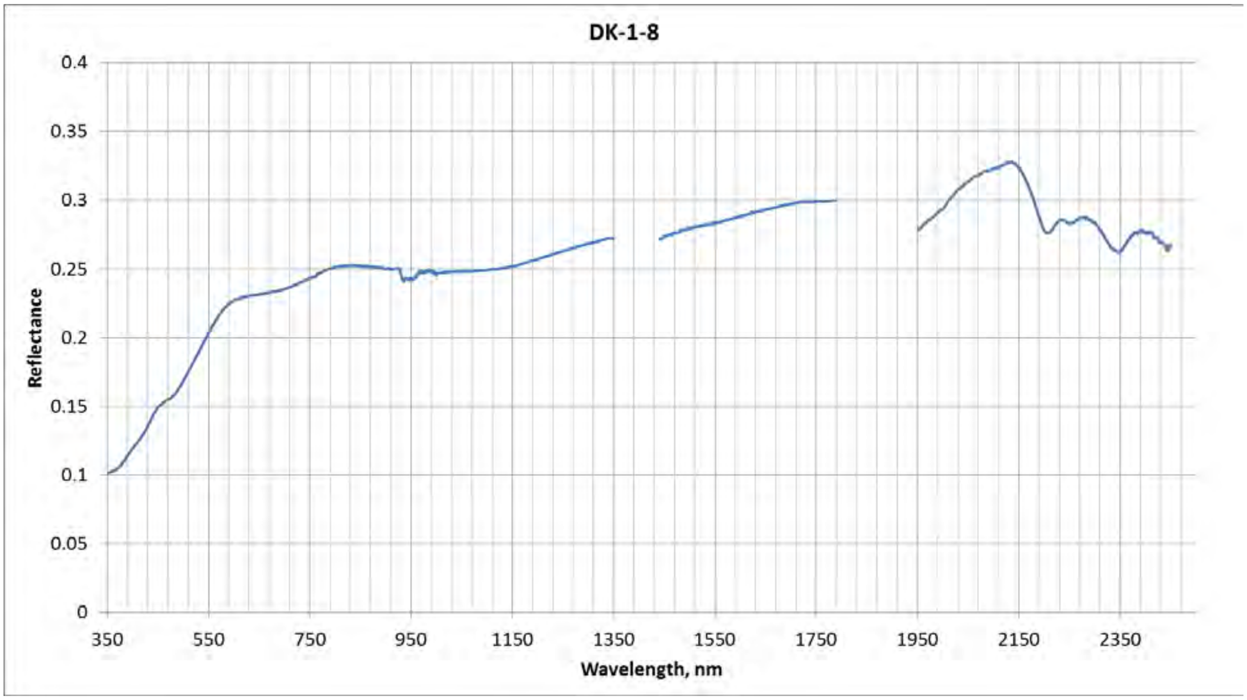
DK-1-8
Reflectance
Wavelength, nm
0.4
0.35
0.3
0.25
0.2
0.15
0.1
0.05
0
350
550
750
950
1150
1350
1550
1750
1950
2150
2350

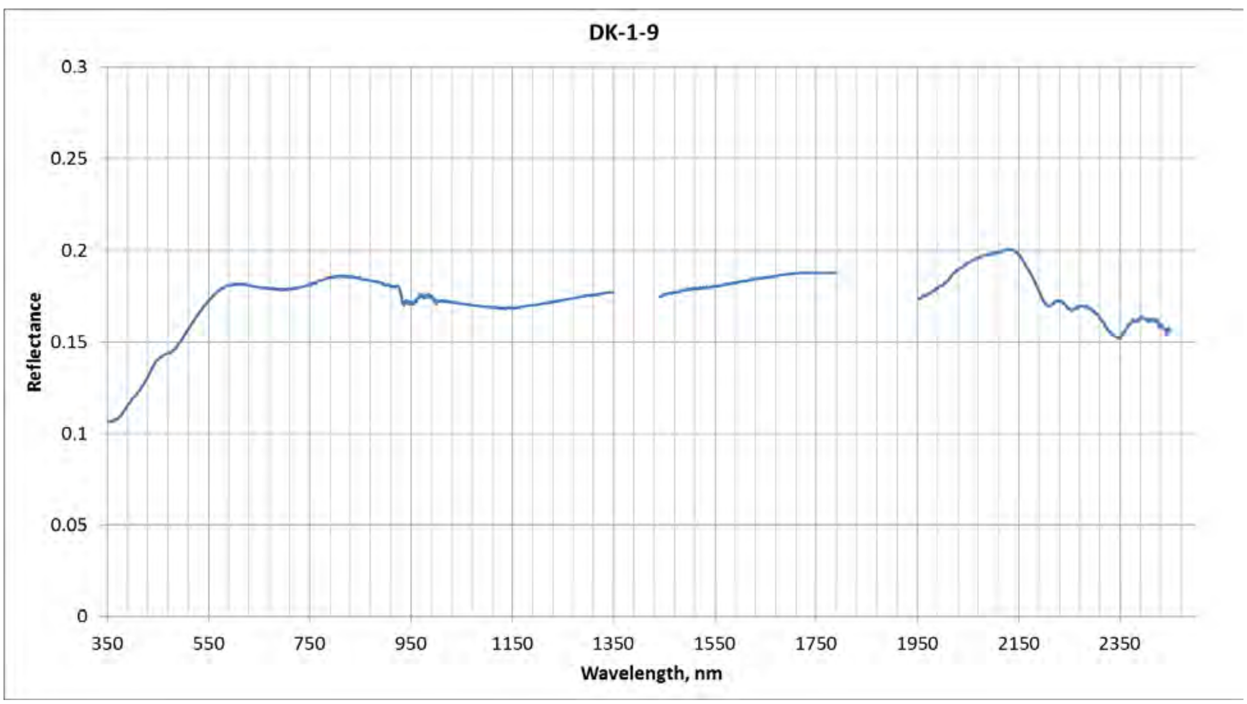
DK-1-9
Reflectance
Wavelength, nm
0.3
0.25
0.2
0.15
0.1
0.05
0
350
550
750
950
1150
1350
1550
1750
1950
2150
2350

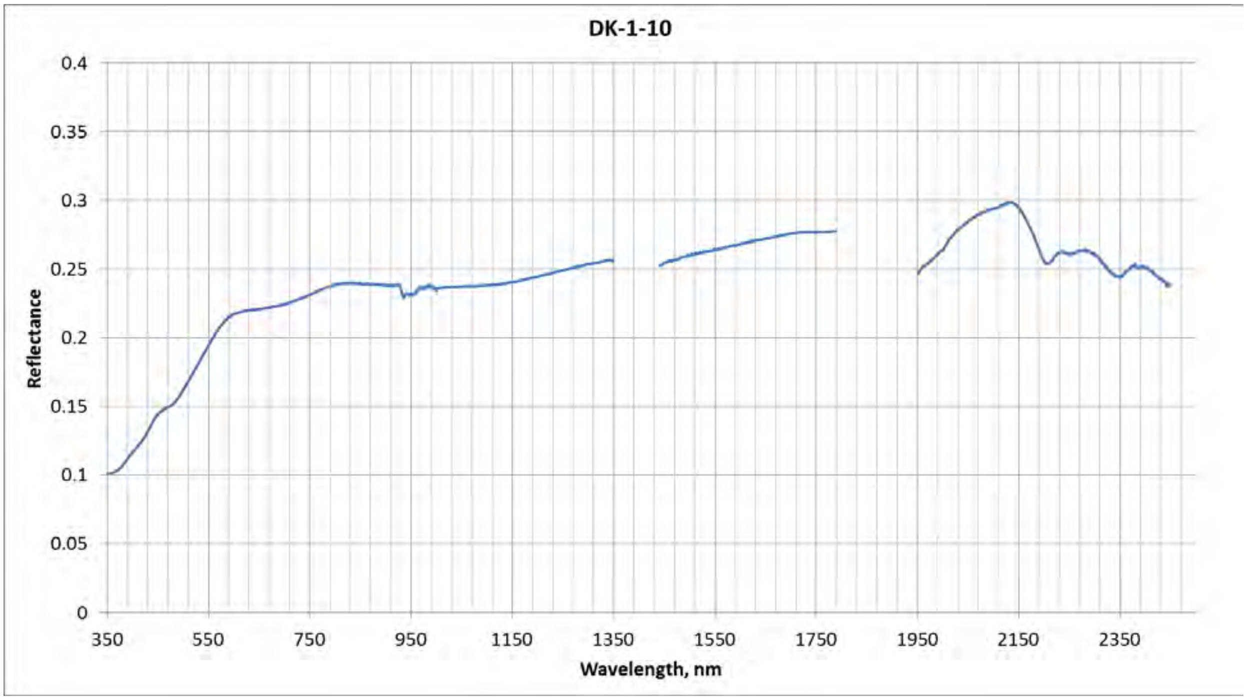
DK-1-10
Reflectance
0.4
0.35
0.3
0.25
0.2
0.15
0.1
0.05
0
350
550
750
950
1150
1350
1550
1750
1950
2150
2350
Wavelength, nm

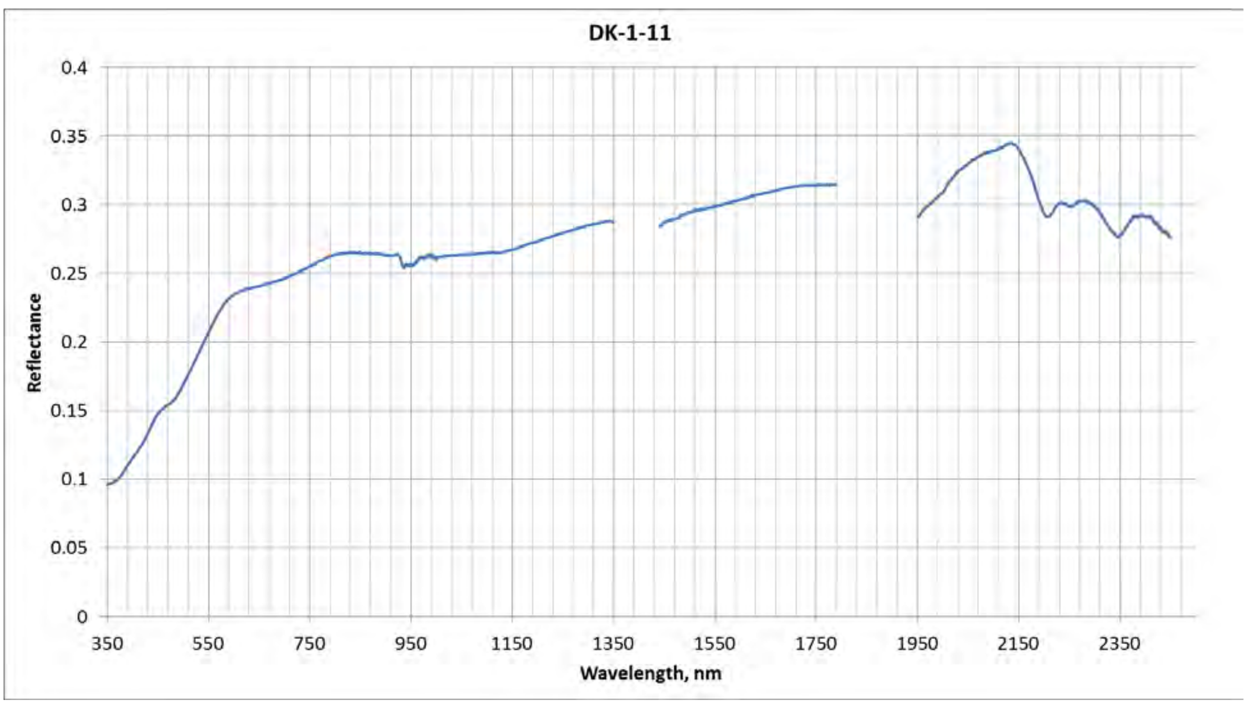
DK-1-11
Reflectance
0.4
0.35
0.3
0.25
0.2
0.15
0.1
0.05
0
350
550
750
950
1150
1350
1550
1750
1950
2150
2350
Wavelength, nm

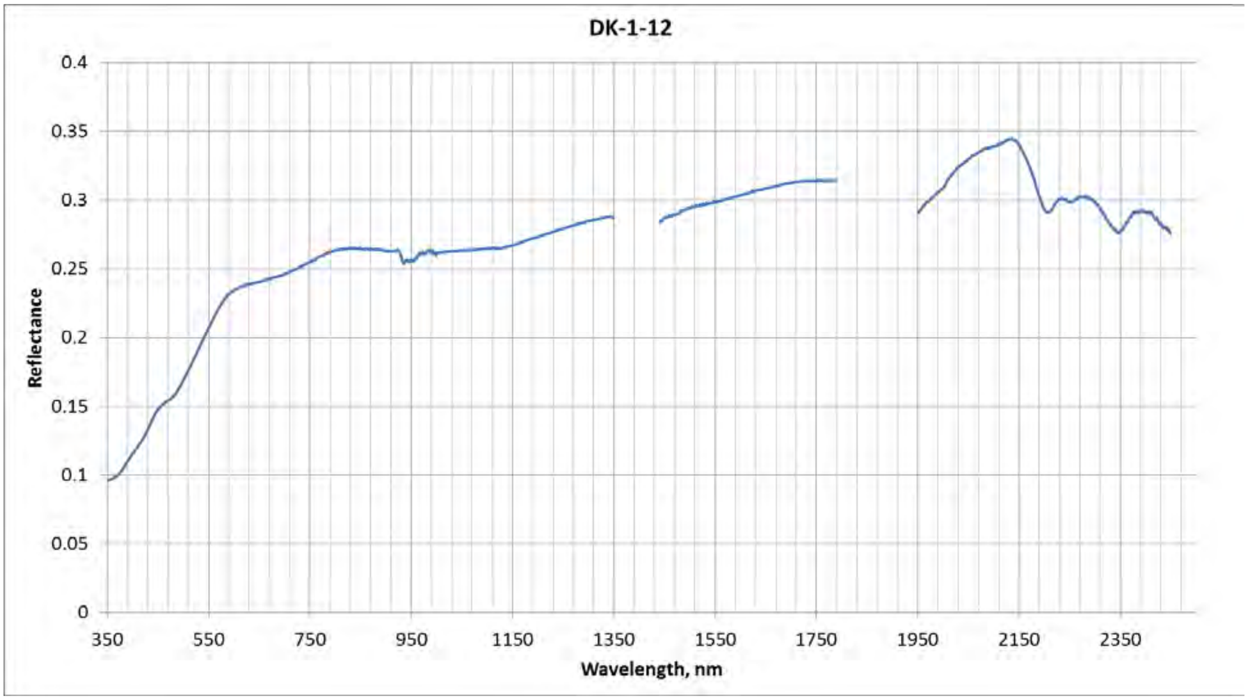
DK-1-12
Reflectance
Wavelength, nm
0.4
0.35
0.3
0.25
0.2
0.15
0.1
0.05
0
350
550
750
950
1150
1350
1550
1750
1950
2150
2350

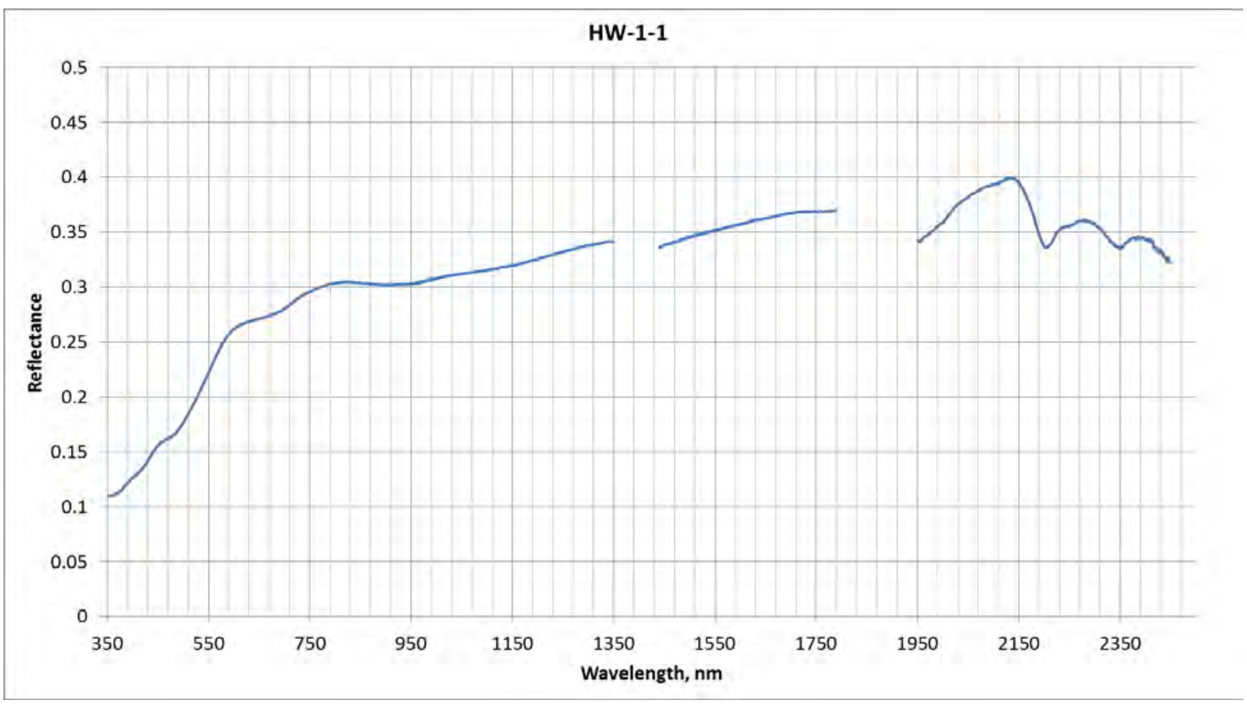
HW-1-1
Reflectance
Wavelength, nm
0.5
0.45
0.4
0.35
0.3
0.25
0.2
0.15
0.1
0.05
0
350
550
750
950
1150
1350
1550
1750
1950
2150
2350

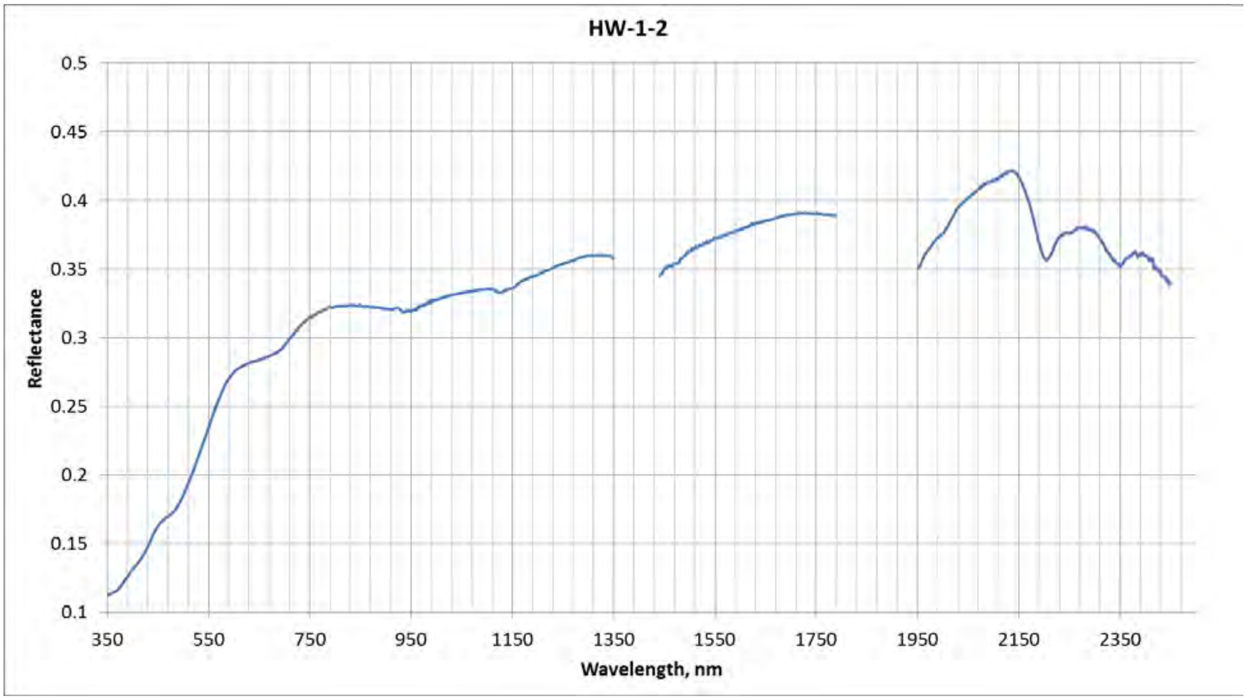
HW-1-2
Reflectance
Wavelength, nm
0.5
0.45
0.4
0.35
0.3
0.25
0.2
0.15
0.1
350
550
750
950
1150
1350
1550
1750
1950
2150
2350

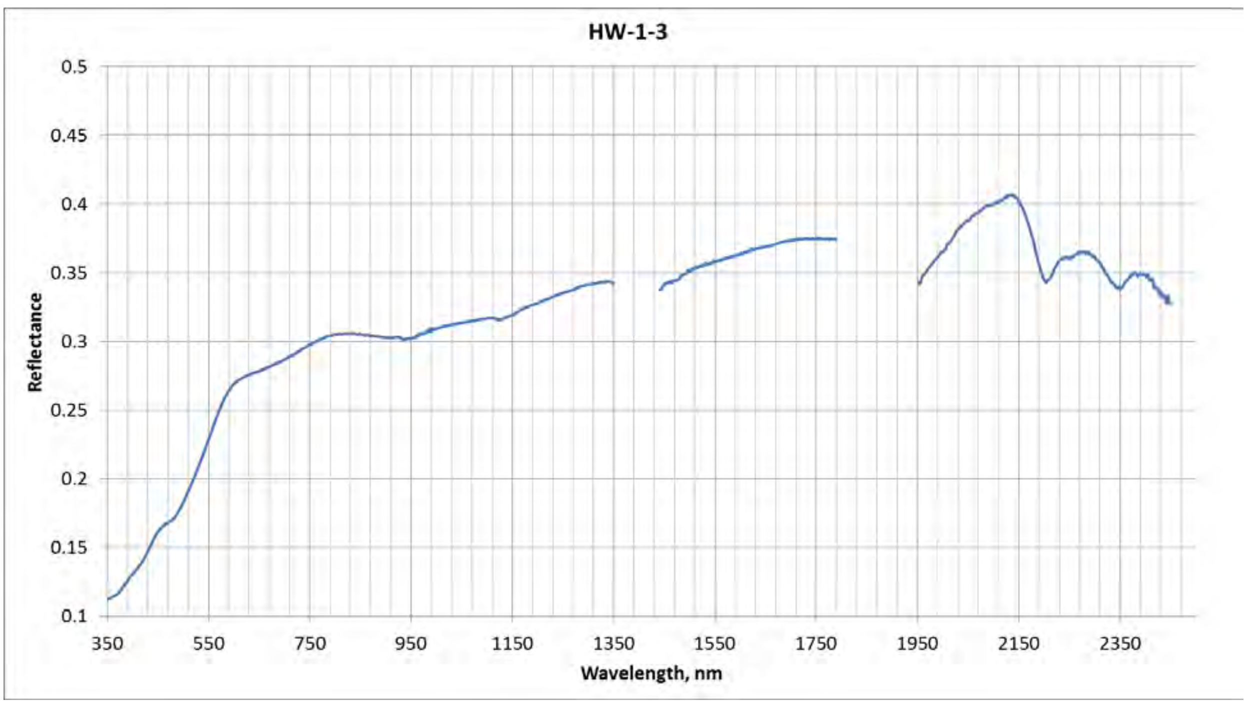
HW-1-3
Reflectance
Wavelength, nm
0.5
0.45
0.4
0.35
0.3
0.25
0.2
0.15
0.1
350
550
750
950
1150
1350
1550
1750
1950
2150
2350

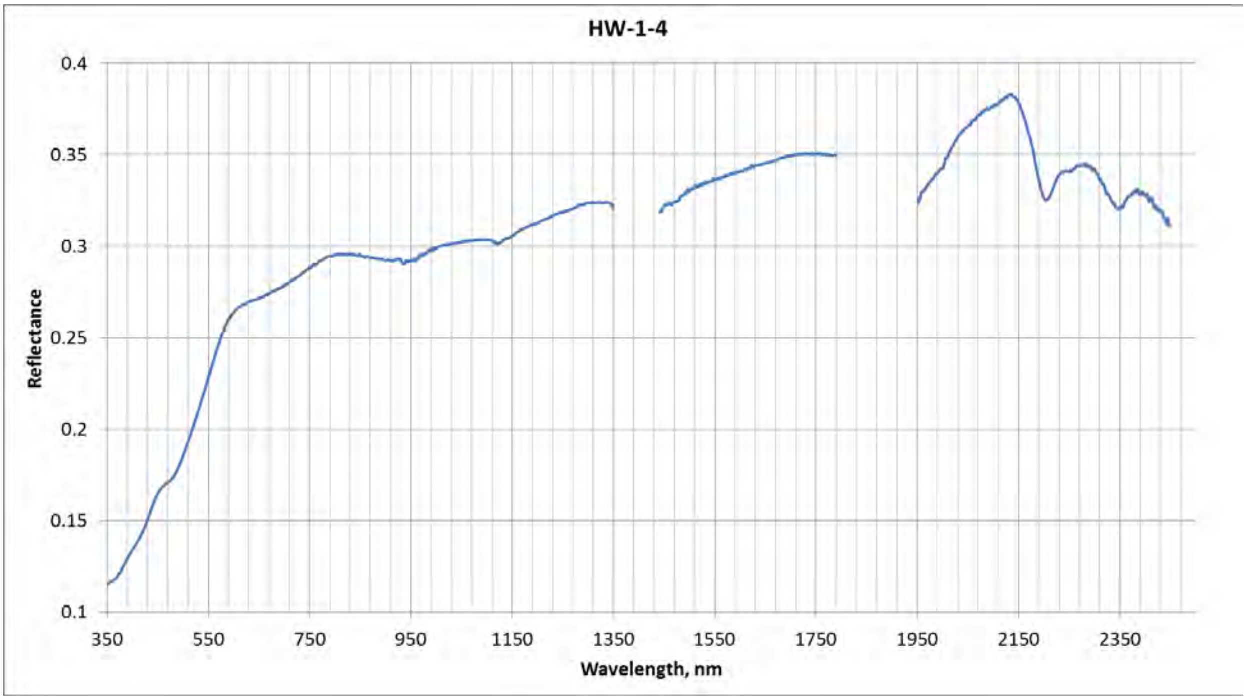
HW-1-4
Reflectance
Wavelength, nm
0.4
0.35
0.3
0.25
0.2
0.15
0.1
350
550
750
950
1150
1350
1550
1750
1950
2150
2350

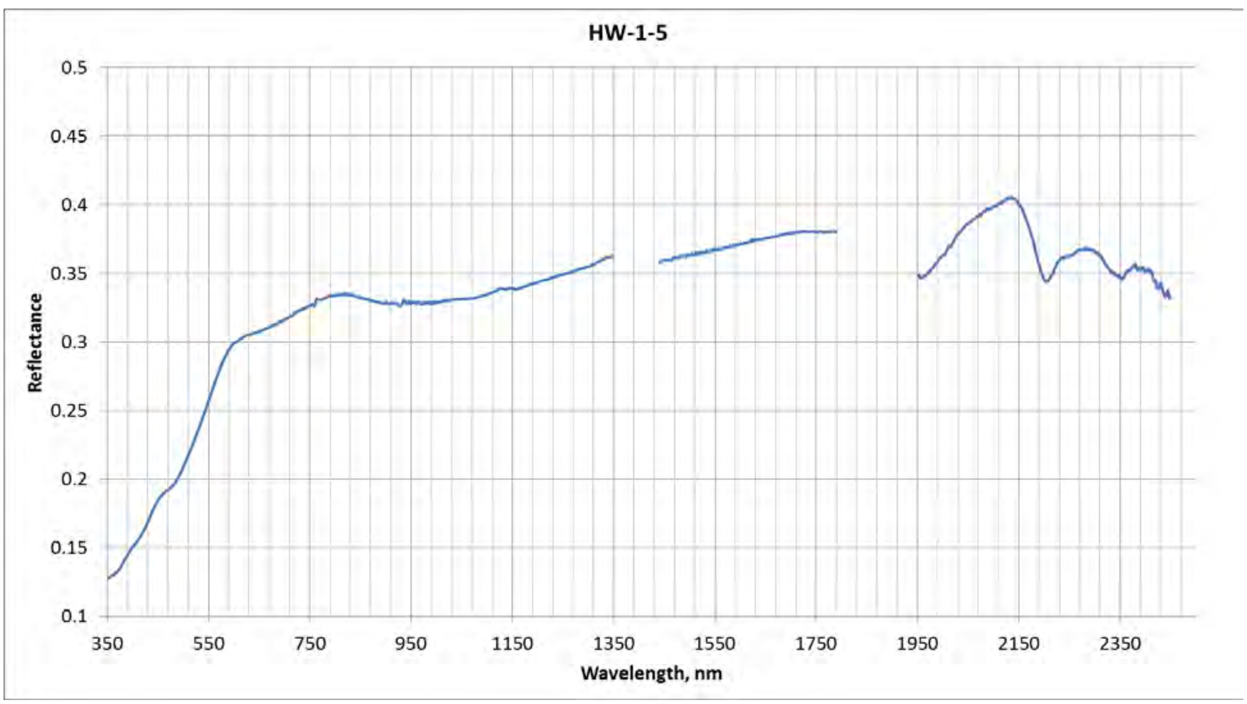
HW-1-5
Reflectance
Wavelength, nm
0.5
0.45
0.4
0.35
0.3
0.25
0.2
0.15
0.1
350
550
750
950
1150
1350
1550
1750
1950
2150
2350

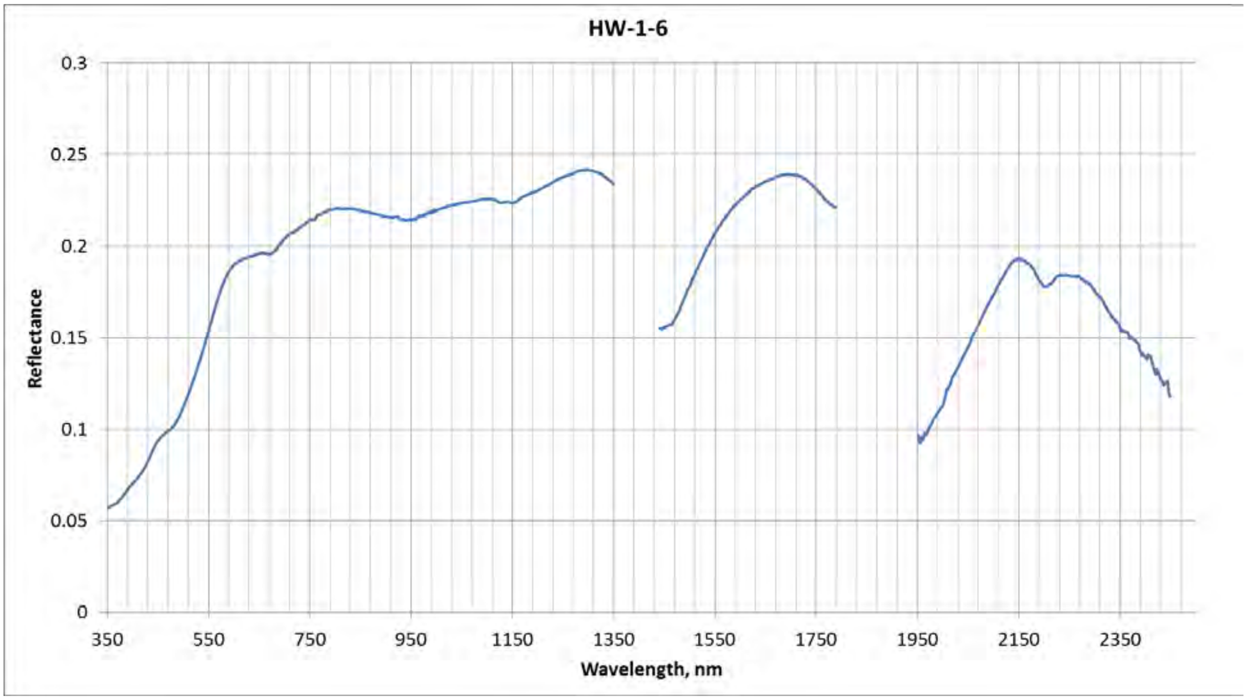
HW-1-6
Reflectance
Wavelength, nm
0.3
0.25
0.2
0.15
0.1
0.05
0
350
550
750
950
1150
1350
1550
1750
1950
2150
2350


HW-1-7
Reflectance
Wavelength, nm
0.3
0.25
0.2
0.15
0.1
0.05
0
350
550
750
950
1150
1350
1550
1750
1950
2150
2350

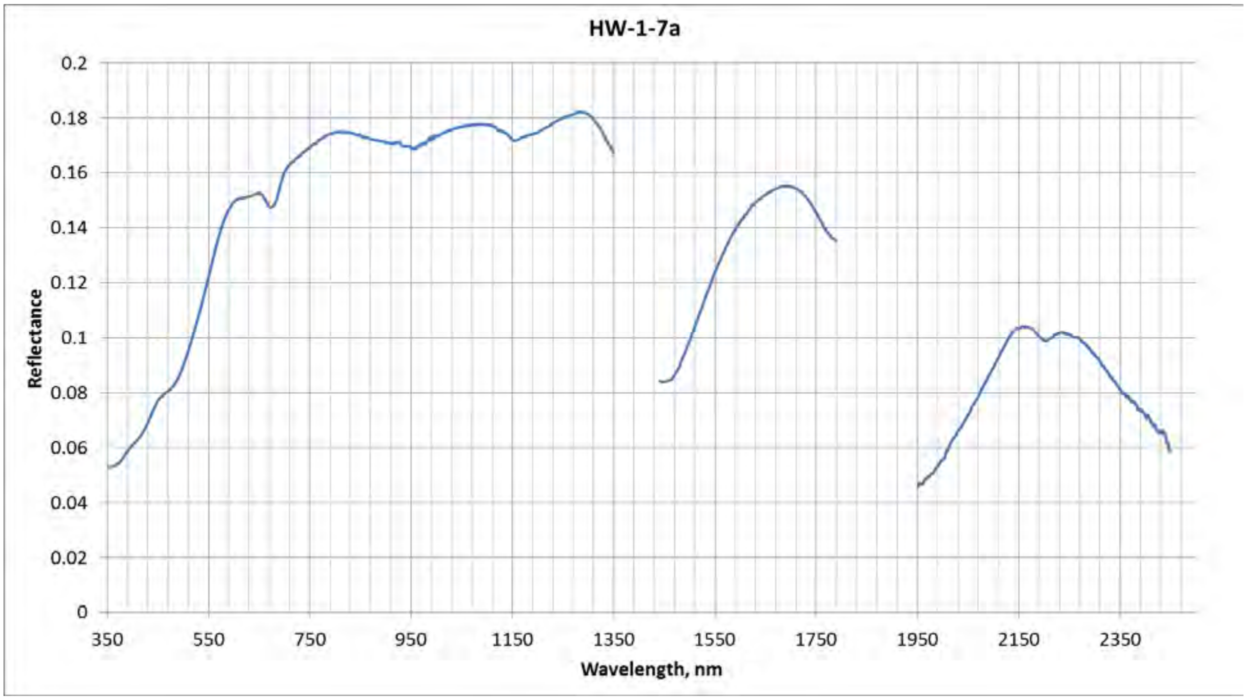
HW-1-7a
Reflectance
Wavelength, nm
0.2
0.18
0.16
0.14
0.12
0.1
0.08
0.06
0.04
0.02
0
350
550
750
950
1150
1350
1550
1750
1950
2150
2350

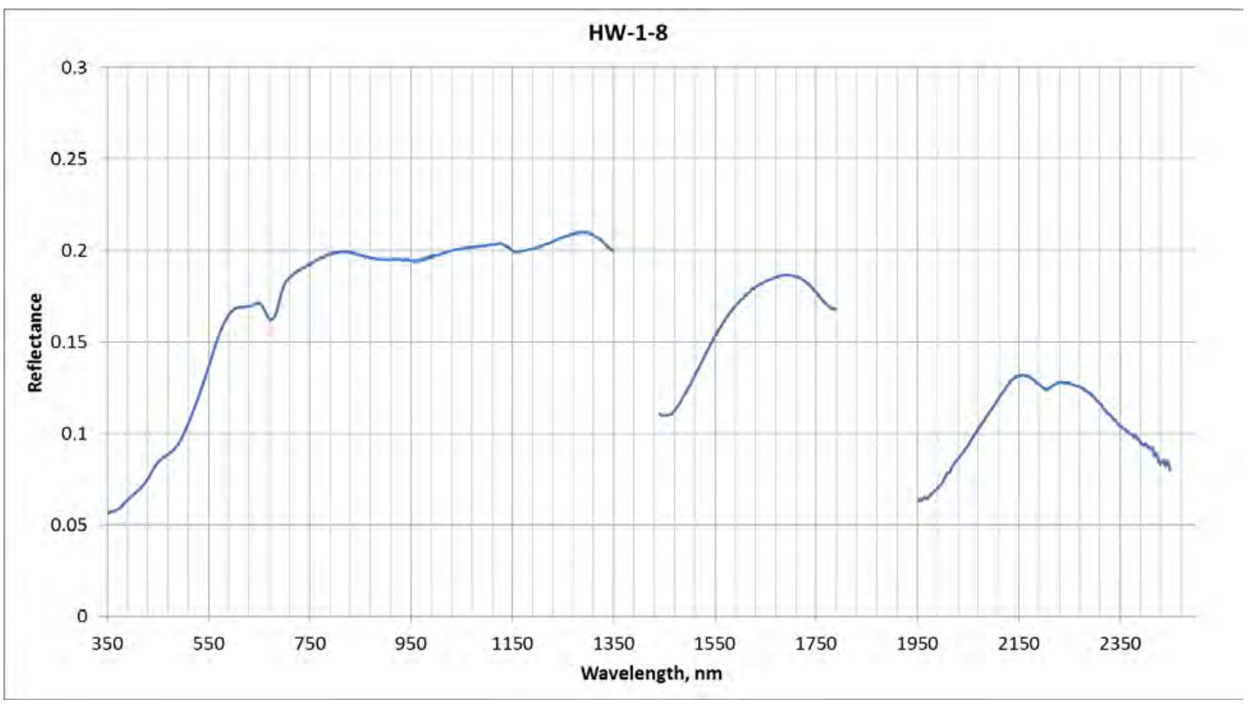
HW-1-8
Reflectance
Wavelength, nm
0.3
0.25
0.2
0.15
0.1
0.05
0
350
550
750
950
1150
1350
1550
1750
1950
2150
2350

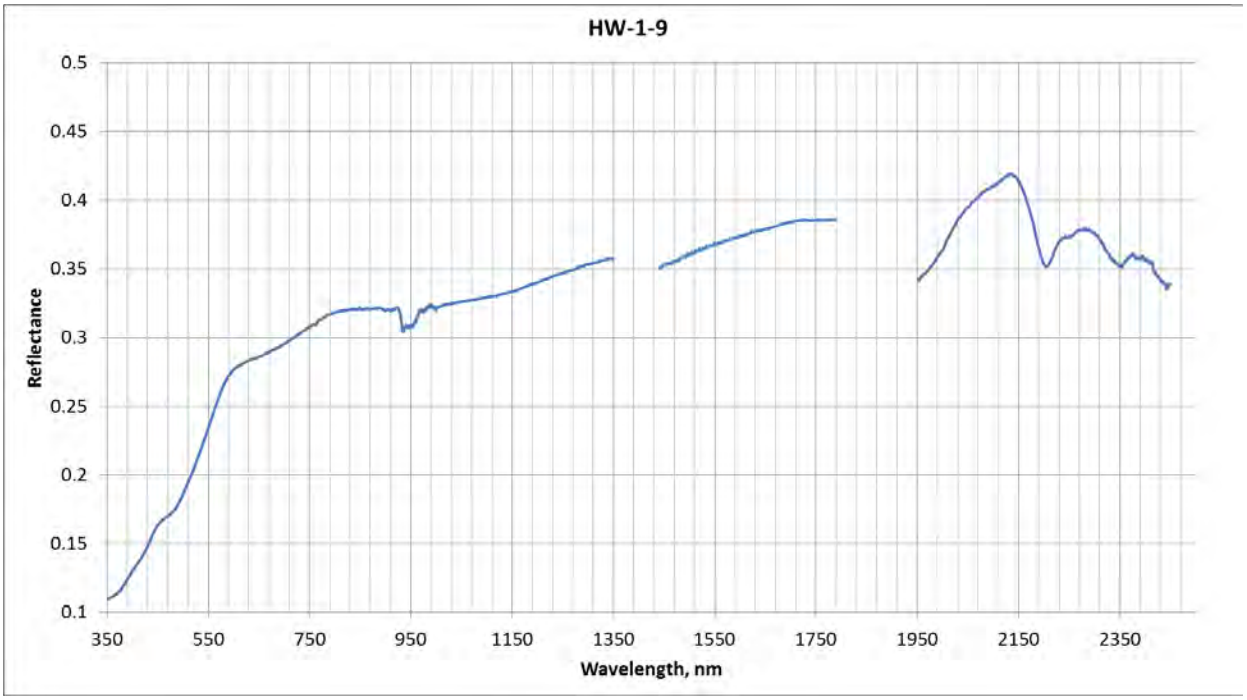
HW-1-9
Reflectance
Wavelength, nm
0.5
0.45
0.4
0.35
0.3
0.25
0.2
0.15
0.1
350
550
750
950
1150
1350
1550
1750
1950
2150
2350

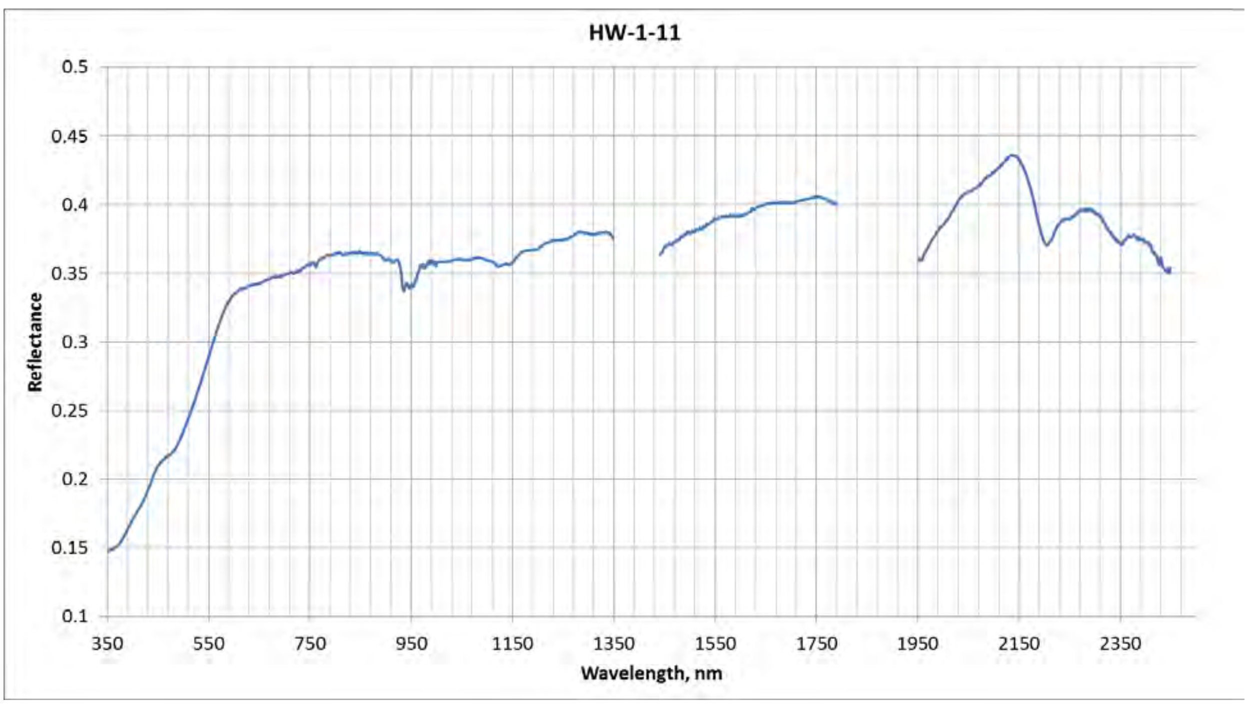
HW-1-11
Reflectance
Wavelength, nm
0.5
0.45
0.4
0.35
0.3
0.25
0.2
0.15
0.1
350
550
750
950
1150
1350
1550
1750
1950
2150
2350

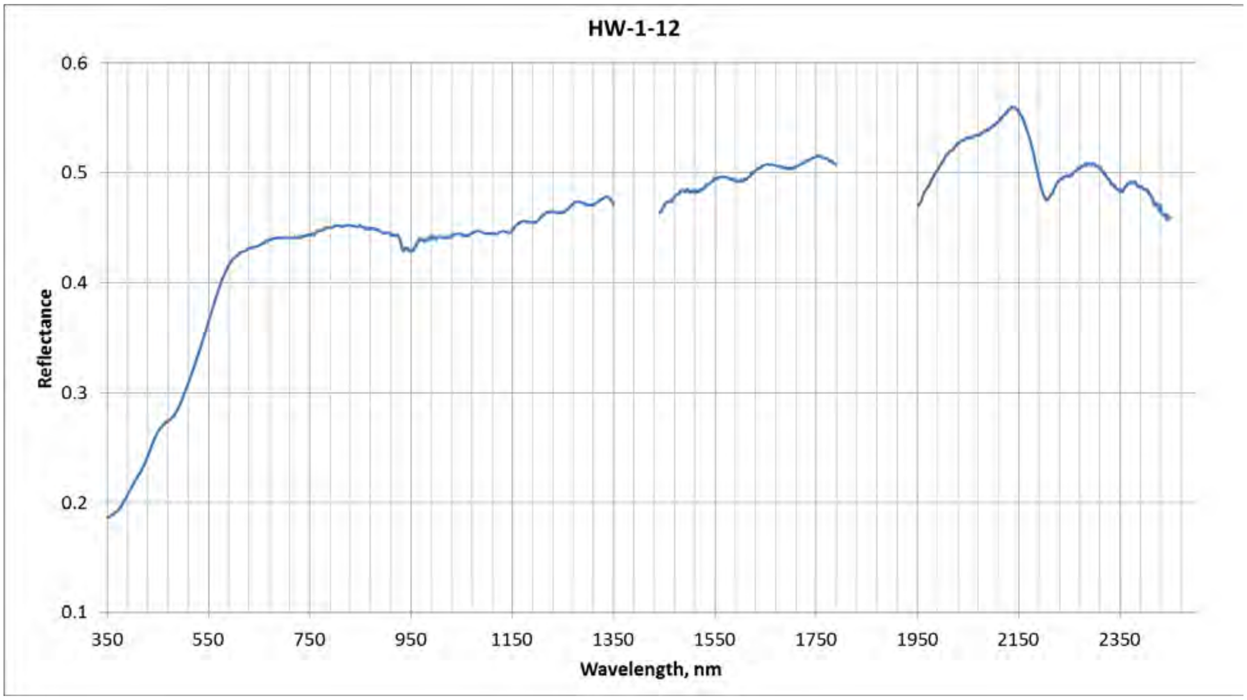
HW-1-12
0.6
0.5
0.4
0.3
0.2
0.1
Reflectance
350
550
750
950
1150
1350
1550
1750
1950
2150
2350
Wavelength, nm

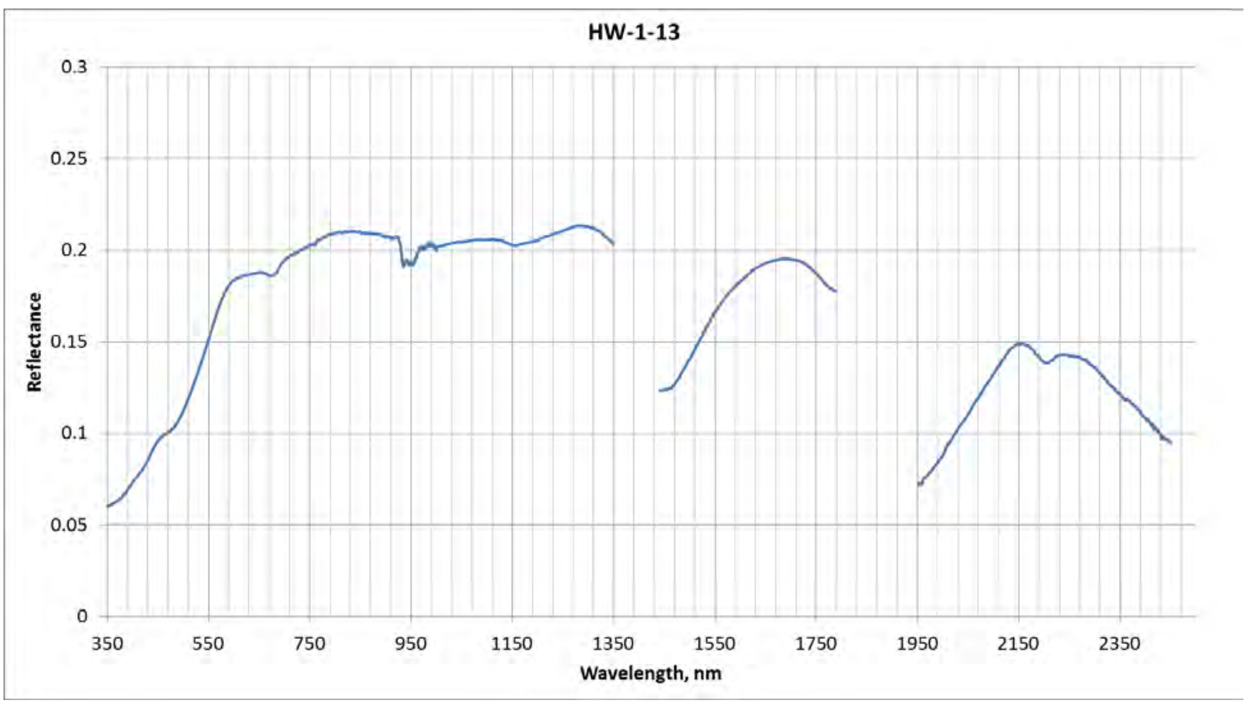
HW-1-13
0.3
0.25
0.2
0.15
0.1
0.05
0
Reflectance
350
550
750
950
1150
1350
1550
1750
1950
2150
2350
Wavelength, nm

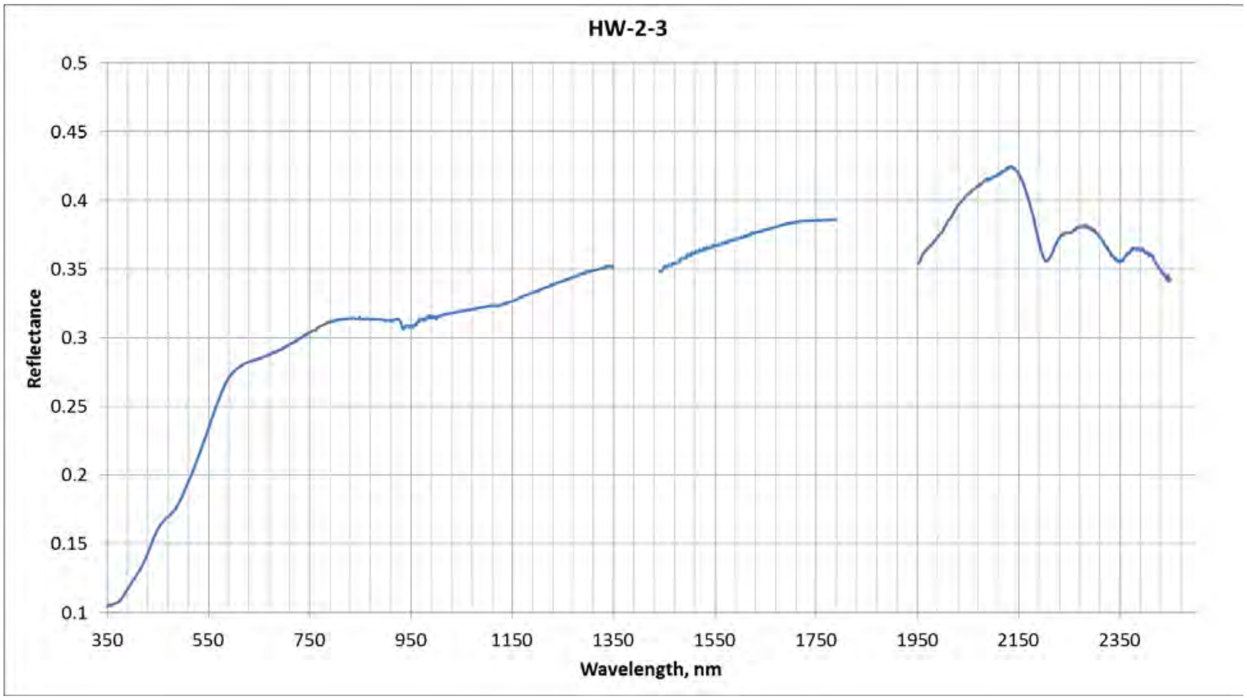
HW-2-3
Reflectance
0.5
0.45
0.4
0.35
0.3
0.25
0.2
0.15
0.1
350 550 750 950 1150 1350 1550 1750 1950 2150 2350
Wavelength, nm

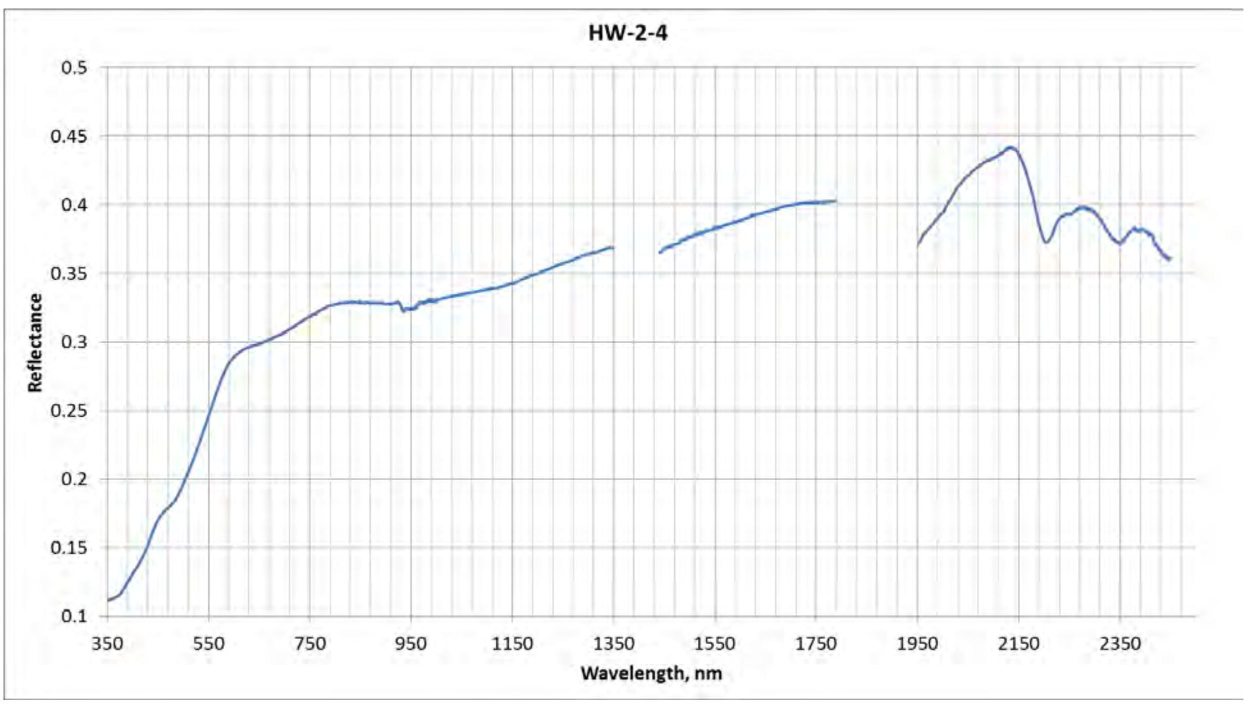
HW-2-4
Reflectance
0.5
0.45
0.4
0.35
0.3
0.25
0.2
0.15
0.1
350 550 750 950 1150 1350 1550 1750 1950 2150 2350
Wavelength, nm

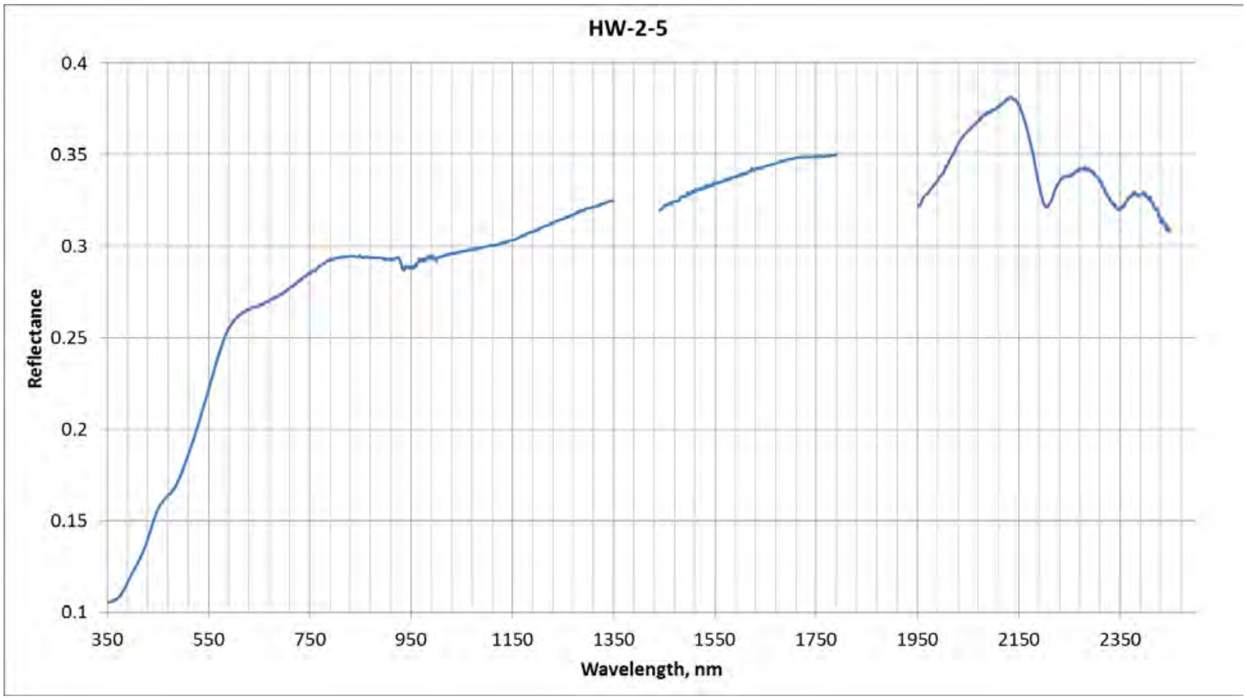
HW-2-5
Reflectance
Wavelength, nm
0.4
0.35
0.3
0.25
0.2
0.15
0.1
350
550
750
950
1150
1350
1550
1750
1950
2150
2350

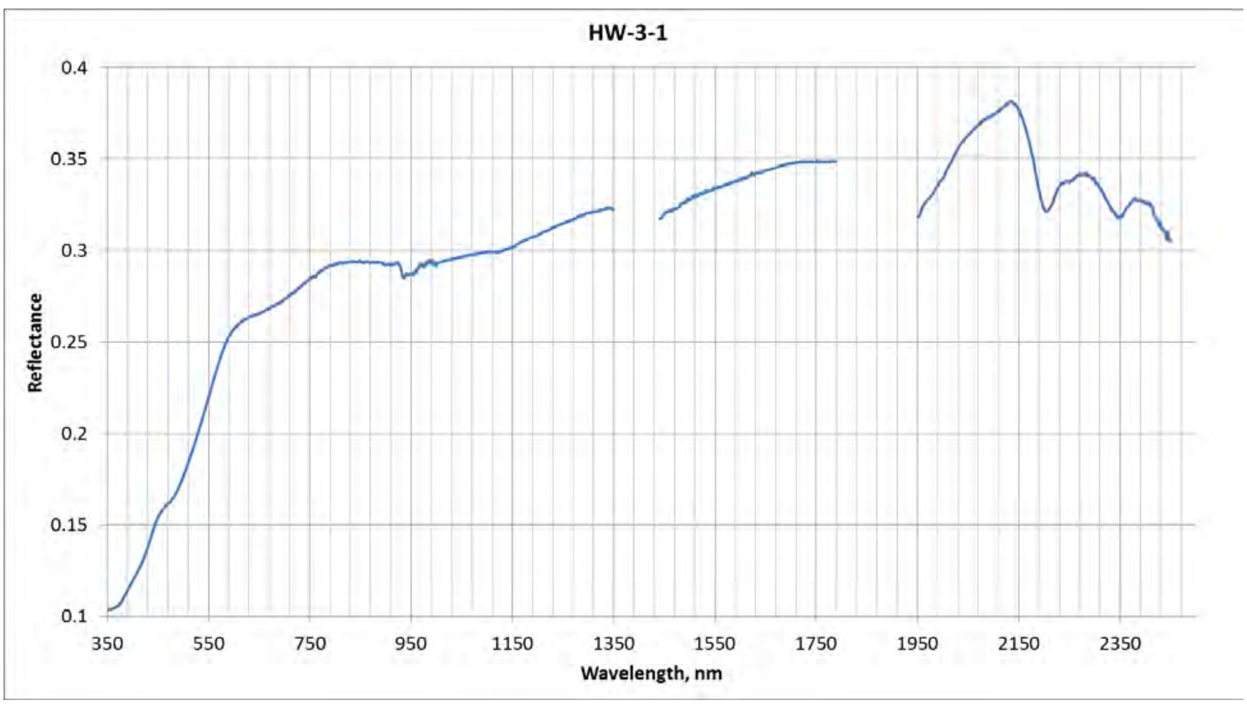
HW-3-1
Reflectance
Wavelength, nm
0.4
0.35
0.3
0.25
0.2
0.15
0.1
350
550
750
950
1150
1350
1550
1750
1950
2150
2350

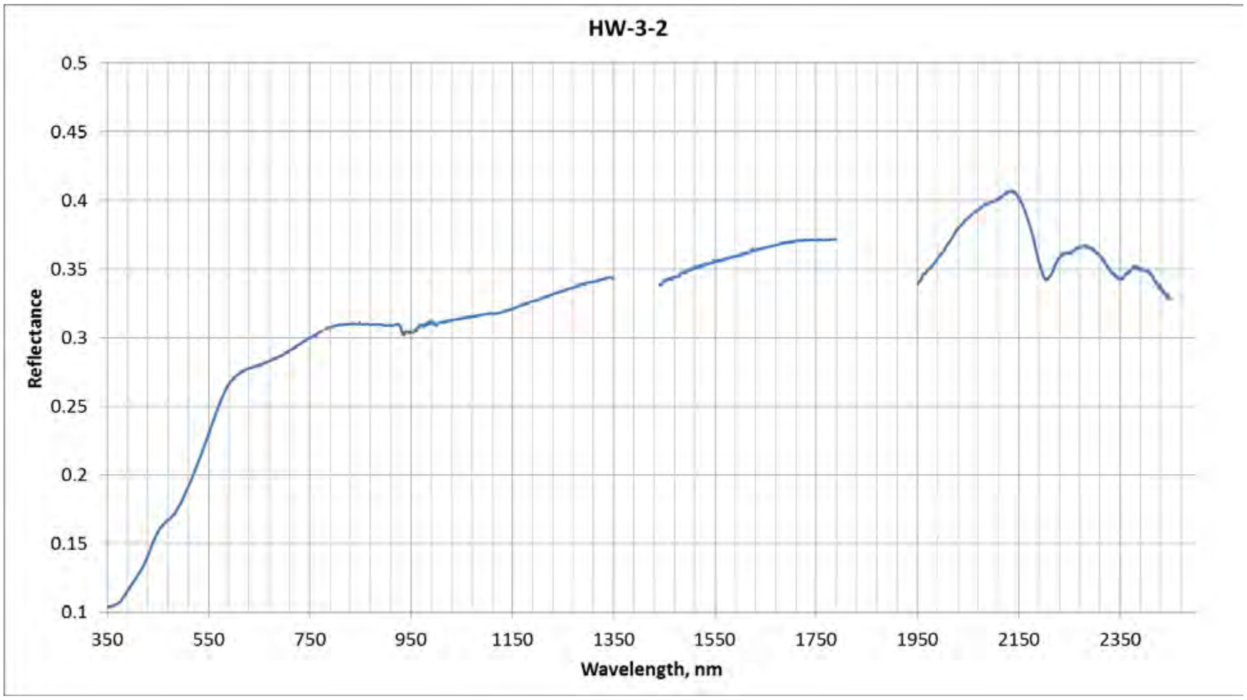
HW-3-2
Reflectance
0.5
0.45
0.4
0.35
0.3
0.25
0.2
0.15
0.1
350
550
750
950
1150
1350
1550
1750
1950
2150
2350
Wavelength, nm

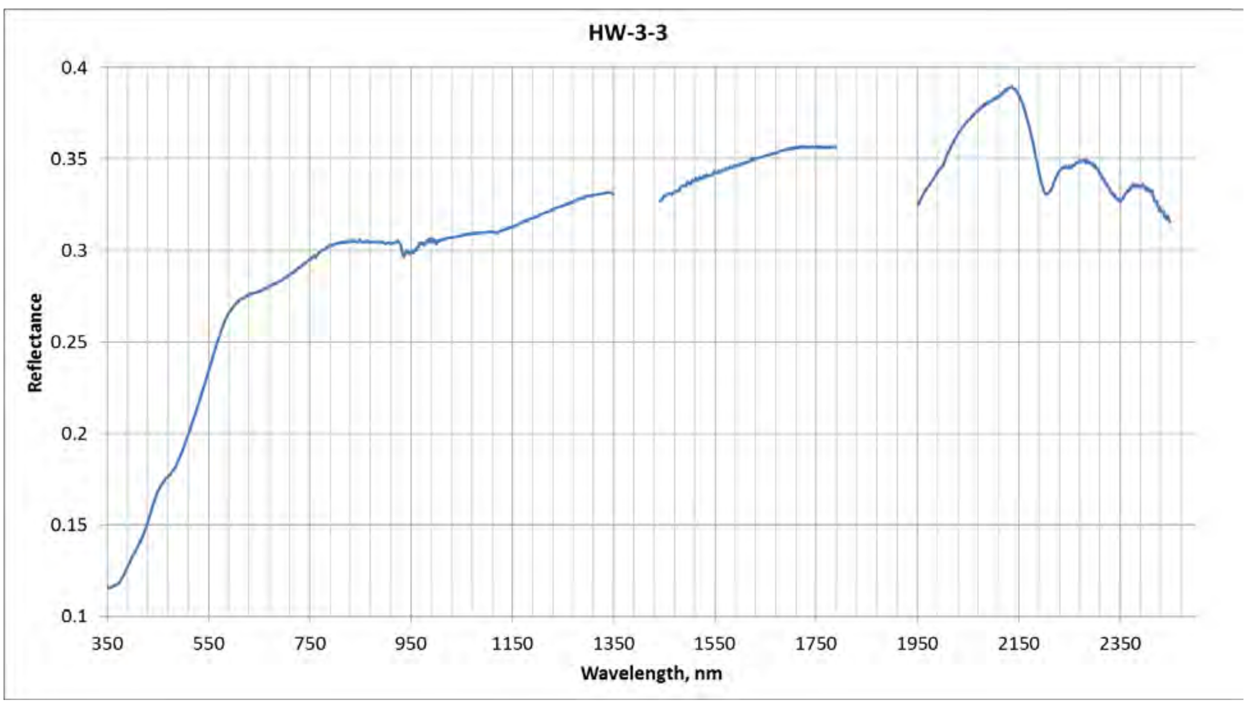
HW-3-3
Reflectance
0.4
0.35
0.3
0.25
0.2
0.15
0.1
350
550
750
950
1150
1350
1550
1750
1950
2150
2350
Wavelength, nm

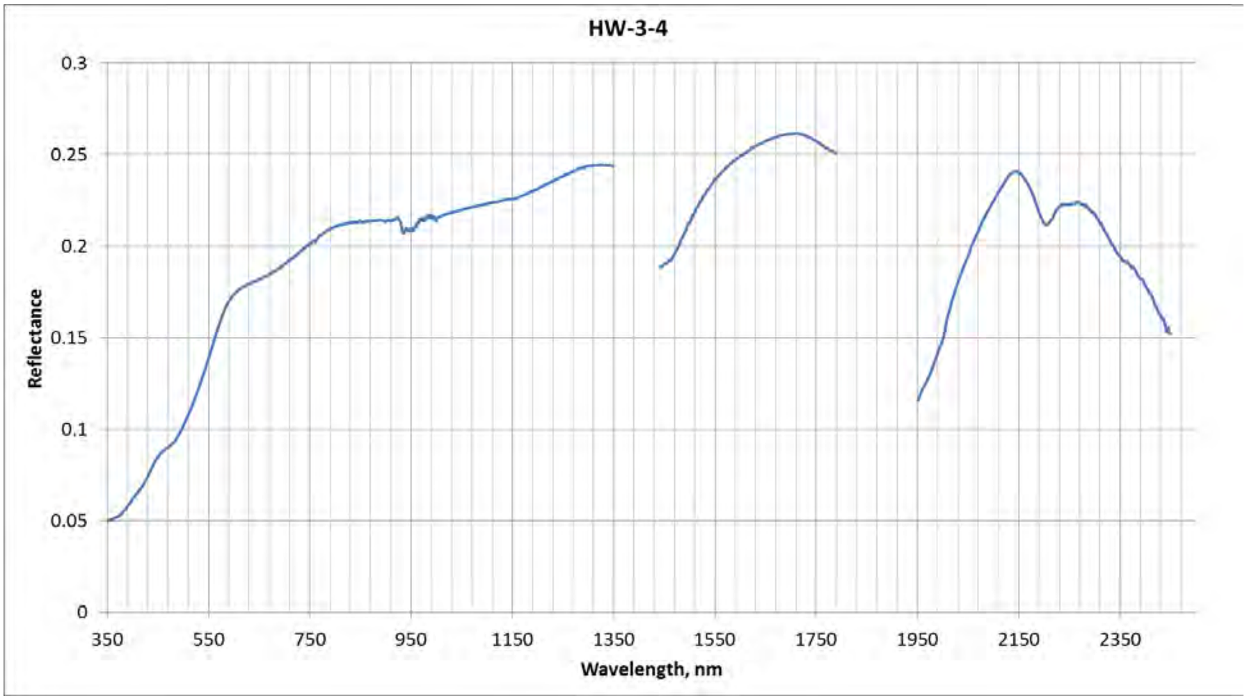

BRDF Reflectance Spectra

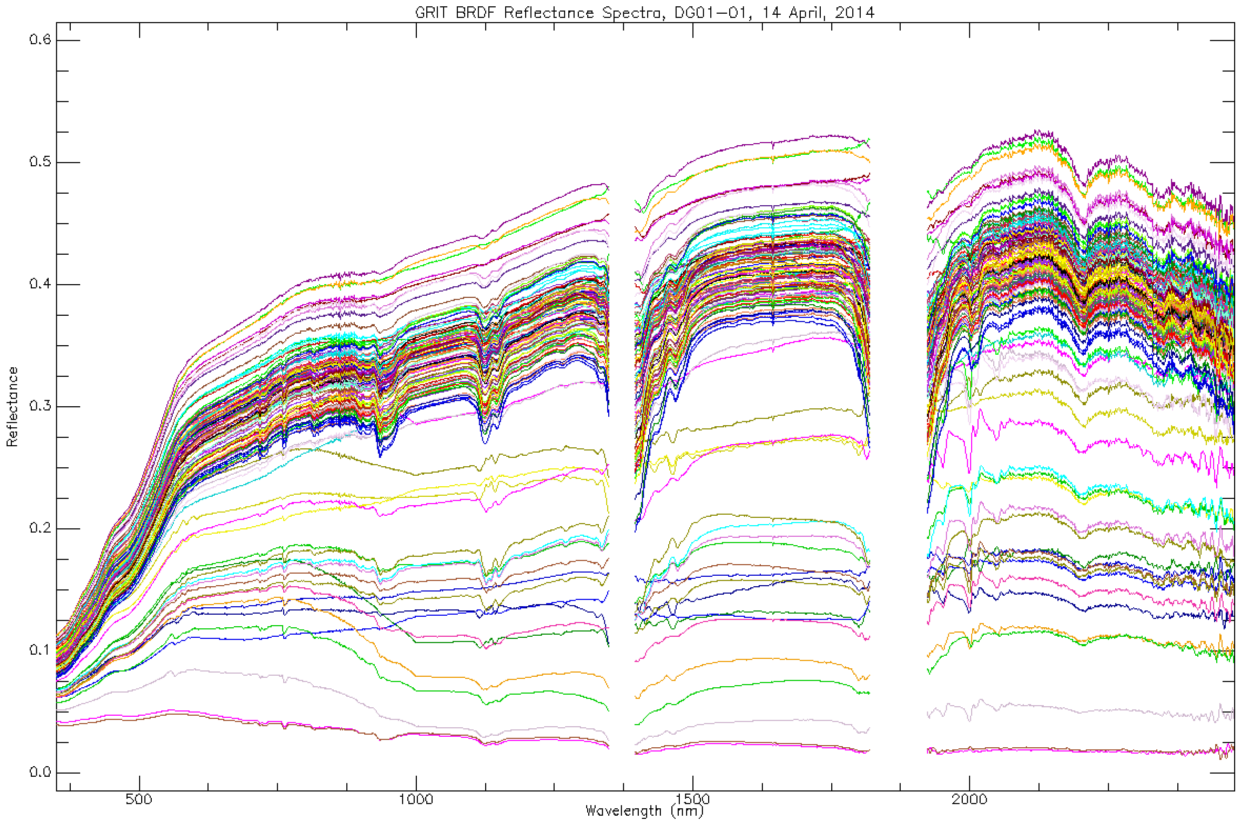

GRIT BRDF Reflectance Spectra, DG01-01, 14 April, 2014
Reflectance
Wavelength (nm)
0.0
0.1
0.2
0.3
0.4
0.5
0.6
500
1000
1500
2000

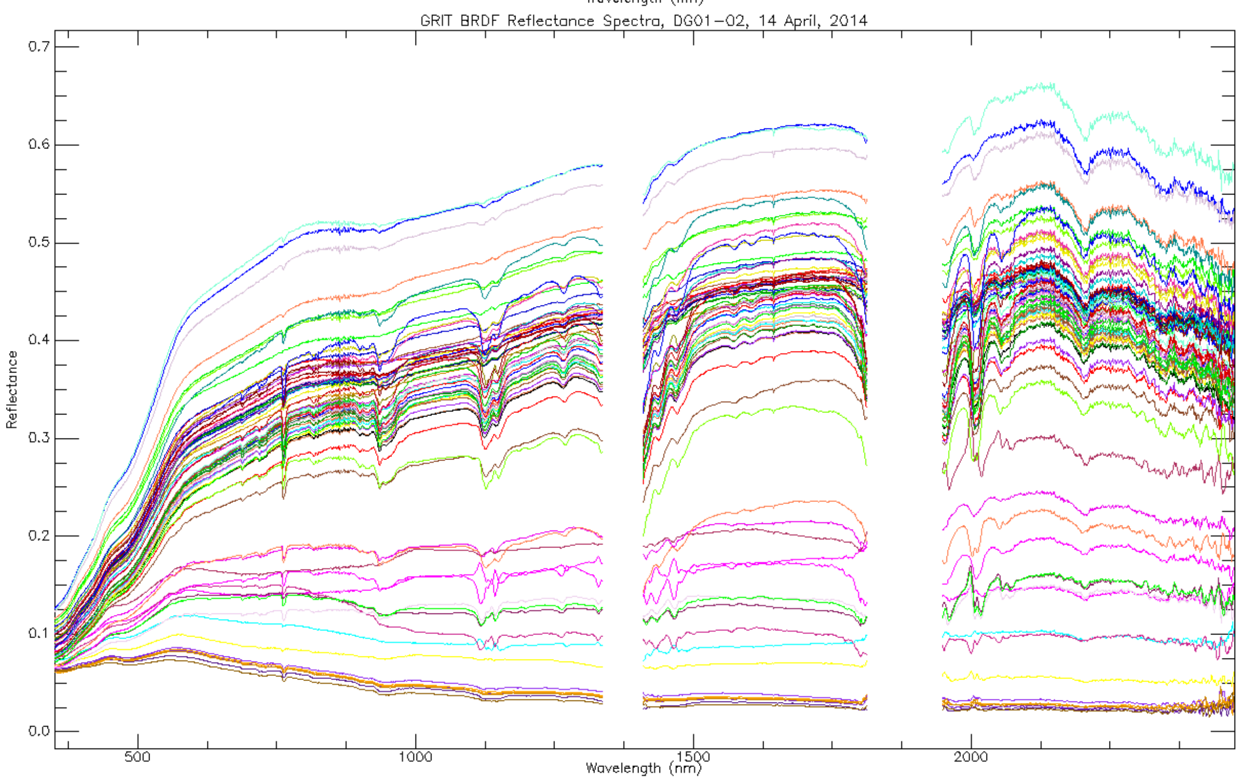

GRIT BRDF Reflectance Spectra, DG01-02, 14 April, 2014
Reflectance
Wavelength (nm)
0.0
0.1
0.2
0.3
0.4
0.5
0.6
0.7
500
1000
1500
2000

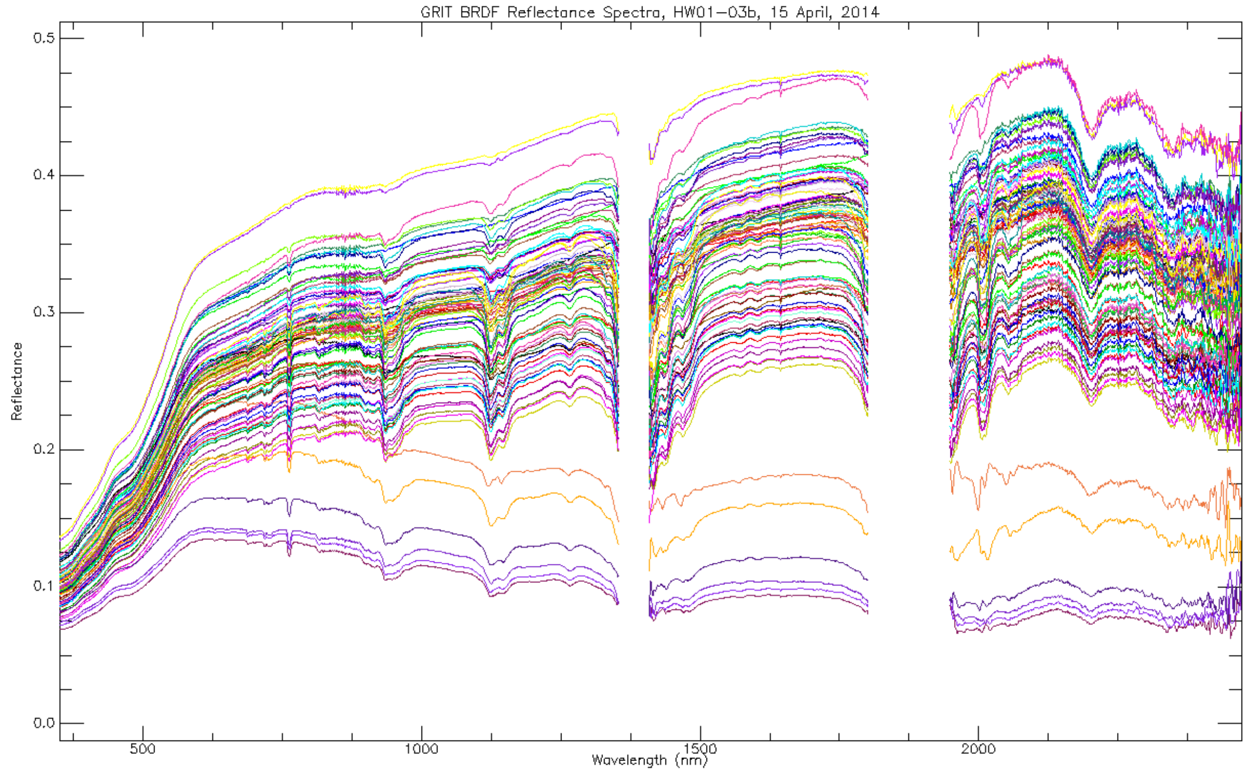

GRIT BRDF Reflectance Spectra, HW01-03b, 15 April, 2014
Reflectance
Wavelength (nm)

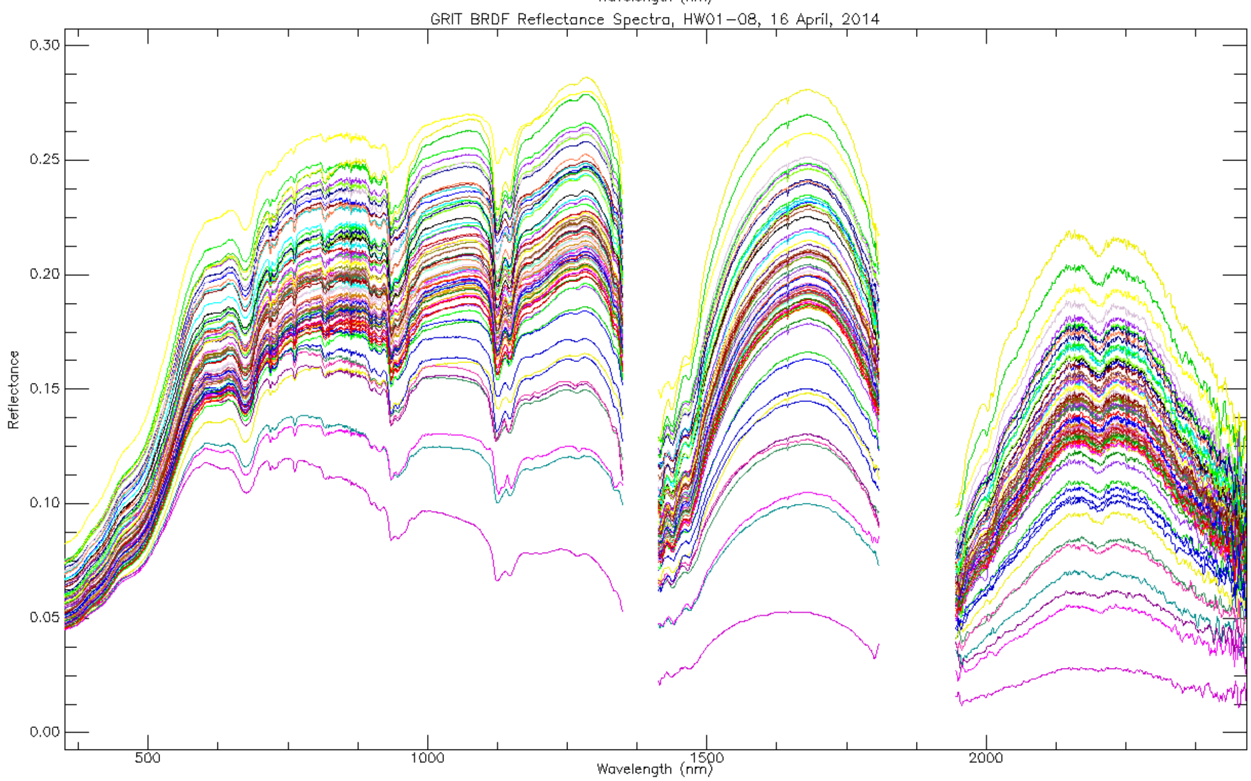

GRIT BRDF Reflectance Spectra, HW01-08, 16 April, 2014
Reflectance
Wavelength (nm)

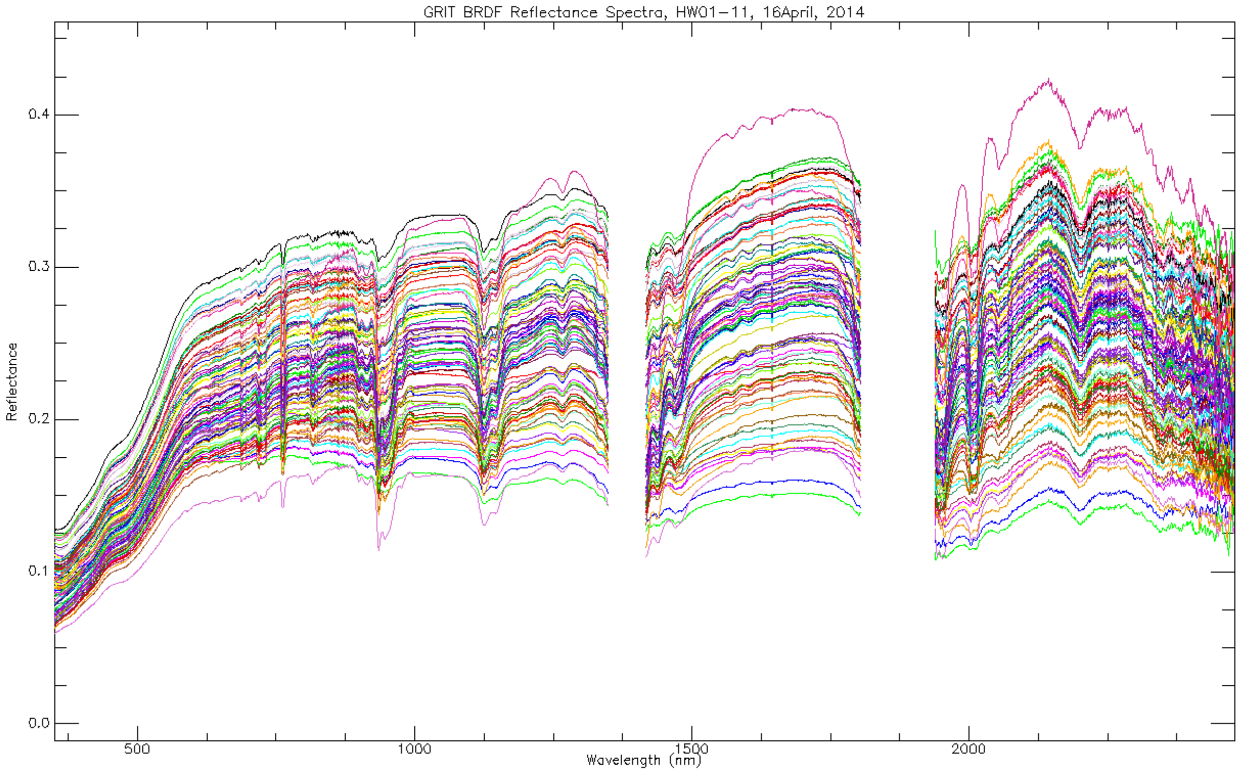
GRIT BRDF Reflectance Spectra, HW01-11, 16April, 2014
Reflectance
Wavelength (nm)
0.0
0.1
0.2
0.3
0.4
500
1000
1500
2000

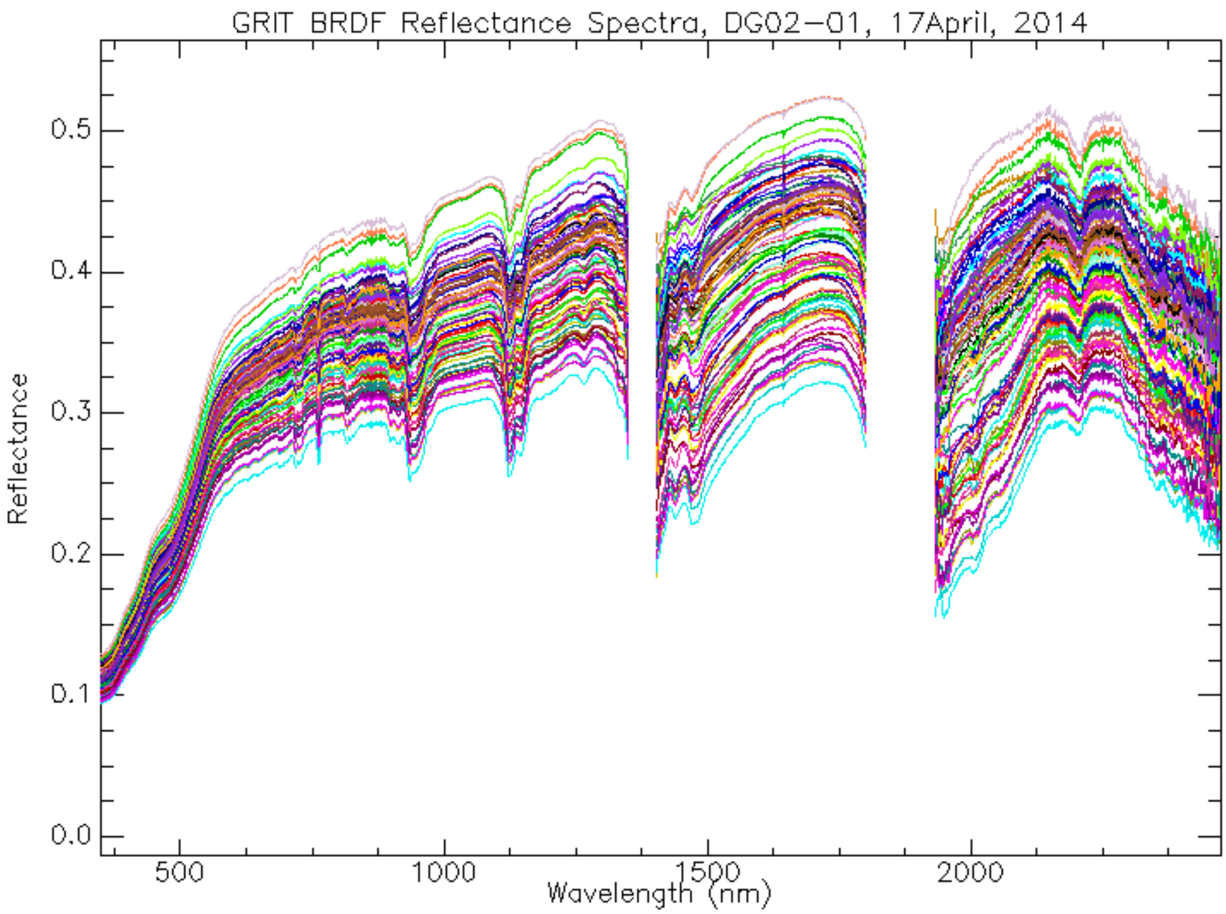
GRIT BRDF Reflectance Spectra, DG02-01, 17April, 2014
Reflectance
Wavelength (nm)
0.0
0.1
0.2
0.3
0.4
0.5
500
1000
1500
2000

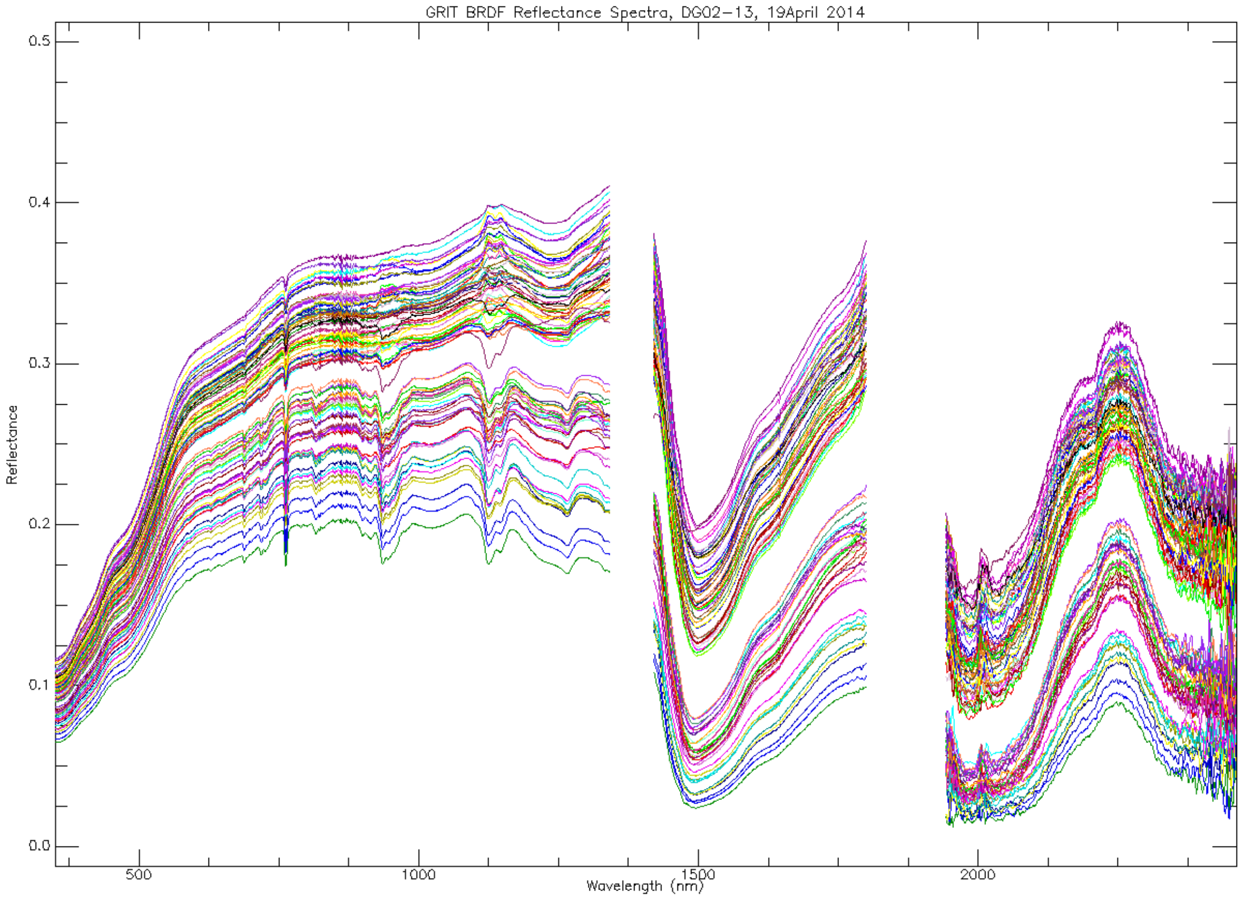

GRIT BRDF Reflectance Spectra, DG02-13, 19April 2014
Reflectance
Wavelength (nm)
0.0
0.1
0.2
0.3
0.4
0.5
500
1000
1500
2000

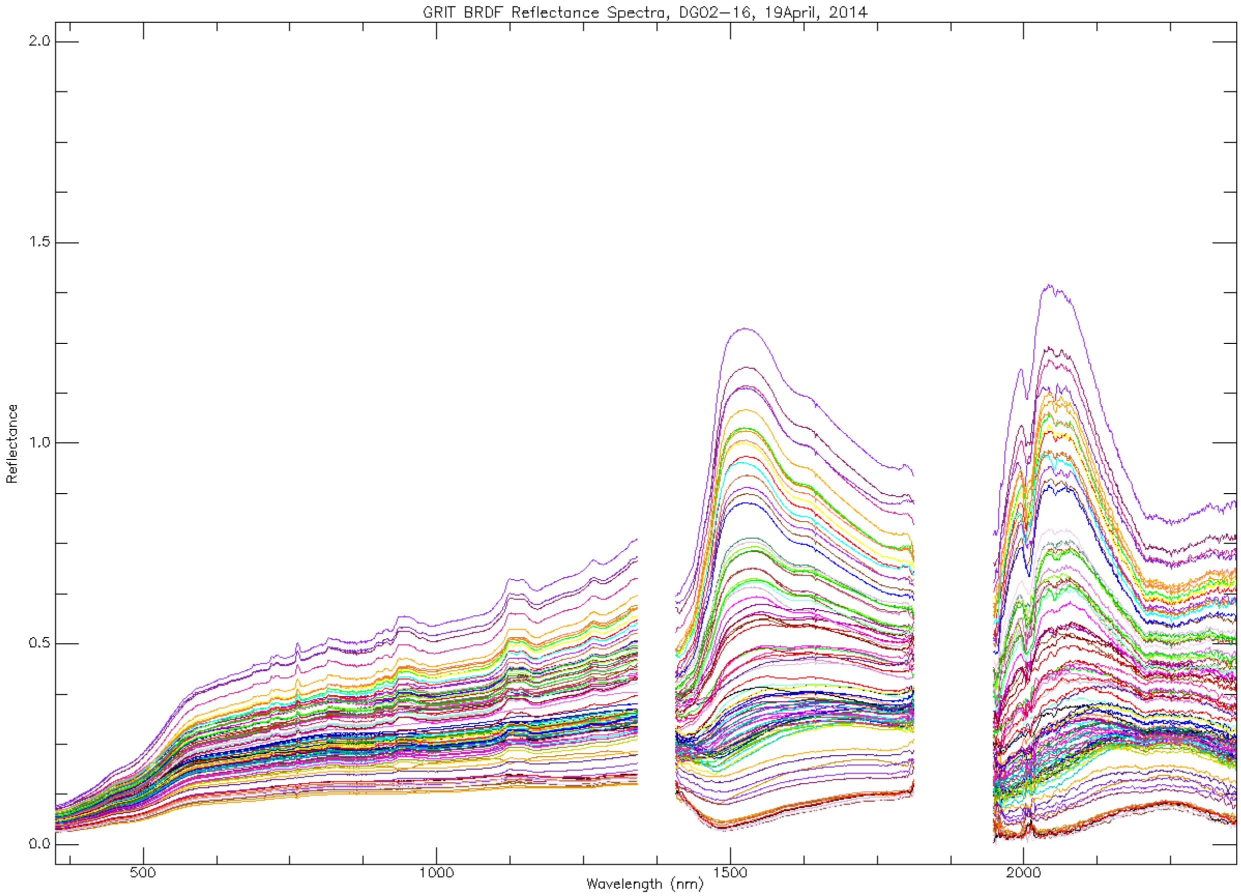
GRIT BRDF Reflectance Spectra, DG02–16, 19April, 2014
Reflectance
Wavelength (nm)
2.0
1.5
1.0
0.5
0.0
500
1000
1500
2000

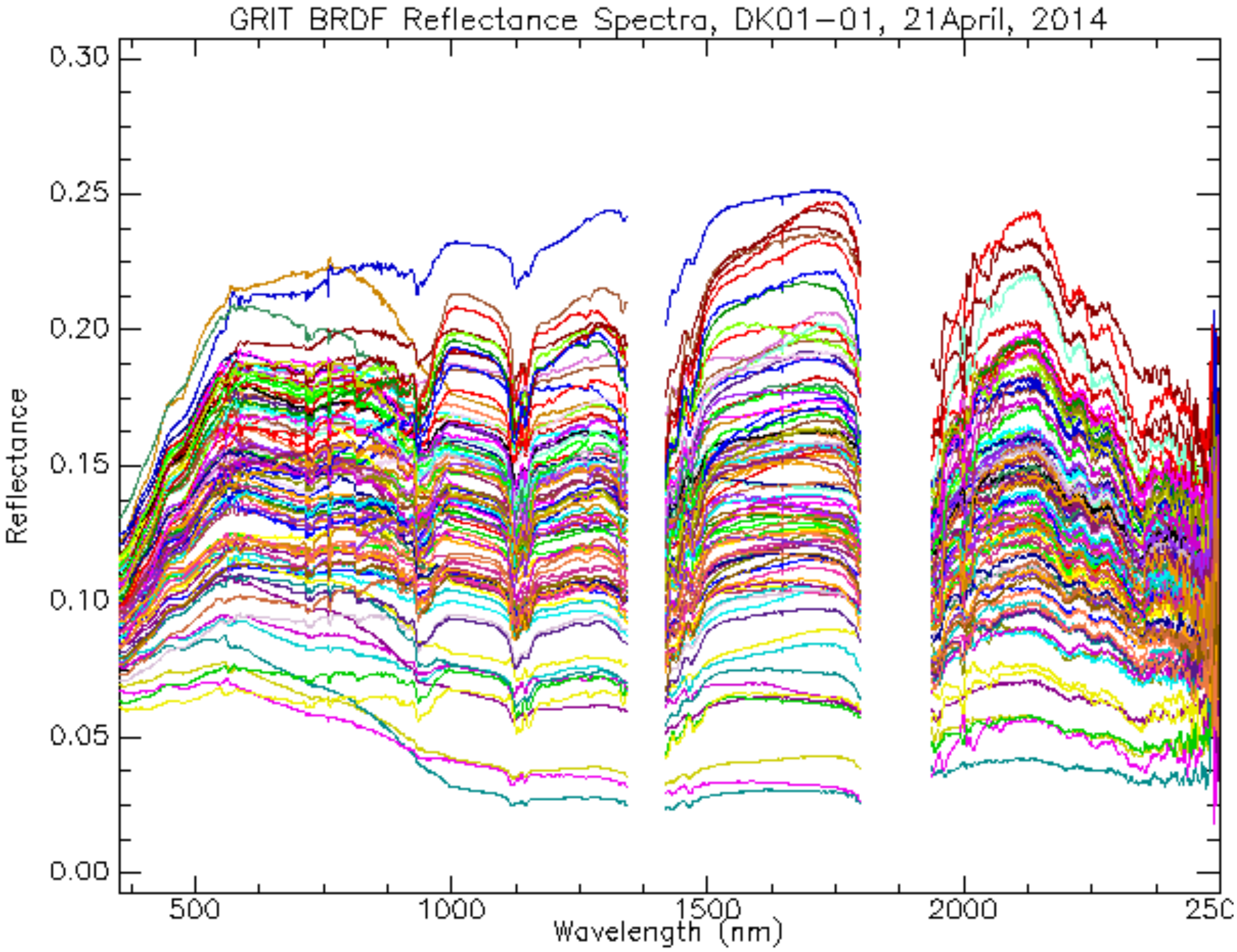
GRIT BRDF Reflectance Spectra, DK01-01, 21April, 2014
Reflectance
0.00
0.05
0.10
0.15
0.20
0.25
0.30
500
1000
1500
2000
250
Wavelength (nm)

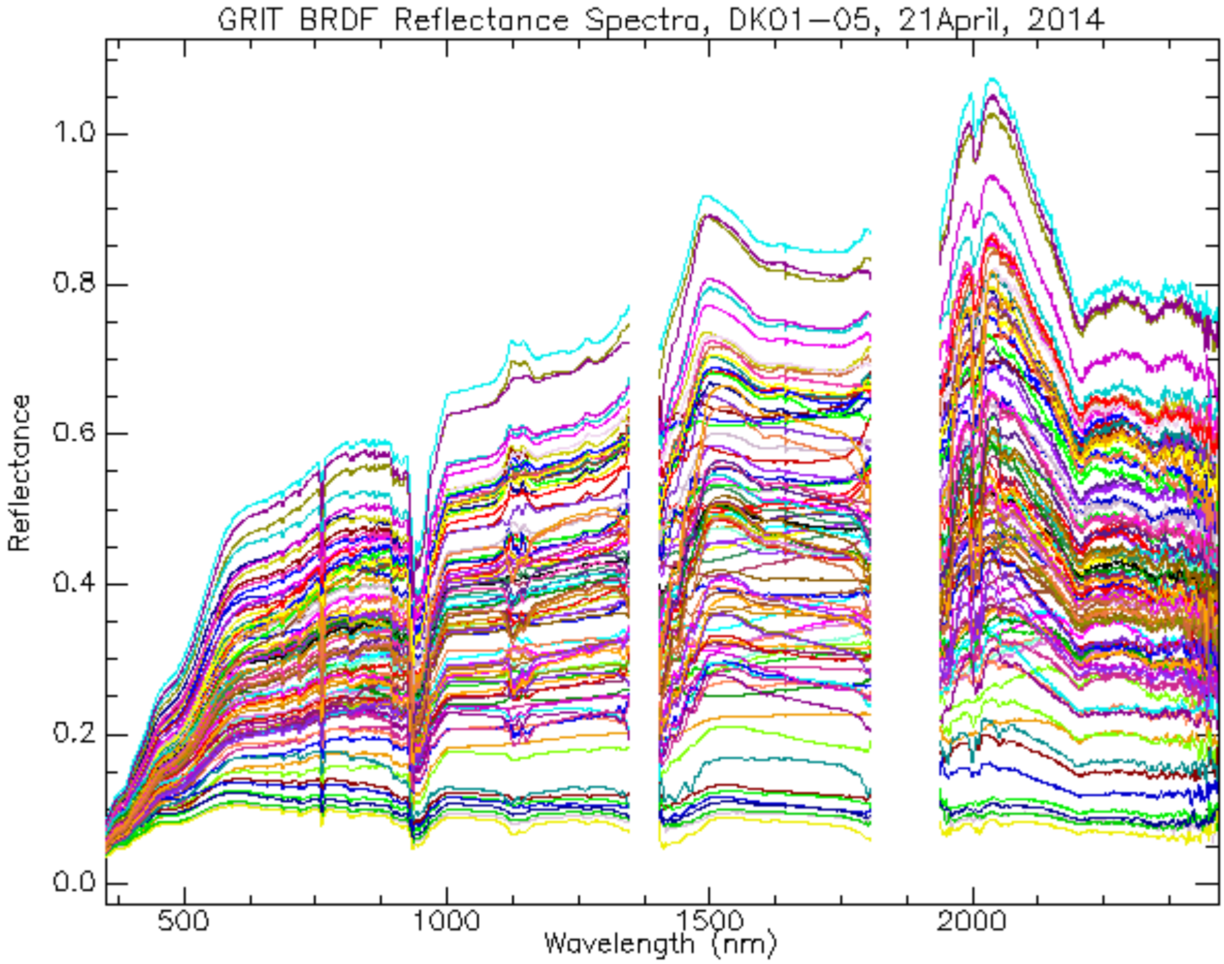

GRIT BRDF Reflectance Spectra, DK01-05, 21April, 2014
Reflectance
Wavelength (nm)
0.0
0.2
0.4
0.6
0.8
1.0
500
1000
1500
2000

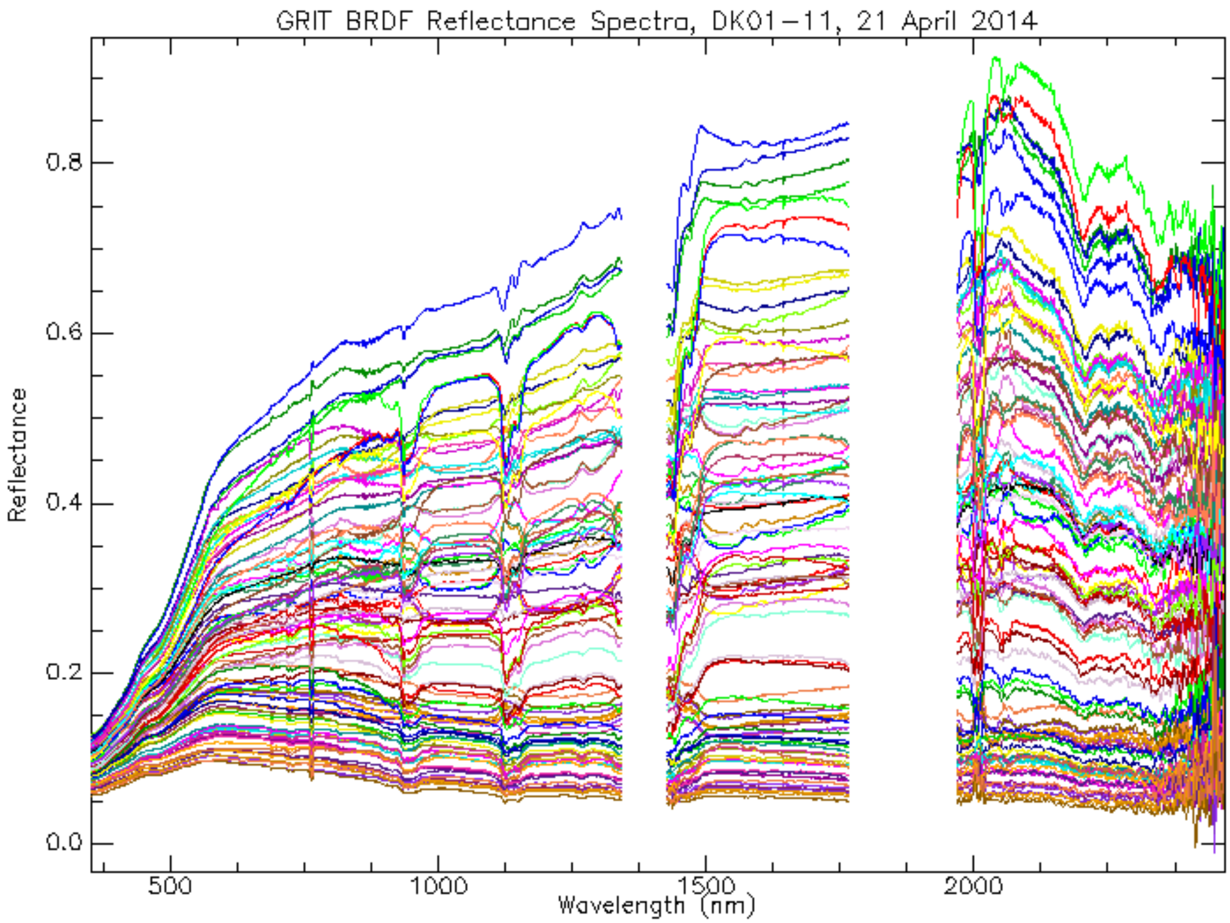

GRIT BRDF Reflectance Spectra, DK01-11, 21 April 2014
Reflectance
0.0
0.2
0.4
0.6
0.8
500
1000
1500
2000
Wavelength (nm)

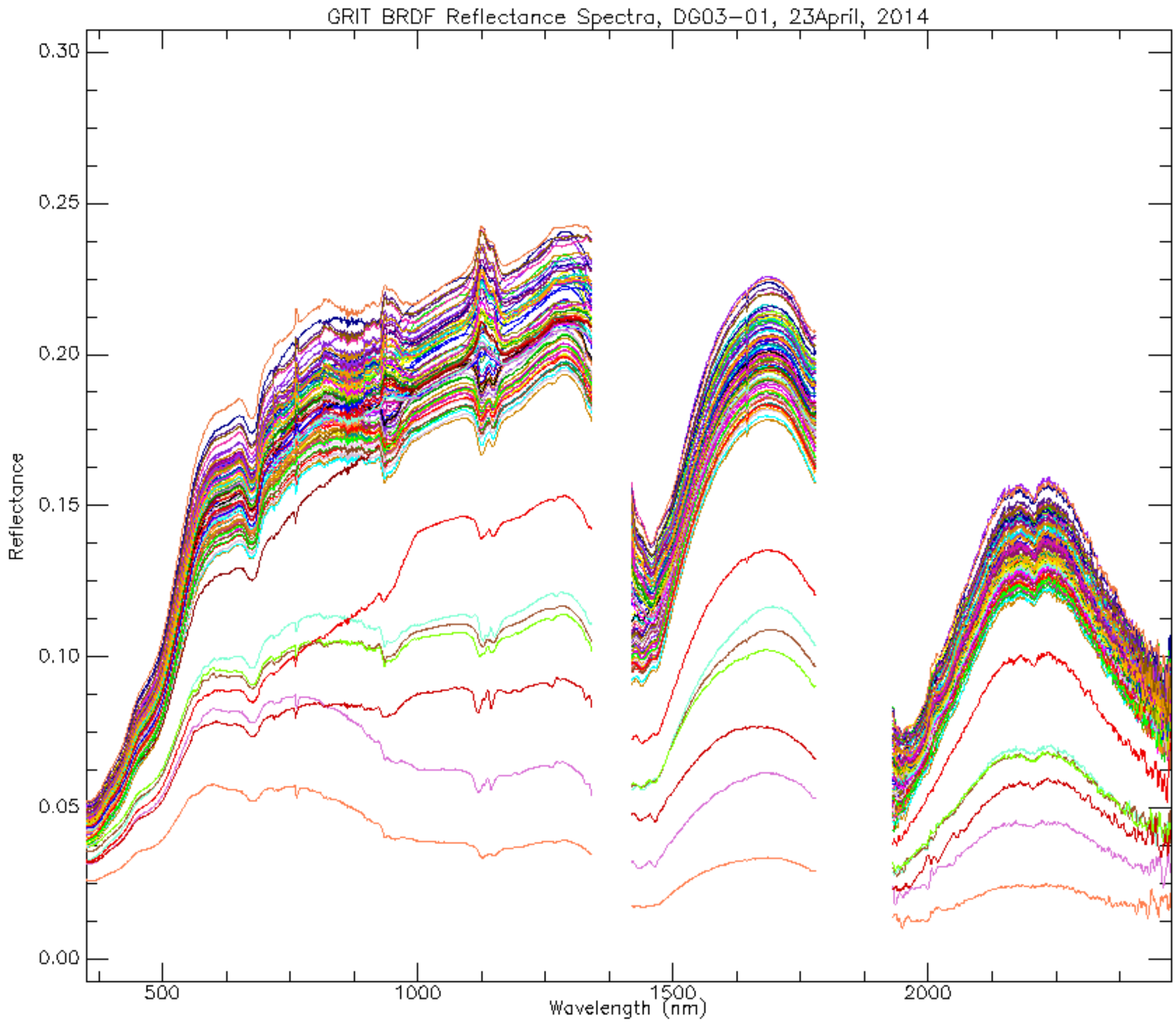
GRIT BRDF Reflectance Spectra, DG03-01, 23April, 2014
Reflectance
Wavelength (nm)
0.30
0.25
0.20
0.15
0.10
0.05
0.00
500
1000
1500
2000

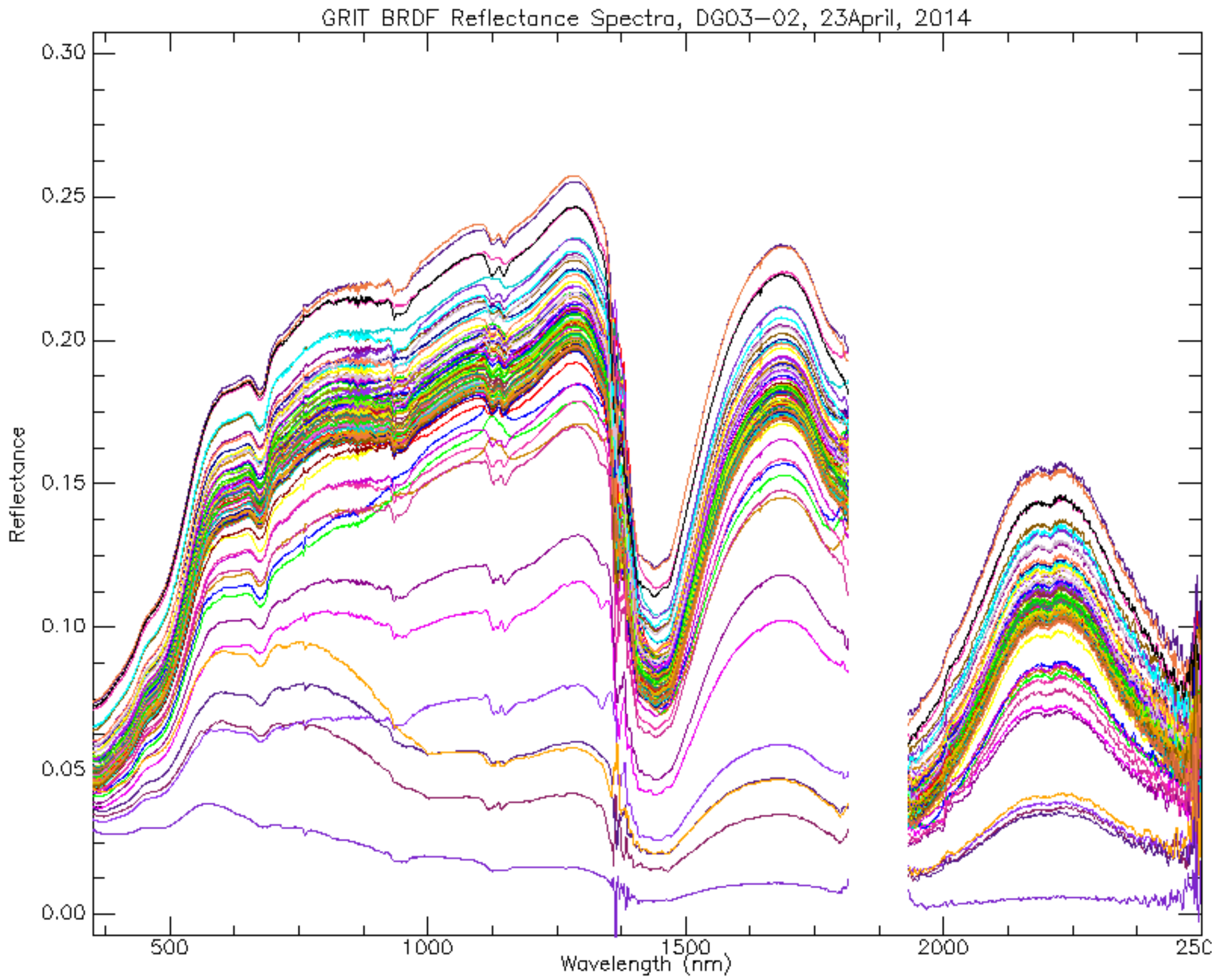
GRIT BRDF Reflectance Spectra, DG03-02, 23April, 2014
Reflectance
Wavelength (nm)
0.30
0.25
0.20
0.15
0.10
0.05
0.00
500
1000
1500
2000
250

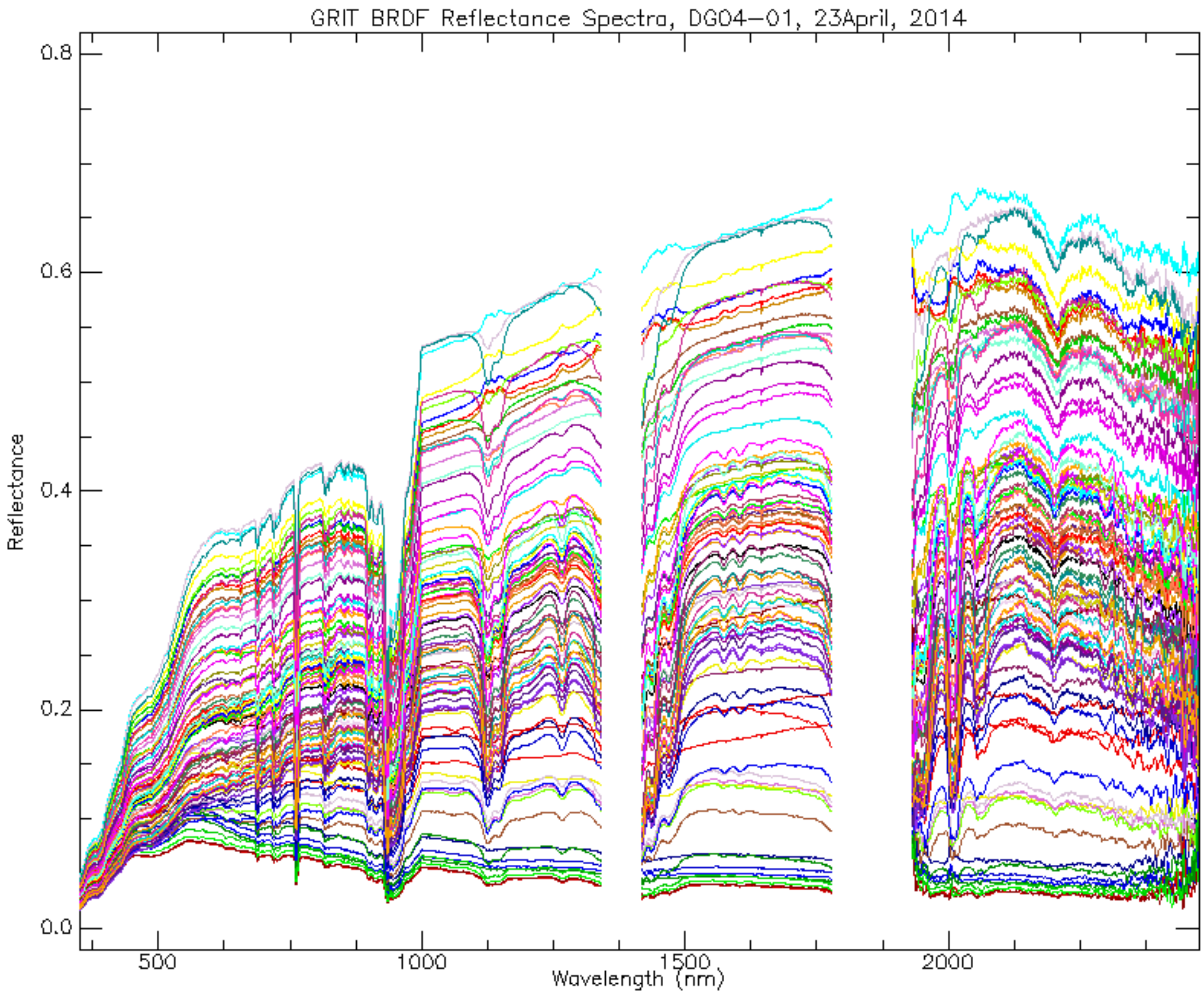
GRIT BRDF Reflectance Spectra, DG04-01, 23April, 2014
0.8
0.6
0.4
0.2
0.0
Reflectance
500
1000
1500
2000
Wavelength (nm)

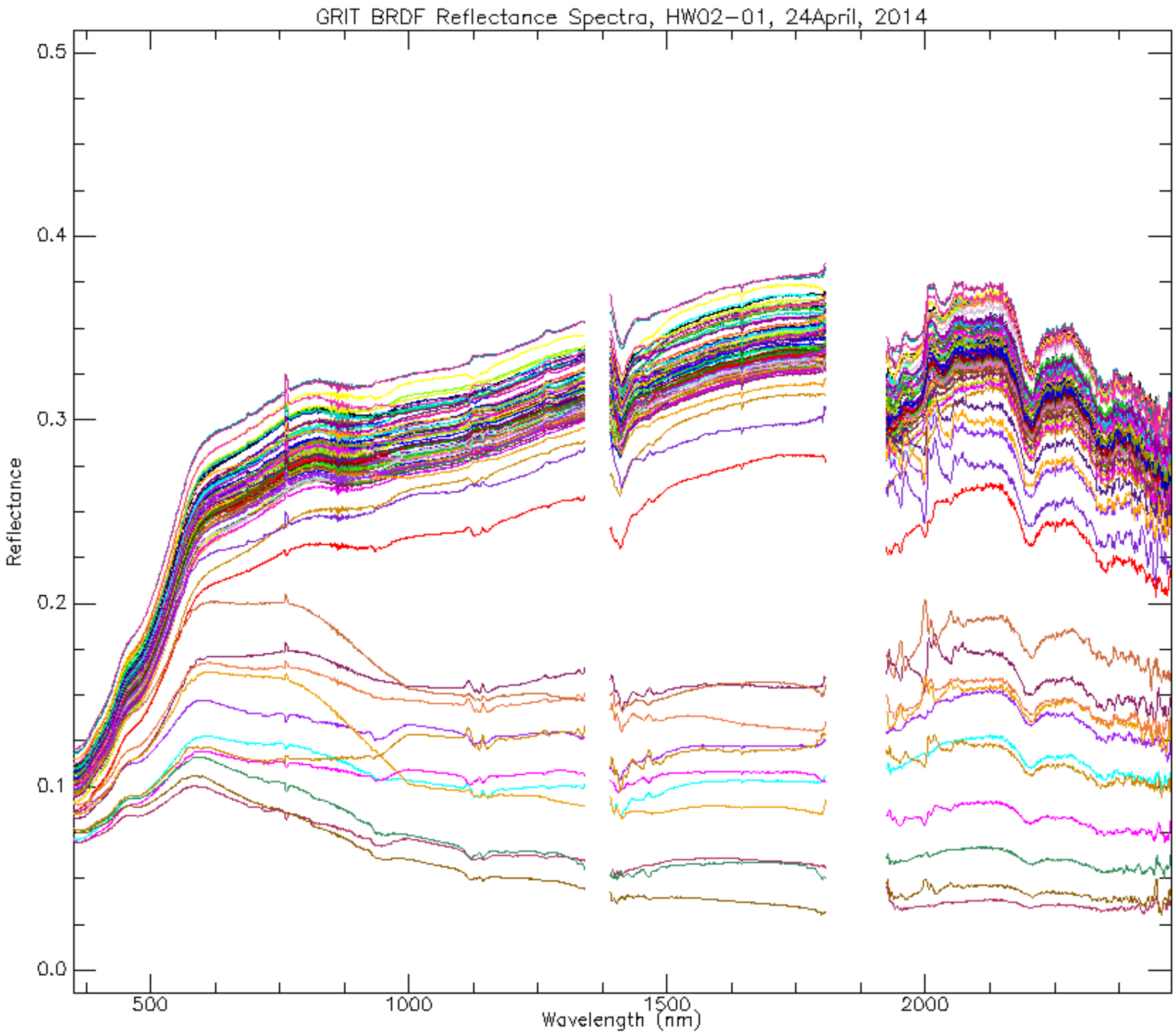

GRIT BRDF Reflectance Spectra, HW02-01, 24April, 2014
Reflectance
Wavelength (nm)
0.0
0.1
0.2
0.3
0.4
0.5
500
1000
1500
2000

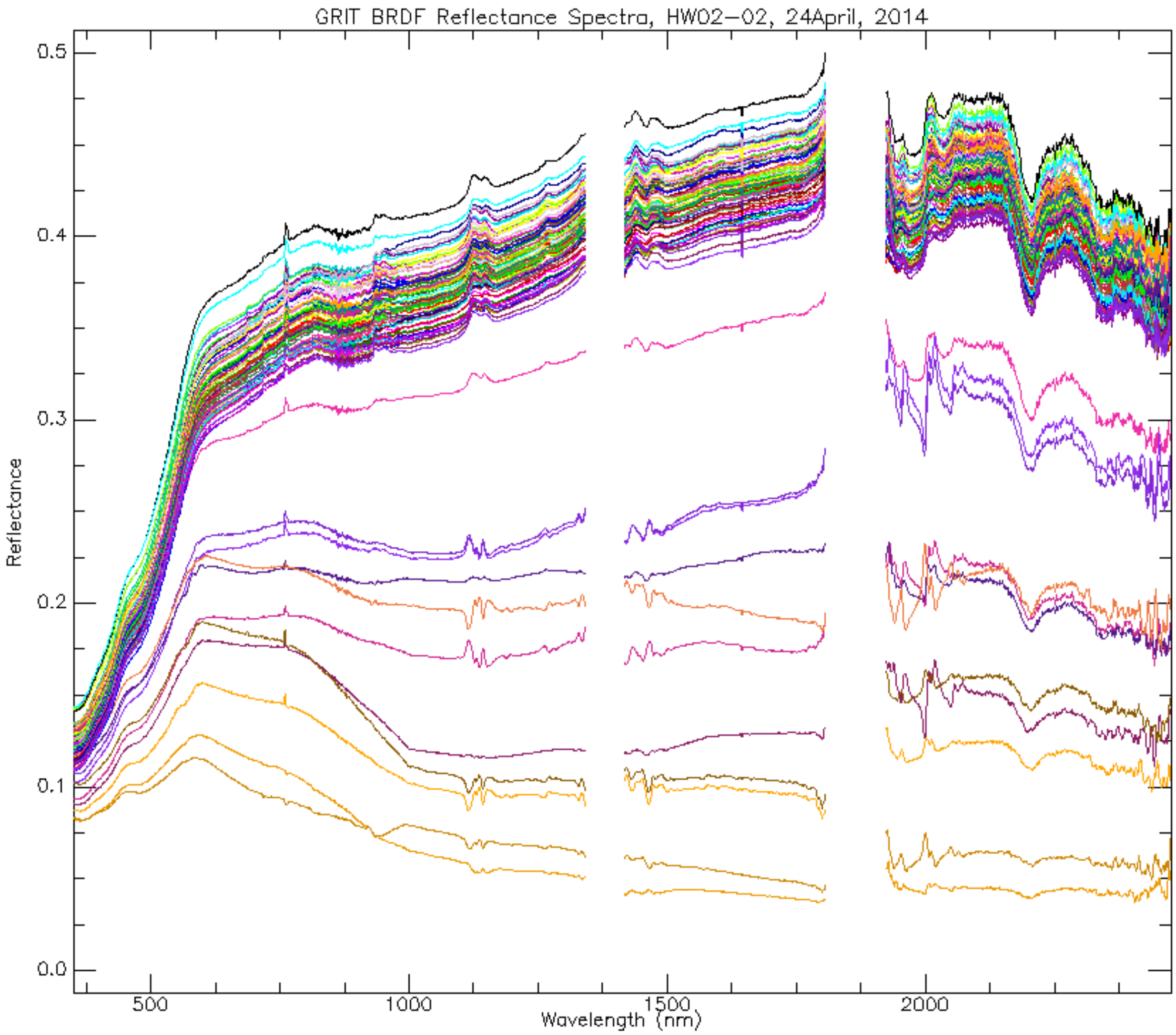
GRIT BRDF Reflectance Spectra, HW02-02, 24April, 2014
Reflectance
0.5
0.4
0.3
0.2
0.1
0.0
500
1000
1500
2000
Wavelength (nm)

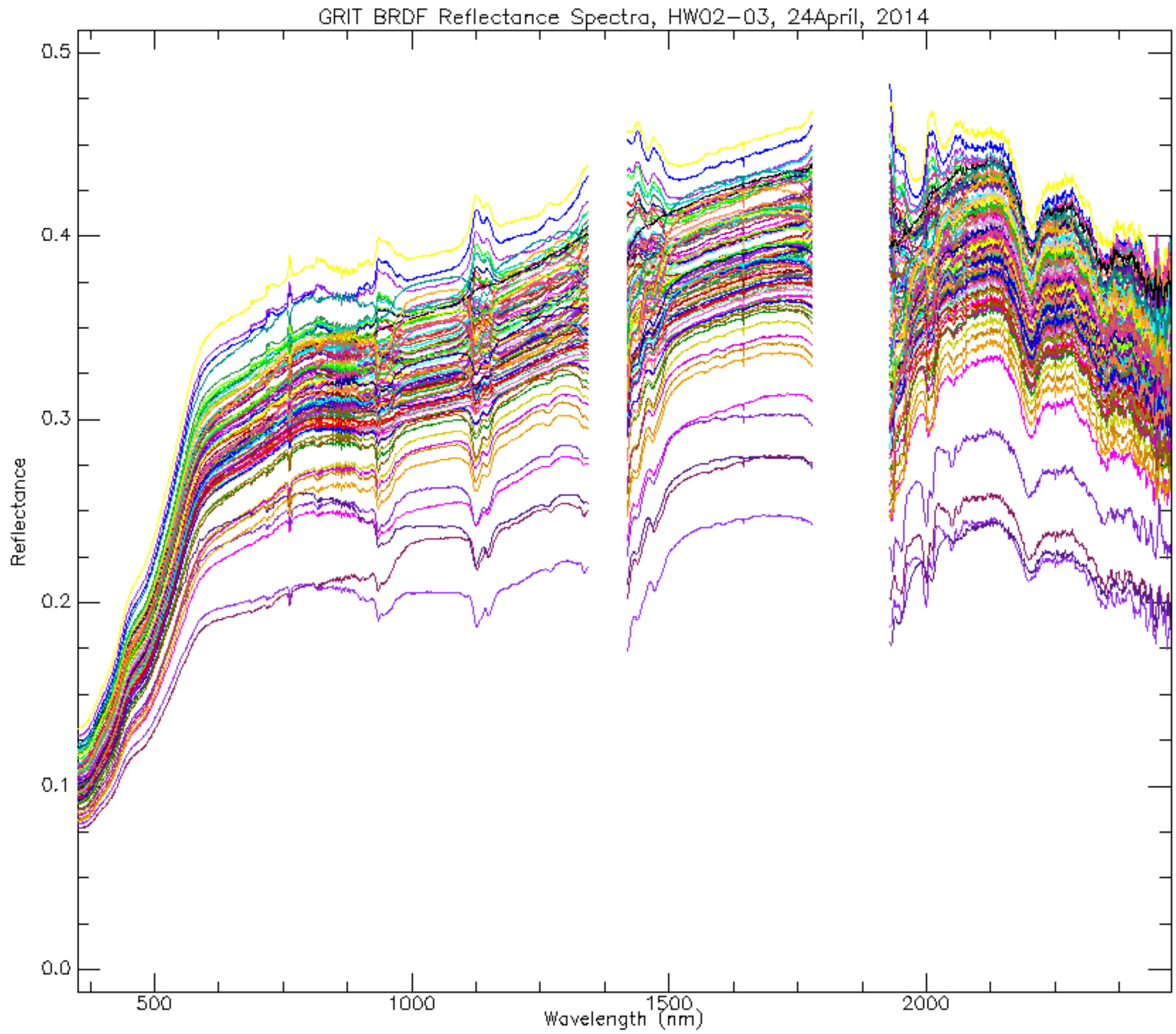
GRIT BRDF Reflectance Spectra, HW02-03, 24April, 2014
Reflectance
Wavelength (nm)
0.0
0.1
0.2
0.3
0.4
0.5
500
1000
1500
2000

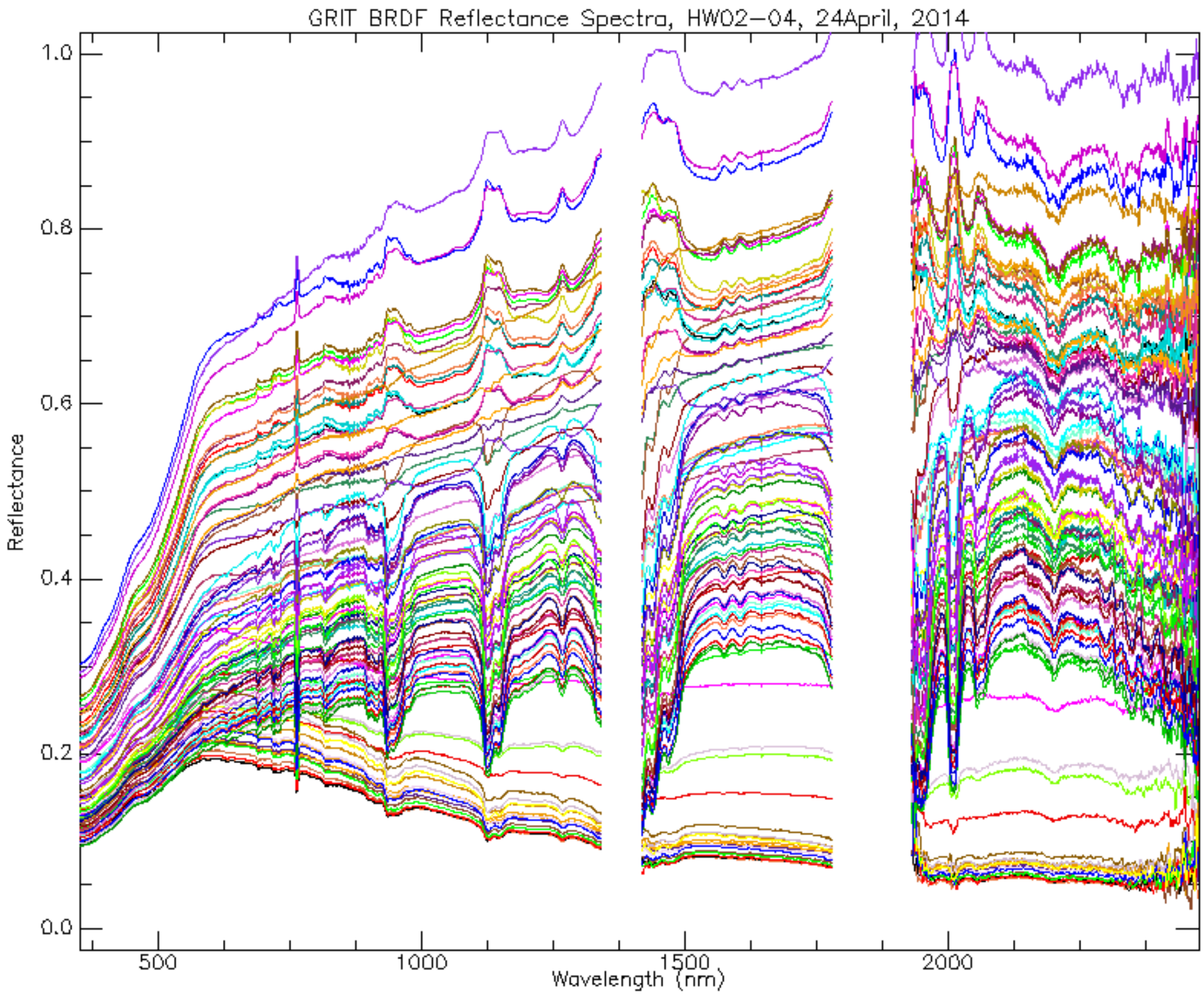
GRIT BRDF Reflectance Spectra, HW02-04, 24April, 2014
Reflectance
Wavelength (nm)
0.0
0.2
0.4
0.6
0.8
1.0
500
1000
1500
2000

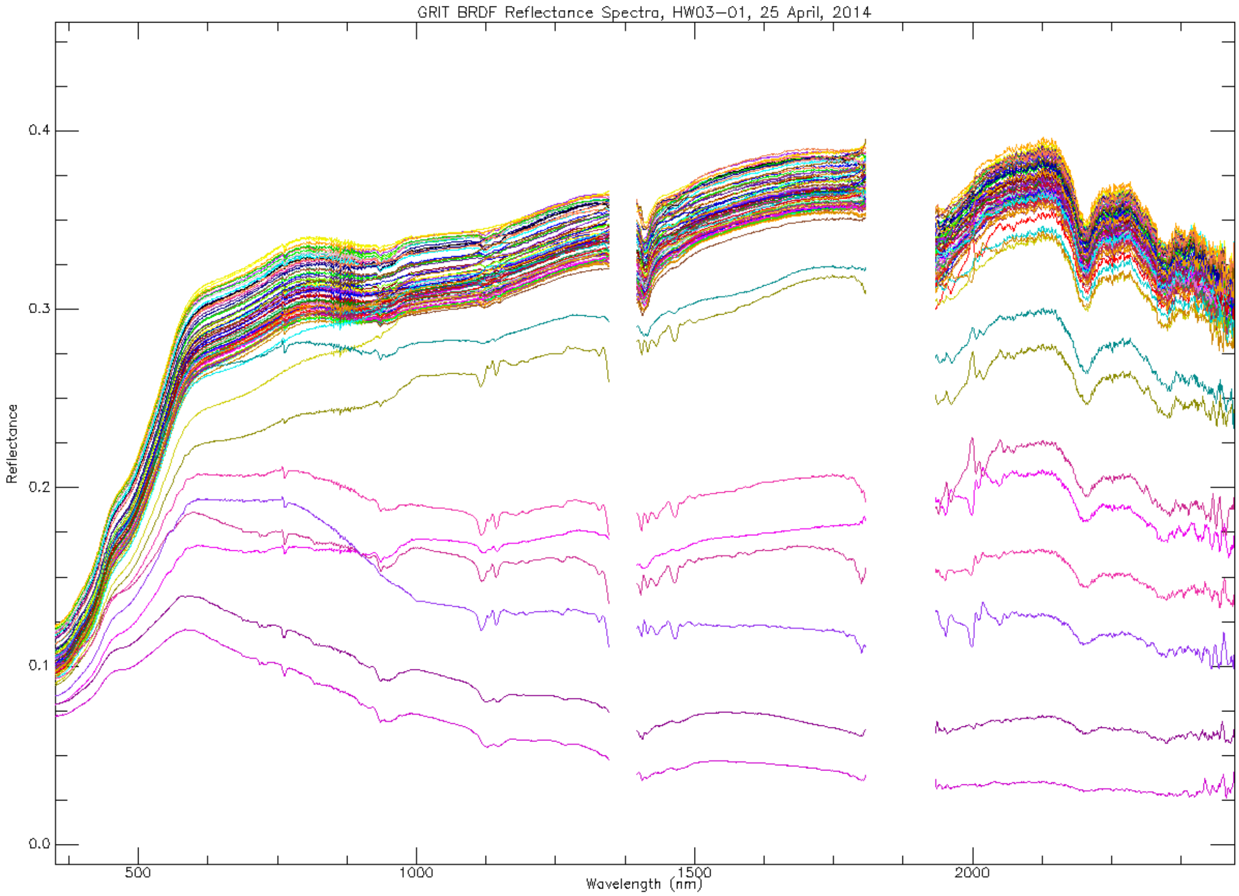
GRIT BRDF Reflectance Spectra, HW03-01, 25 April, 2014
Reflectance
Wavelength (nm)
0.0
0.1
0.2
0.3
0.4
500
1000
1500
2000

APPENDIX H

LiDAR

Introduction

LiDAR data collected during the Ssang Yong Remote Sensing Experiment has been processed into Disc Image (.img) and LAS (.las) formats. The Disc Image files have been viewed within ESRI's ArcMap software (see Figure H-1) and the LAS format files have been viewed within open source CloudCompare software (see Figure H-2). Georeferencing has not been accomplished. Tables including geocoordinates scan location along with fiducials within the scanned areas have been uploaded to the Project Geodatabase and may be viewed with the Map Document (Ssang Yong 2014\SsangYong2014.mxd) (see Table H-1). Notes have also been included in a separate table to support processing of LiDAR data in the Map Document and an Excel Workbook (Ssang Yong 2014\Data.xlsx) under the tab LiDAR_Notes (see Table H-2). Images below were produced from the same scan.

Table H- 1. GPS Point taken at LiDAR Postition referencing scan from Figures H-1 and H-2.

Field	**Values**
OBJECTID	7
Shape	Point Z
Date_GPS	4/19/2014
Time_GPS	6:33:30 AM
Latitude	35.997002
Longitude	129.427903
Height_Meters_WGS_84	31.524507
File	93209933
Notes	LiDAR Position
Receiver_Type	Trimble R-8
MSL_Above_WGS_84_Meters	29.518824
Height_Above_MSL_Meters	2.005683

Table H- 2. Information linked to scan in Figures H-1 and H-2.

Date	Time	File	Beach	Facing	Position	Top Base Plate Height (cm)	Notes
19-Apr-14	1505	065225	Dogu	Away From Water	L9	162	Perpendicular to Water, (Scan 18) Repeat, S of Scan Area

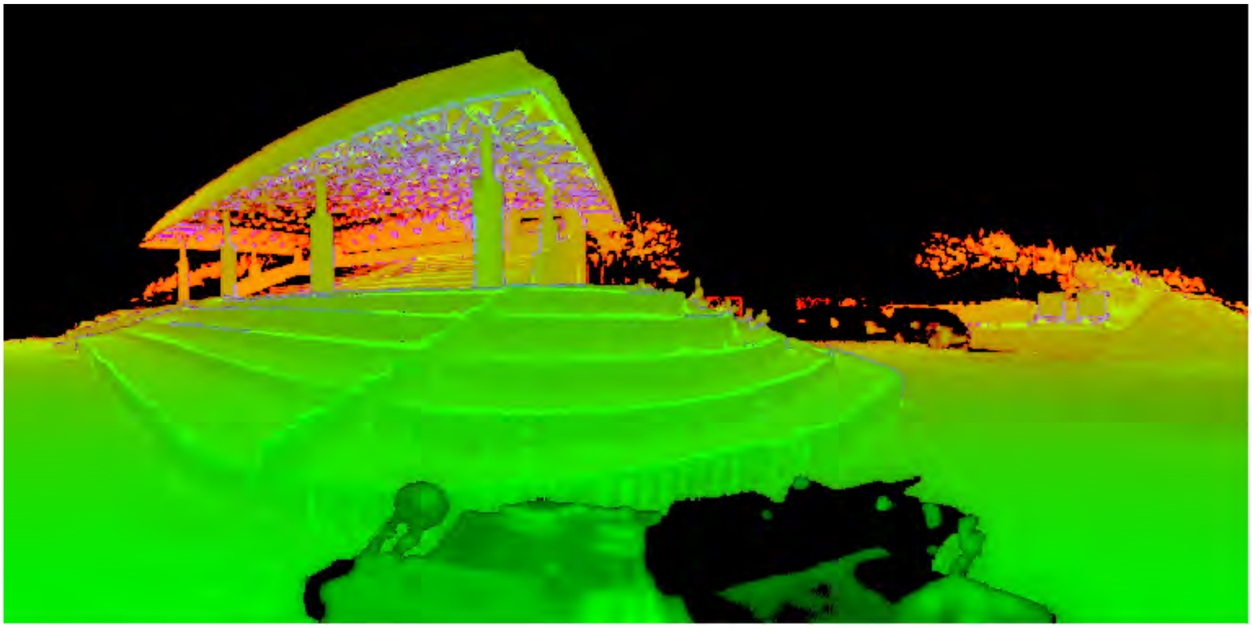
Figure H- 1. ArcMap view of a Disc Image file. Filename: SICK_NONE_2014-04-19_065225.img.

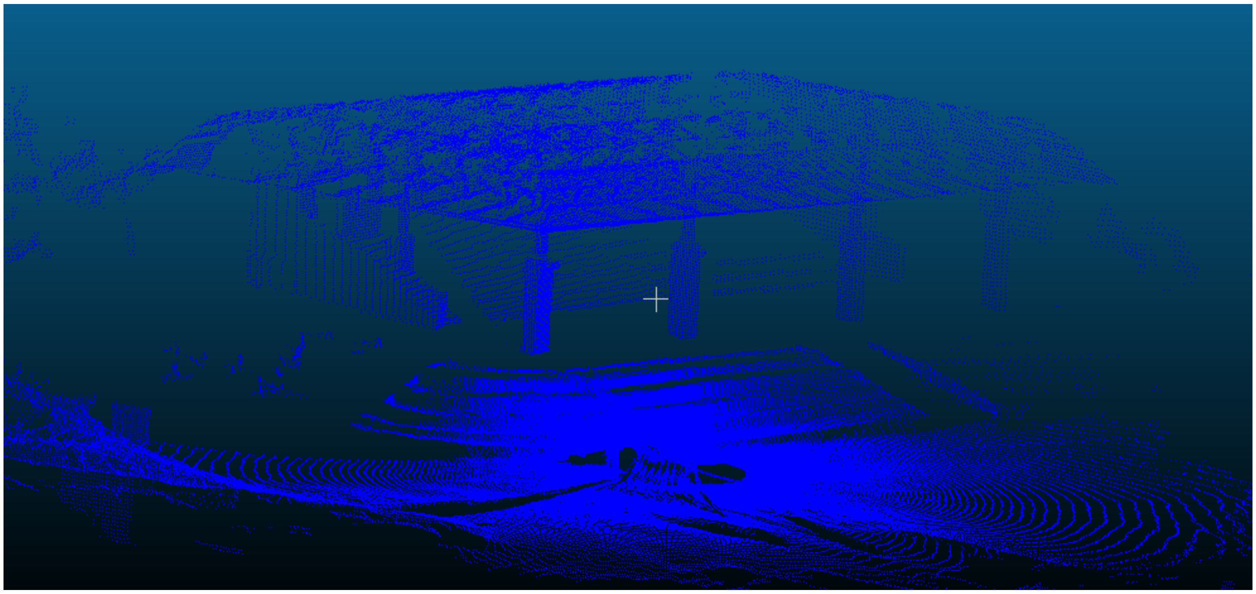
Figure H- 2. LAS image viewed in CloudCompare. Filename: SICK_NONE_2014-04-19_065225.las.

APPENDIX I

Meteorological Station

Table of Contents

List of Figures

List of Tables

Introduction

A HOBO meteorological station was set up at Camp Mujuk (Lat. 35.955, Long. 129.428) during the Ssang Yong 2014 Experiment for data collection (see Figure I-1). The location is georeferenced in the Ssang Yong 2014 Geodatabase (see Figure I-2). Meteorological data were collected for use in analysis of imagery, e.g., removal of atmospheric effects. Observations from the weather station include relative humidity, temperature, wind speed, wind direction, barometric pressure and down-welling irradiance (PAR meter). The weather station was installed on the 15 April 2014 and data were collected starting 11:11 AM local in ten second intervals. All data were collected in local time (UTC +9). Observations were stopped on the first night at 6:23 PM and resuming at 8:57 AM on the 16th. Ensuing records were continuous with three minute gaps for battery changes and data retrieval every few days. The last observation was made on 26 April 2014 at 3:30 PM. Summary figures of the data are provided in Figure I-3 through I-7. The data were processed and loaded into an Excel Workbook and archived in the Ssang Yong 2014 Geodatabase (Ssang Yong 2014/Attribute_Data/Weather/Meteorological_Station).

As a quality control measure U (East) and V (North) wind components are plotted in Figure I-8. The Camp Mujuk weather station winds are not representative of winds occurring at the beaches. Barometric pressure was rising throughout the period. April and May tend to be the sunniest months in Pohang, South Korea.

Atmospheric correction of WorldView-2 imagery is a critical processing task. By accounting for field weather conditions, applicable products can be developed in a timely manner. Meteorological data provided in this appendix have been made available for use with atmospheric correction programs such as FLAASH and Tafkaa.

Figure I- 1. Google Earth Image with Meteorological Station Marked.

Figure I- 2. Meteorological Station Assembled at Camp Mujuk.

File	Start Date/Time	End Date/Time
1	15Apr14/1111	15Apr14/1823
2	16Apr14/0857	17Apr14/0842
3	17Apr14/0843	20Apr14/1449
4	20Apr14/1453	22Apr14/1303
5	22Apr14/1306	26Apr14/1530

Table I-1. Date and Time for Figures Below.

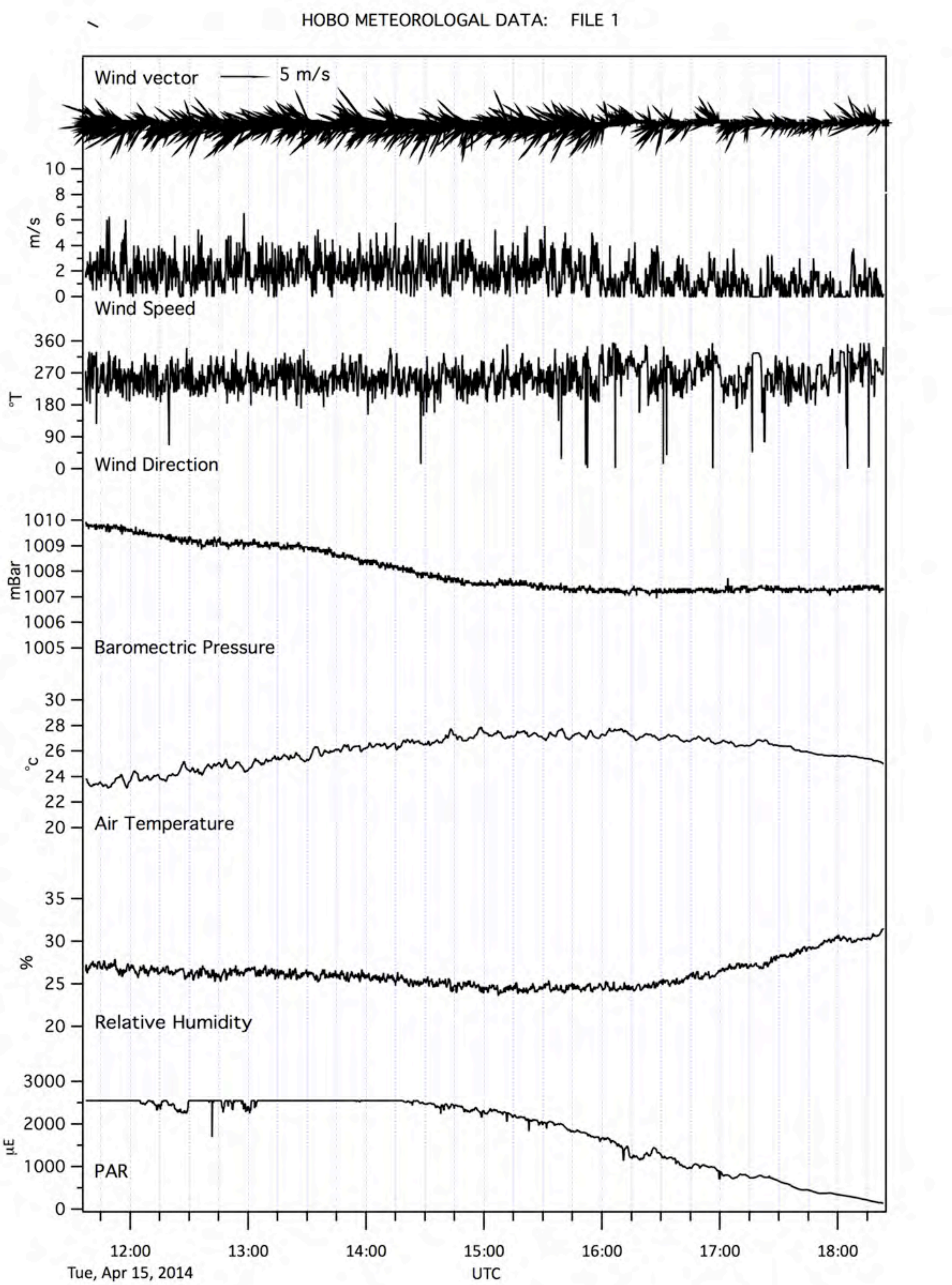

Figure I- 3. HOBO Meteorological Data File 1.

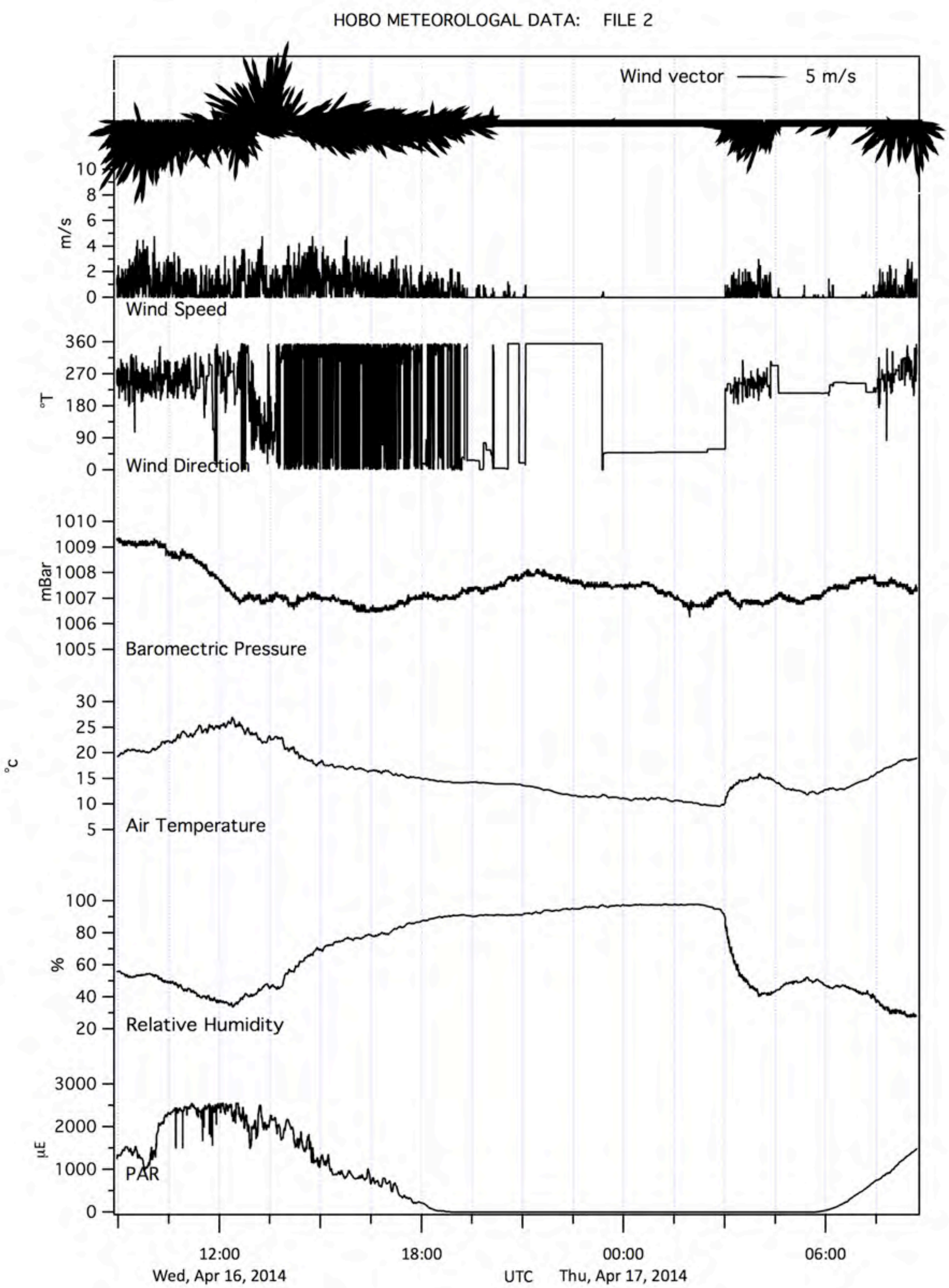

Figure I- 4. HOBO Meteorological Data File 2.

HOBO METEOROLOGAL DATA: FILE 3

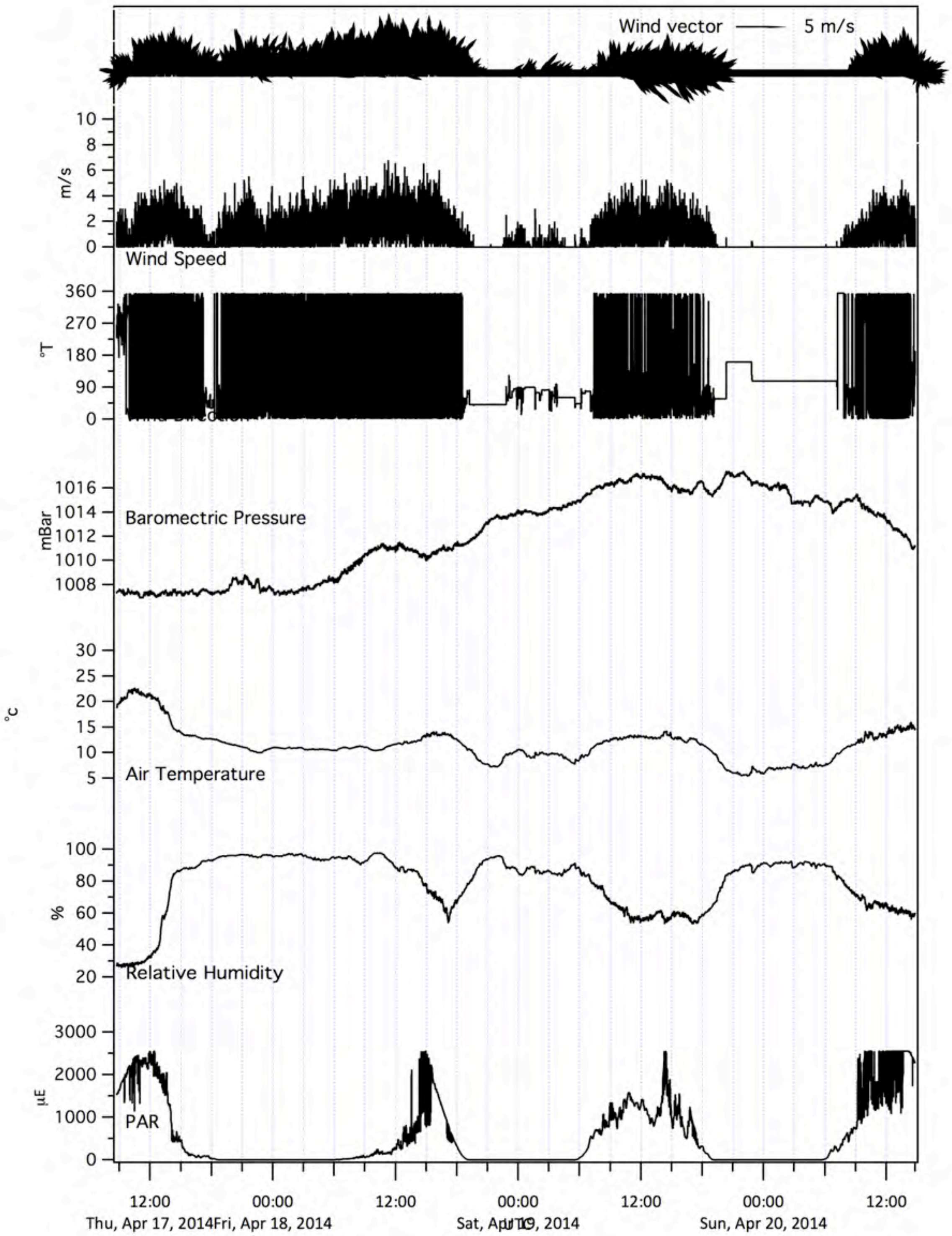

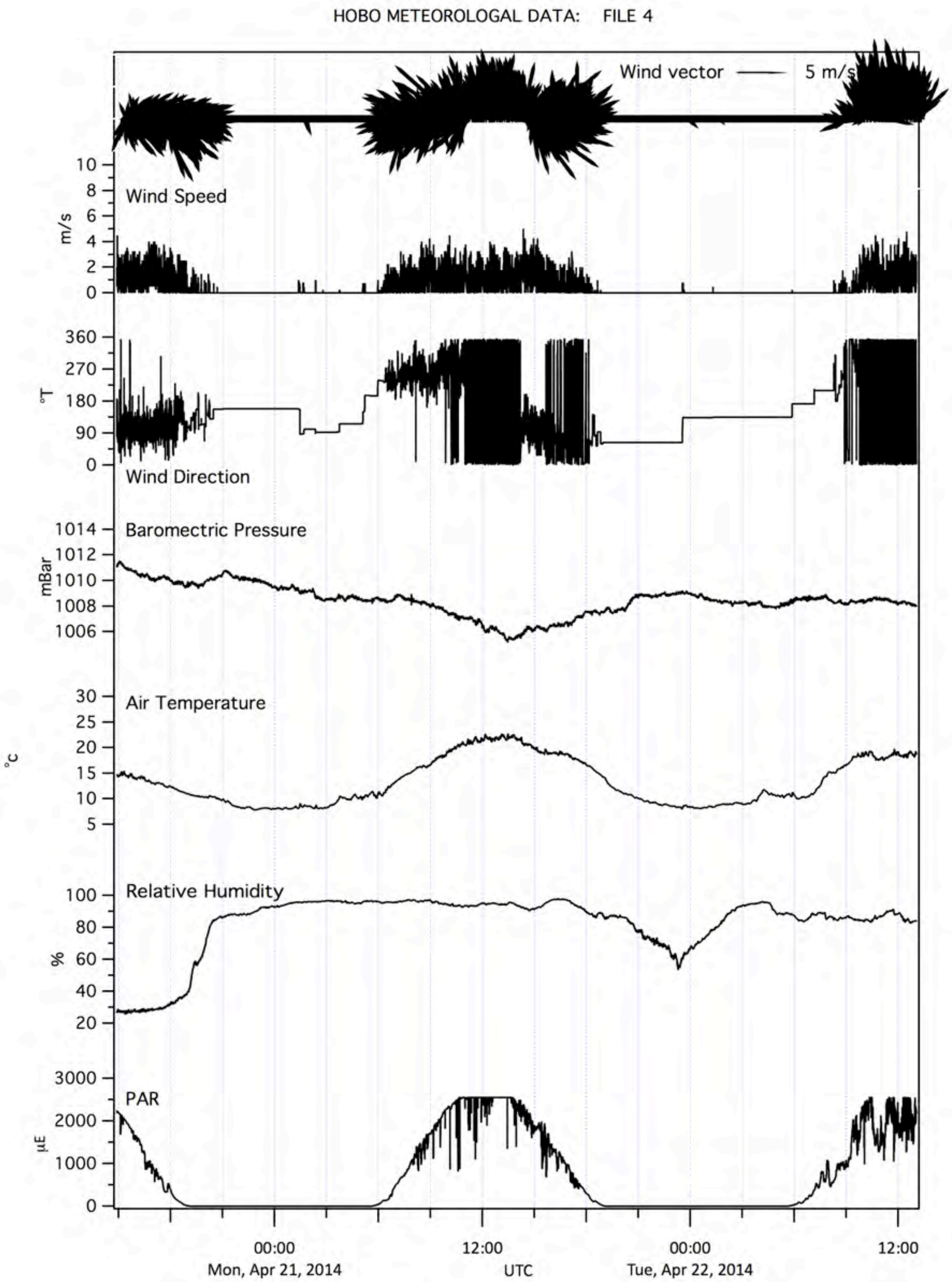

Figure I-5. HOBO Meteorological Data File 3.

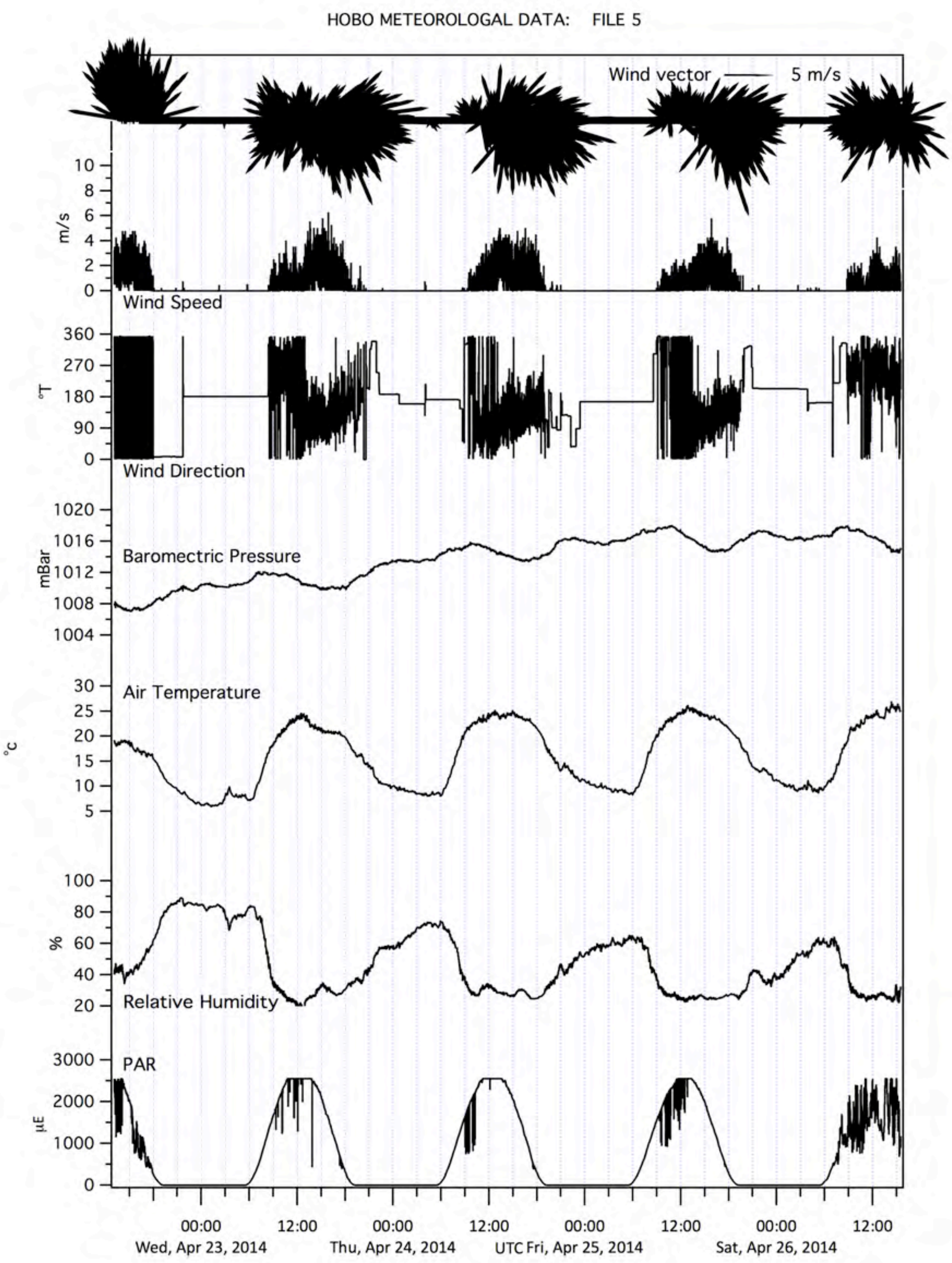

Figure I-6. HOBO Meteorological Data File 5.

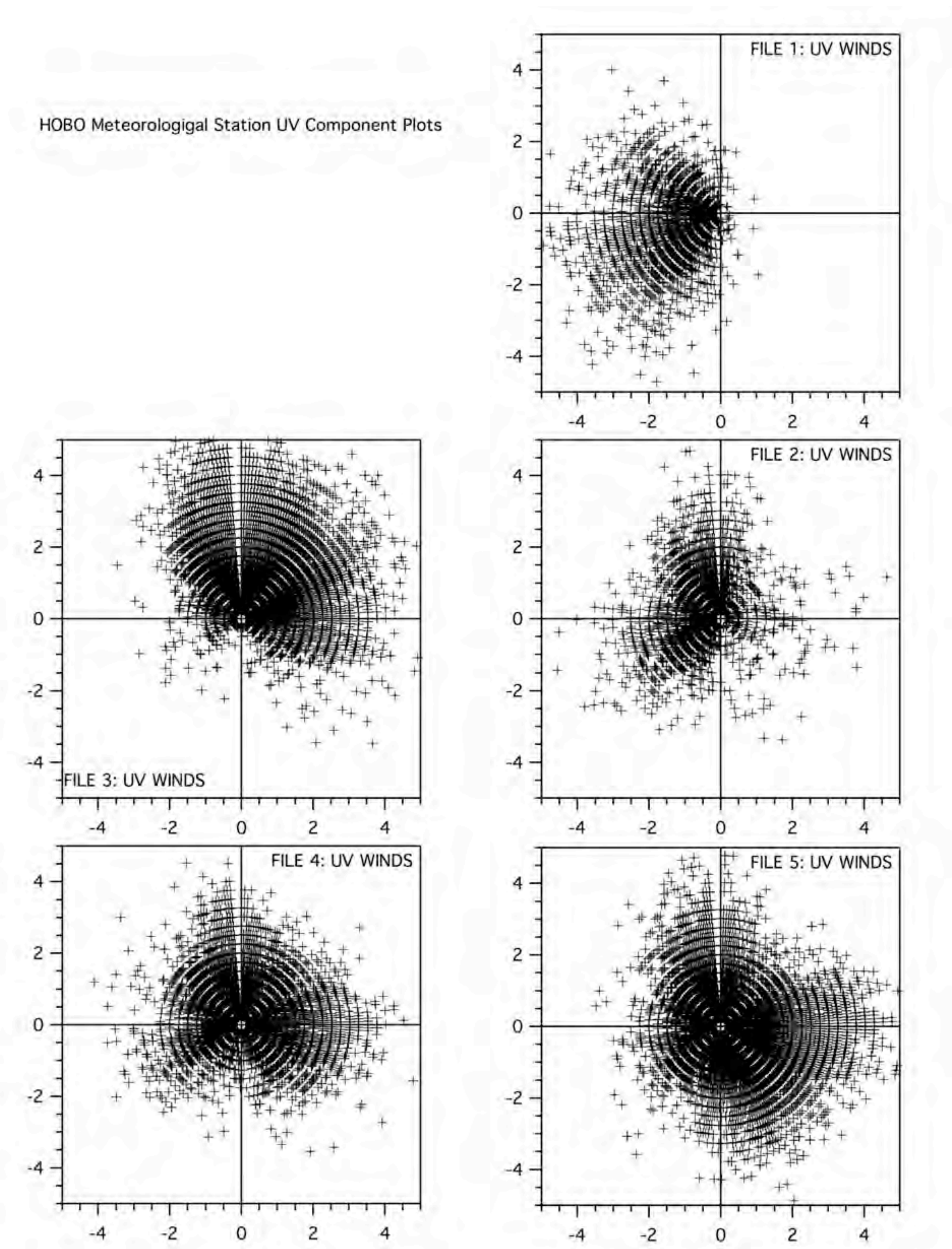

Figure I-7. HOBO Meteorological Data UV Component Scatter Plots.

APPENDIX J

Aerosols

Table of Contents

List of Figures

List of Tables

Introduction

Atmospheric correction of spectral region imagery requires consideration of surface roughness and correction of the actual surface pressure from the standard pressure of 1013 MB, the correction of the deviation of the actual ozone column content from a standard value of 350 Dobson Units (DU), and correction for water vapor and other gases such as Nitrogen Oxide (NO_2).

The range of DU along the central east coast of the Republic of Korea is listed in Table J-1 and graphed in Figure J-1 from 14-25 April 2014.

April 2014	Dobson Unit		April 2014	Dobson Unit	
	Low	High		Low	High
14	300	325	20	300	325
15	325	350	21	300	325
16	300	325	22	300	325
17	300	325	23	350	375
18	325	350	24	350	375
19	275	300	25	325	350
Ozone and UV Monitoring, Environment Canada. Available online. URL: http://exp-studies.tor.ec.gc.ca/clf2/e/main.html. Accessed on May 7, 2014.					

Table J- 1. Range of Dobson Units for Central East Coast of Korea

Monitoring of the ozone layer is performed by Environment Canada, Science and Technology Branch, Atmospheric Science and Technology Directorate, Air Quality Research Division. The below maps (Figure J-1) were computed from ground-based measurements and specialized sensors on satellites, such as the Total Ozone Mapping Spectrometer (TOMS), the Stratospheric Aerosol and Gas Experiment and the Solar Backscatter Ultra Violet spectrometer. The DU is the measure of ozone concentration. One DU is the number of molecules of ozone that would be required to create a layer of pure ozone 0.01 millimeters thick at a temperature of 0 ºC and a pressure of one atmosphere. The world average is about 300 units, it varies geographically from about 230 to 500 DUs.

These data are of potential value to remote sensing, especially for the atmospheric correction of WorldView-2 imagery and also for field spectroscopy.

The Ozone Monitoring Instrument measures ozone profiles at a spatial resolution of 36 x 48 km. It also measures key air quality components such as NO_2, SO_2, BrO, OClO, and aerosol characteristics.

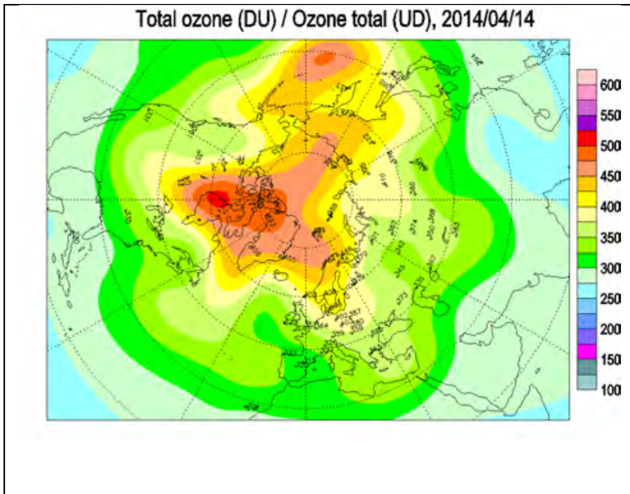
Total ozone (DU) / Ozone total (UD), 2014/04/14
600
550
500
450
400
350
300
250
200
150
100

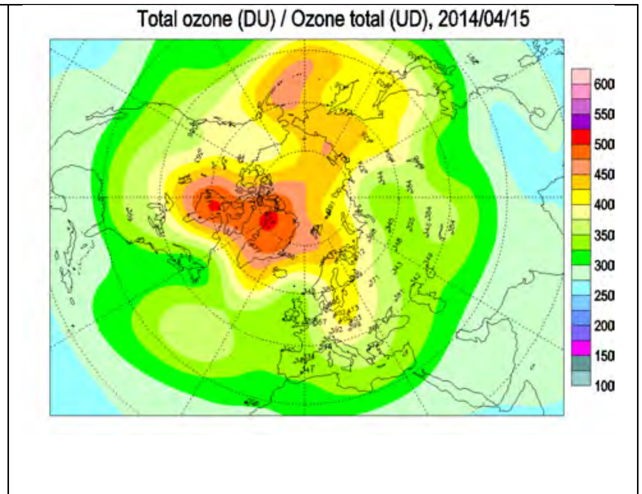
Total ozone (DU) / Ozone total (UD), 2014/04/15
600
550
500
450
400
350
300
250
200
150
100

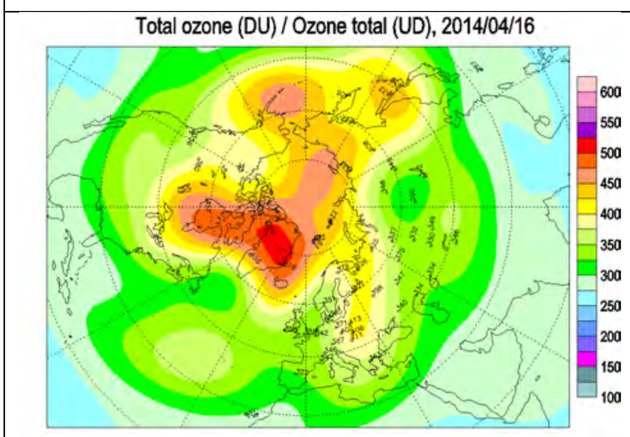
Total ozone (DU) / Ozone total (UD), 2014/04/16
600
550
500
450
400
350
300
250
200
150
100

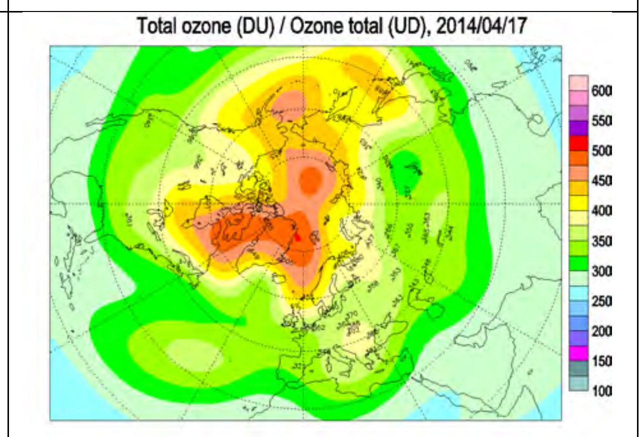
Total ozone (DU) / Ozone total (UD), 2014/04/17
600
550
500
450
400
350
300
250
200
150
100

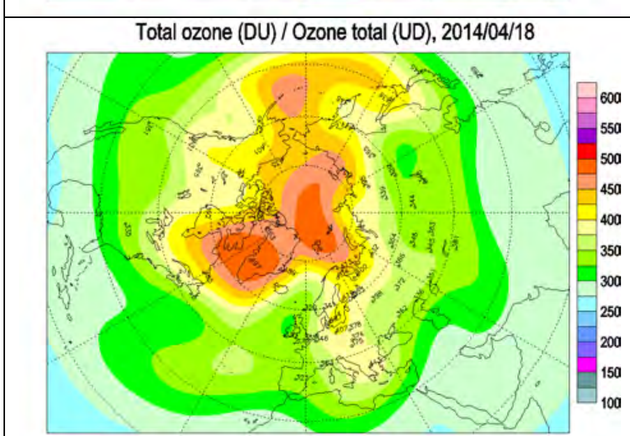
Total ozone (DU) / Ozone total (UD), 2014/04/18
600
550
500
450
400
350
300
250
200
150
100

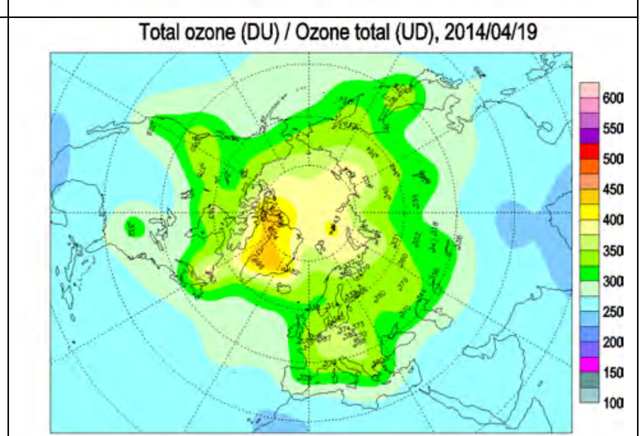
Total ozone (DU) / Ozone total (UD), 2014/04/19
600
550
500
450
400
350
300
250
200
150
100

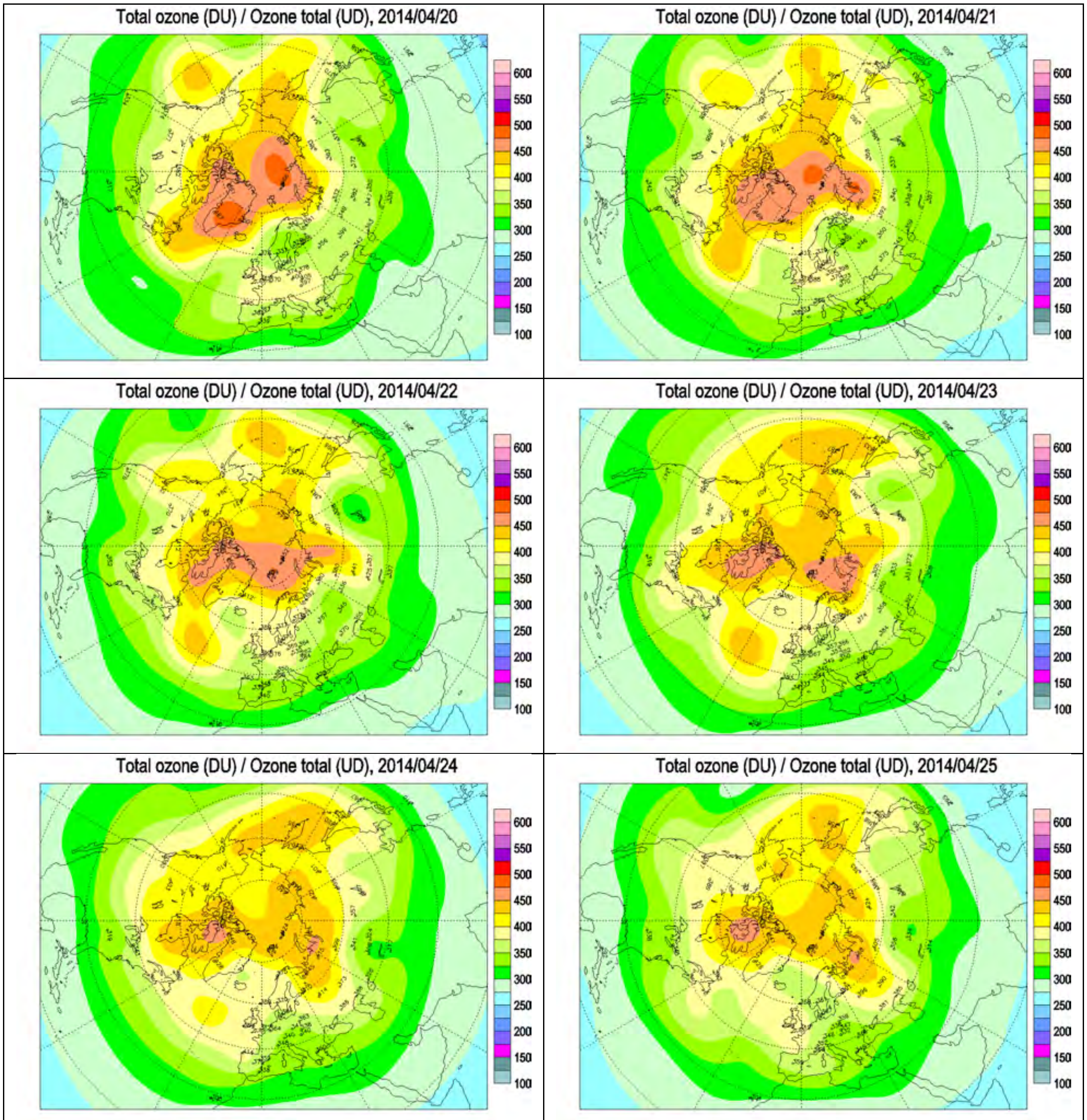

Environment Canada. Ozone and UV Monitoring. Available online. URL: http://exp-studies.tor.ec.gc.ca/clf2/e/main.html. Accessed on May 7, 2014.

Figure J- 1. Northern Hemisphere Ozone Map from 14-25 April 2014.

DU data for the ozone near Dogu Beach were also collected online from NOAA. The input information is in Table J-2 and the output is shown in Table J-3.

Table J- 2. Data Entered at NOAA Website with Results in Table J-3.

Field	Value
Latitude:	35.999
Longitude:	129.426
Start Date:	2014-04-14
End Date:	2014-04-25
All Data:	False
Entry Cnt:	9

Table J- 3. Daily Average Total Column Ozone values in Dobson Units from: Latitude 35.999. Longitude 129.426.

Year	Month	Day	Julian	OMI_O3 (Dobson)	Lat_Diff	Lon_Diff
2014	4	14	104	314	0.124	0.051
2014	4	16	106	337	0.124	0.051
2014	4	17	107	336	0.124	0.051
2014	4	18	108	326	0.124	0.051
2014	4	19	109	335	0.124	0.051
2014	4	20	110	325	0.124	0.051
2014	4	21	111	369	0.124	0.051
2014	4	23	113	327	0.124	0.051
2014	4	25	115	346	0.124	0.051
OMI Ozone Time Series Data. URL: http://www.esrl.noaa.gov/gmd/grad/neubrew/OmiDataTimeSeries.jsp						

APPENDIX K

Bathymetry

Table of Contents

Table of Figures

Introduction

Bathymetric soundings integrated with GPS coordinates were collected using the HydroLite-TM™ along the approaches of landing beaches at Dogu, Doksuk-ri, and Hwajin-ri. Hydrographic survey data have been archived in the Ssang Yong 2014 Geodatabase. These data were used to create point, TIN, Raster, and contour features, which may be used for comparison with older surveys and imagery-derived bathymetric retrievals. The measured and logged depths were used with other GPS survey data to create beach profiles and to characterize obstacles and man-made features. The following figures highlight very shallow water and surf zone soundings collected offshore of each landing beach.

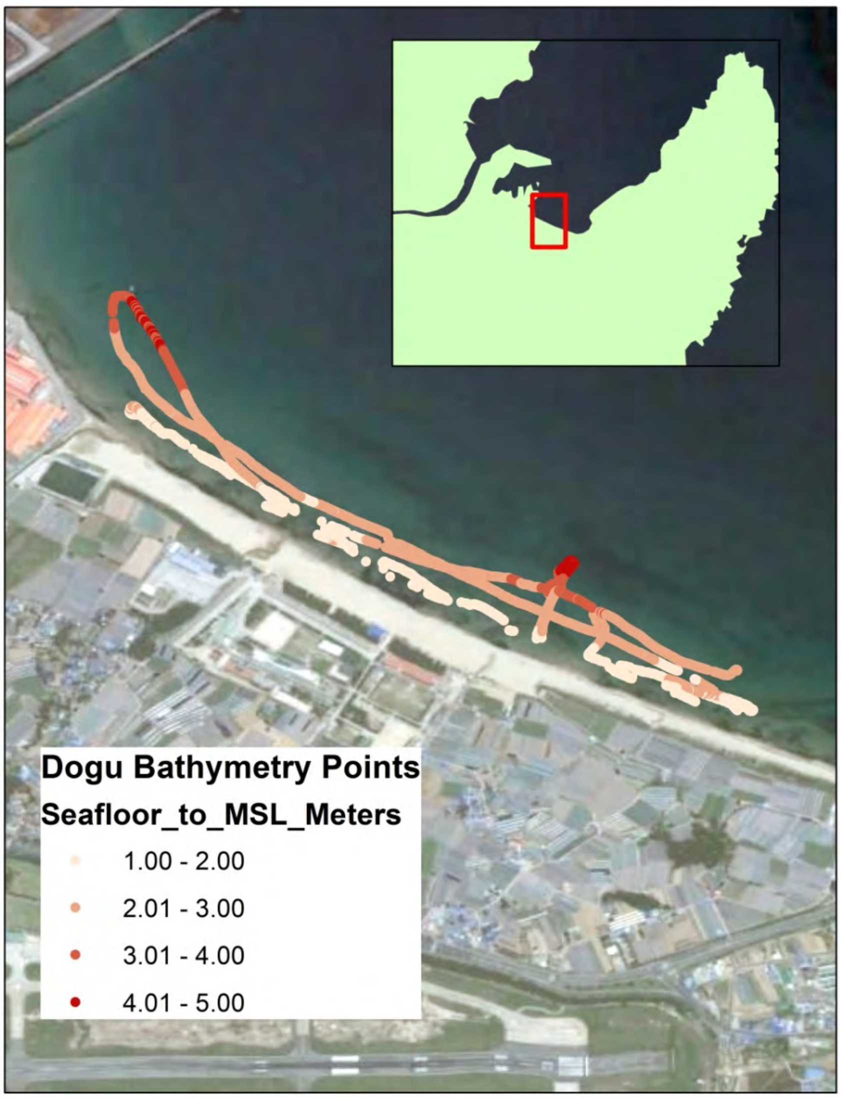

Figure K- 1. Dogu beach in Pohang, South Korea. Bathymetric soundings support surf zone breaching by amphibious craft and the installation of floating or elevated causeways for Combined/Joint Logistics Over the Shore.

Figure K- 2. Doksuk-ri beach in Republic of Korea. Updated very shallow water hydrography supports amphibious planners concerned with the impact of waves, tides, and very shallow processes on surf zone

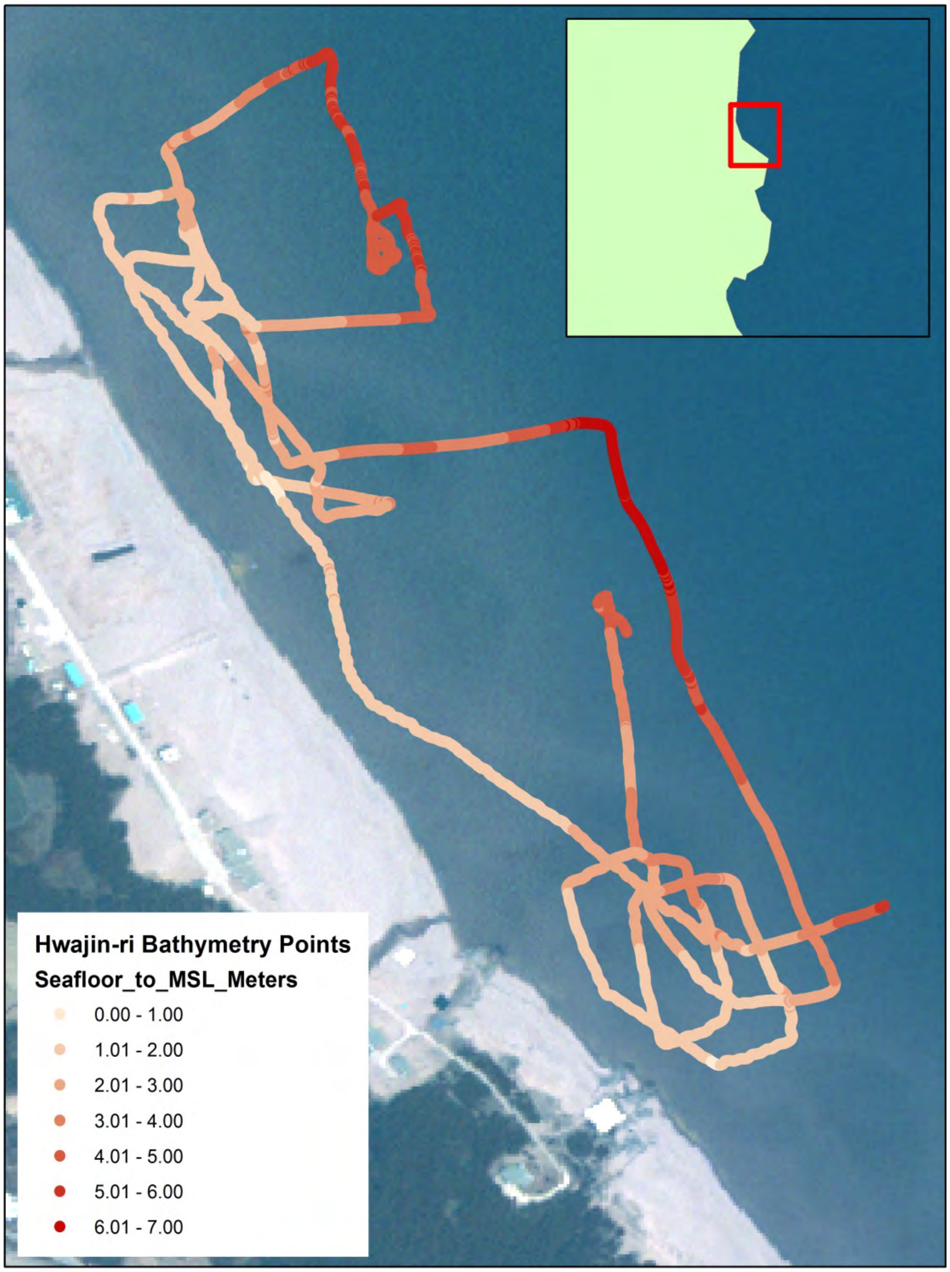

Figure K- 3. Hwajin-ri beach in republic of Korea. Updated very shallow water bathymetry provides littoral situational awareness for the amphibious landing, which is the culminating event for Exercise Ssang Yong.

APPENDIX L

Tide Predictions

Introduction

Tide predictions were obtained from the Korea Hydrographic and Oceanic Administration (KHOA). This information includes the predicted high and low waters for April 2014. The predicted values are graphed in Figure L-1. Tidal data are also listed in Table L-1. Spring tides occurred in concert with the full moon around April 14, 2014. During this period, high tides were higher than usual and the low tides were lower. Tide predictions have also been obtained for March and May, which may be found copied into \SsangYong 2014\Attribute_Data\Oceanic\Predictive_Tide_Data\Pohang_March_May2014.docx of the Ssang Yong 2014 Geodatabase.

Scientists carefully monitored the tides while working with equipment on the beach or in vessels during shallow water operations. Besides using this data to protect equipment and safeguard personnel, the information is useful to predict how much beach is available for maneuver at all phases of the tide. Knowledge of the tides was used to synchronize imagery, planning the timing for beach studies, and to avoid grounding during hydrographic surveys.

This information was also useful in planning the time for the collection of geotechnical data and spectra to characterize trafficability parameters.

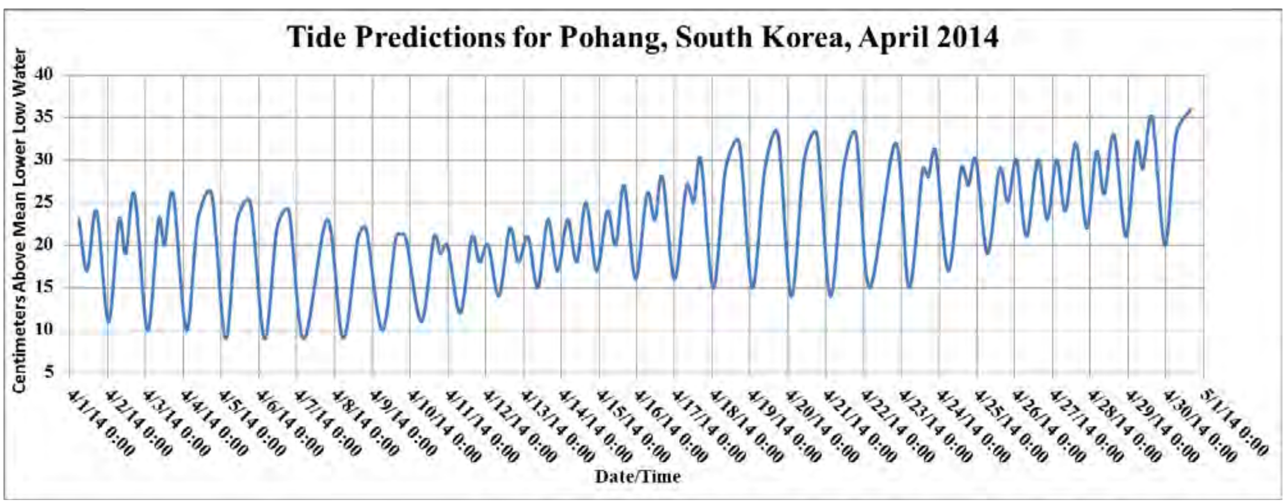

Figure L- 1. Tide predictions for Pohang in South Korea. Predictions from KHOA are referenced to mean lower low water.

Table L-1. April 2014 Pohang Tide Forecast obtained from KHOA. Times are local (UTC +9).

▲ : High water ▼ : Low water   h: m (height) / (hour : minute (cm))   Tide datum: mean lower low water

Lunar phase	Date	h : m (height)	h : m (height)	h : m (height)	h : m (height)	Lunar
	1	05 : 40 (23) ▲	10 : 48 (17) ▼	16 : 30 (24) ▲		03/02
	2	00 : 23 (11) ▼	07 : 05 (23) ▲	11 : 22 (19) ▼	16 : 55 (26) ▲	03/03
	3	01 : 10 (10) ▼	08 : 12 (23) ▲	11 : 58 (20) ▼	17 : 25 (26) ▲	03/04
	4	01 : 56 (10) ▼	09 : 11 (23) ▲	17 : 56 (26) ▲		03/05
	5	02 : 43 (9) ▼	10 : 11 (23) ▲	18 : 28 (25) ▲		03/06
	6	03 : 32 (9) ▼	11 : 27 (22) ▲	18 : 59 (24) ▲		03/07
◐	**7**	04 : 26 (9) ▼	19 : 26 (23) ▲			03/08
	8	05 : 22 (9) ▼	15 : 00 (21) ▲	19 : 58 (22) ▲		03/09
	9	06 : 16 (10) ▼	15 : 09 (21) ▲	21 : 01 (21) ▲		03/10
	10	07 : 04 (11) ▼	15 : 09 (21) ▲	19 : 15 (19) ▼	23 : 43 (20) ▲	03/11
	11	07 : 46 (12) ▼	15 : 08 (21) ▲	20 : 01 (18) ▼		03/12
	12	01 : 34 (20) ▲	08 : 25 (14) ▼	15 : 16 (22) ▲	20 : 46 (18) ▼	03/13
	13	02 : 49 (21) ▲	09 : 04 (15) ▼	15 : 28 (23) ▲	21 : 35 (17) ▼	03/14
	14	03 : 57 (23) ▲	09 : 47 (18) ▼	15 : 43 (25) ▲	22 : 24 (17) ▼	03/15
○	**15**	05 : 13 (24) ▲	10 : 34 (20) ▼	15 : 57 (27) ▲	23 : 09 (16) ▼	03/16
	16	06 : 26 (26) ▲	11 : 24 (23) ▼	16 : 13 (28) ▲	23 : 51 (16) ▼	03/17
	17	07 : 29 (27) ▲	12 : 03 (25) ▼	16 : 35 (30) ▲		03/18
	18	00 : 32 (15) ▼	08 : 25 (29) ▲	17 : 02 (32) ▲		03/19
	19	01 : 14 (15) ▼	09 : 19 (29) ▲	17 : 36 (33) ▲		03/20
	20	01 : 59 (14) ▼	10 : 13 (30) ▲	18 : 17 (33) ▲		03/21
	21	02 : 49 (14) ▼	11 : 15 (29) ▲	19 : 10 (33) ▲		03/22
◑	**22**	03 : 45 (15) ▼	20 : 18 (32) ▲			03/23
	23	04 : 44 (15) ▼	13 : 32 (29) ▲	17 : 08 (28) ▼	21 : 45 (31) ▲	03/24
	24	05 : 43 (17) ▼	13 : 57 (29) ▲	18 : 26 (27) ▼	23 : 22 (30) ▲	03/25
	25	06 : 38 (19) ▼	14 : 20 (29) ▲	19 : 35 (25) ▼		03/26
	26	01 : 01 (30) ▲	07 : 27 (21) ▼	14 : 38 (30) ▲	20 : 39 (23) ▼	03/27
	27	02 : 31 (30) ▲	08 : 10 (24) ▼	14 : 48 (32) ▲	21 : 39 (22) ▼	03/28
	28	03 : 53 (31) ▲	08 : 46 (26) ▼	14 : 59 (33) ▲	22 : 33 (21) ▼	03/29
●	**29**	05 : 14 (32) ▲	09 : 19 (29) ▼	15 : 17 (35) ▲	23 : 21 (20) ▼	04/01
	30	06 : 27 (33) ▲	15 : 41 (36) ▲			04/02

For additional tide predictions refer to URL: http://khoa.go.kr.

APPENDIX M

Water Level Buoys

Introduction

Two water level buoys were deployed during the Ssang Yong 2014 Remote Sensing Experiment in order to collect *in-situ* tide information. A pelican case with Trimble R-8 GPS sensors were strapped onto the center of each buoy and deployed at Dogu beach and Doksuk-ri beach. The sensors recorded data every 15 seconds while deployed. Table M-1 provides buoy locations and average height above the ellipsoid for the data collected. Figures M-1 and M-2 provide time series of the water level fluctuations. Data downloads and battery changes occurred on 17, 21, and 24 April 2014 causing small gaps in the time series (see Table M-2). These gaps may be filled using either predictions or water level gage data. A picture of a deployed buoy off of Doksuk-ri beach is provided in Figure M-3.

Table M- 1. Information on Buoys deployed during Ssang Yong 2014.

Buoy Location	Latitude	Longitude	Average Height Above WGS 84
Dogu Beach	35.99865	129.43170	29.519
Doksuk-ri Beach	36.22835	129.38346	29.434

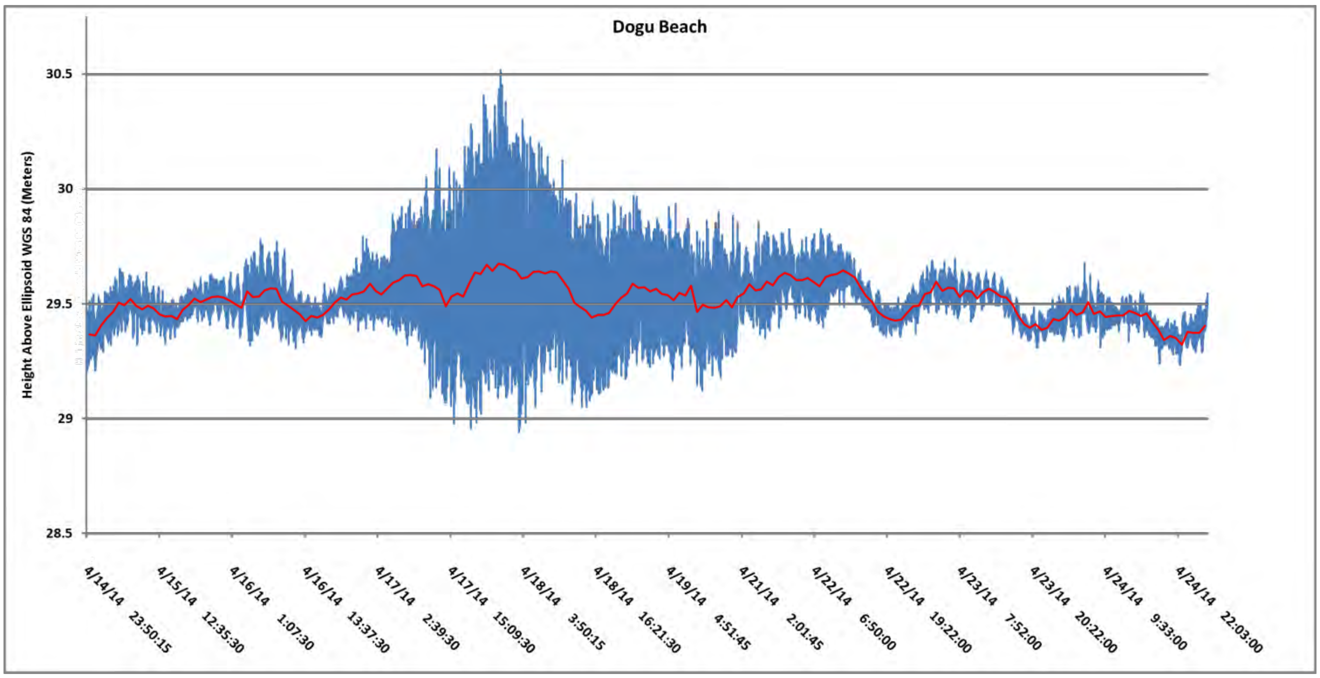

Figure M- 1. Water level data from Dogu beach. Hourly average water levels are in red.

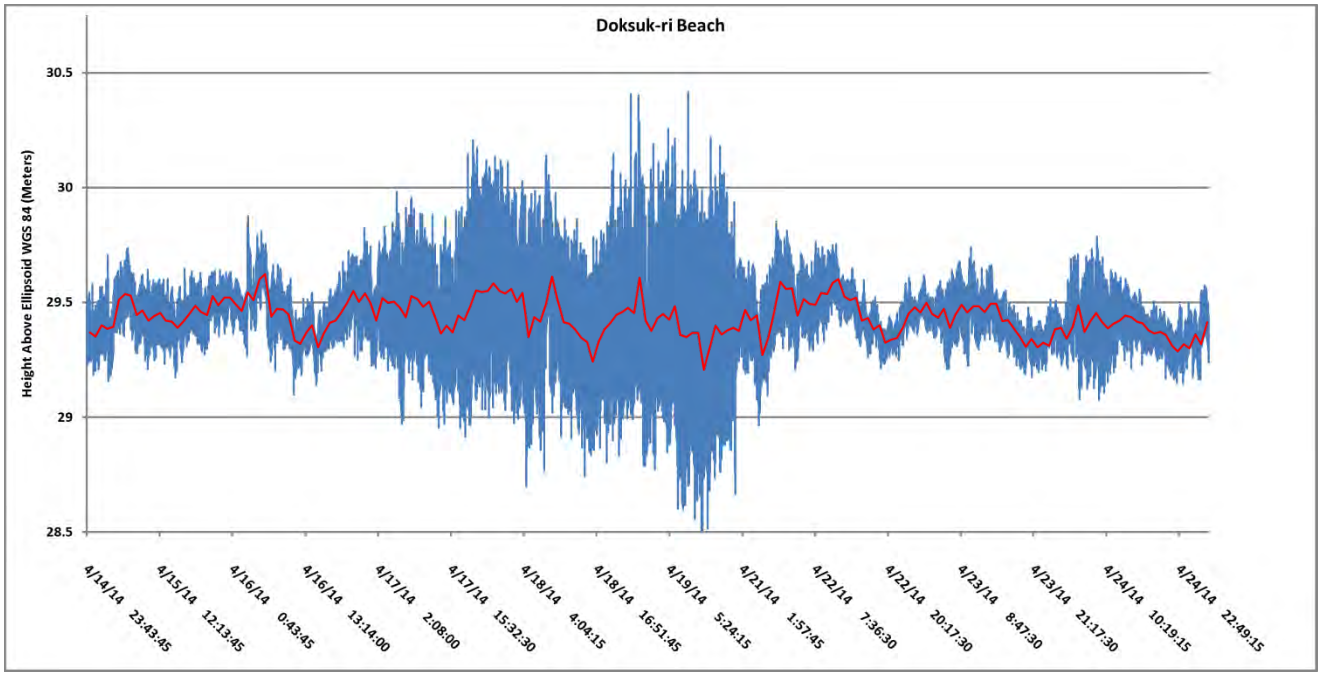

Figure M- 2. Water level data from Doksuk-ri Beach. Hourly averaged water levels are in red.

Table M- 2. Start and stop times for buoy data collection during battery exchange and data downloads.

Buoy Location	Collecting Data	Date	Local Time (UTC +9)
Dogu	Stopped	17April2014	09:29:45
Doksuk-ri			15:54:00
Dogu	Started	17April2014	09:52:15
Doksuk-ri			16:16:45
Dogu	Stopped	21April2014	09:46:00
Doksuk-ri			12:04:15
Dogu	Started	21April2014	10:18:30
Doksuk-ri			12:44:30
Dogu	Stopped	24April2014	08:59:45
Doksuk-ri			12:17:00
Dogu	Started	24April2014	09:22:45
Doksuk-ri			12:33:30

Figure M- 3. Water Level Buoy sited near Doksuk-ri beach. Data downloads and battery changes were accomplished with a RHIB.

APPENDIX N

Water Loggers

Table of Contents

List of Figures

List of Tables

Introduction

The water loggers were placed in the nearshore at Dogu beach, Hwajin-ri beach, and Doksuk-ri beach. These loggers measure temperature and pressure, which were used to determine water height in reference to mean sea level in order to de-tide very shallow water hydrographic survey data from the nearshore zone at Dogu, Hwajin-ri, and Doksuk-ri . Below are the methods used to convert the raw data into usable and readable format. For a summary of the data see Figure N-1 at the end of this appendix.

Methods

Determination of water level from HOBO U20 water level data logger:

During the Ssang Yong 2014 Remote Sensing Exercise, water level data were measured with three HOBO U20 Water Level Data Loggers. Specifications for the water level sensor can be found online at http://ww.onsetcomp.com. Upon completion of the exercise, water level data were transferred to binary data files for storage and subsequent processing. The data from each sensor were further processed from binary to ascii readable text with provided software. The resulting output file contained ascii tab delimited text containing Date, Time (sec), Absolute Pressure (mBars), and Temperature (°C).

Water level was determined from Absolute Pressure by the following:

1. $P_{abs} = P_{water} + P_{air}$ where P_{abs} is the Pressure (mbar) recorded by the sensor $P_w = \rho g h$ and P_{air} is atmospheric pressure recorded from a nearby station ρ is water density (kg m^{-3}), $\boldsymbol{g}$ is gravitational acceleration and is assumed to be 9.8 m/s^2 , and $\boldsymbol{h}$ is the height (m) of the water column above the sensor. Rearranging terms and applying unit conversions (mbar to Pa) to the data yields the necessary algorithm for converting P_{abs} to $\boldsymbol{h}$ and $\boldsymbol{c}$ is the unit conversion factor from mbar to Pa

$$h = \frac{c\left(P_{abs} - P_{air}\right)}{\rho_w g} = \frac{100\left(P_{abs} - P_{air}\right)}{\rho_w \,\mathrm{x}9.8}$$

2. The seawater density was calculated from the temperature time series records and salinity climatology, since conductivity (which is used to derive salinity) was not available. An estimate for salinity was obtained from the literature (citation needed). Note: variations in density due to isothermal compression are negligible (<< 1%) for depths less than a 1000 m (Pond and Pickard, 1983). Table 1 below provides the values used for the density calculation. An average temperature was determined from each time series record. Uncertainty in the salinity estimate is considerably more of a problem than the small variations (< 0.5 ºC) in the temperature record for density calculation.

Table N- 1. Values used for Seawater Denstiy Estimate.

Location	Temperature (ºC)	Salinity PSU	Density (kg m^{-3})
Dogu	14.6± 0.42	35	1026
Doksuk-ri	14.5± 0.37	33	1024
Hwajin-ri	14.2± 0.48	35	1026

3.Once the density was determined for each station, the algorithm in Paragraph 1 was applied to each time series to obtain the atmospherically corrected water levels. Absolute pressure data was recorded at 30s intervals while atmospheric pressure was sampled at 10 s intervals. To match the different time series it was necessary to resample the atmospheric pressure record to 30s intervals. The resulting output from each time series is shown in the subsequent figure (indicated by the black trace). Subsequently a 3-Hour Low Pass (HLP) Boxcar filter was applied to the data to resolve the tidal signature more clearly. The 3 HLP filtered signal is denoted by the red trace. The 3 HLP filter consisted of a 2M+1 window where M = 360 and is given by

$$\bar{h}(i) = \frac{1}{2M+1}\sum_{j=-M}^{M} x(i+j)$$

where $\bar{h}(i)$ is the replaced average value of the time series at the position *i*

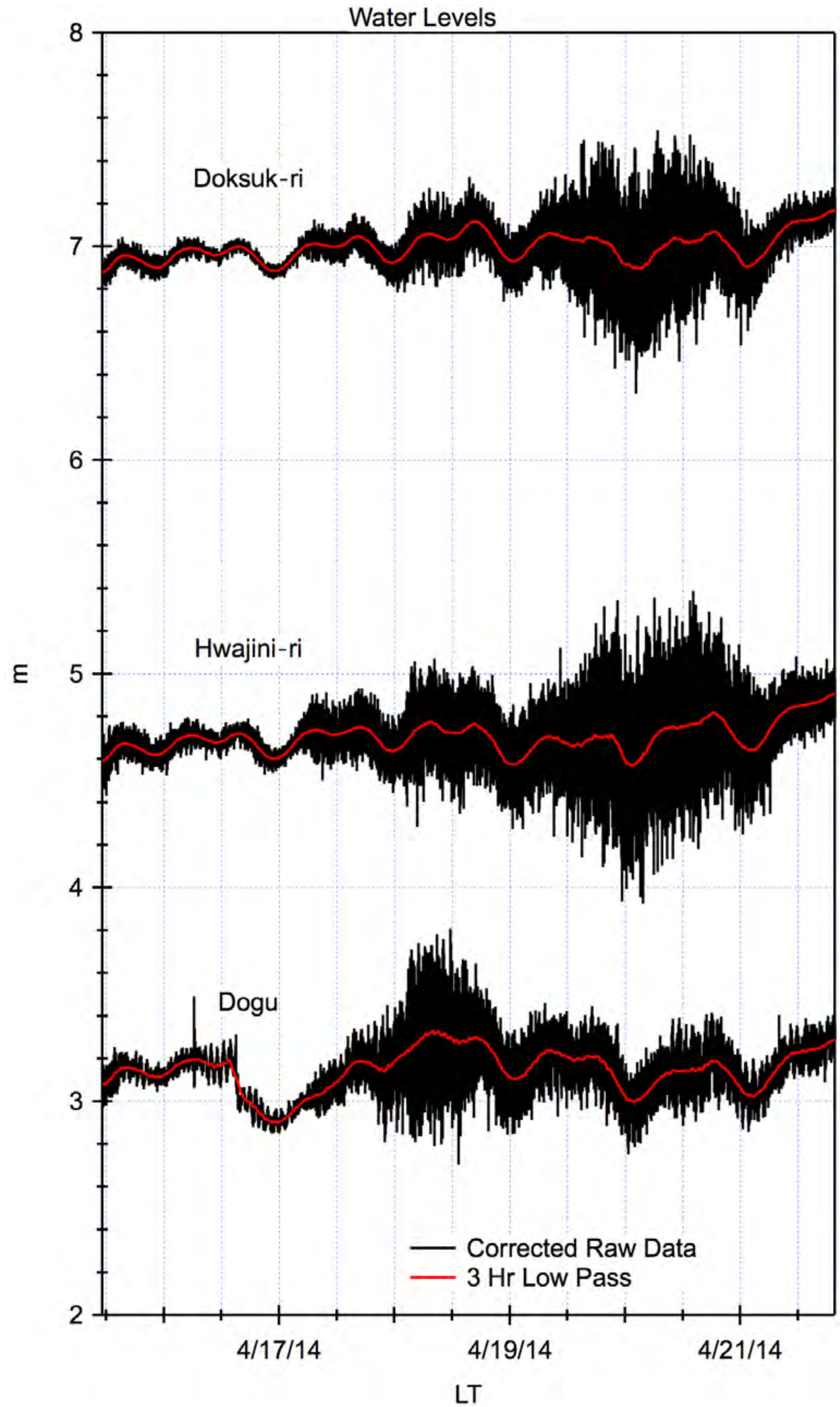

Figure N- 1. Summary of Water Level fluctuations from HOBO water level gages.

APPENDIX O

Ssang Yong 2014 Geodatabase

Table of Contents

List of Figures

List of Tables

Introduction

A file geodatabase was created using ArcGIS. It is a collection of files in a folder on disk that can store, query, and manage both spatial and non-spatial data. The geodatabase uses a very efficient data structure that is optimized for performance and storage. This appendix is designed to show information within the Geodatabase. Additional information to help a user navigate the SsangYong2014.mxd map document is provided in Appendix P.

Presently the directory *Ssang Yong 2014* contains three sub-directories: (a) Attribute_Data, (b) GIS_Data, (c) Products, and (d) SsangYong2014.gdb. Files include (a) Data.xlsx, which is an Excel workbook and (b) SsangYong2014.mxd, which is an ESRI ArcMap map document (see Figure 1). For this work, the SsangYong2014 directory (ending in .gdb) is in the ESRI File Geodatabase Format, which has an open Advanced Programming Interface (API) which many 3rd party programs can read. This allowed previous work with the Australian Defence Force to be used with GlobalMapper.

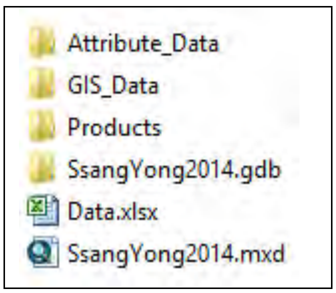

Figure O-1. Contents of Ssang Yong 2014 Geodatabase. The file geodatabase contains both spatial and non-spatial data.

Summary of Contents and Appendix Design Information

The Attribute_Data sub-directory was created for storing data collected during the Ssang Yong 2014 experiment, and baseline data collected in advance of the experiment, in raw and processed formats. Additional ArcMap documents and Triangulated Irregular Networks (TINs) are located within the GIS_Data sub-directory. The Products sub-directory contains the Data Report and images created from ESRI ArcMap and Environment for Visualizing Images (ENVI) software. ESRI's File Geodatabase includes a variety of GIS file formats. The geodatabase is the native data structure for ArcGIS and is the primary data format used for editing and data management. The contents of the geodatabase include feature classes, raster datasets, tables, and relationship classes. Feature classes have similar spatial representations, such as points, lines, or polygons, and a common set of attribute columns, e.g., a point feature class may represent GPS point data of sampled locations. Attributes are descriptive pieces of information that describe the geographic features represented in the spatial dataset. Raster data sets are made of rows and columns, where individual cells contain attribute values and location coordinates. Tables, when uploaded to a GIS, may be linked to other feature classes through linking identifiers within the data. Relationship classes are used to link feature

classes or a feature class to a table. The Excel Workbook contains spreadsheets of various types of data that were collected during the experiment and is linked to the map document interface. Associated ReadMe text files stored within the database describe the data and any issues encountered during collection or data processing.

The manner in which different data types are being stored in the Ssang Yong 2014 Geodatabase are described in Figures O-2 through O-11. Information for each of the three sub-directories (Attribute_Data, GIS_Data, Products) is described in three panels. The first two panels show the respective directory and sub-directories through highlights. Important folder contents are listed in the third panel on the right side of each figure. To access the ESRI File Geodatabase (SsangYong2014.gdb), open ArcMap or ArcCatalog. The various data types used in the file geodatabase are described in Table O-1. The Excel Workbook (Data) contents are described in Table O-2.

Contents of \Ssang Yong 2014\Attribute_Data
Contents of \Ssang Yong 2014\Attribute_Data\ASD

Spectral nadir data collected with a portable ASD field spectrometer rover unit and ASD base station mounted on a tripod are provided in Figure O-2.

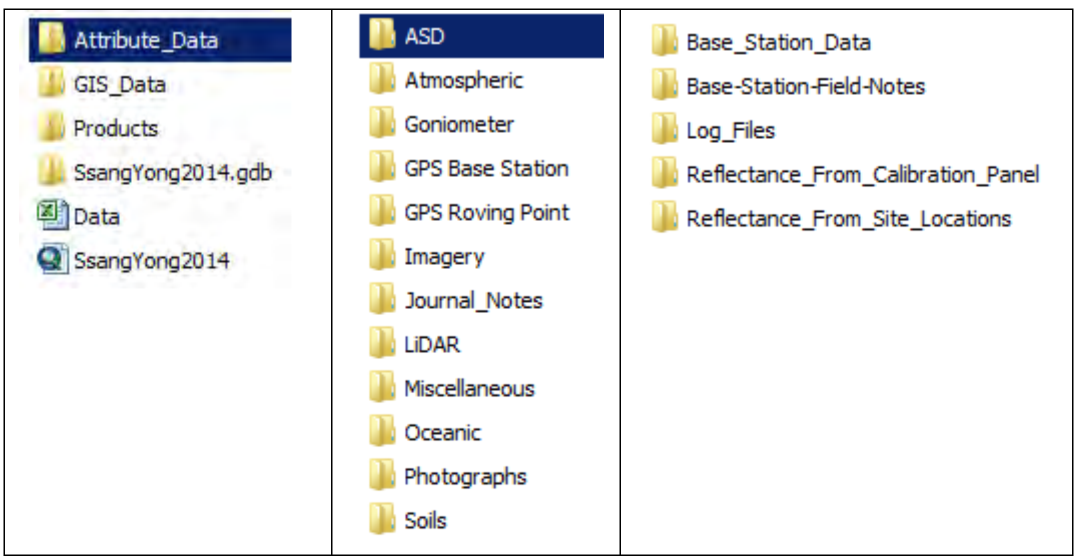

Figure O-2. \Ssang Yong 2014\Attribute_Data\ASD.

Contents of \Ssang Yong 2014\Attribute_Data\Atmosphere

The Atmosphere directory (see Figure O-3) contains raw and processed weather station date along with aerosol information and climate data.

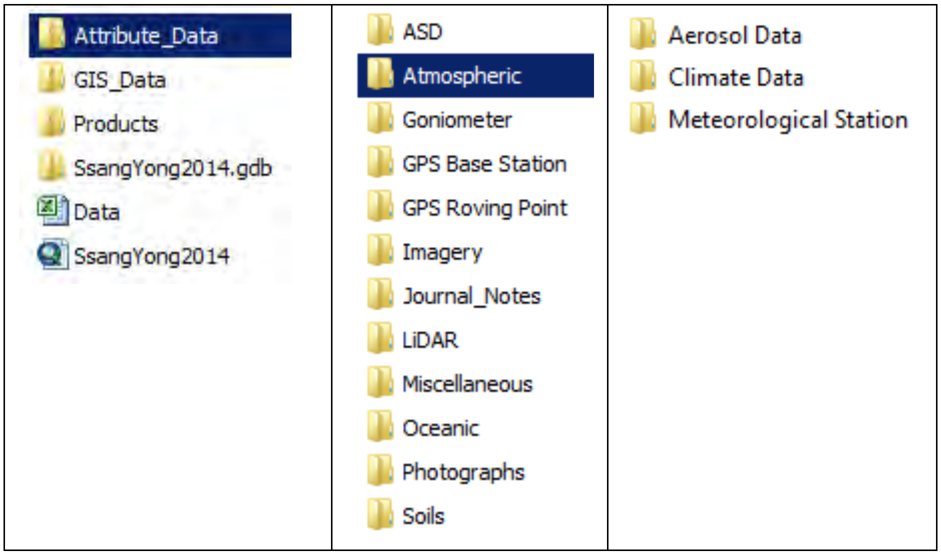

Figure O-3. \Ssang Yong 2014\Attribute_Data\Atmospheric.

Contents of \Ssang Yong 2014\Attribute_Data\Goniometer

GRIT ASD spectral files, relevant field notes, and GOPRO photographs have been uploaded to the Goniometer folder (see Figure O-4).

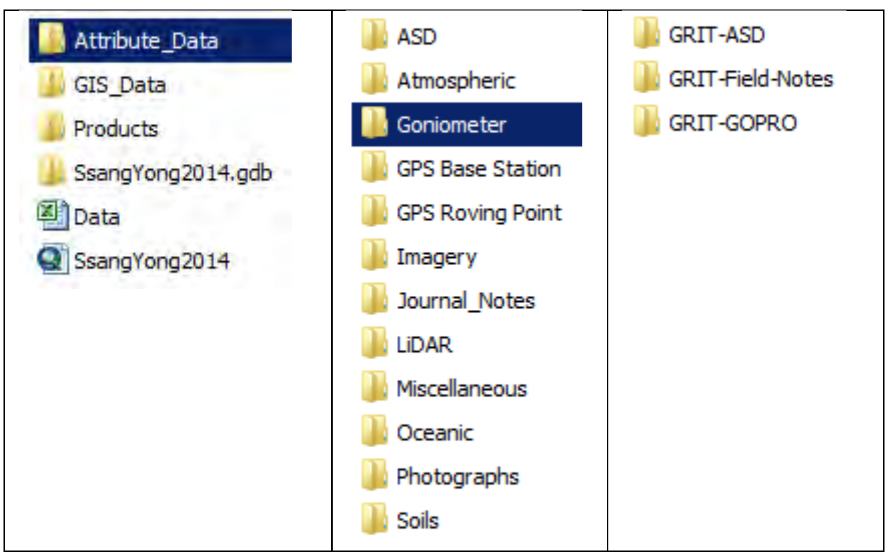

Figure O-4. \Ssang Yong 2014\Attribute_Data\Goniometer.

Contents of \Ssang Yong 2014\Attribute_Data\GPS Base Station

Figure O-5 describes the archival of raw GPS base station data, RINEX conversions, and NOAA's online OPUS solutions. Receiver Independent Exchange Format (RINEX) is a data interchange format for raw satellite navigation system data. This allowed the team to post-process the received data to produce more accurate results. NOAAs Online

Positioning User Service (OPUS) provided simple access to high-accuracy National Spatial Reference System (NSRS) coordinates.

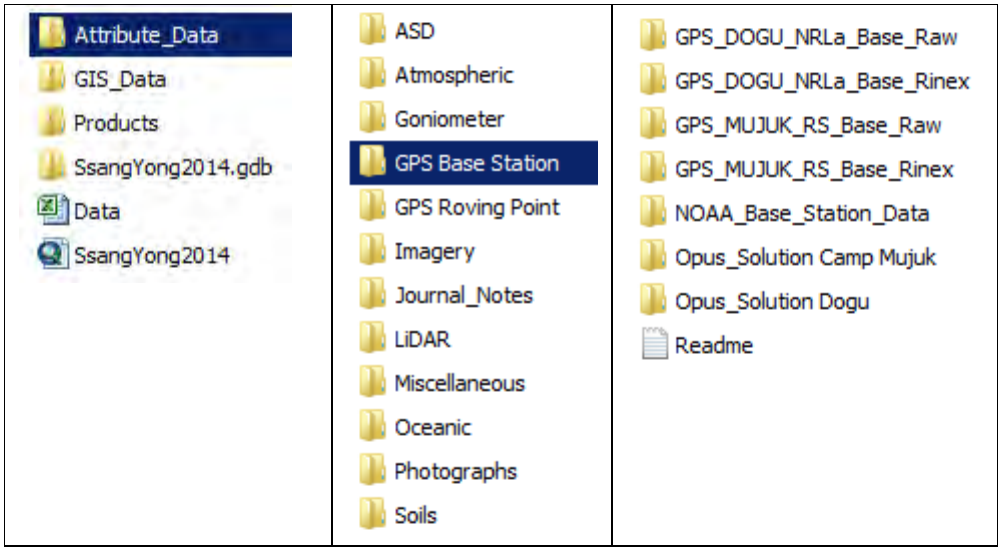

Figure O-5. \Ssang Yong 2014\Attribute_Data\GPS Base Statioin.

Contents of \Ssang Yong 2014\Attribute_Data\GPS Roving Point

To see where all point and roving GPS data collected during the experiment in original download, RINEX, and final processed formats, see Figure O-6. The Excel Workbook located in the GPS Roving Point directory contains notes taken for GPS points on the dates from 23 to 25 April 2014.

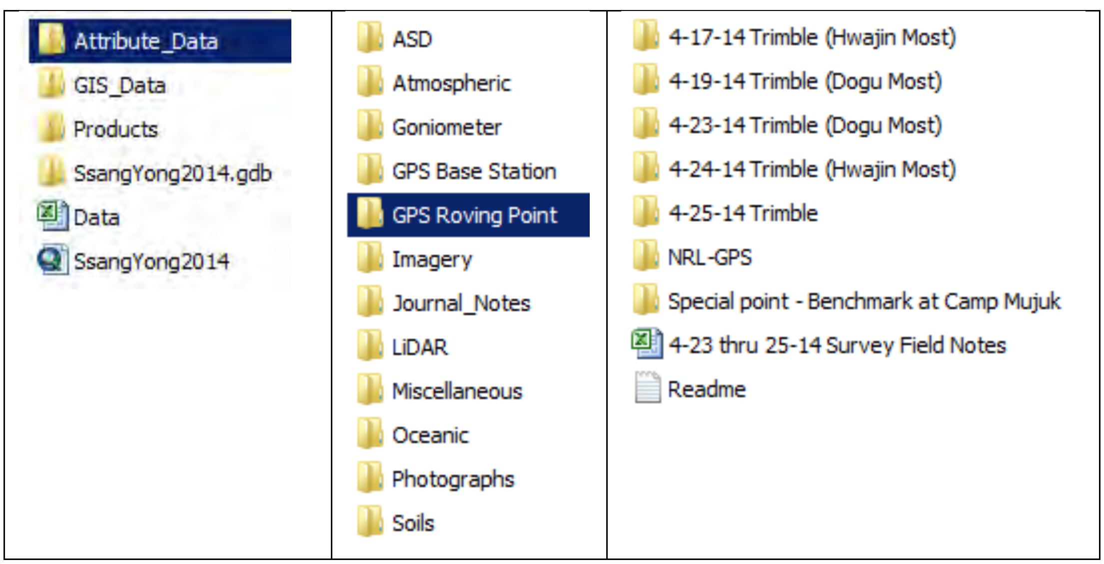

Figure O-6. \Ssang Yong 2014\Attribute_Data\GPS Roving Point.

Contents of \Ssang Yong 2014\Attribute_Data\Imagery

Refer to Figure O-7 to see the location of imagery from USGS (Landsat 5 and 8), Digital Globe (WorldView-2), and NASA (MODIS). The Word document and Landsat 5 Bands text file, located in the Imagery folder, contain spectral band information.

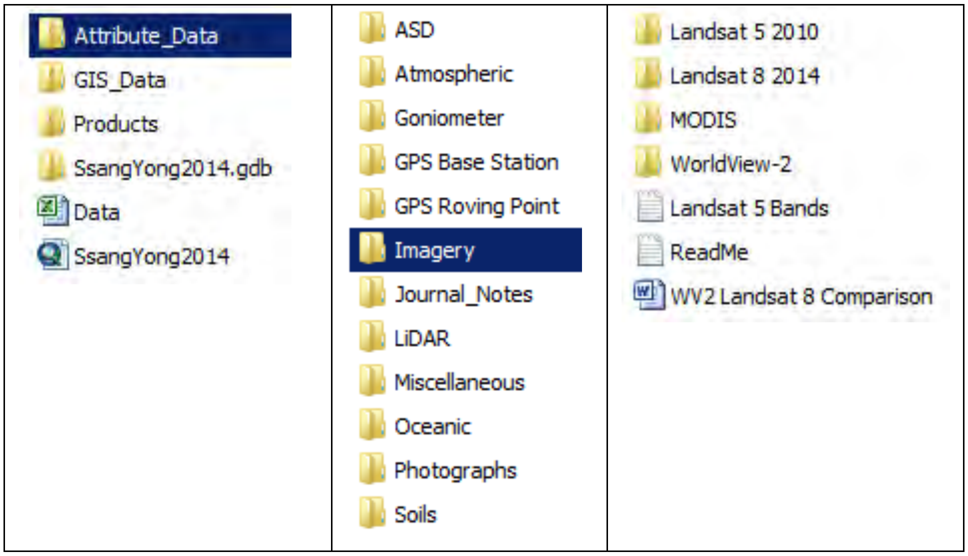

Figure O-7. \Ssang Yong 2014\Attribute_Data\Imagery.

Contents of \Ssang Yong 2014\Attribute_Data\Journal_Notes

Scientific observations were also recorded in field notes, which included instrument set-up and operation information along with observations about the samples, the collecting event, and the surrounding environment. Occasionally, drawings or photographs supplemented the written documentation. Scanned handwritten notes from two scientific journals by personnel involved in the experiment are included in the Journal_Notes directory (see Figure O-8). The field notes describe important information relevant to the collection of GPS survey data, the locations of LiDAR scan positions and fiducials, details relevant to hydrographic surveys, and the deployment and recovery of instruments from the RHIB boat.

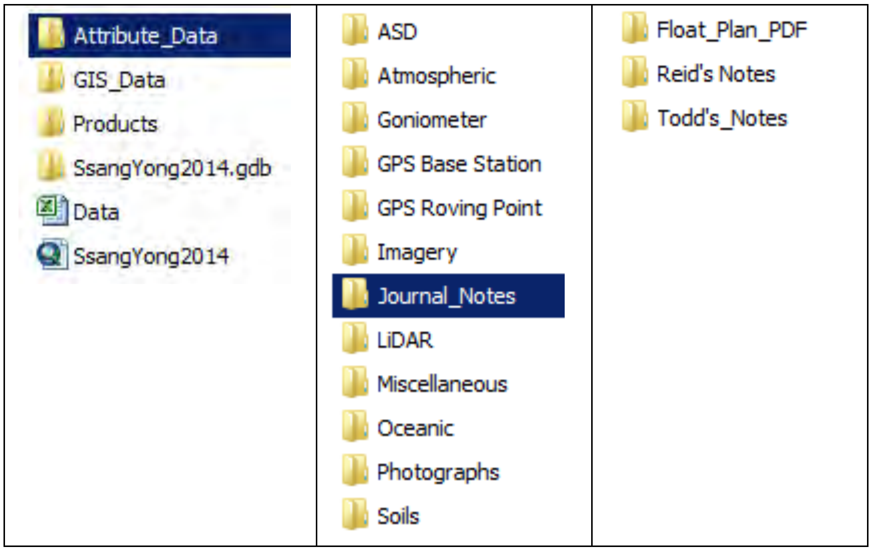

Figure O- 8. \Ssang Yong 2014\Attribute_Data\Journal_Notes. Entries include physical characteristics of the sampling location, sketches, instrument names and serial numbers, environment, location, date, and time.

Contents of \Ssang Yong 2014\Attribute_Data\LiDAR

This directory contains original LiDAR sensor data, post processed into Differential Scattering (DISC) image files and files that have been reprocessed into LASer (LAS) format. The LAS file format is a public file format for the interchange of 3-dimensional point cloud data between data users. Notes for the LiDAR data collected are contained within the Excel Workbook that is described in Table O-2.

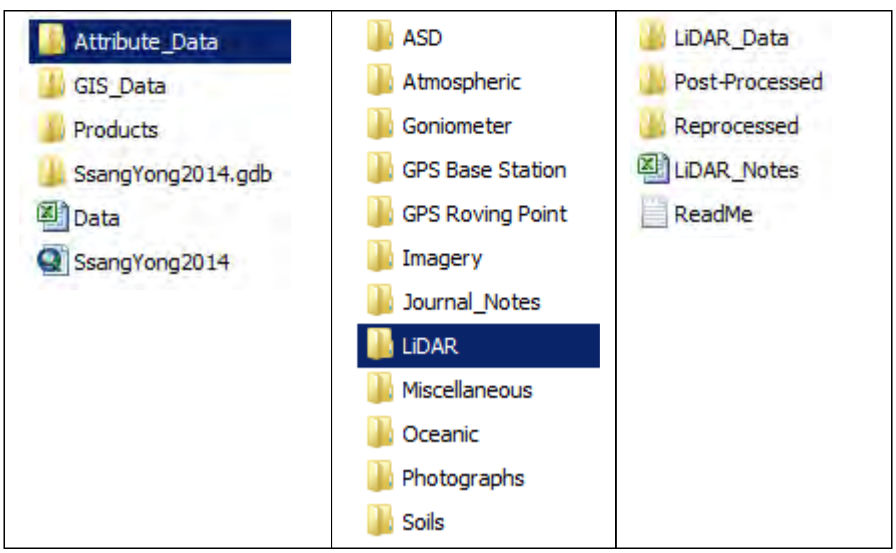

Figure O- 9. \Ssang Yong 2014\Attribute_Data\LiDAR.

Contents of \Ssang Yong 2014\Attribute_Data\Miscellaneous

Selected climatic information from the Korea Meteorological Administration (KMA) has been archived and is especially useful to support DQA. Other geospatial products saved in this directory include, a Notice to Mariners created by Korea Hydrographic and Oceanographic Administration, Littoral Planning Charts, recently updated Sailing Directions published by the National Geospatial-Intelligence Agency, and photographs downloaded from the Defense Video & Imagery Distribution System (see dvidshub.net) for Exercise Ssang Yong 2014. These photographs and imagery are relevant since the science experiment occurred immediately following the amphibious landing.

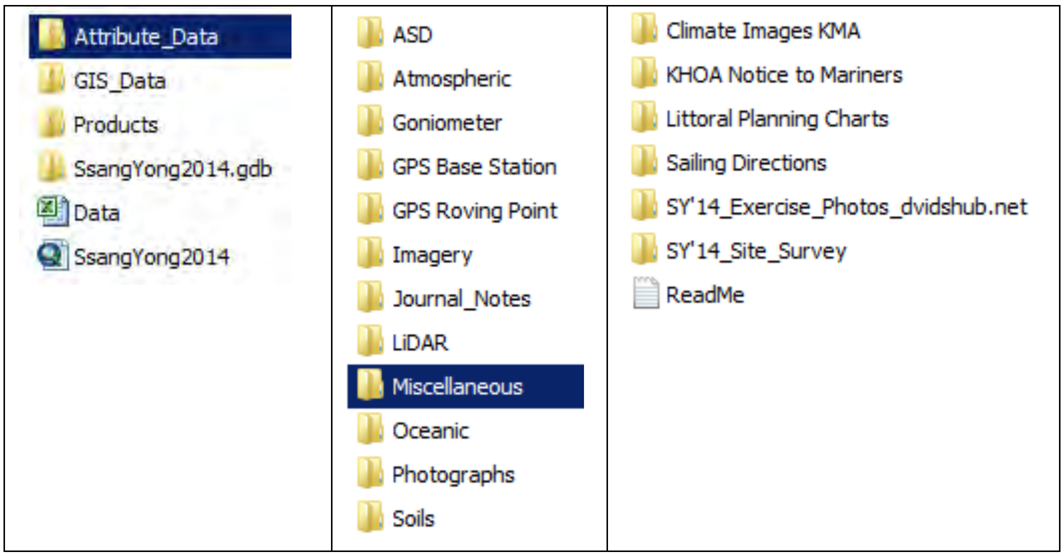

Figure O- 10. \Ssang Yong 2014\Attribute_Data\Miscellaneous.

Contents of \Ssang Yong 2014\Attribute_Data\Oceanic

The Oceanic directory contains raw and processed sensor data from survey instruments, water level loggers, and water level buoys (see Figure O-11). Tide predictions which were useful to de-tide soundings are provided for the period from March through May 2014. Tide predictions were obtained from the Korea Hydrographic and Oceanographic Administration.

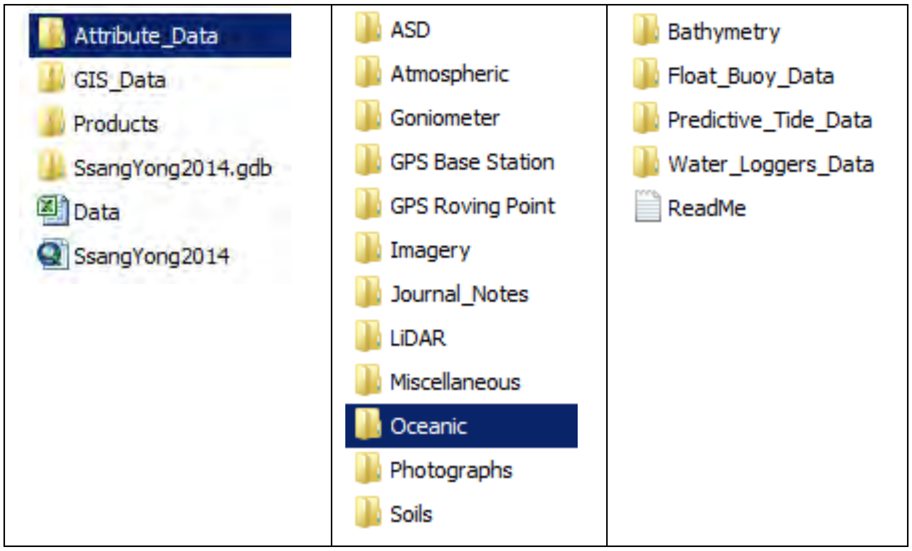

Figure O- 11. \Ssang Yong 2014\Attribute_Data\Oceanic.

Contents of \Ssang Yong 2014\Attribute_Data\Photographs

Many of the images within the sub-directories of the Photographs directory are linked to the map document, so any movement of these will break links (see Figure O-12). Many of the photographs that have been included were tagged with latitude and longitudes. Project photographs include pictures of key locations at Camp Mujuk, key terrain or landmarks that were surveyed, and locations where equipment was stored, instruments were operated, and data processing occurred. Descriptive photographs were taken to support transportation and to identify local plants, man-made objects, and obstacles. Directories have been established to save photographs taken at the various landing beaches.

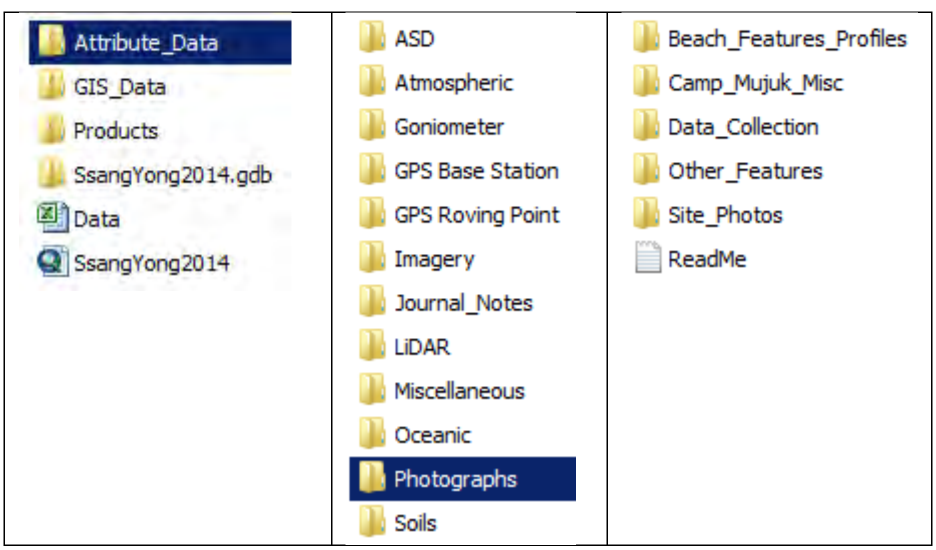

Figure O- 12. \Ssang Yong 2014\Attribute_Data\Photographs.

Contents of \Ssang Yong 2014\Attribute_Data\Soils

Microscope photographs of a geotechnical nature that were taken at various site locations were uploaded to the Soils directory along with data collected at specific site locations that includes moisture content, specific gravity, grain size, and density tests (see Figure O-13).

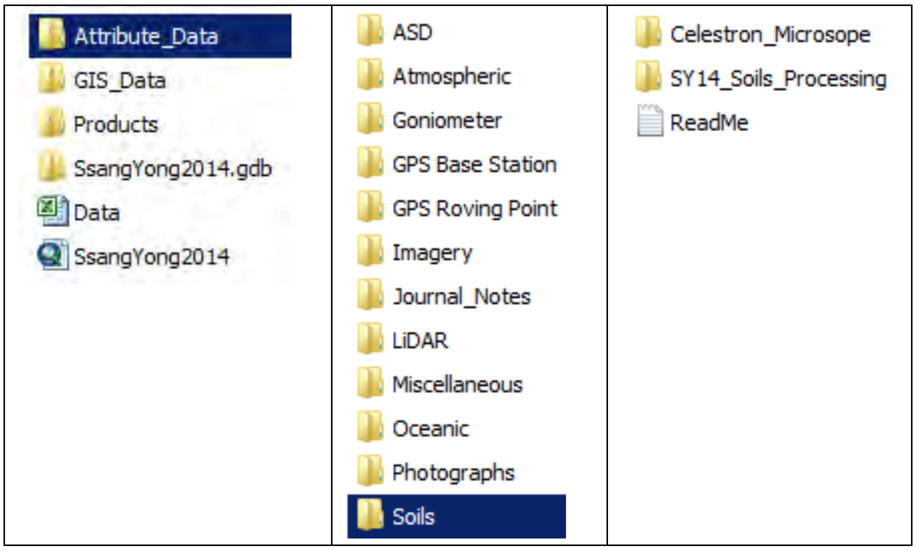

Figure O- 13. \Ssang Yong 2014\Attribute_Data\Soils.

Contents of \Ssang Yong 2014\GIS_Data
Contents of \Ssang Yong 2014\GIS_Data\MXDs

Map document (.mxd) files used to create maps and compare products derived from the Ssang Yong Experiment with the current Littoral Planning Chart are found in the MXDs directory (see Figure O-14).

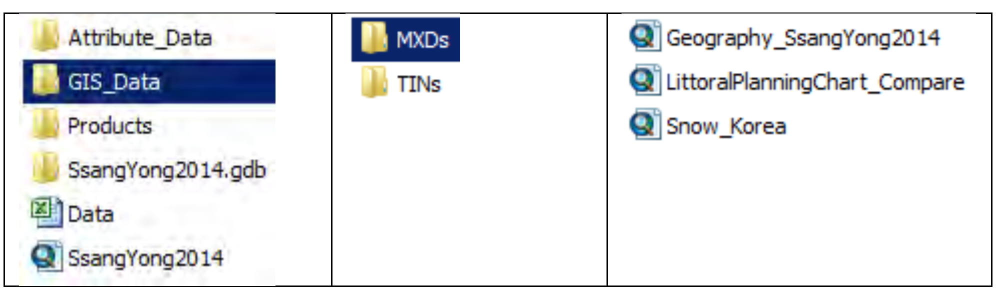

Figure O- 14. \Ssang Yong 2014\GIS_Data\MXDs.

Contents of \Ssang Yong 2014\GIS_Data\TINs

TINs are linked to the main map document**.** TINs are a digital data structure used to characterize terrain or bathymetric features in three dimensions.

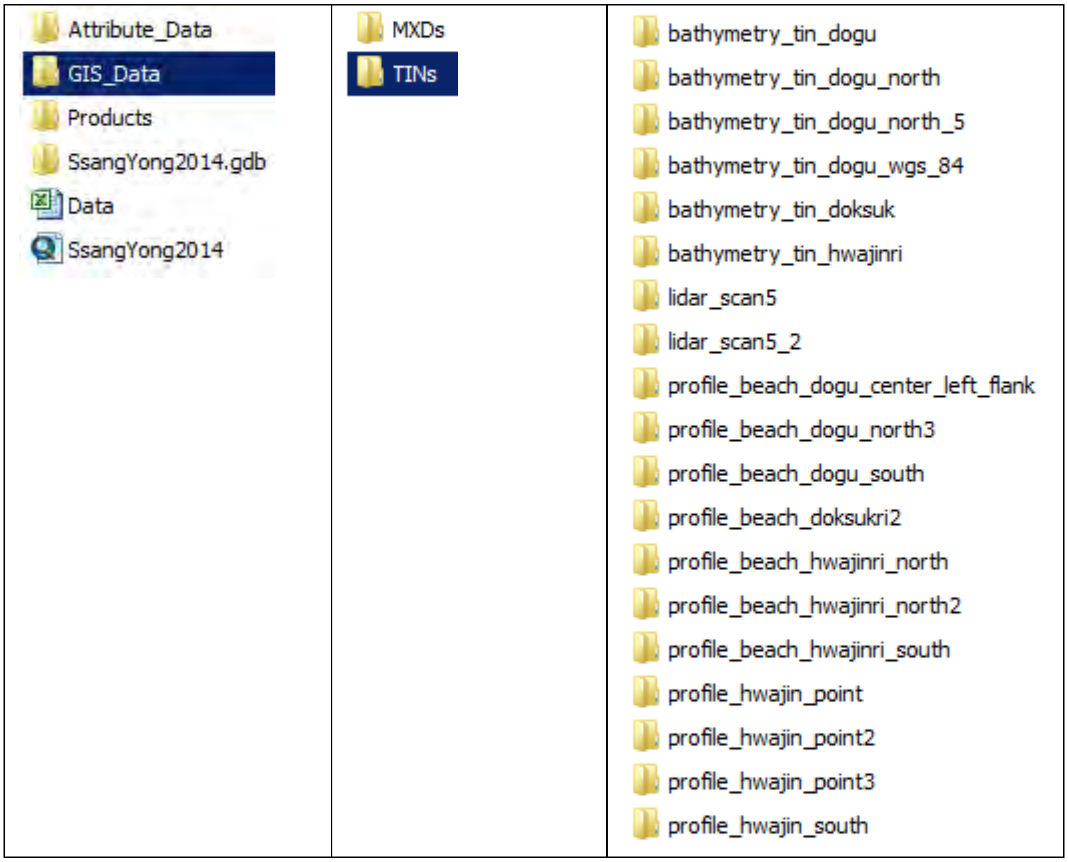

Figure O- 15. \Ssang Yong 2014\GIS_Data\TINs.

Contents of \Ssang Yong 2014\Products

The Products folder illustrated in Figure O-16 includes information on where images were created in the ArcMap environment, the Data Report and Appendices as separate word documents, figures created using ENVI software, and the Data Report with Appendices as a single Word and PDF Document.

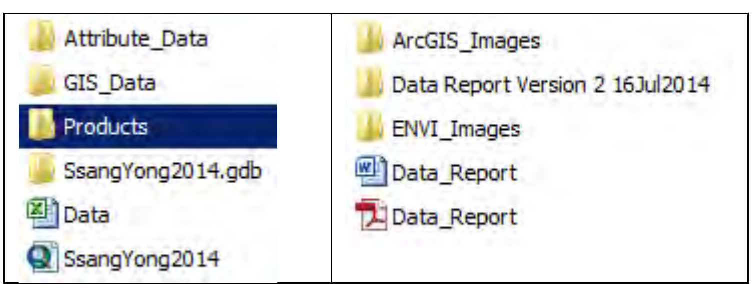

Figure O- 16. \Ssang Yong 2014\Products.

Contents of \Ssang Yong 2014\SsangYong2014.gdb

The contents of the ESRI ArcGIS File Geodatabase must be viewed in either the ArcCatalog or ArcMap application. A user can open ArcCatalog by itself. When operating in the ArcMap environment it is ArcCatalog that is being used within ArcMap to view the File Geodatabase. To open ArcMap Left-click the ArcMap icon (see Figure O-17) and open a blank map as illustrated below:

Figure O- 17. ArcMap Icon.

Left-click My Templates, left-click Blank Map and left-click the OK button to open a blank map (see Figure O-18).

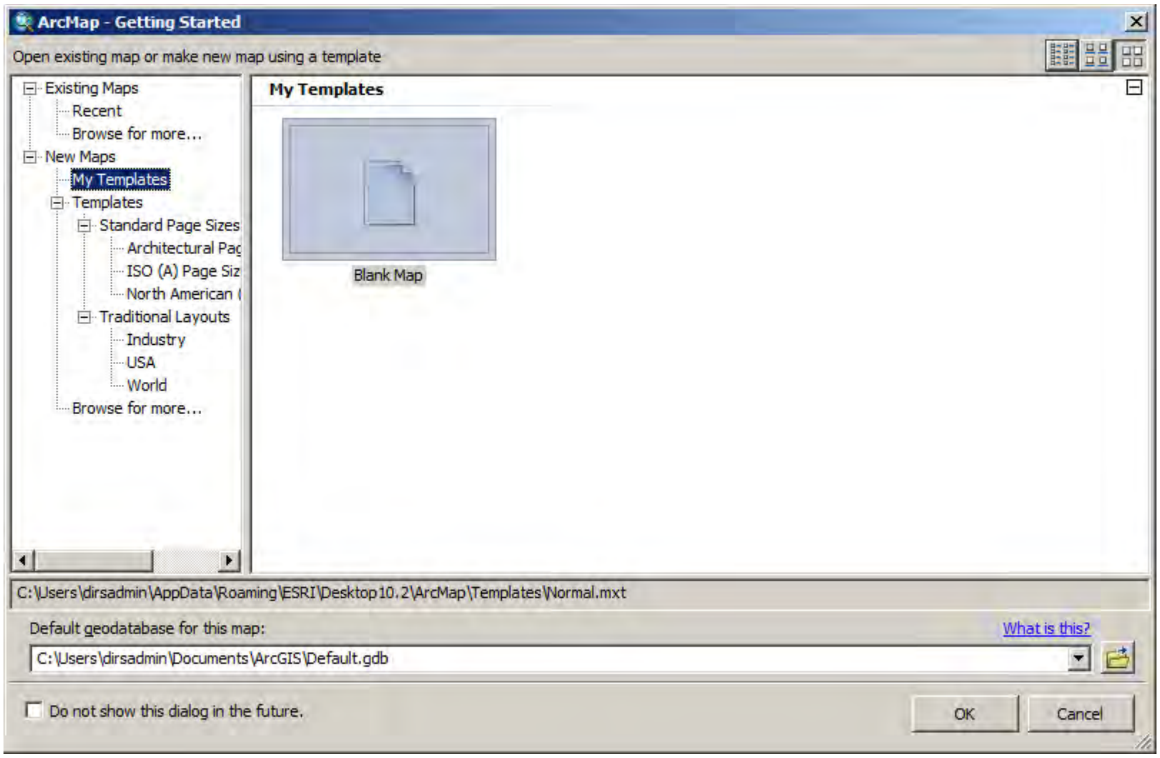

Figure O- 18. ArcMap Getting Started window.

If ArcCatalog is not open, left-click the ArcCatalog icon (Figure O-19) to access the window (see Figure O-20).

Figure O- 19. ArcCatalog Icon in ArcMap Environment.

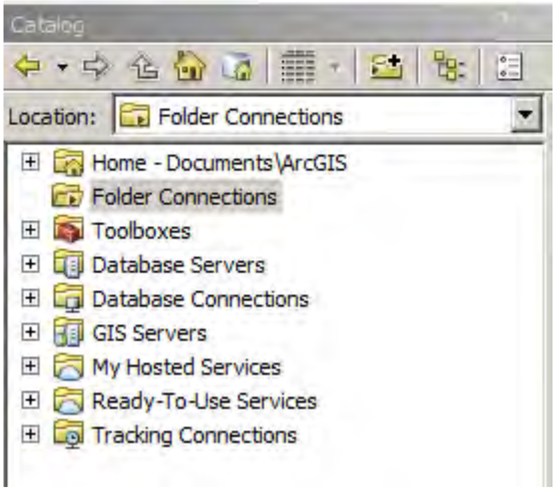

Figure O- 20. ArcCatalog within the ArcMap Environment.

If the File Geodatabase is not seen in the Catolog window, left-click the Connect to Folder button (see Figure O-21).


Figure O- 21. Connect to Folder Icon.

Navigate to the Ssang Yong 2014 Geodatabase, highlight Ssang Yong 2014, and left-click OK to connect to the folder highlighted (see Figure O-22).

Figure O- 22. Connect to Folder Window.

Expand the Ssang Yong 2014 Geodatabase (see Figure O-23) and SsangYong.gdb (see Figure O-24) to view the contents of the File Geodatabase by left-clicking the plus symbols next to their identifiers.

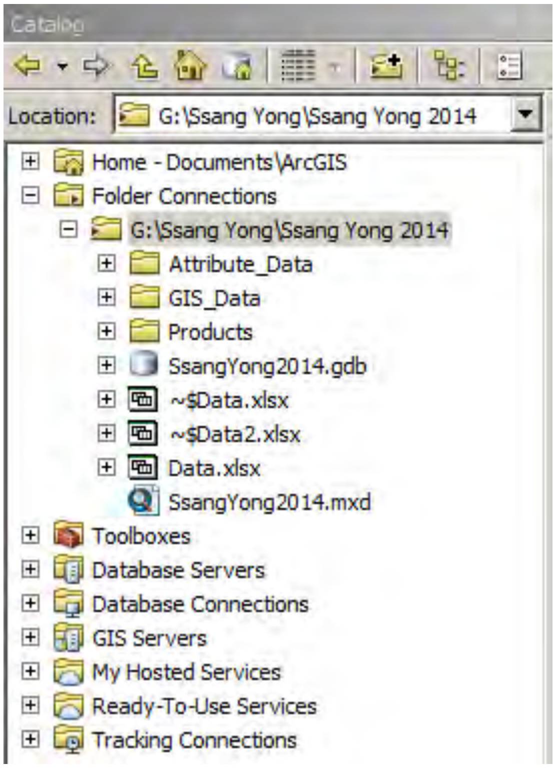

Figure O- 23. Ssang Yong 2014 Geodatabase Expanded in ArcCatalog.

- SsangYong2014.gdb
  - Korea_Base_Layers
  - Base_Station_Camp_Mujuk
  - Base_Station_Dogu
  - Bathymetry_Contours_Dogu
  - Bathymetry_Contours_Doksukri
  - Bathymetry_Contours_Hwajinri
  - Bathymetry_Line_Dogu
  - Bathymetry_Points_Dogu
  - Bathymetry_Points_Dogu_Line
  - Bathymetry_Points_Doksuk
  - Bathymetry_Points_Hwajin
  - Bathymetry_Raster_Dogu_Seafloor
  - Bathymetry_Raster_Doksukri_Seafloor
  - Bathymetry_Raster_Hwajinri_Seafloor
  - Benchmark_Camp_Mujuk
  - Boat_Ramps_Used
  - Buildings_Hwajinri
  - Buoy_Dogu
  - Buoy_Doksukri
  - Cal_Pan_White_Ref_Pan
  - Calibration_Panels_Camp_Mujuk
  - Contour_Profile1
  - Data
  - Data_Report
  - Data_Report2
  - Data_Report3
  - Dune_Grass_Line_Dogu
  - Dune_Grass_Line_Dogu2
  - Dune_Grass_Line_Dogu3
  - Dune_Grass_Line_Dogu4
  - Export_Output
  - Export_Output_2
  - Features_GeoTaggedPhotosToPo7__ATTACH
  - Features_GeoTaggedPhotosToPo7__ATTACHR
  - Features_GeoTaggedPhotosToPo7_Doksuk
  - Gate_Dogu
  - GPS_Ground_Control
  - GPS_Points_Dogu
  - GPS_Points_Doksukri
  - GPS_Points_Hwajinri
  - GPS_Sample_Locations
  - GPS_Sample_Locations_Dogu
  - GPS_Sample_Locations_Doksukri
  - GPS_Sample_Locations_Hwajinri
  - GRIT_Hwajin
  - GRIT_Points_Dogu
  - GRIT_Points_Doksuk
  - Hwajinri_Parking_Lot
  - Information_Boundary_Box
  - Korea_China
  - LC81140352014104LGN00_B1_Com
  - LC81140352014136LGN00_B1_Com
  - LiDAR_Dogu
  - LiDAR_Doksuk
  - LiDAR_Fiducials_Dogu
  - LiDAR_Fiducials_Doksuk
  - LiDAR_Fiducials_Hwajin
  - LiDAR_Hwajin
  - LiDAR_Positions_Dogu
  - LiDAR_Positions_Dogu_2
  - LiDAR_Positions_Dogu_Merge
  - LiDAR_Positions_Dogu2
  - LiDAR_Positions_Doksuk
  - LiDAR_Positions_Hwajin
  - LiDAR_Scan_16Apr2014_Hwajin
  - LiDAR_Scan_19Apr2014_Dogu
  - LiDAR_Scan_21Apr2014_Doksuk
  - LiDAR_Scan_23Apr2014_Dogu
  - LiDAR_Scan_24Apr2014_Hwajin
  - LiDAR_Scan_DG_1
  - LiDAR_Scan_DG_2
  - LiDAR_Scan_DK_1
  - LiDAR_Scan_HW_1
  - LiDAR_Scans_HW_2
  - Littoral_Planning_Chart_T130031
  - Littoral_Planning_Chart_T35181
  - Littoral_Planning_Chart_T35182
  - Littoral_Planning_Chart_T40171
  - Littoral_Planning_Chart_T41174
  - Littoral_Planning_Chart_T803470
  - Littoral_Planning_Chart_T806902
  - Littoral_Planning_Chart_T806967
  - Locations_Equipment_BoatRamps
  - LT51140352010173HAJ01_B1_Com
  - LT51140352010173HAJ01_B51
  - Meteorological_Station
  - Meteorological_Station_Data
  - Meter_Cutout_Doksuk
  - Meter_Square_Hwajinri
  - Notice_to_Mariners
  - Pacific_Ocean_Southern_Asia
  - Parking_Lot_Hwajinri
  - Photos_Dogu_From_Beach_Facing_Left_Flank
  - Photos_Dogu_From_Beach_Facing_Left_Flank__ATTACH
  - Photos_Dogu_From_Beach_Facing_Left_Flank__ATTACHR
  - Photos_Dogu_From_Beach_Facing_Ocean
  - Photos_Dogu_From_Beach_Facing_Ocean__ATTACH
  - Photos_Dogu_From_Beach_Facing_Ocean__ATTACHREL
  - Photos_Dogu_From_Beach_Facing_Right_Flank
  - Photos_Dogu_From_Beach_Facing_Right_Flank__ATTACH
  - Photos_Dogu_From_Beach_Facing_Right_Flank__ATTACH
  - Photos_Dogu_From_Land_Facing_Hinterland__ATTACHRE

Photos_Dogu_From_Land_Facing_Land
Photos_Dogu_From_Land_Facing_Land__ATTACH
Photos_Dogu_From_Ocean_Facing_Hinterland__ATTACHF
Photos_Dogu_From_Ocean_Facing_Land
Photos_Dogu_From_Ocean_Facing_Land__ATTACH
Photos_Dogu_From_Ocean_Panoramic
Photos_Dogu_From_Ocean_Panoramic___ATTACH
Photos_Dogu_From_Ocean_Panoramic___ATTACHREL
Photos_Dogu_Panoramic__ATTACH
Photos_Dogu_Panoramic__ATTACHREL
Photos_Dogu_Panoramic_Facing_Hinterland
Photos_Geotagged_Hwajinri
Photos_Geotagged_Hwajinri__ATTACH
Photos_Geotagged_Hwajinri__ATTACHREL
Photos_Geotagged_Plants_Hwajinri
Photos_Geotagged_Plants_Hwajinri__ATTACH
Photos_Geotagged_Plants_Hwajinri__ATTACHREL
Profile_Beach_Dogu_North_Contours2
Profile_Beach_Dogu_North_Points2
Profile_Beach_Dogu_North_Raster2
Profile_Beach_Dogu_South_Contours2
Profile_Beach_Dogu_South_Points2
Profile_Beach_Dogu_South_Raster2
Profile_Beach_Doksukri_Contours
Profile_Beach_Doksukri_Raster2
Profile_Beach_Hwajinri_North_Contours
Profile_Beach_Hwajinri_North_Points
Profile_Beach_Hwajinri_North_Raster
Profile_Beach_Hwajinri_South_Contours
Profile_Beach_Hwajinri_South_Points
Profile_Beach_Hwajinri_South_Raster
profile_hwaj_north
profile_hwaj_north_contour
profile_hwaj_south
profile_hwaj_south_contour
Profile_Hwajin_North
Profile_Hwajin_Points
Profile_Hwajin_South_Points
Profile_Line_Hwajinri
Profile_Side_Hwajinri1
rastercalc10
rastercalc11
rastercalc13
rastercalc14
rastercalc15
rastercalc3
rastercalc7
RasterT_rasterc3
Roads_Polygons_Hwajinri
Rocks_Hwajinri
Shoreline_WV2_25Apr2014_0239
Shorelines_Hwajin_WV2_25Apr2014_023915_UTC
Shorelines_Landsat_2010_Dogu
Shorelines_Landsat_2010_Hwajin_Doksuk

Shorelines_North_Beaches_WV2_25Apr2014_023915_UTC
Shrubery_North_Corner_Dogu
SICK_NONE_20140416_051538_AS
SICK_NONE_20140416_051538_xy
Snow_Covered_Korea
Soils_Gr_Sz_Dogu
Soils_Gr_Sz_Doksuk
Soils_Gr_Sz_Hwajin
Soils_Grain_Size
Soils_Max_Dens_Dogu
Soils_Max_Dens_Doksuk
Soils_Max_Dens_Hwajin
Soils_Max_Density
Soils_Min_Dens_Fun_Dogu
Soils_Min_Dens_Fun_Doksuk
Soils_Min_Dens_Fun_Hwajin
Soils_Min_Dens_Grad_Dogu
Soils_Min_Dens_Grad_Doksuk
Soils_Min_Dens_Grad_Hwajin
Soils_Min_Density_Funnel
Soils_Min_Density_Graduated_Cyl
Soils_Moisture_Content
Soils_Moisture_Content_Dogu
Soils_Moisture_Content_Dok
Soils_Moisture_Content_Simple
Soils_Moisture_Content_Simple
Soils_Spec_Grav_Dogu
Soils_Spec_Grav_Doksuk
Soils_Spec_Grav_Hwajin
Soils_Specific_Gravity
Spectral_Plots_Nadir_Sites
Streamlet
Streamlet_Dogu_North
Streamlet_South_Dogu
Streamlets_WV2_25Apr2014_023915_UTC
Structure_Dogu
Structure_Dogu_South
Structure_Dogu_South2
Structure_North_Side_Hwajinri
Structure_South_Side_Hwajinri
Structures_Polygons_Hwajinri
Swash_Zone_Dogu
T14MAY09022351_M1BS_500119110010_01
T14MAY19025422_M1BS_500123114010_01
T14MAY22024425_M1BS_500123677010_01_P001_geo
Tower_Dogu
Tower_Dogu2
Transect_Dogu1
Transect_Dogu2
Transect_Hwajin3
Transect_Hwajin4
Wall_Corner_North_Dogu
Water_Logger_Dogu
Water_Logger_Doksukri

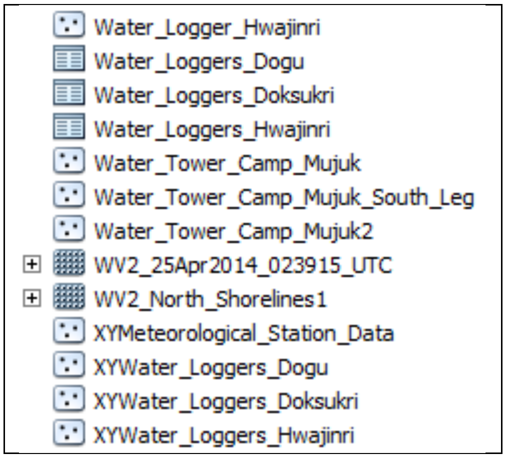

Figure O- 24. \Ssang Yong 2014\SsangYong2014.gdb.

The SsangYong2014 File Geodatabase consists of Feature Classes (Point, Line, Polygon), Feature Datasets, Relationship Classes, Tables, and Raster Datasets. These data are further described in Table O-1.

Table O- 1. Data Types used in SsangYong2014 File Geodatabase.

File Image	File Type	Description
	Point Feature Class	Store Point Features/GPS Points of Sampled Locations
	Line Feature Class	Store Line Features/Contour Lines
	Polygon Feature Class	Store Area Features/Buildings
	Feature Dataset	Collection of Feature Classes with Same Spatial Attributes
	Relationship Class	Links a Table to a Feature Class
	Table	Store Tabular Information
	Raster Dataset	Stores Continuous Images/Satellite Imagery/Photographs

To View an item from the File Geodatabase: Left-click-drag a desired file for viewing, in this case Raster Dataset WV2_25Apr2014_023915_UTC, from the File Geodatabase into the center of the Data View area and release-click to view the file in ArcMap.

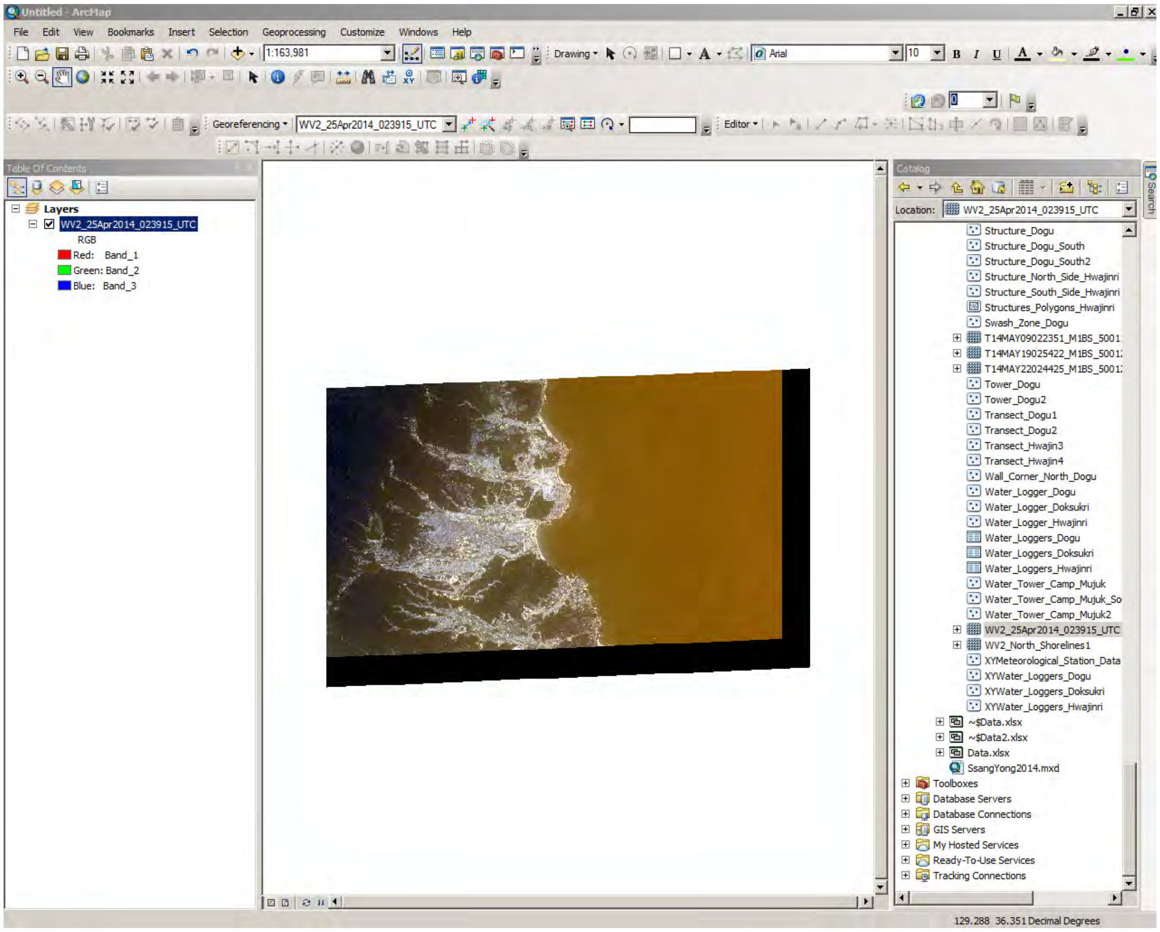

Figure O- 25. ArcMap Data View with Raster Dataset Shown.

Contents of \Ssang Yong 2014\Data

Considerable amounts of data were stored and processed using Microsoft Excel. The Excel workbook is a flat file that contains one or more worksheets or spreadsheets. The worksheet is the primary document for storage of data in Excel. The Excel Workbook (Data) contents are described in Table O-2. This table was explained in earlier sections of this appendix.

Table O- 2. \Ssang Yong 2014\Data

Labels of Workbook Tabs	Description of Content
Locations	Coordinates of test equipment, boat ramps used, and calibration panels at Camp Mujuk.
Buoy_Dogu	Processed data of buoy deployed near Dogu Beach.
Buoy_Doksuk	Processed data of buoy deployed near Doksuk-ri Beach.
Ground_Control	All locations that may provide ground control points.

Dogu_Profile	All GPS points collected at Dogu Beach.
Doksuk_Profile	All GPS points collected at Doksuk-ri Beach.
Hwajin_Profile	All GPS points collected at Dosuk-ri Beach.
Site_Locations	Locations of interest during the experiment.
Grain_Size	Grain size analysis data.
Moisture_Content	Moisture content analysis data.
Specific_Gravity	Specific gravity analysis data.
Min_Dens_Grad_Cyl	Minimum density analysis test data using a graduated cylinder.
Min_Dens_Fun	Minimum density analysis test data using a funnel.
Max_Density	Maximum density test data.
Met_Station	Meteorological station data.
Water_Loggers	Water logger data all beaches.
Bathy_Dogu	Bathymetry data at Dogu Beach.
Bathy_Doksuk	Bathymetry data at Doksuk-ri Beach.
Bathy_Hwajin	Bathymetry data at Hwajin-ri Beach.
LiDAR_Notes	LiDAR notes.
Nadir_Spec_Plots	Site locations nadir spectral plots.

Conclusion

The geodatabase supports the need to map characteristics, or attributes, of different littoral regions surrounding three landing beaches. These thematic maps can be used to support the military decision making process. Examples of thematic maps might include maps of the beach, wetlands, very shallow water, and inland terrain. Much of the attribute data was collected during April 2014 following Exercise Ssang Yong 2014.

APPENDIX P

Map Document

Table of Contents

List of Figures

1. Introduction

A geodatabase (geographic database) stores spatial information as objects with attributes. In fact, a geodatabase may also be described as an object-relational model. In ArcGIS, the geodatabase objects persist as rows in Data Base Management System (DBMS) tables that have identity. Attribute tables are arranged so that each row represents a feature and each column represents one feature attribute. In raster datasets, each row of an attribute table corresponds to a certain zone of cells having the same value.

ESRI ArcGIS 10.2 software was used to create the file geodatabase to store spatial components along with data collected during the experiment and other relevant sources. ArcMap is one component of ArcGIS and was the primary software used and will be needed to analyze or edit the files within the Ssang Yong 2014 Geodatabase. Non-spatial components are connected through a table, photograph, PDF, or other format to a particular experiment location or object. For raster datasets, the attribute values can be used to find, query, and symbolize features or raster cells.

2. Navigating the Map Document (SsangYong2014.mxd)

ArcGIS Maps provide the mechanism to share GIS information. Each interactive GIS map is a specification for how data are integrated and displayed.

To automatically open ArcMap 10.2 software, double left-click the **Ssang Yong 2014>SsangYong2014** map document. This will allow you to view the interface created for accessing geodatabase files (see Figure P-1, P-2, and P-3).

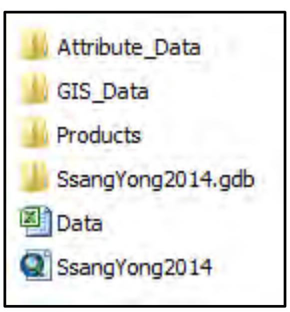

Figure P- 1. Contents of Ssang Yong 2014 Geodatabase.

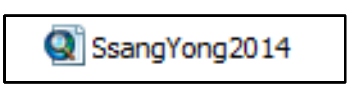

Figure P- 2. ArcMap Map Document file used to store a previously designed interface.

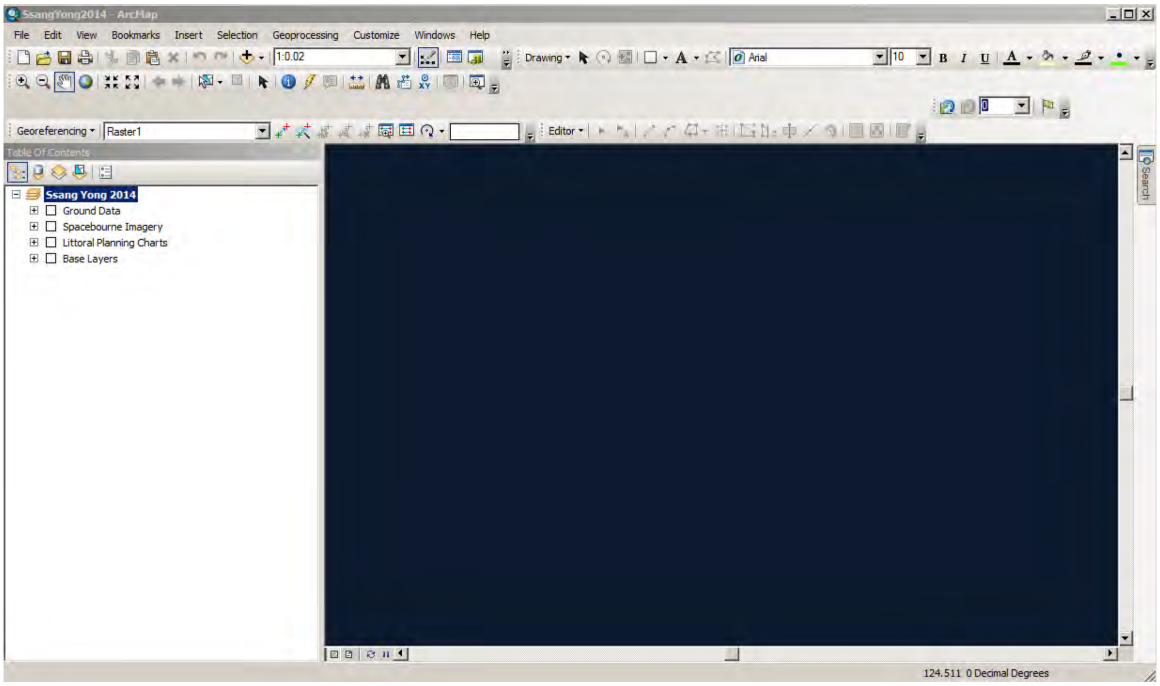

Figure P- 3. ArcMap software interface.

Once the map document is open, ensure that the left most button is highlighted under the **Table of Contents >List By Drawing Order**, if not, left-click the far left button (see Figure P-4 and P-5).

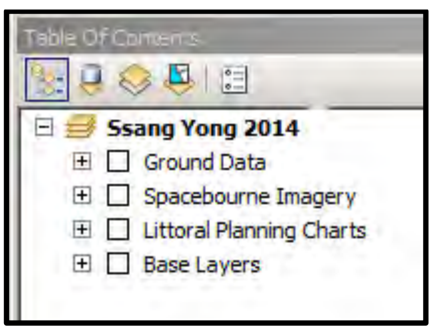

Figure P- 4. Showing far left button highlighted.

Figure P- 5. Button left-clicked for viewing data. Button is named the *List By Drawing Order* button.

Under the **Table of Contents**, you can choose what to observe by expanding any component with a plus symbol and checking the empty boxes with a left-click of the mouse when the cursor is hovering over the plus or the empty box respectively (see Figure P-6 and P-7).

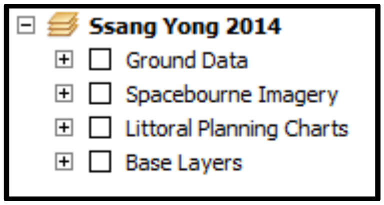

Figure P- 6. First layer of components in Map Document.

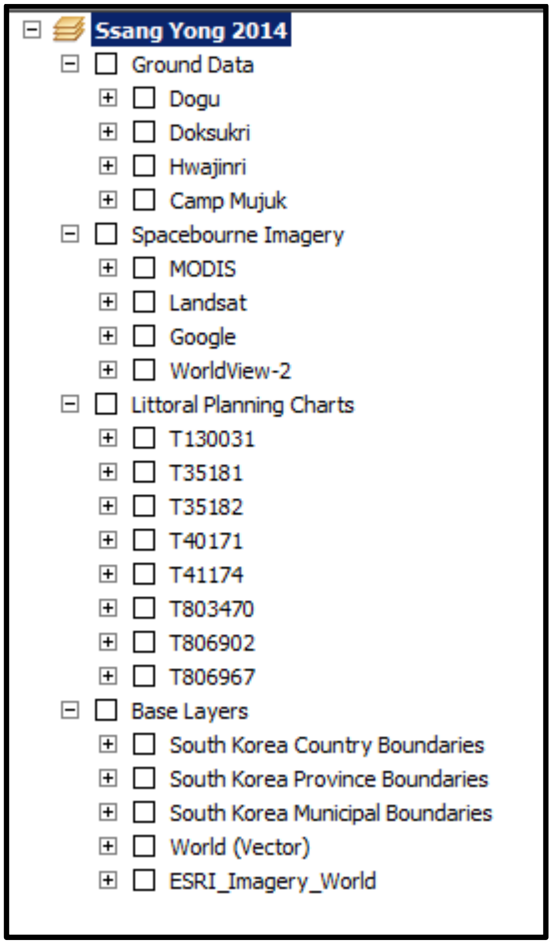

Figure P- 7. Second Layer of Map Document.

To find the layer at the bottom of the **Table of Contents** the **Ssang Yong 2014>Base Layers>ESRI_Imagery_World** box must be checked by left-clicking along with any higher layer it is connected to, in this case the **Ssang Yong 2014>Base Layers** box (see Figure P-8).

Figure P- 8. Showing checked boxes to access ESRI_Imagery_World imagery.

Once the boxes are correctly checked, the imagery is shown in the **Data View** area (see Figure P-9). If you do not see the checked items you may need to right-click the desired selection (e.g., Dogu) and choose **Zoom to Layer** on the drop down menu or you may need to expand the selection component chosen to see if there are more choices that require other boxes to be checked.

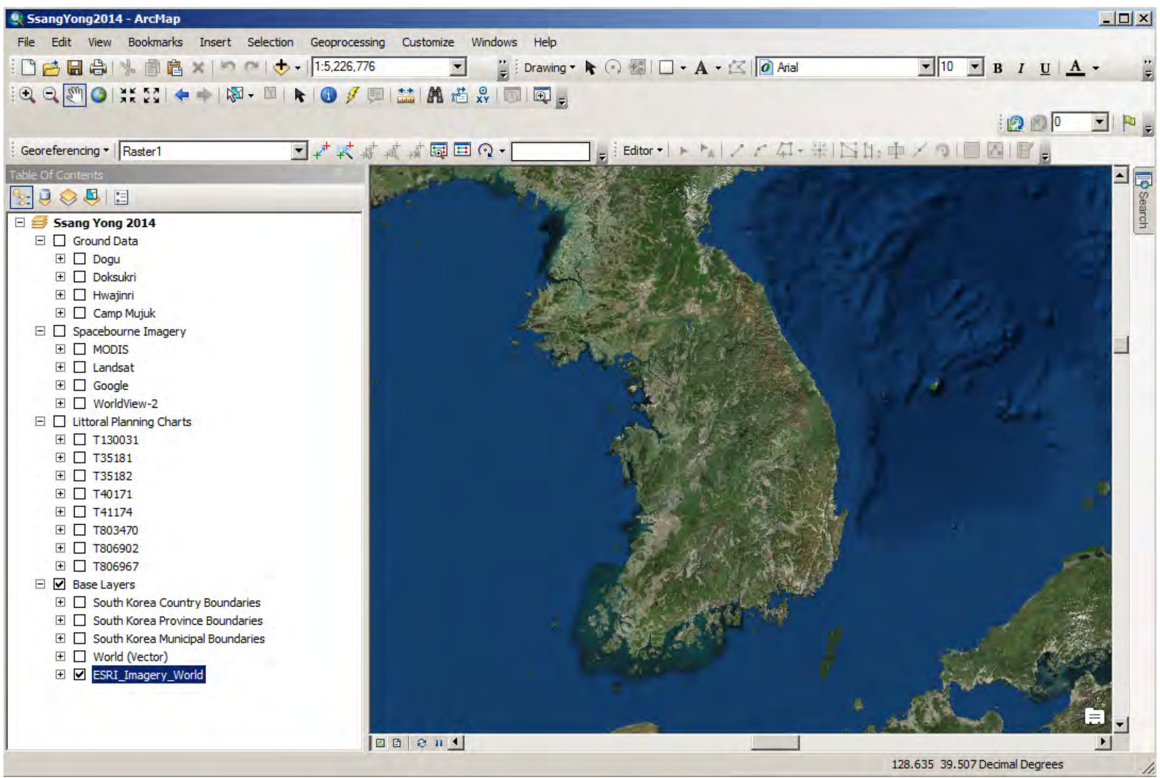

Figure P- 9. Showing ESRI_Imagery_World imagery.

The many components under **Ssang Yong 2104>Base Layer** and **Ssang Yong 2014>Littoral Planning Charts** have a single layer and when checked they will display in the viewer. The components under **Ssang Yong 2014>Ground Data** and **Ssang Yong 2014>Spacebourne Imagery** have multiple layers and must be expanded down to the smallest layer and checked before they are displayed in the viewer. The **Ssang Yong 2014>Littoral Planning Charts** and **Ssang Yong 2014>Base Layers** can be shrunk by left-clicking the minus symbols next to the layer names respectively, to focus on the

Ssang Yong 2014>Ground Data and **Ssang Yong 2014>Spacebourne Imagery** (see Figure P-10).

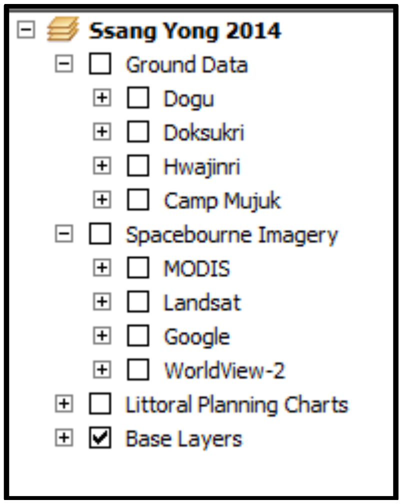

Figure P- 10. Only Ground Data and Spacebourne Imagery expanded to the second layer.

Ssang Yong 2014>Spacebourne Imagery>Google imagery will not be shown since it was only used for general reference and will not be in the final interface. Within the layer **Ssang Yong 2014>Spacebourne Imagery>MODIS** there is a single multispectral image obtained from NASA depicting snow cover on the Korean peninsula (see Figure P-11).

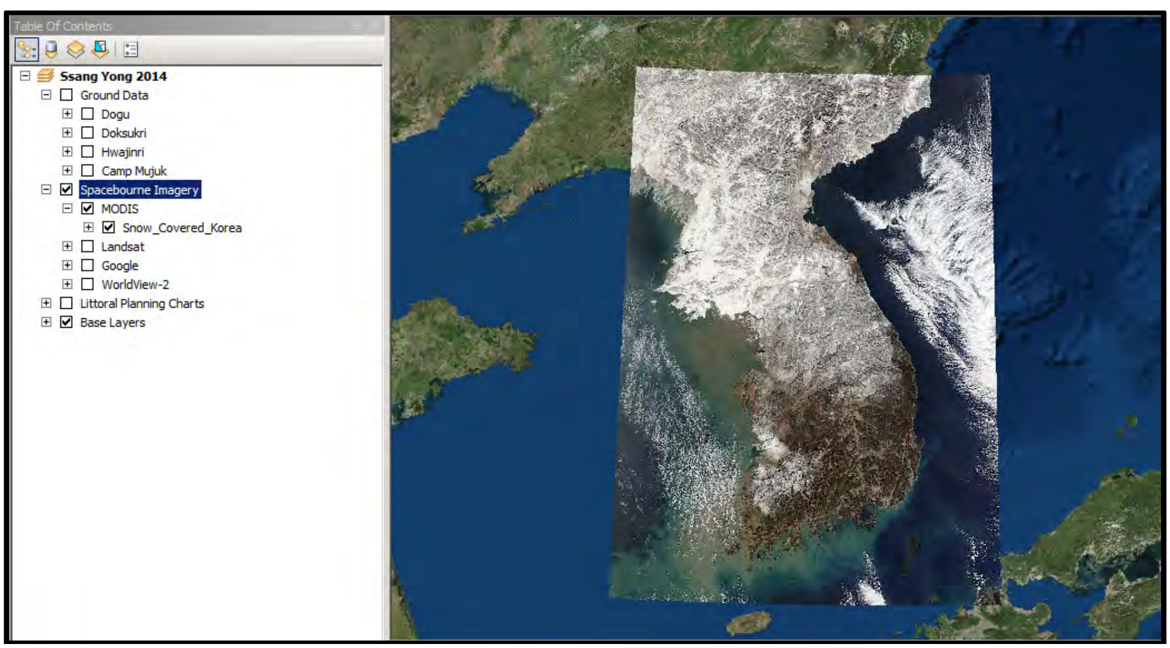

Figure P- 11. Snow covered Korea in January 3, 2010. (Obtained online from http://rapidfire.sci.gsfc.nasa.gov/subsets/?subset=FAS_Korea.2010003.terra.1km). Geophysical parameters describing the Earth's surface (land and ocean) and atmosphere (including clouds) can be derived from MODIS imagery.

Choose either **Ssang Yong 2014>Spacebourne Imagery>Landsat** image to be viewed then right-click and choose **Zoom to Layer** in the drop down menu (see Figure P-12). This image is particularly valuable given Landsat 8's improved ability to detect variations in colors, sediment patterns can be seen in the East Sea as well as potentially problematic algae, indicated by higher chlorophyll concentrations in Yeongil Bay.

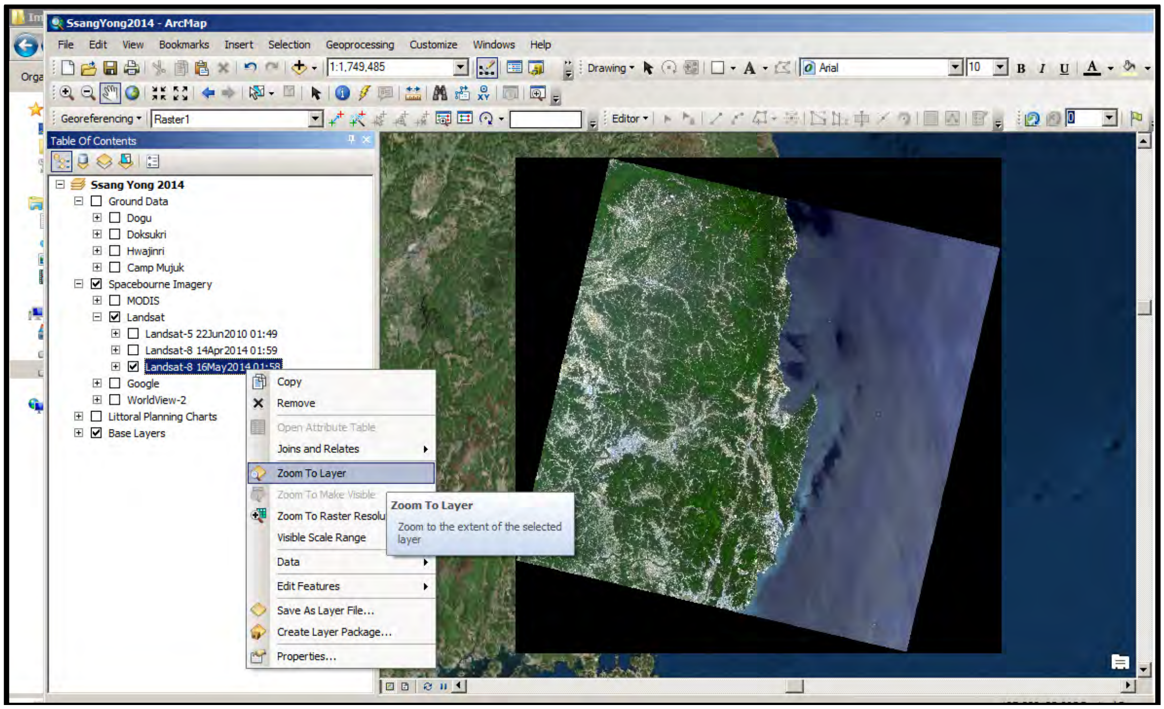

Figure P- 12. Landsat 8 imagery. Slight variations in the color of coastal water due to algae or sediments can be used to understand processes that impact amphibious operations such as sediment transport.

Left-click **Ssang Yong 2014>Spacebourne Imagery>WorldView-2>25Apr2014>imagery** to see image (see Figure P-13). Waterline and streamlet extractions for Hwajin-ri can be displayed by checking the respective boxes.

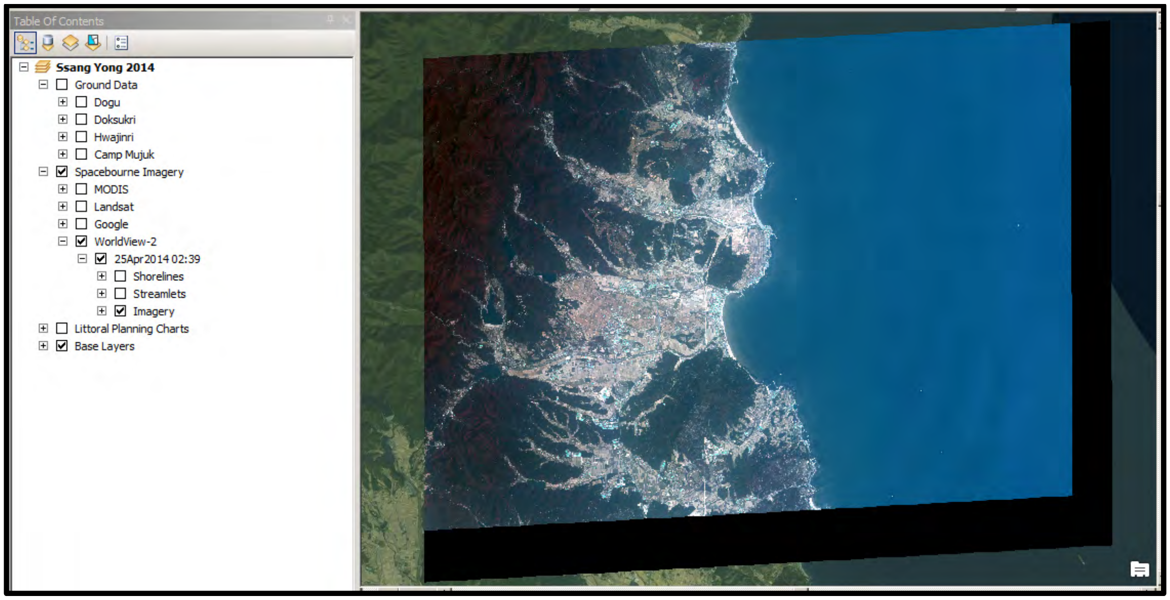

Figure P- 13. WorldView-2 imagery of Doksuk-ri and Hwajin-ri beaches..Most of the east coast of South Korea is rocky. There are some sand, gravel, and cobble beaches located between the headlands.

To zoom into an area of interest, left-click on the **Magnifying Tool** and create a box by left-clicking-dragging, then release-click when finished. The box created will be the new extent when the left-click button is released (see Figure P-14, P-15, and P-16).

Figure P- 14. Button used for zooming in or creating a box for a new extent.

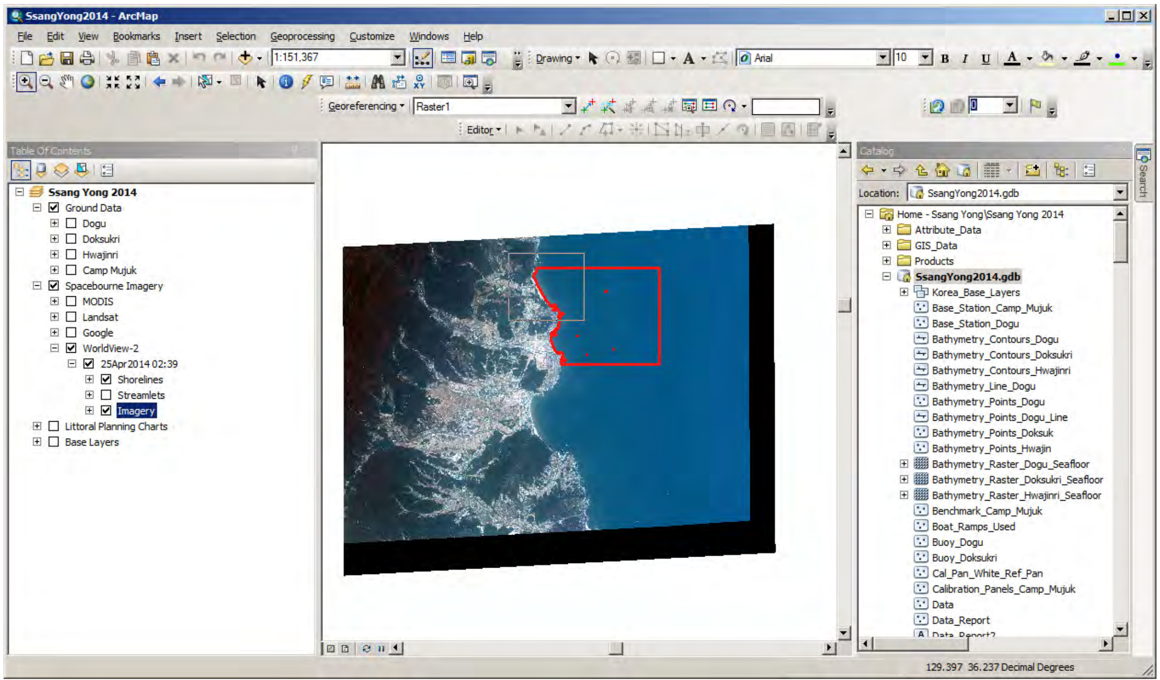

Figure P- 15. Image with new extent drawn over Hwajin-ri beach. This beach near Pohang, South Korea is used to load and offload vehicles from amphibious craft such as the Landing Craft Air Cushion (LCAC).

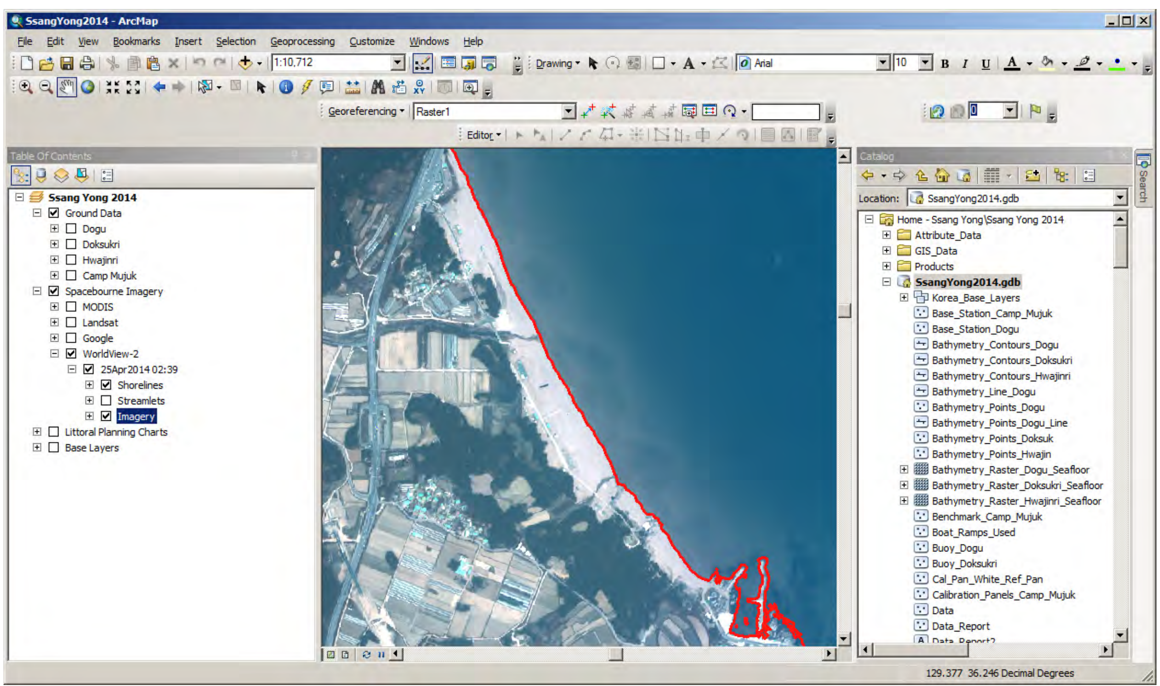

Figure P- 16. Hwajin-ri Beach showing waterline extraction. The waterline is the land-sea interface at time of imaging. Tidal fluctuations are small (microtidal) since the East Sea is bounded by the rocky east coast of South Korea and the Japanese archipelago.

Click off the **Shorelines** to view the types of Ground Data. Ensure **Ssang Yong 2014>Ground Data** is checked. If not, left-click the empty box to select the appropriate the location and expand the location by left-clicking the plus symbol next to the name. Figure P-17 illustrates the selection of geospatial data contained within **Ssang Yong 2014>Ground Data>Hwajinri.**

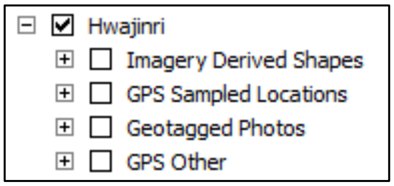

Figure P- 17. Contents under Hwajin-ri Layer. Data are especially useful as ground control for remote sensing and mapping applications.

Figure P-18 highlights the use of geodatabase with the raster Littoral Planning Charts (LPCs). The folder **Ssang Yong 2014>Ground Data>Hwajin-ri>Imagery Derived Products** contains examples of imagery extracted features that are not depicted on the LPCs used for amphibious planning during Exercise Ssang Yong 2014. Several significant rock formations on the landing-beach are missing along with man-made features such as a parking lot to the north, retaining walls, several roads, and buildings located near roads that parallel the beach. This example was only created for Hwajin-ri Beach (see Figure P-18) and the data contain other changes for Doksuk-ri and Dogu beaches.

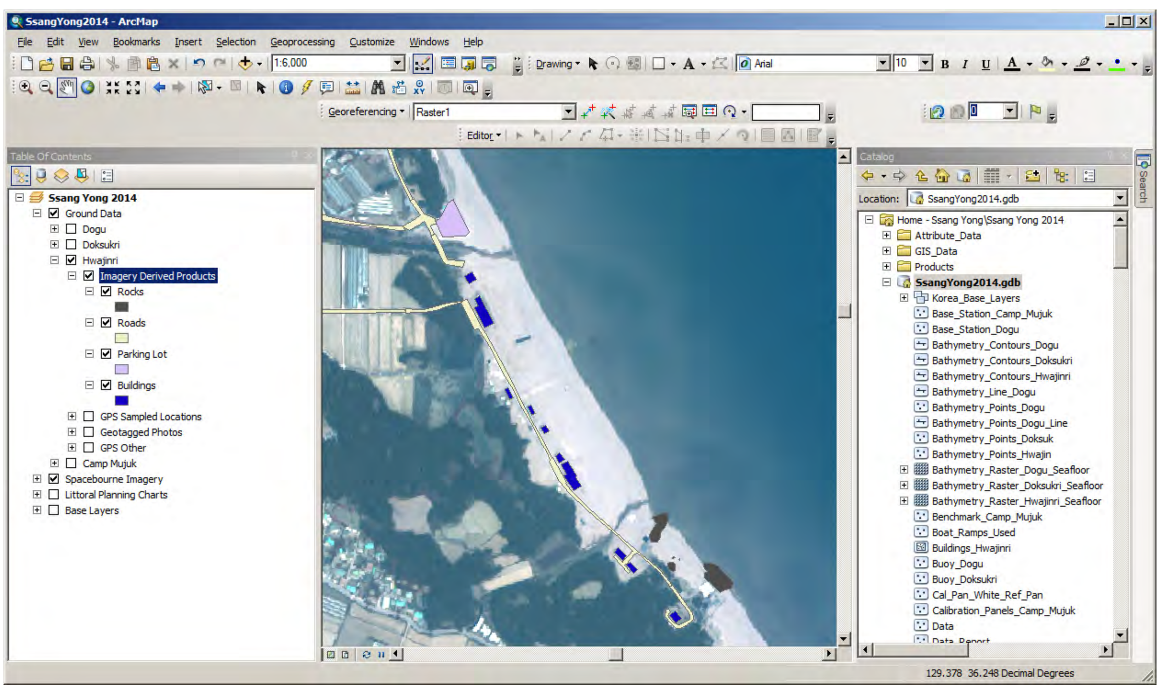

Figure P- 18. Example geospatial value-add Features for Littoral Planning Charts. Data collected through the analysis of satellite imagery and photographs provide information that answers questions that are listed in the General Intelligence Requirements Handbook (MCIA, 1995).

Raw and processed data are stored in the **Ssang Yong 2014>Products>Data Report, Ssang Yong 2014>Attribute_Data>Photographs**, and **Ssang Yong 2014>Data**. The directory **Ssang Yong 2014>Ground Data>Hwajinri>GPS Sampled Locations** contains point data from locations where soil/sediments were sampled along with spectra that were collected with a goniometer/spectrometer (see Figure P-19). These data are also linked to the **Ssang Yong 2014>Data** spreadsheet that contains geotechnical information from laboratory analyses.

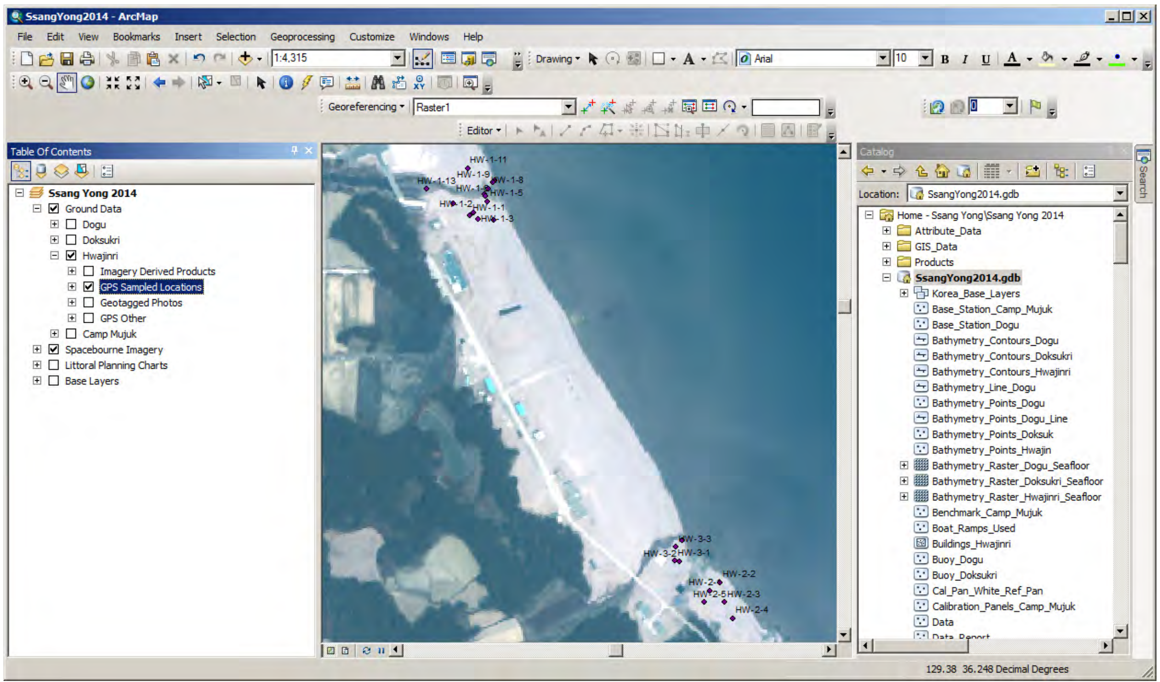

Figure P- 19. Showing GPS Sample Location on Hwajin-ri. Data collected will be used to build products that support the amphibious landing where assault ships, amphibious assault vehicles, LCACs, Marines, helicopters, airplanes, and fighter jets are all operating in the dynamic littorals.

Figure P-20 shows the procedure to zoom into a collection of points using the **Magnifying Tool**.

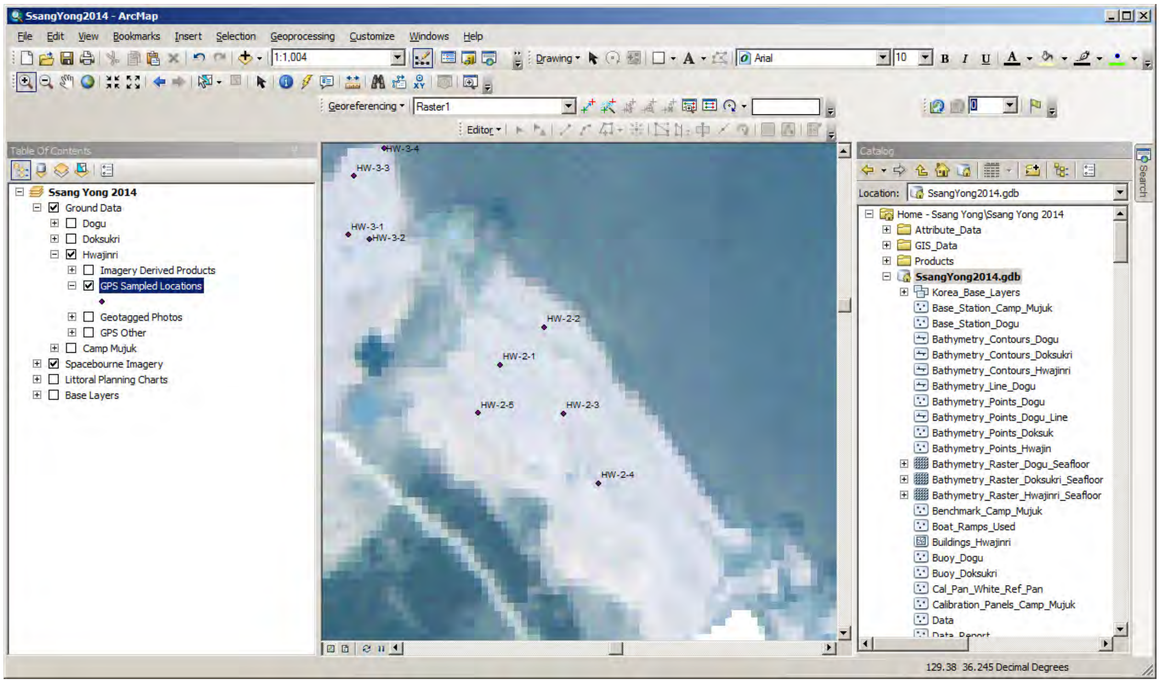

Figure P- 20. Zoomed into a set of sampled point at Hwajin-ri beach. Land drainage to the sea along the landing beaches is primarily through streamlets. The Hyeongsan River, was the only river located along the studied coastal region. It empties into Pohang Harbor, which is located approximately 23k south of Hwajin-ri.

To open the **Data** spreadsheets, the **Data Report**, or other data linked to the Hwanjin-ri study location, click on the identify icon (see Figure P-21), then click on a point of interest.

Figure P- 21. Identify Icon. The Identify tool that can be accessed from the Tools toolbar.

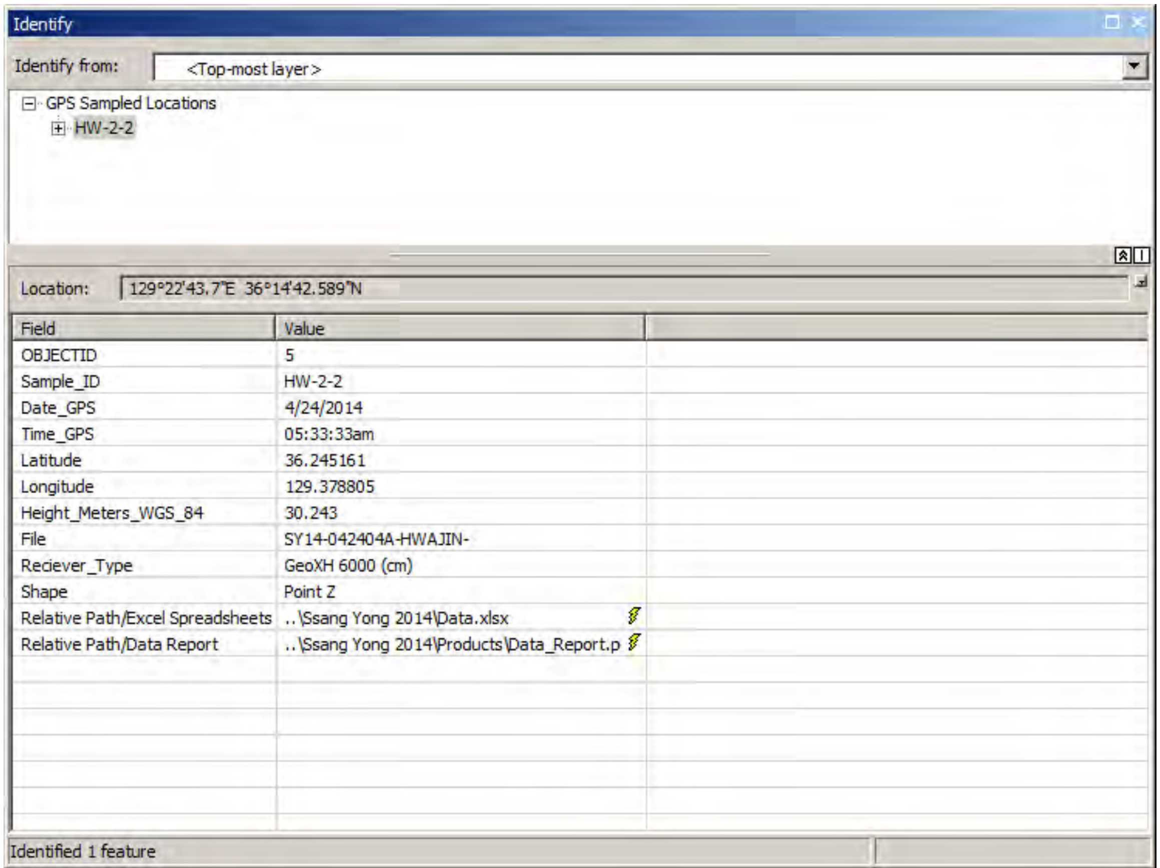

Figure P- 22. Window that appears when Identify tool is used on a GPS Sample Point. This option allows the user to view attribute values for a feature.

Information is shown about the point selected. At the bottom there are lightning bolts that may be clicked to open the **Data** spreadsheets and the **Data Report**. For information linked to this point, expend the **HW-2-2** by left-clicking the plus symbol next to the location name toward the top of the Window.

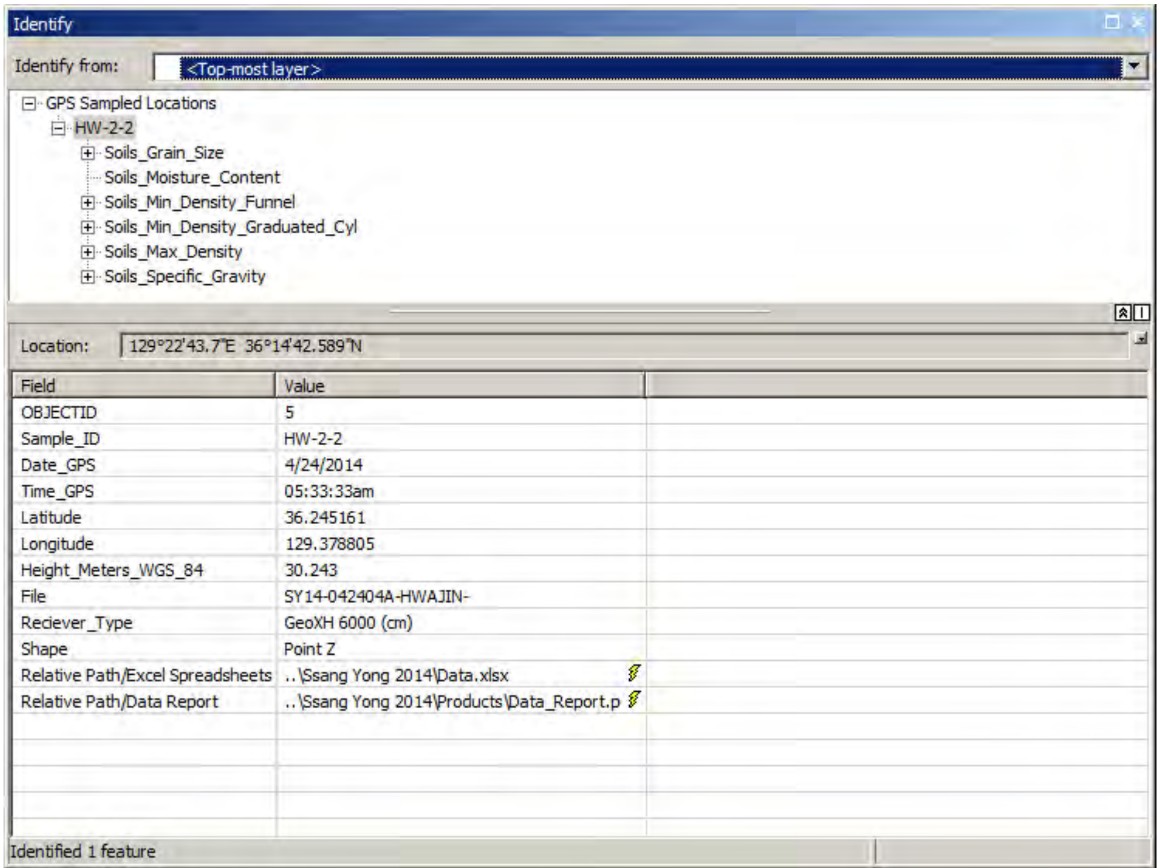

Figure P- 23. Showing tables available by expanding HW-2-2 at top of Window. When you click on a feature with the Identify tool, the *Identify* window lists the feature(s) at the identify location. Attributes are listed in the below panel.

You can left-click a feature in the feature list and see its attributes in the bottom panel. You can also right-click a feature to navigate to it, select it for other operations, define hyperlinks for it, and so on. For example, in Figure P-24 to see soil grain size attributes left-click the number, **52**, within the location designation symbol (**HW-2-2**). The number 52 is a row number that is generated by ArcGIS.

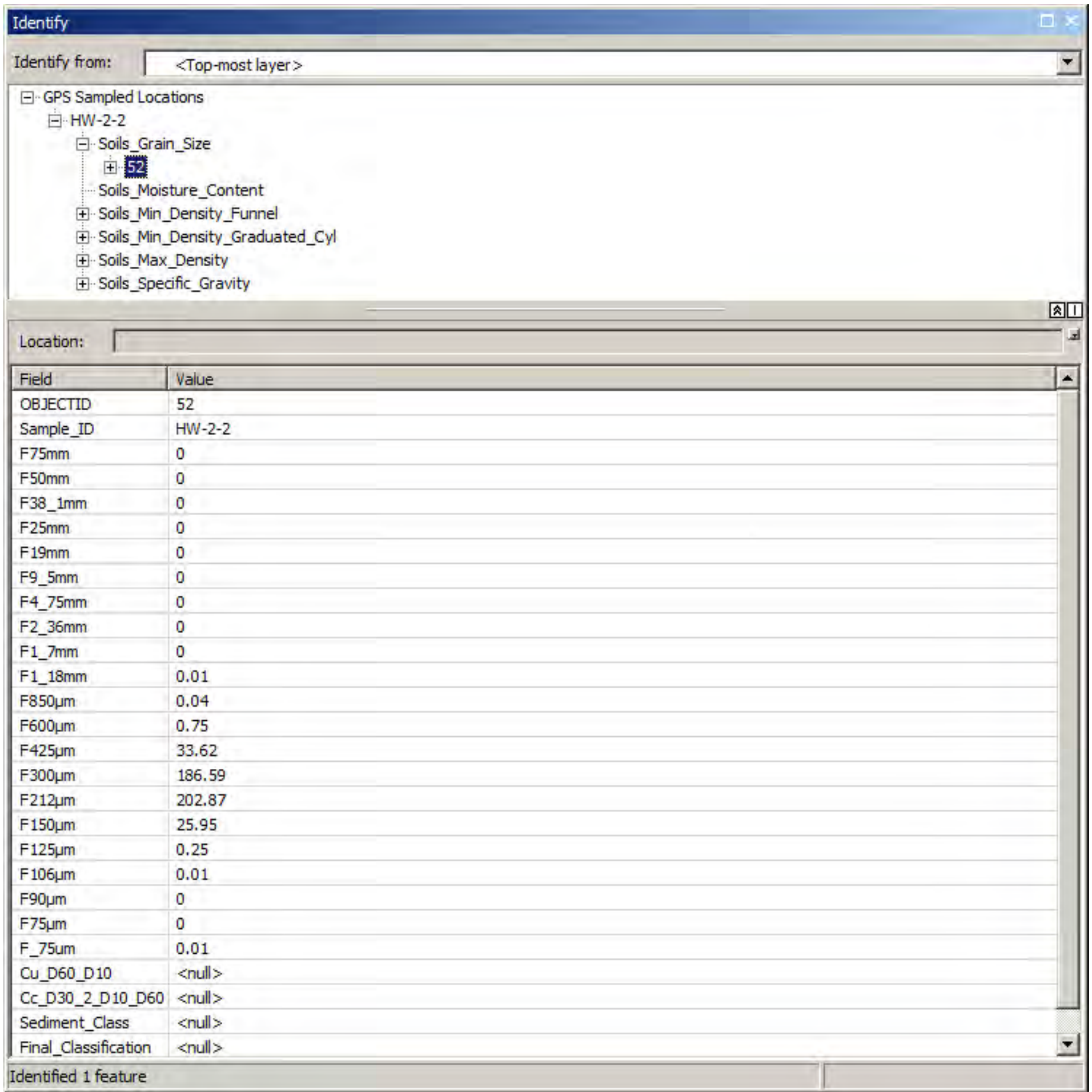

Figure P- 24. Showing attribute information in a table linked to HW-2-2.

To see the full table of a specific soils attribute, right-click on **Ssang Yong 2014>Ground Control>Hwajinri>GPS Sample Locations** layer and left-click **Open Attribute Table**. Under the **Table of Contents** choose one of the tables under **Related Tables** (see Figure P-25).

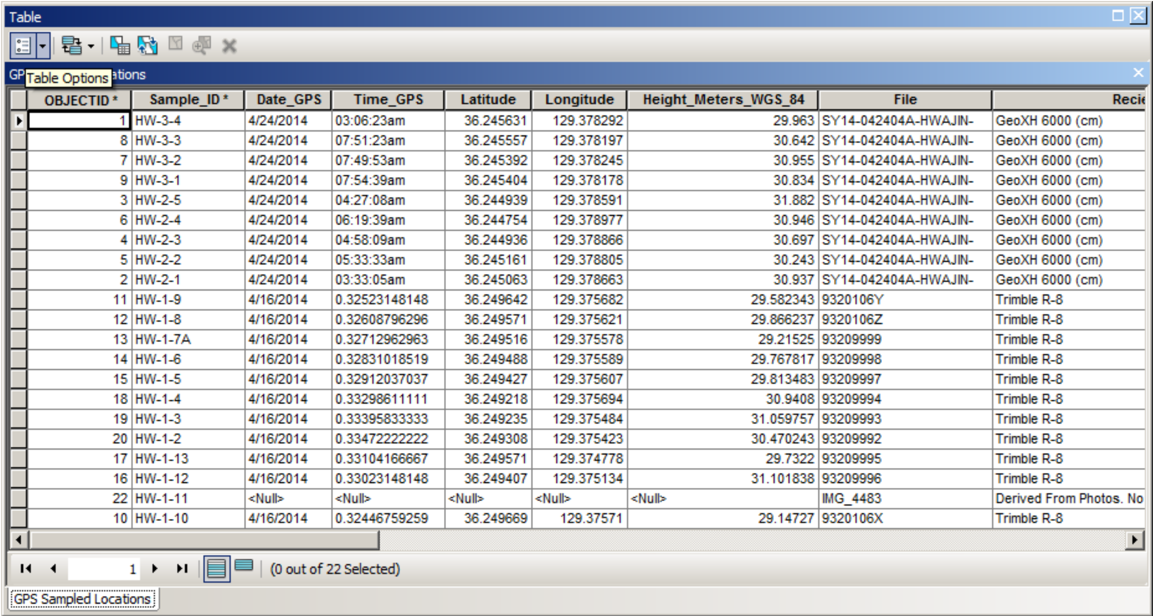

OBJECTID *	Sample_ID *	Date_GPS	Time_GPS	Latitude	Longitude	Height_Meters_WGS_84	File	Reci
1	HW-3-4	4/24/2014	03:06:23am	36.245631	129.378292	29.963	SY14-042404A-HWAJIN-	GeoXH 6000 (cm)
8	HW-3-3	4/24/2014	07:51:23am	36.245557	129.378197	30.642	SY14-042404A-HWAJIN-	GeoXH 6000 (cm)
7	HW-3-2	4/24/2014	07:49:53am	36.245392	129.378245	30.955	SY14-042404A-HWAJIN-	GeoXH 6000 (cm)
9	HW-3-1	4/24/2014	07:54:39am	36.245404	129.378178	30.834	SY14-042404A-HWAJIN-	GeoXH 6000 (cm)
3	HW-2-5	4/24/2014	04:27:08am	36.244939	129.378591	31.882	SY14-042404A-HWAJIN-	GeoXH 6000 (cm)
6	HW-2-4	4/24/2014	06:19:39am	36.244754	129.378977	30.946	SY14-042404A-HWAJIN-	GeoXH 6000 (cm)
4	HW-2-3	4/24/2014	04:58:09am	36.244936	129.378866	30.697	SY14-042404A-HWAJIN-	GeoXH 6000 (cm)
5	HW-2-2	4/24/2014	05:33:33am	36.245161	129.378805	30.243	SY14-042404A-HWAJIN-	GeoXH 6000 (cm)
2	HW-2-1	4/24/2014	03:33:05am	36.245063	129.378663	30.937	SY14-042404A-HWAJIN-	GeoXH 6000 (cm)
11	HW-1-9	4/16/2014	0.32523148148	36.249642	129.375682	29.582343	9320106Y	Trimble R-8
12	HW-1-8	4/16/2014	0.32608796296	36.249571	129.375621	29.866237	9320106Z	Trimble R-8
13	HW-1-7A	4/16/2014	0.32712962963	36.249516	129.375578	29.21525	93209999	Trimble R-8
14	HW-1-6	4/16/2014	0.32831018519	36.249488	129.375589	29.767817	93209998	Trimble R-8
15	HW-1-5	4/16/2014	0.32912037037	36.249427	129.375607	29.813483	93209997	Trimble R-8
18	HW-1-4	4/16/2014	0.33298611111	36.249218	129.375694	30.9408	93209994	Trimble R-8
19	HW-1-3	4/16/2014	0.33395833333	36.249235	129.375484	31.059757	93209993	Trimble R-8
20	HW-1-2	4/16/2014	0.33472222222	36.249308	129.375423	30.470243	93209992	Trimble R-8
17	HW-1-13	4/16/2014	0.33104166667	36.249571	129.374778	29.7322	93209995	Trimble R-8
16	HW-1-12	4/16/2014	0.33023148148	36.249407	129.375134	31.101838	93209996	Trimble R-8
22	HW-1-11	<Null>	<Null>	<Null>	<Null>	<Null>	IMG_4483	Derived From Photos. No
10	HW-1-10	4/16/2014	0.32446759259	36.249669	129.37571	29.14727	9320106X	Trimble R-8

Figure P- 25. Attribute table for GPS Sampled Locations.

To view contents within the attribute table, Left-click on the far left icon, **Table Options** then choose a table under **Related Tables**. The result is displayed in Figure 26.

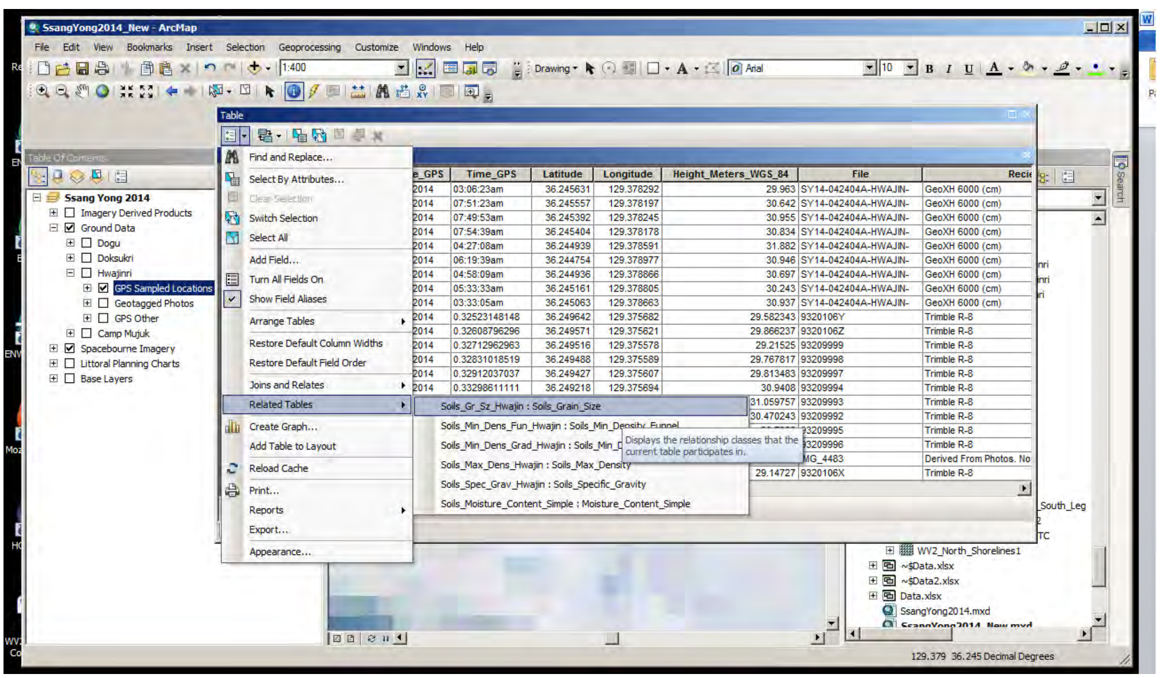

Figure P- 26. A direct method to show which related tables are linked to the Hwajin-ri GPS Sampled Locations layer.

If the table comes up blank (see Figure P-27).

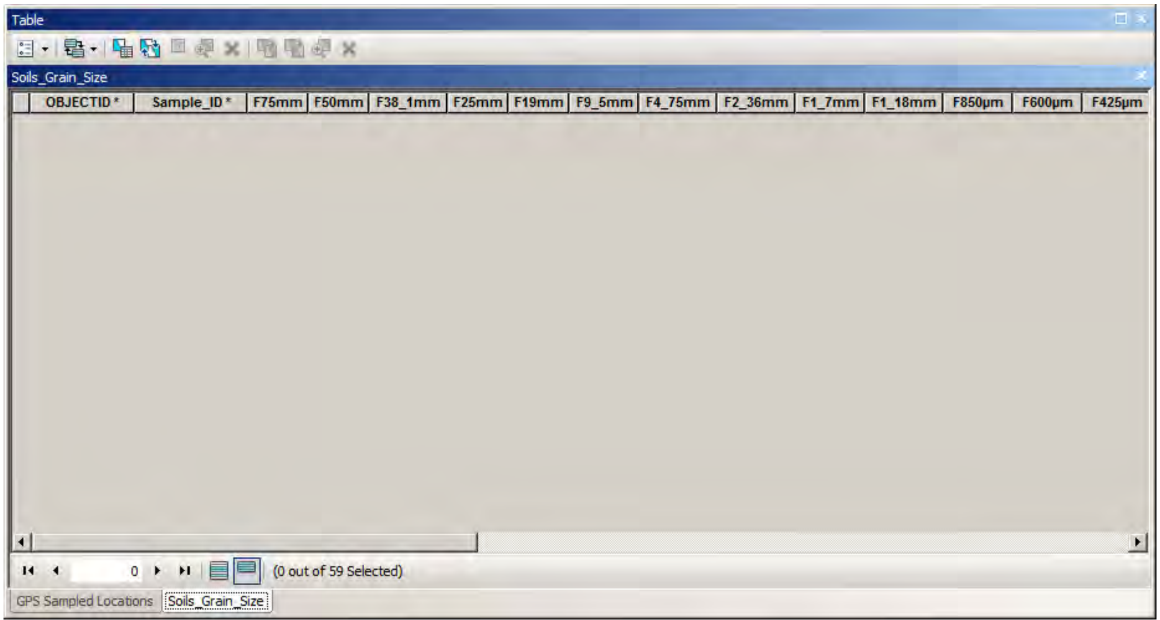

Figure P- 27. A blank window may appear when no attributes are selected for the Soils_Grain_Size Table.

Once the **Show all Records** tab is selected at the bottom of the Soils_Grain_Size table, the attributes will be displayed (see Figure P-28).

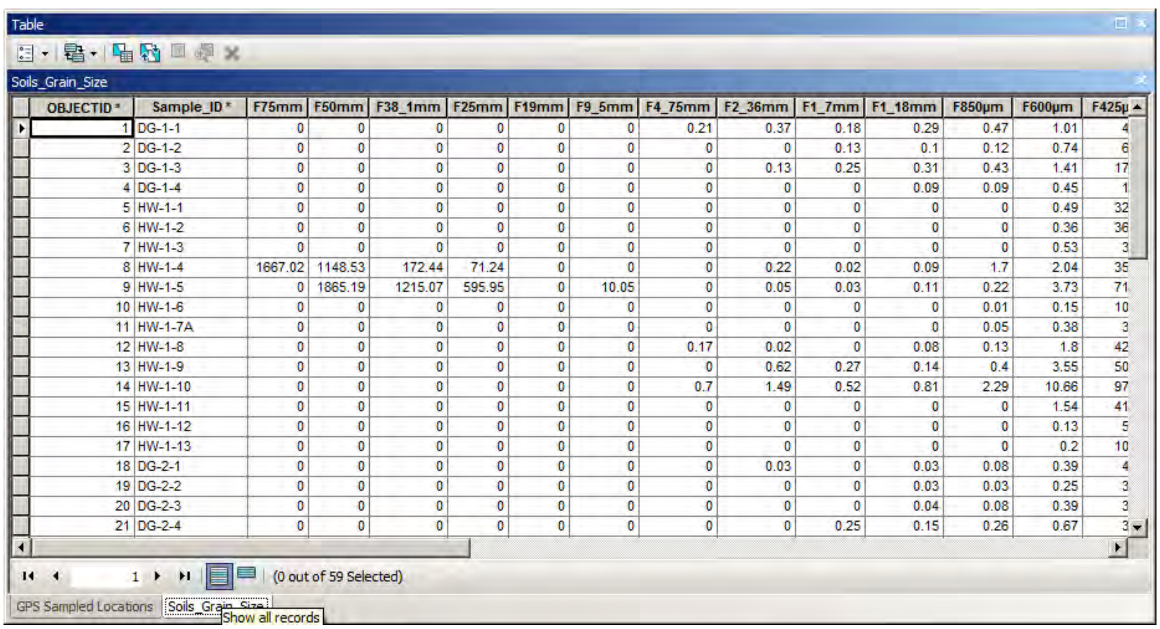

OBJECTID *	Sample_ID *	F75mm	F50mm	F38_1mm	F25mm	F19mm	F9_5mm	F4_75mm	F2_36mm	F1_7mm	F1_18mm	F850µm	F600µm	F425µ
1	DG-1-1	0	0	0	0	0	0	0.21	0.37	0.18	0.29	0.47	1.01	4
2	DG-1-2	0	0	0	0	0	0	0	0	0.13	0.1	0.12	0.74	6
3	DG-1-3	0	0	0	0	0	0	0	0.13	0.25	0.31	0.43	1.41	17
4	DG-1-4	0	0	0	0	0	0	0	0	0	0.09	0.09	0.45	1
5	HW-1-1	0	0	0	0	0	0	0	0	0	0	0	0.49	32
6	HW-1-2	0	0	0	0	0	0	0	0	0	0	0	0.36	36
7	HW-1-3	0	0	0	0	0	0	0	0	0	0	0	0.53	3
8	HW-1-4	1667.02	1148.53	172.44	71.24	0	0	0	0.22	0.02	0.09	1.7	2.04	35
9	HW-1-5	0	1865.19	1215.07	595.95	0	10.05	0	0.05	0.03	0.11	0.22	3.73	71
10	HW-1-6	0	0	0	0	0	0	0	0	0	0	0.01	0.15	10
11	HW-1-7A	0	0	0	0	0	0	0	0	0	0	0.05	0.38	3
12	HW-1-8	0	0	0	0	0	0	0.17	0.02	0	0.08	0.13	1.8	42
13	HW-1-9	0	0	0	0	0	0	0	0.62	0.27	0.14	0.4	3.55	50
14	HW-1-10	0	0	0	0	0	0	0.7	1.49	0.52	0.81	2.29	10.66	97
15	HW-1-11	0	0	0	0	0	0	0	0	0	0	0	1.54	41
16	HW-1-12	0	0	0	0	0	0	0	0	0	0	0	0.13	5
17	HW-1-13	0	0	0	0	0	0	0	0	0	0	0	0.2	10
18	DG-2-1	0	0	0	0	0	0	0	0.03	0	0.03	0.08	0.39	4
19	DG-2-2	0	0	0	0	0	0	0	0	0	0.03	0.03	0.25	3
20	DG-2-3	0	0	0	0	0	0	0	0	0	0.04	0.08	0.39	3
21	DG-2-4	0	0	0	0	0	0	0	0	0.25	0.15	0.26	0.67	3

Figure P-28. Showing "Show all records" tab selected to view data in attribute table.

Close the table. To see photographs linked to this site, left-click on the lightning bolt (Hyperlink Tool) to the right of the Identify Icon from the Tools toolbar (see Figure 29).

Figure P- 29. Hyperlink Icon. The cursor will be transformed into a lightning bolt.

Once the Hyperlink Tool is activated, all of the features with a hyperlink will turn blue. When you hover the pointer over a feature for which a hyperlink exists, the mouse pointer turns into a black lightning bolt with a flash, and you see a pop-up tip with the link location. Click on one of the blue points to view linked data (see Figure P-30).

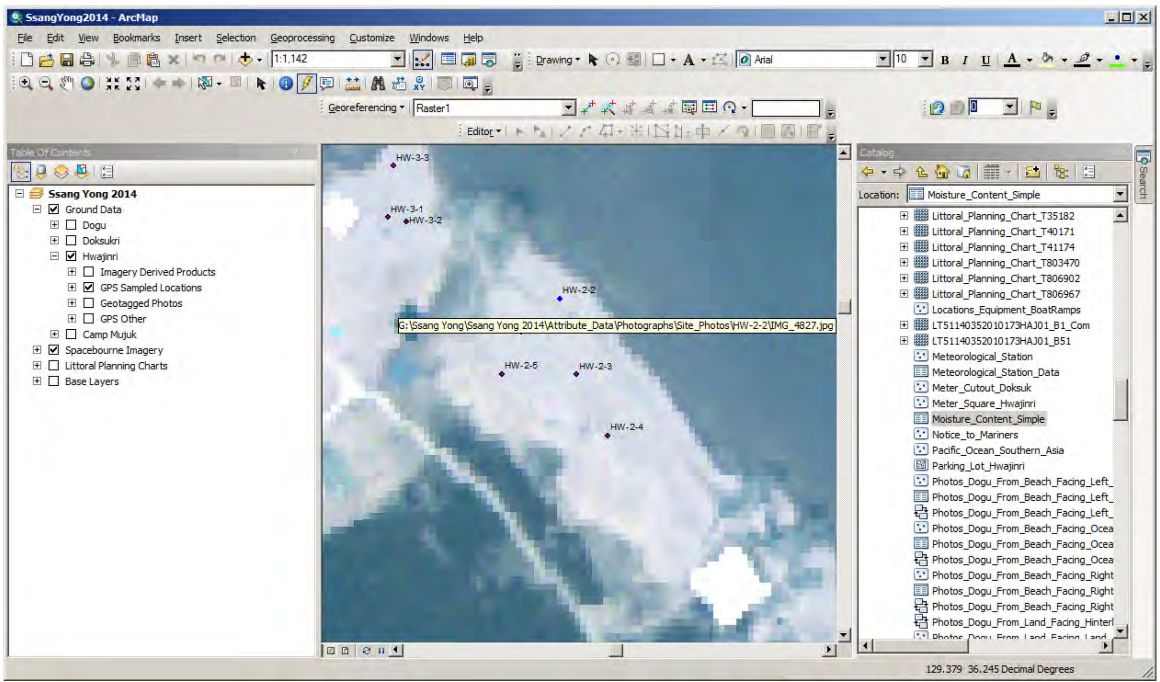

Figure P- 30. Hwajin-ri Beach showing blue hyperlinked points of the GPS sample locations.

Once a blue hyperlinked point is left-clicked, a primary photograph for this sample location will Pop-up (see Figure P-31).

Figure P- 31. Primary photograph hyperlinked to HW-2-2 site GPS point.

Once the primary picture is displayed, the user can view more pictures for this site location by clicking through the navigation tool displayed at the bottom of the window. All photographs will be made available through a single folder for the respective sampling location.

To view the contents of the Geotagged Photos layer, close the picture, left-click the checked box for **Ssang Yong 2014>Ground Data>Hwajinri>GPS Sample Locations** to uncheck it, and left-click the box for **Ssang Yong 2014>Ground Data>Hwajinri>Geotagged Photos** to check it, under **Table of Contents** (see Figure P-32).

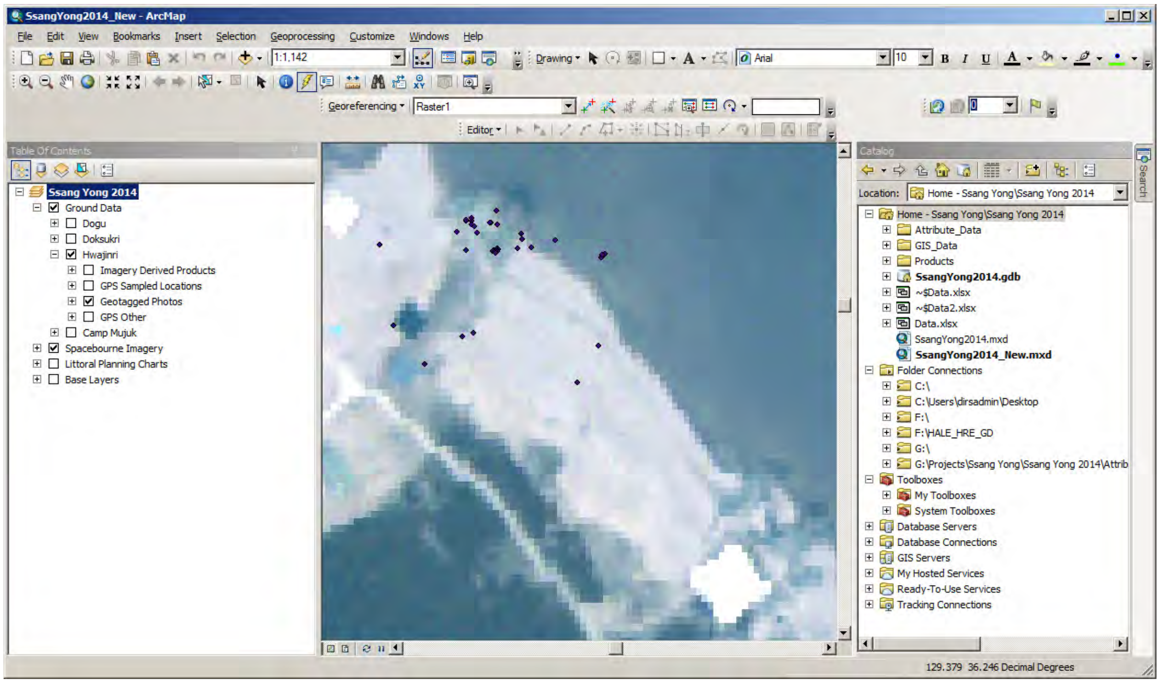

Figure P- 32. Locations of geotagged photos at Hwajin-ri Beach.

Metadata for the photographs are provided in the attribute table. Left-click **HTML Popup** button (Figure P-33), then left-click on the desired point (see Figure P-32). The result is the photograph with metadata as shown in Figure P-34. This button can also be used to see the primary **Attribute Table** linked to each point.

Figure P- 33. HTML Popup button.

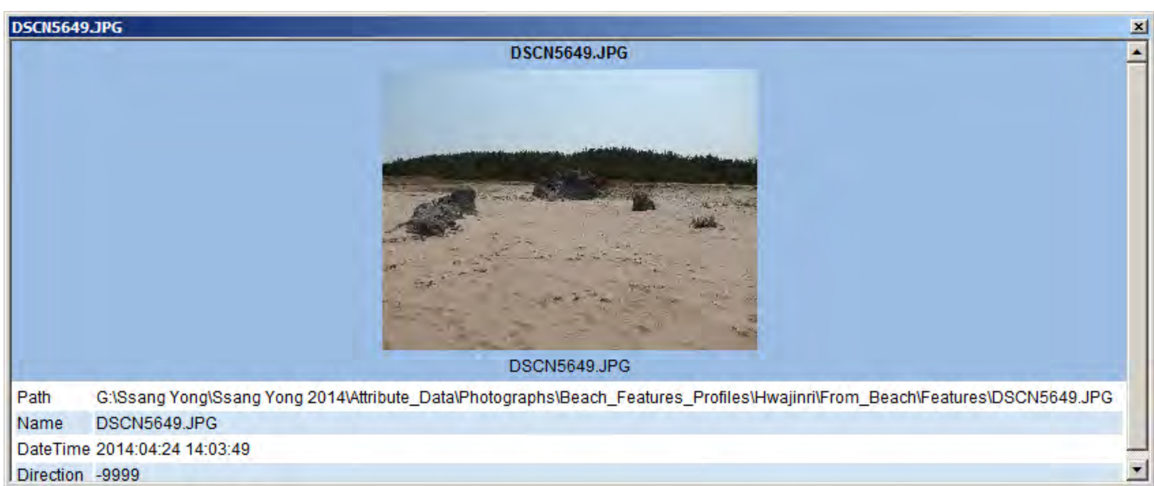

Figure P- 34. Geotagged Photograph. During the experiment there were three different cameras that provided geotagged photographs.

To see an enlarged view of the photograph, left-click on the image. To view this photograph in Windows Photo Viewer, left-click on the point with the **Identify** icon and left-click on the **Attachments** section with the paper clip or click on the lightning bolt in the table to the far right of the **Path** field (see Figure P-35 and P-36).

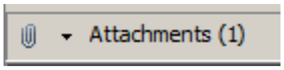

Figure P- 35. Used to open attachments. In this case a photograph.

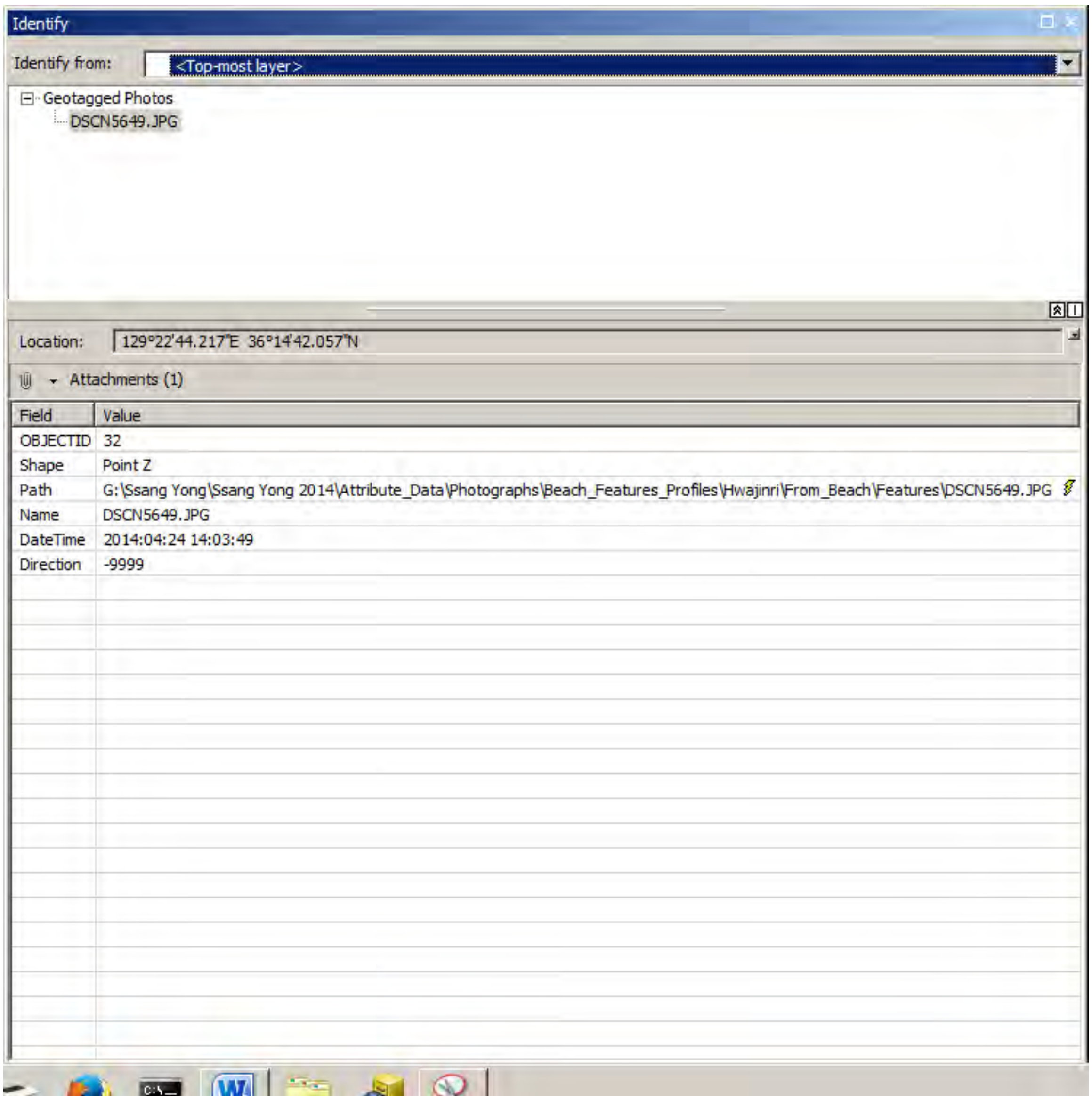

Figure P- 36. Used to open photographs in Windows Photo Viewer.

The GPS Other folder provides considerable survey data. To access this folder left-click **Ssang Yong 2014>Ground Data>Hwajinri>Geotagged** Photos, left-click

Ssang Yong 2014>Ground Data>Hwajinri>GPS Other, and expand by left-clicking the plus symbol (to the left of the folder name) (see Figure P-37).

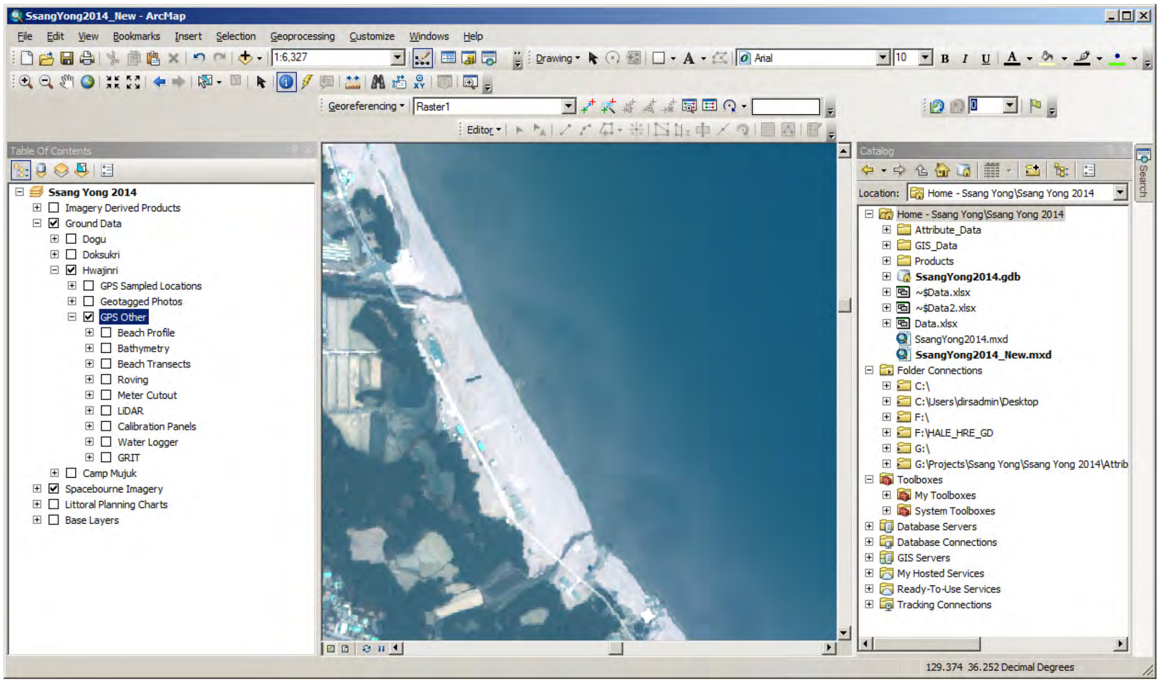

Figure P- 37. GPS Other. This includes terrestrial lidar and beach profiles.

Under **Ssang Yong 2014>Ground Data>Hwajinri>GPS Other>Beach Profile** TINs, Rasters, and Contours have been created from the points collected at the northern and southern parts of Hwajin-ri Beach. In the Table of Contents, all folder names ending in 1 refer to the northern beach and 2 the southern part of the beach (see Figure P-38).

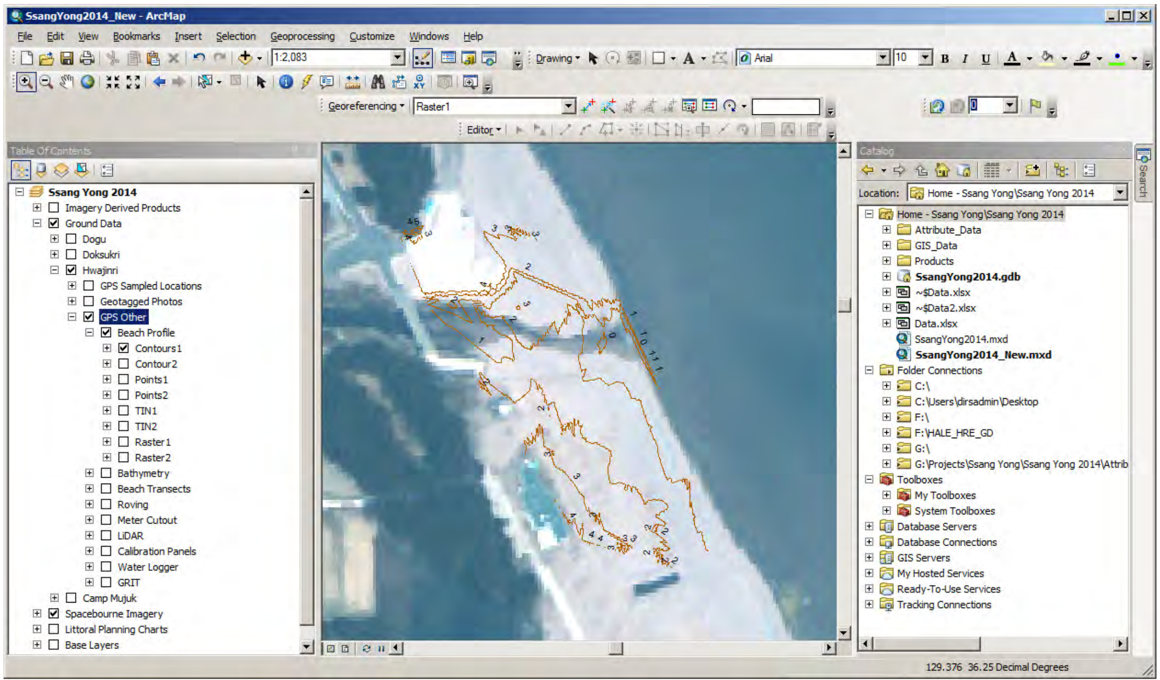

Figure P-38. Contour lines located on northern Hwajin-ri beach from GPS surveys

Figure P-39 depicts hydrographic survey data collected in the near-shore regions of Hwajin-ri beach. These data are accessed under **Ssang Yong 2014>Ground Data>Hwajinri>Bathymetry.** The folder names are **Contours**, **Points**, **TINs**, and **Raster.**

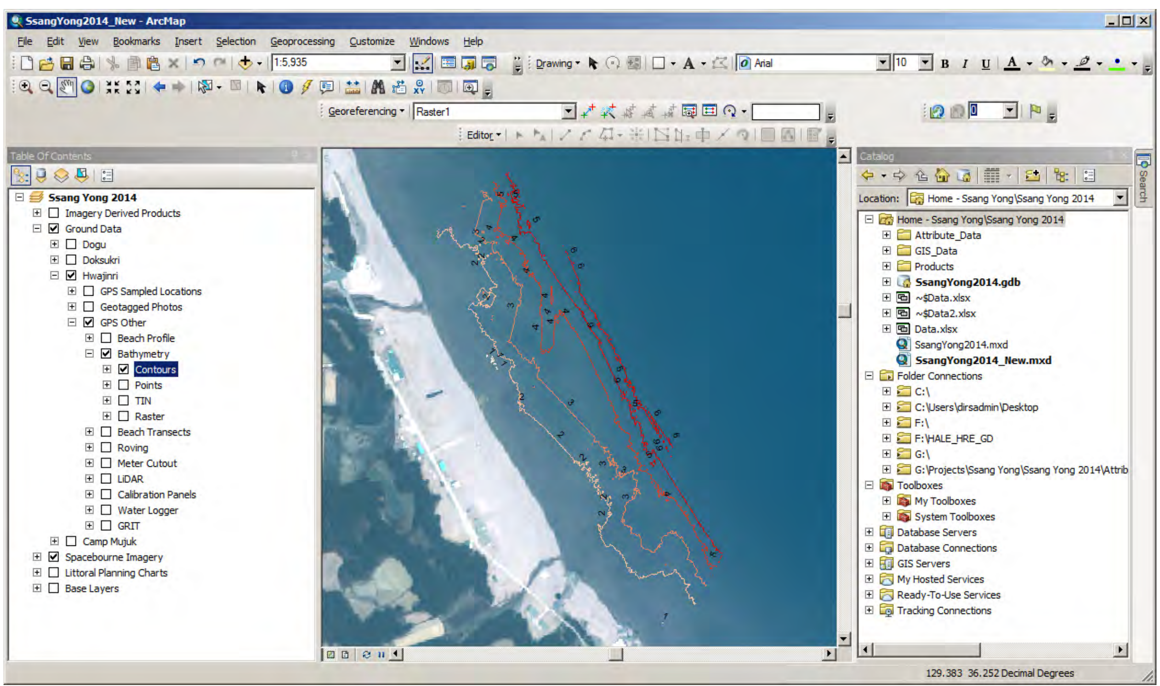

Figure P- 39. Very Shallow Water bathymetric contours for Hwajin-ri beach.

Figure P-40 depicts beach profiles from data stored under **Ssang Yong 2014>Ground Data>Hwajinri>GPS Other>Beach Transects**.

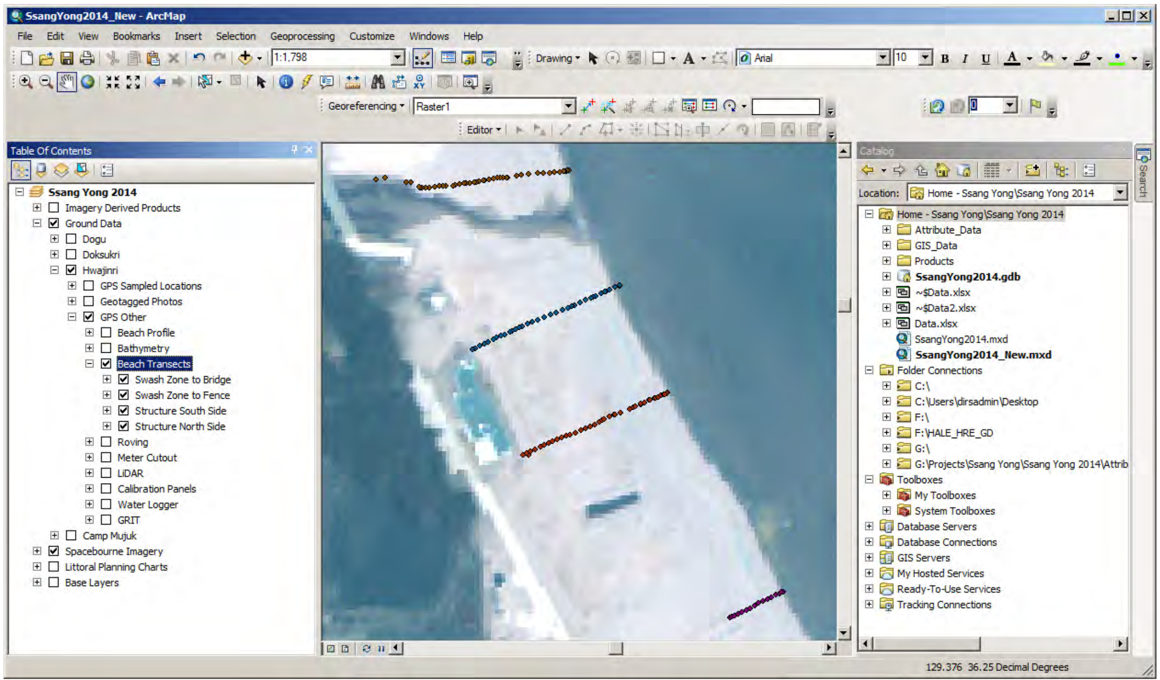

Figure P- 40. Beach transects at Hwajin-ri.

Differential GPS involves the use of two receivers, one that's stationary and another that's roving making position measurements. The stationary receiver ties all the satellite measurements into an accurate and precise local reference. Data collected from the roving unit are stored under **Ssang Yong 2014>Ground Data>Hwajinri>GPS Other>Roving.** Significant ground control is also stored as GPS roving data, e.g., the parking lot, revetment, and steep slope located on south side.

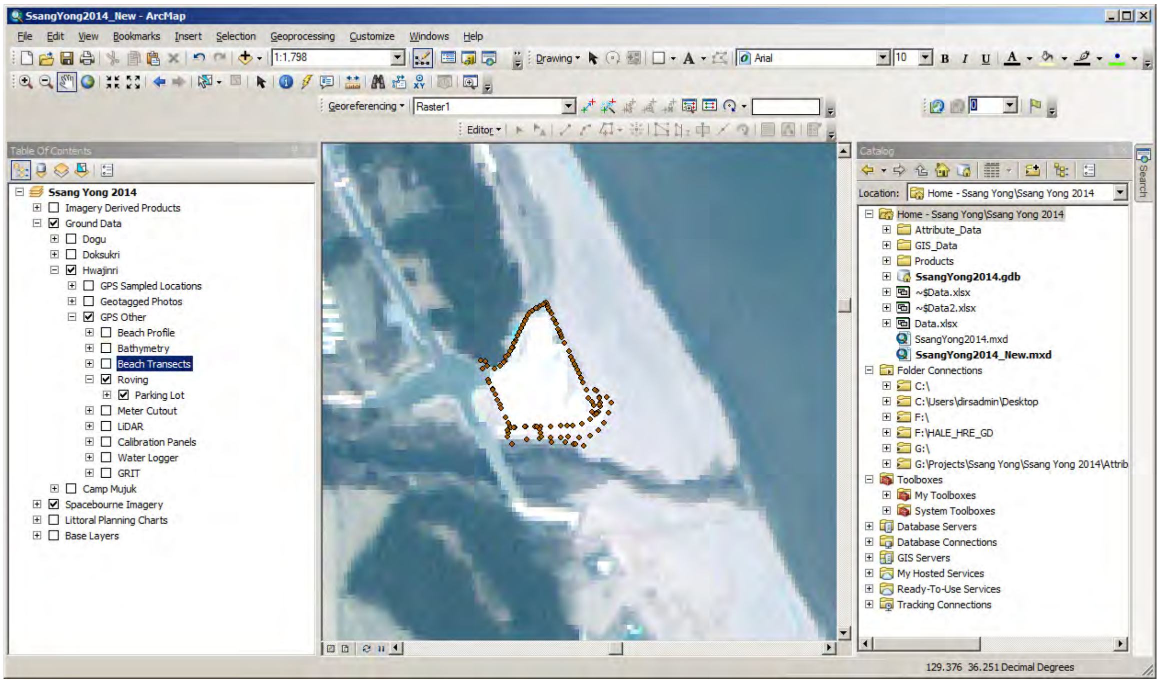

Figure P- 41. The parking lot at Hwajin-ri beach. This feature which includes a significant revetment was not identified on the Littoral Planning Chart for Exercise Ssang Yong 2014.

Some field expedient 1 m^2 quadrats were cut out of tarps to quickly estimate the amount of sand found on beaches that presented patches of gravel and cobble. Figure P-42 depicts the quadrats that include percent sand, gravel, and cobble under **Ssang Yong 2014>Ground Data>Hwajinri>GPS Other>Meter Cutout.** To view the photographs, click on the **Hyperlink** icon (Lightning Bolt) then click a point.

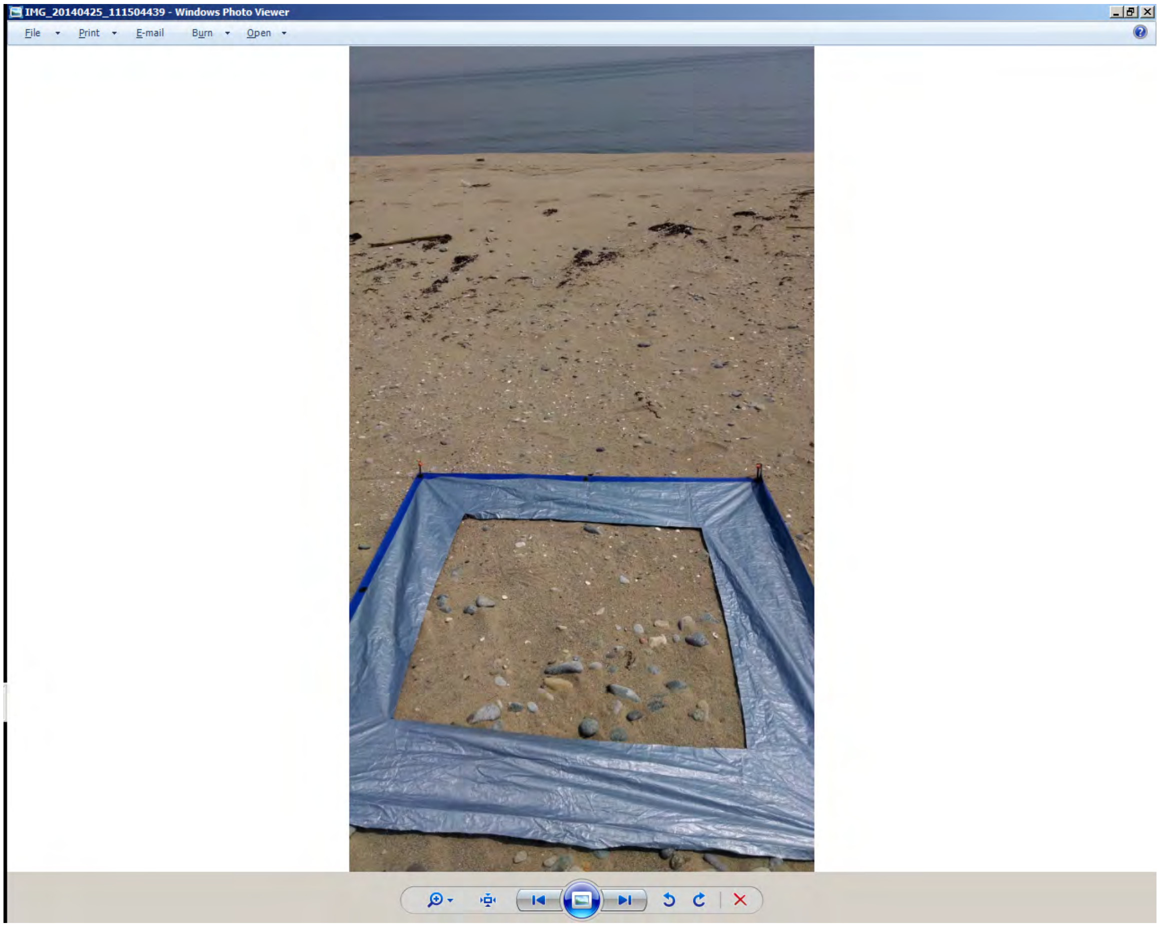

Figure P- 42. A tarp with one square meter cut out deployed on Hwajin-ri beach. These were made quickly to get an appreciation for the spatial distribution of gravel and cobble.

Figure P-43 illustrates the cut section for the quadrat.

Figure P- 43. Showing meter stick in one meter square cut-out in tarp.

Sub-aerial beach topography was measured using terrestrial LiDAR point clouds from a tripod-based LiDAR and can be found under **Ssang Yong 2014>Ground Data>Hwajinri>GPS Other>LiDAR**. Sub-layers include **Fiducials** and **Positions** (see Figure P-44).

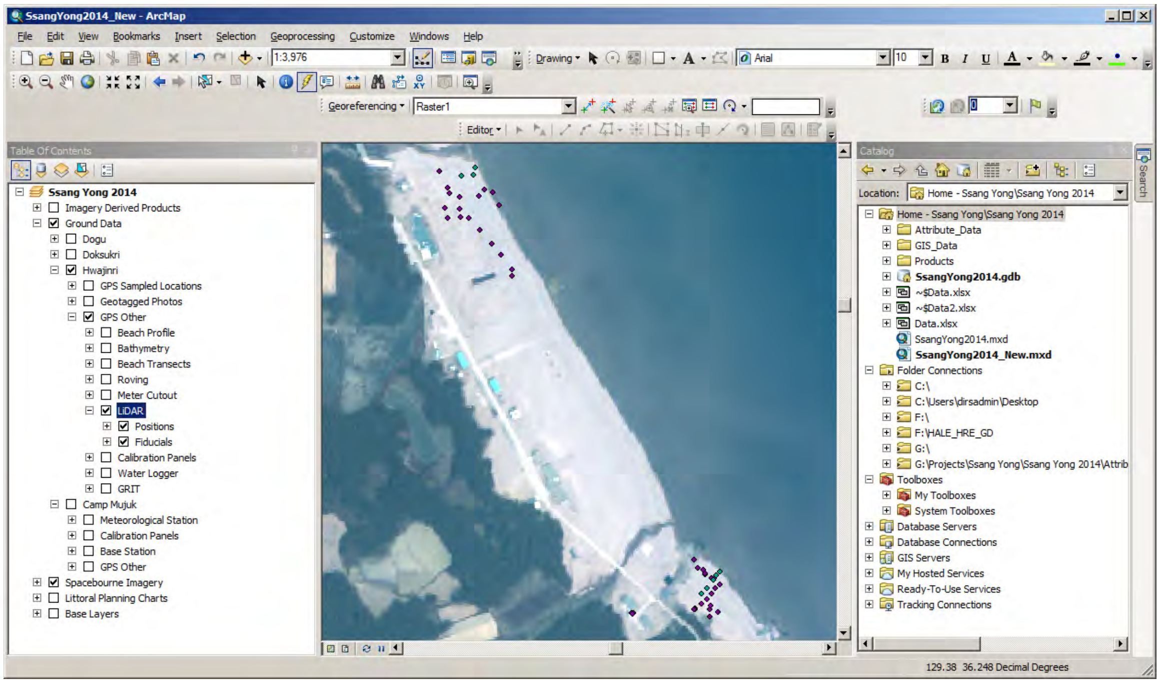

Figure P- 44. Showing LiDAR Scan positions and LiDAR Fiducials.

Figure P-45 demonstrates the method to zoom into a cluster of LiDAR related points. These points include fiducials and multiple scan locations. Significant features and placed targets are termed "fiducial" because they represent reference positions for the LiDAR survey.

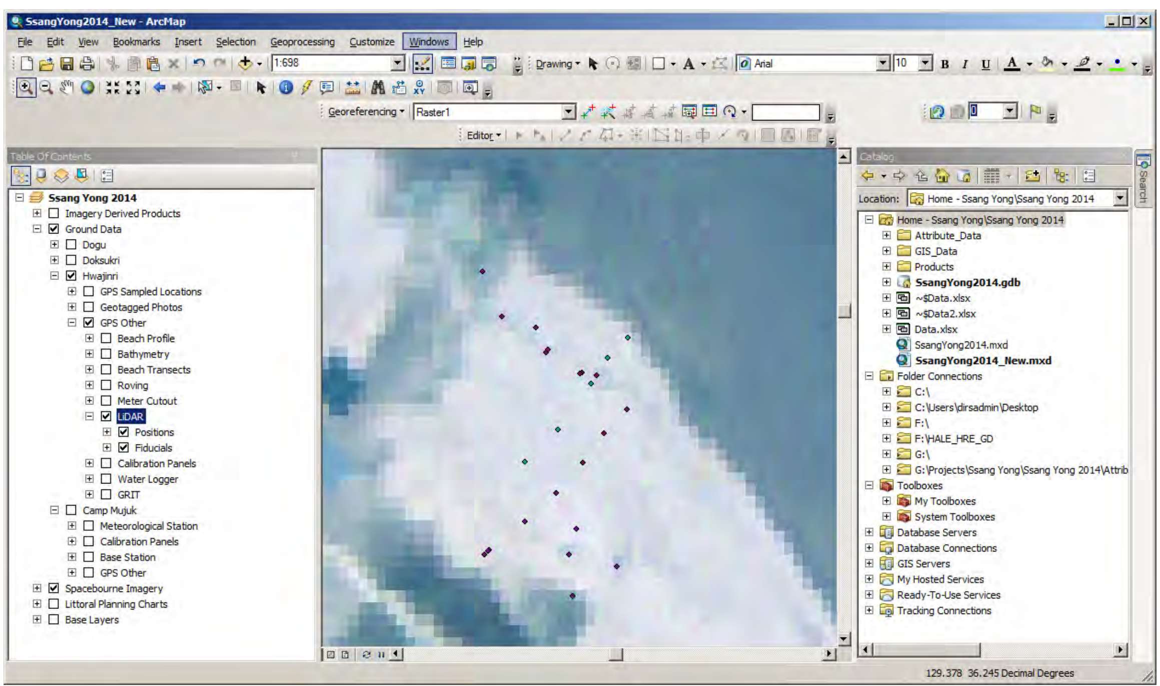

Figure P- 45. Close-up of fiducials (red) and tripod locations (green) for the terrestrial LiDAR. Spatially accurate surveys of large areas can be obtained by combining data from adjacent scans.

In order to locate LiDAR scan locations, left-click on the **HTML Popup** icon then left-click a point to see the information linked to that point (see Figure P-46).

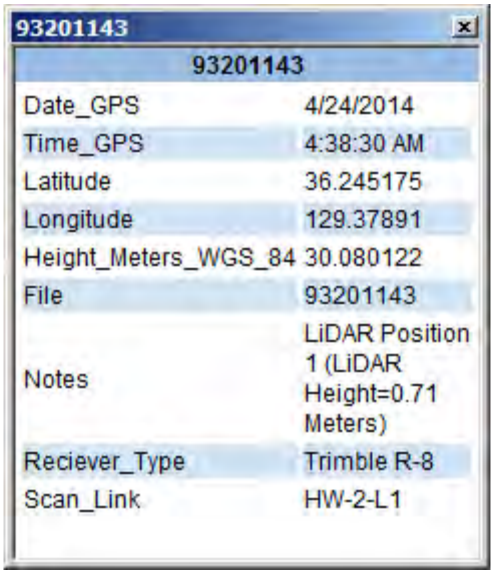

Figure P- 46. HTML Pop-up of LiDAR Position 1 at Hwajin-ri Beach.

Left-click on the **Identify** icon then left-click on a point to see additional information linked to the point (see Figure P-47).

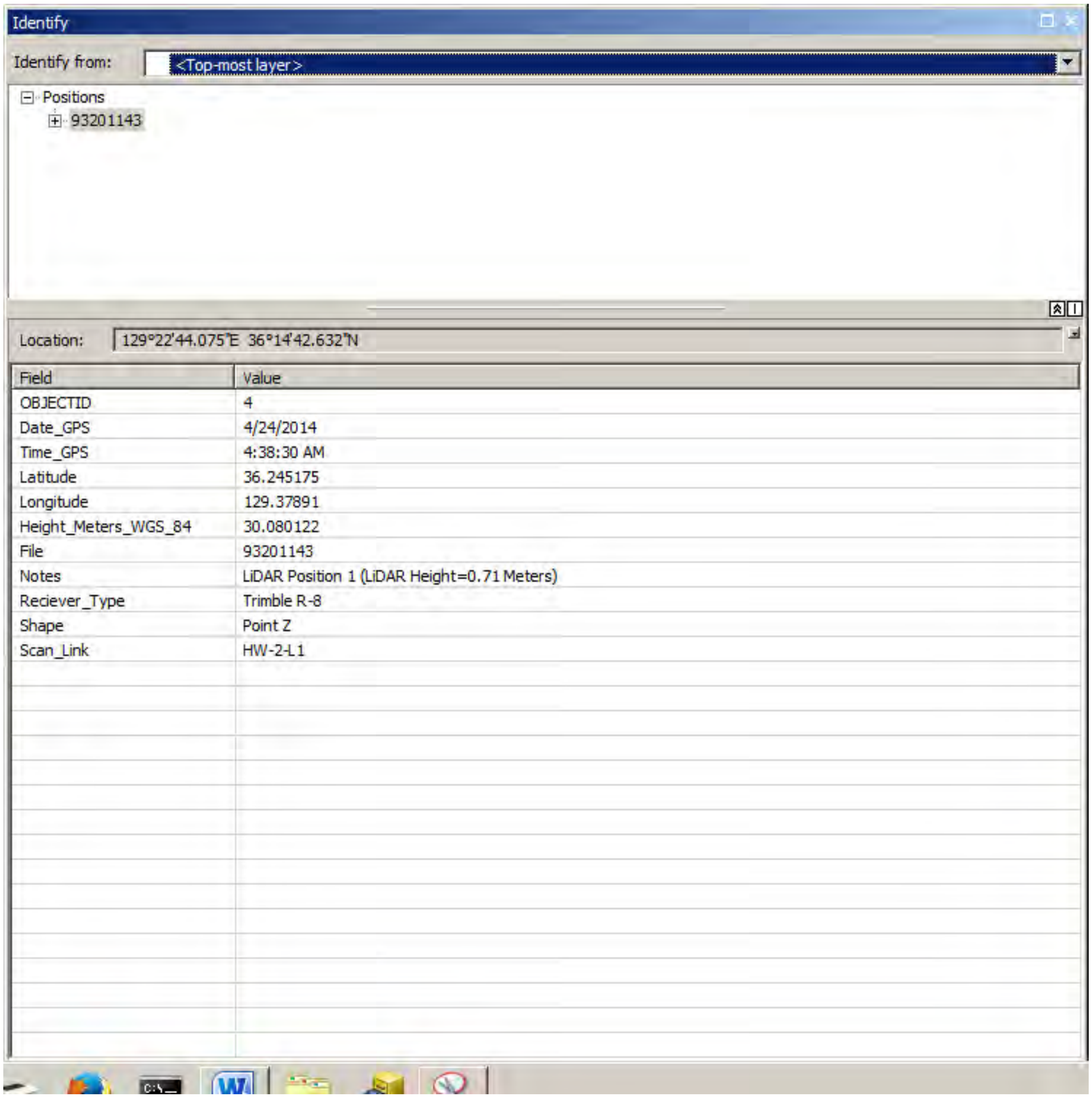

Figure P- 47. Example attribute table that is displayed when the Identify tool is used on a point.

The attribute table shows the same information as the **HTML Pop-up** but has the capability of showing linked tables. By left-clicking the plus symbol to the left of **93201143** (at the top of the table) you can expand the scan and choose one of the layers to see the LiDAR Scan information that is linked to the indicated location (see Figure P-48).

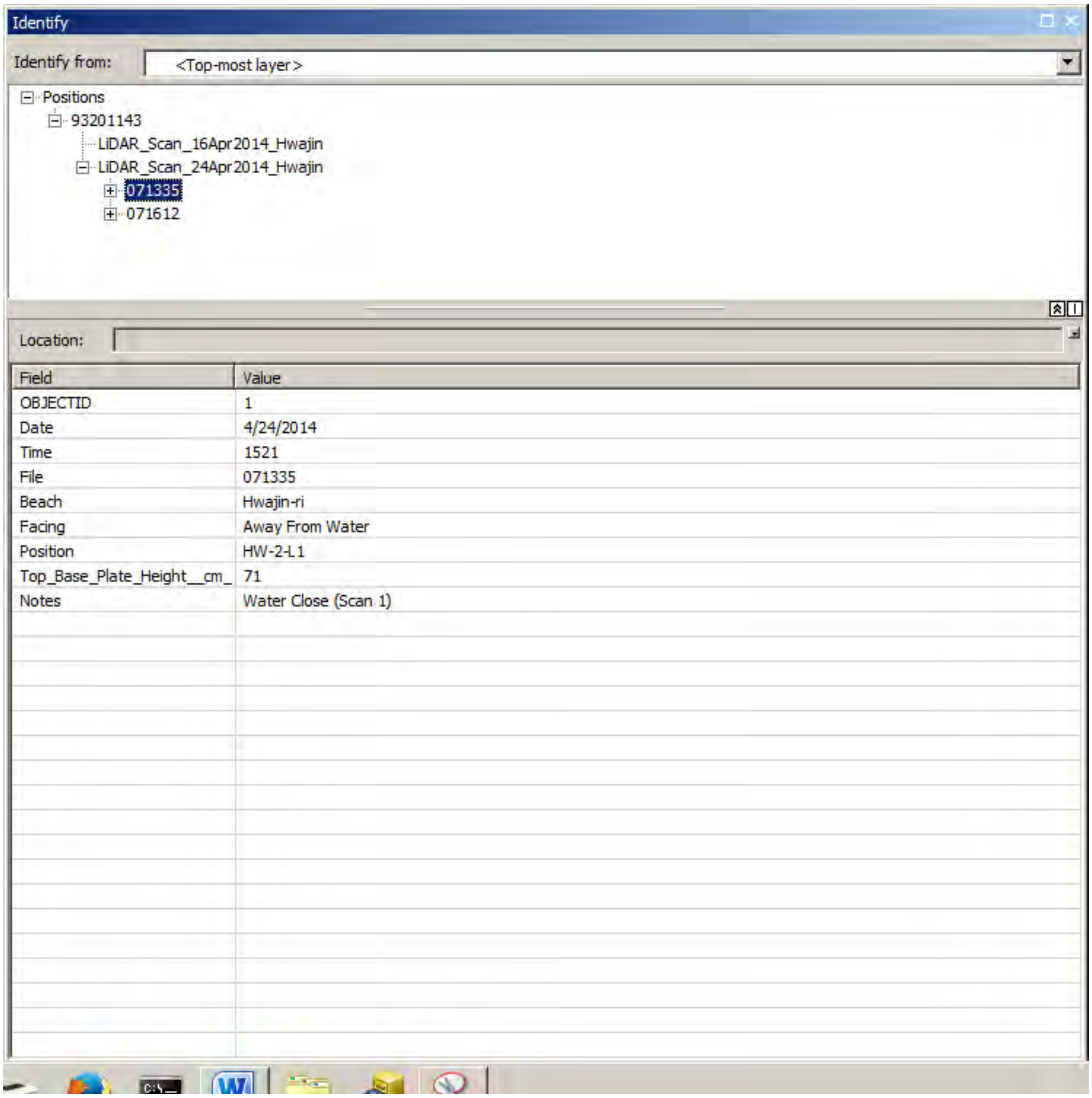

Figure P- 48. Scan data linked to LiDAR position GPS point.

The attribution information above in the bottom panel of Figure P-48 is for a specific scan that shows the File 071335 linked to this geographic point.

Calibration panels of known geometric properties where deployed on the beach and at Camp Mujuk. Imagery was collected of the beach calibration panels from WorldView-2. In addition, GPS positions and nadir spectra were collected at the calibration panels. These data are found under **Ssang Yong 2014>Ground Data>Hwajinri>GPS Other>Calibration Panels** (see Figure P-49).

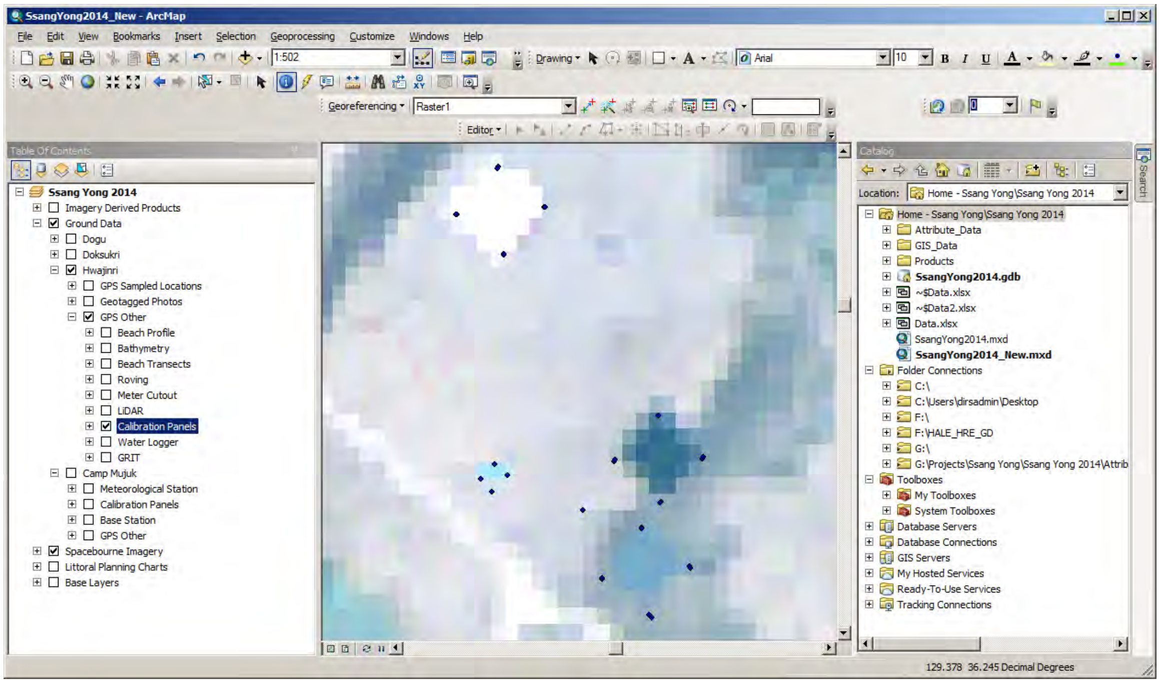

Figure P- 49. Image with calibration panels captured and corresponding GPS points. Image analysis can consider the correspondence between properties of the calibration panel and **distorted** properties of the image.

Water level time series data were collected to tide synchronize images. These time series are located in the **Ssang Yong 2014>Ground Data>Hwajinri>GPS Other>Water Logger** layer. The point location of bottom-mounted pressure gages that were used to derive water levels are linked with the Excel **Data** spreadsheet and **Data Report** (see Figure P-50). Water logger data time series are in the Excel spreadsheet.

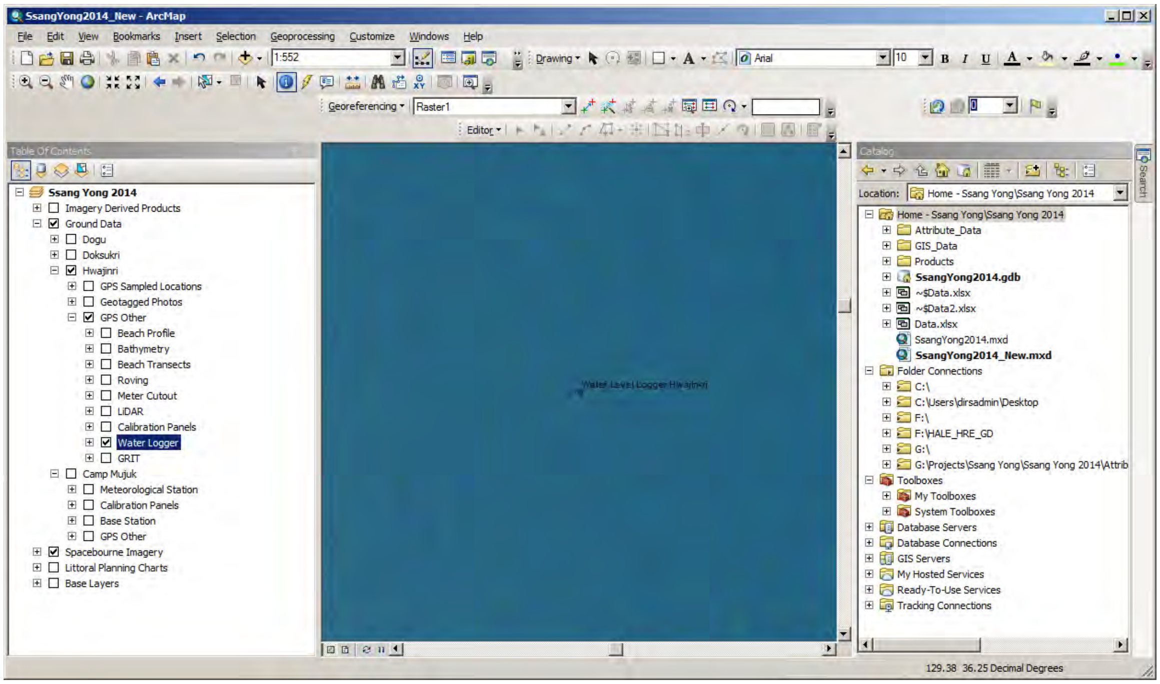

Figure P- 50. Water Logger point at Hwajin-ri Beach. The HOBO pressure-based water level data logger was used to measure water level fluctuations.

In order to characterize an object's reflectance properties on the beach, the Goniometer at Rochester Institute of Technology (GRIT) was used to measure the Bi-directional Reflectance Distribution Function (BRDF). GRIT moves the spectrometer to positions over a hemispherical surface to acquire the same spot from a comprehensive set of azimuth and zenith angles. Storage of the BRDF in the geodatabase is important because this allows users to enhance the libraries to support off-nadir and stand-off viewing geometries to improve the characterization of trafficability in various types of beaches. Goniometer GPS Positions are stored in **Ssang Yong 2014>Ground Data>Hwajinri>GPS Other>GRIT.**

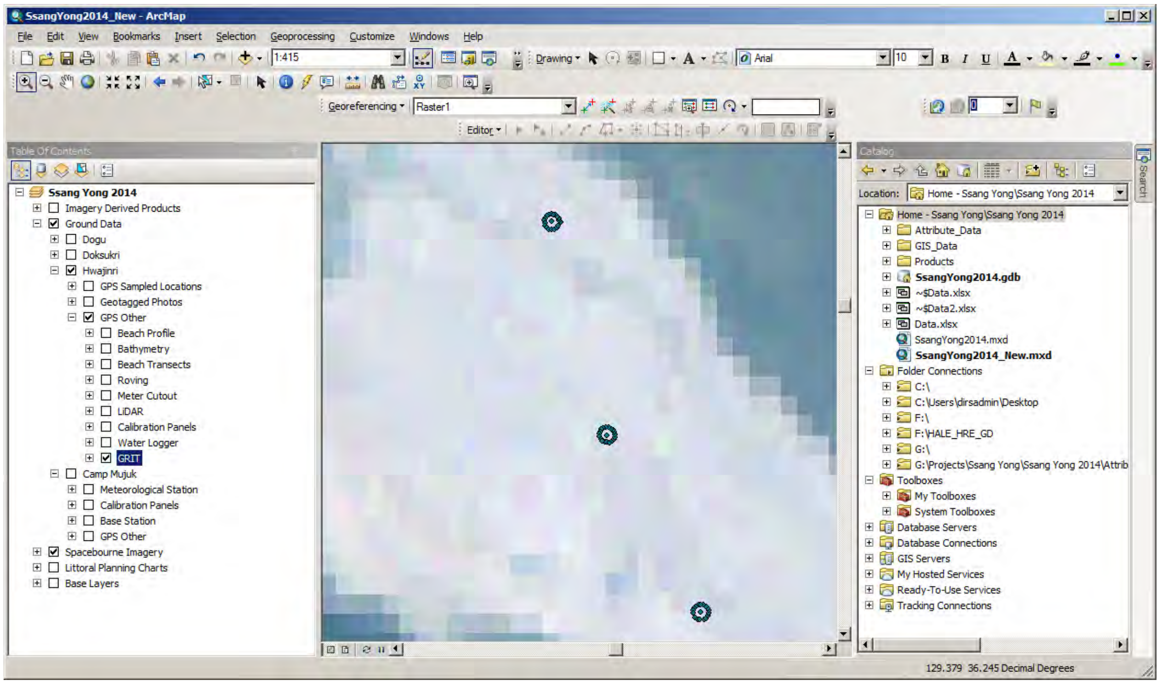

Figure P- 51. Goniometer azimuth GPS positions.

If the user desires to view the attribute table linked to the sampling location, right-click content name under **Table of Contents** and left-click **Open Attribute Table**. In this case right click **GRIT** (see Figure P-52). All information (GPS locations) linked to each point is listed.

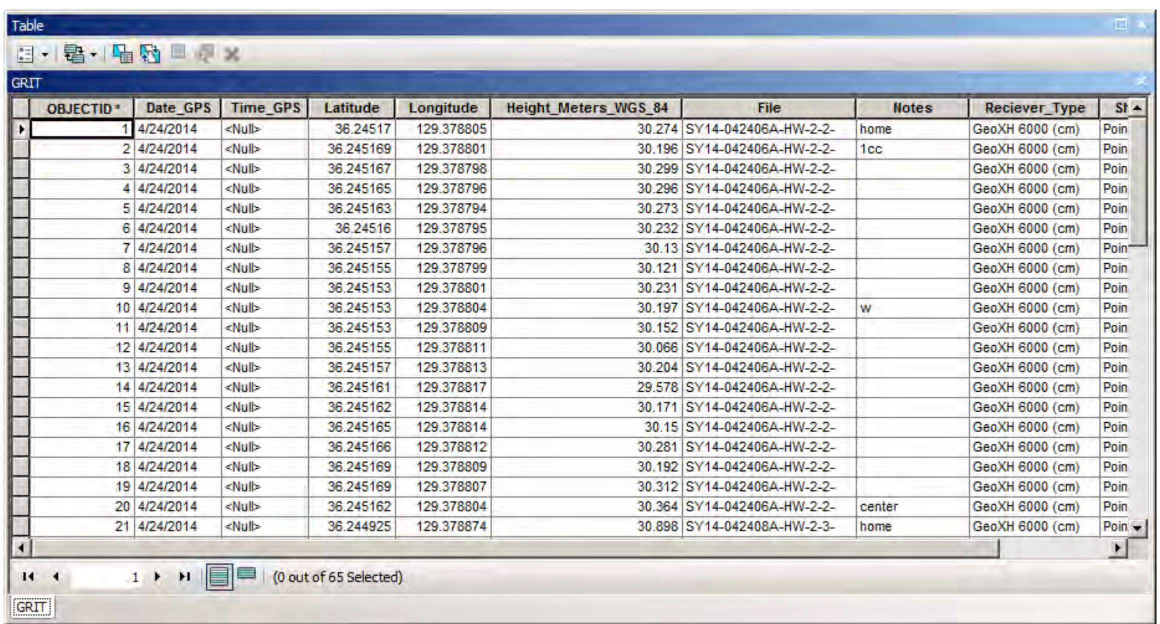

Table

GRIT

OBJECTID *	Date_GPS	Time_GPS	Latitude	Longitude	Height_Meters_WGS_84	File	Notes	Reciever_Type	Sh
1	4/24/2014	<Null>	36.24517	129.378805	30.274	SY14-042406A-HW-2-2-	home	GeoXH 6000 (cm)	Poin
2	4/24/2014	<Null>	36.245169	129.378801	30.196	SY14-042406A-HW-2-2-	1cc	GeoXH 6000 (cm)	Poin
3	4/24/2014	<Null>	36.245167	129.378798	30.299	SY14-042406A-HW-2-2-		GeoXH 6000 (cm)	Poin
4	4/24/2014	<Null>	36.245165	129.378796	30.296	SY14-042406A-HW-2-2-		GeoXH 6000 (cm)	Poin
5	4/24/2014	<Null>	36.245163	129.378794	30.273	SY14-042406A-HW-2-2-		GeoXH 6000 (cm)	Poin
6	4/24/2014	<Null>	36.24516	129.378795	30.232	SY14-042406A-HW-2-2-		GeoXH 6000 (cm)	Poin
7	4/24/2014	<Null>	36.245157	129.378796	30.13	SY14-042406A-HW-2-2-		GeoXH 6000 (cm)	Poin
8	4/24/2014	<Null>	36.245155	129.378799	30.121	SY14-042406A-HW-2-2-		GeoXH 6000 (cm)	Poin
9	4/24/2014	<Null>	36.245153	129.378801	30.231	SY14-042406A-HW-2-2-		GeoXH 6000 (cm)	Poin
10	4/24/2014	<Null>	36.245153	129.378804	30.197	SY14-042406A-HW-2-2-	w	GeoXH 6000 (cm)	Poin
11	4/24/2014	<Null>	36.245153	129.378809	30.152	SY14-042406A-HW-2-2-		GeoXH 6000 (cm)	Poin
12	4/24/2014	<Null>	36.245155	129.378811	30.066	SY14-042406A-HW-2-2-		GeoXH 6000 (cm)	Poin
13	4/24/2014	<Null>	36.245157	129.378813	30.204	SY14-042406A-HW-2-2-		GeoXH 6000 (cm)	Poin
14	4/24/2014	<Null>	36.245161	129.378817	29.578	SY14-042406A-HW-2-2-		GeoXH 6000 (cm)	Poin
15	4/24/2014	<Null>	36.245162	129.378814	30.171	SY14-042406A-HW-2-2-		GeoXH 6000 (cm)	Poin
16	4/24/2014	<Null>	36.245165	129.378814	30.15	SY14-042406A-HW-2-2-		GeoXH 6000 (cm)	Poin
17	4/24/2014	<Null>	36.245166	129.378812	30.281	SY14-042406A-HW-2-2-		GeoXH 6000 (cm)	Poin
18	4/24/2014	<Null>	36.245169	129.378809	30.192	SY14-042406A-HW-2-2-		GeoXH 6000 (cm)	Poin
19	4/24/2014	<Null>	36.245169	129.378807	30.312	SY14-042406A-HW-2-2-		GeoXH 6000 (cm)	Poin
20	4/24/2014	<Null>	36.245162	129.378804	30.364	SY14-042406A-HW-2-2-	center	GeoXH 6000 (cm)	Poin
21	4/24/2014	<Null>	36.244925	129.378874	30.898	SY14-042408A-HW-2-3-	home	GeoXH 6000 (cm)	Poin

1 (0 out of 65 Selected)

GRIT

Figure P- 52. Goniometer (GRIT) Attribute Table.

To view metadata on a layer, right click on the name under the **Table of Contents**, hover the mouse over **Data** to expand it, then left-click **View Item Description** (see Figure P-53).

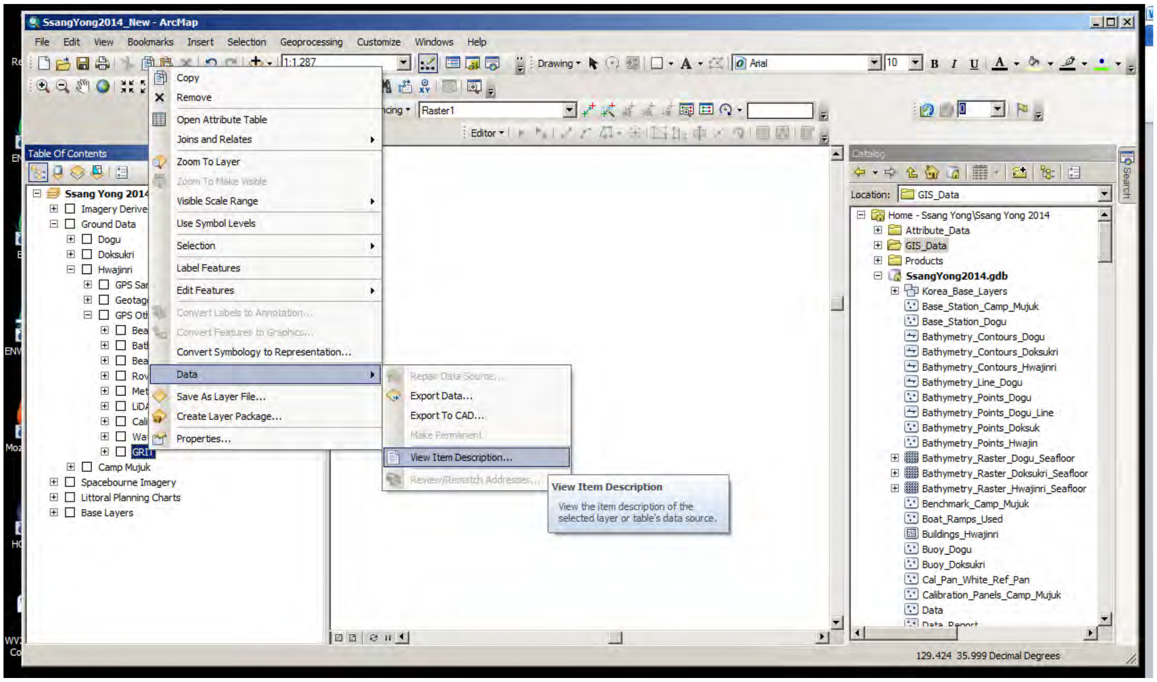

Figure P- 53. Showing how to access Metadata.

3. Summary

The Ssang Yong 2014 database contains a file geodatabase. It is a repository that holds a collection of baseline and scientific data supporting the development of imagery-derived amphibious planning products such as trafficability maps. It has been designed to store different types of data in a file system. Each dataset is held as a file that can scale up to 1 TB in size.

Data and information archived in the Ssang Yong 2014 database are representative of the rocky coastal region found along the east coast of South Korea. This particular geodatabase complements earlier geodatabases that characterize selected biological and physical features that affect maneuver in coral, mangrove, volcanic, barrier-island, and estuarine coasts.

For additional information on how to navigate a file geodatabase, please refer to free tutorials located online at ArcGIS Resources (see http://resources.arcgis.com)

APPENDIX Q

Site Photographs

Introduction

Photographs of test sites, instruments, and procedures were taken by team members throughout the experiment for documentation and reference purposes. Several of the scientists included contextual information like temperature, cloud cover, time, and geo-coordinates with their photographs. The following is a selection of photographs displaying the close-ups of the sediment surface, where the spectral and the geotechnical tests were conducted. The full library of photographs is accessible in the geodatabase under Attribute_Data/Photographs.

<u>Dogu beach</u>

DG-1-1

DG-1-2

DG-1-3

DG-2-1


DG-2-2

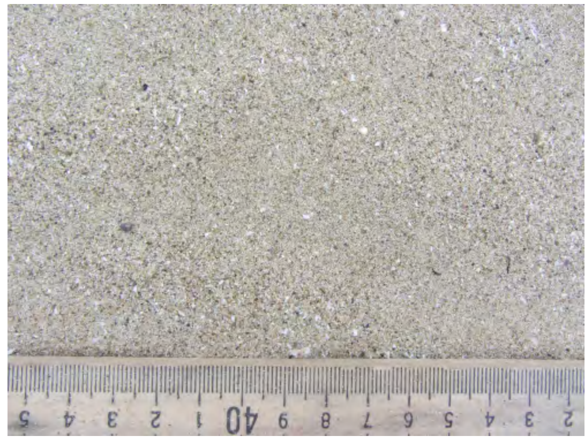
DG-2-3

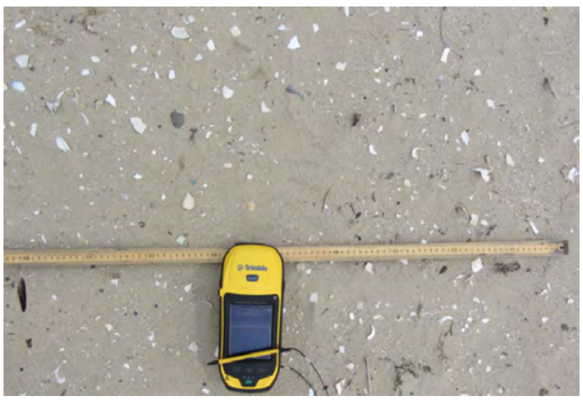
DG-2-4


DG-2-5


DG-2-6


DG-2-7


DG-2-8


DG-2-9


DG-2-10


DG-2-12


DG-2-13


DG-2-16


DG-2-15


DG-2-18


DG-3-1

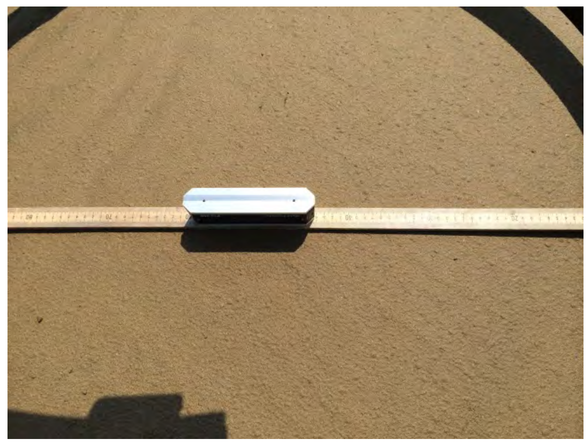
DG-3-2


DG-3-3


DG-3-4

DG-4-1

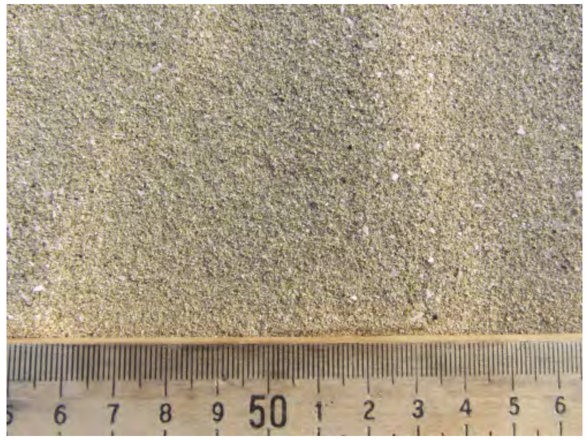

DG-4-2

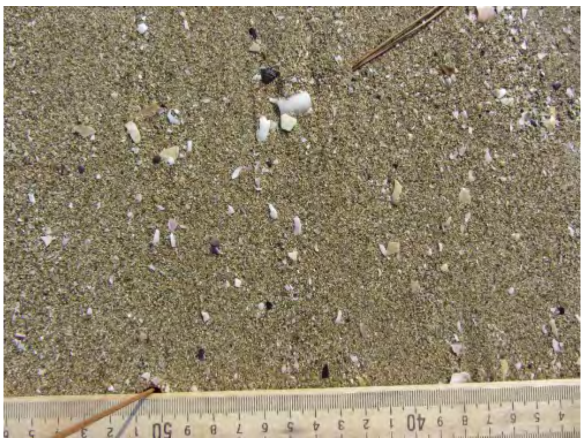

DG-4-3

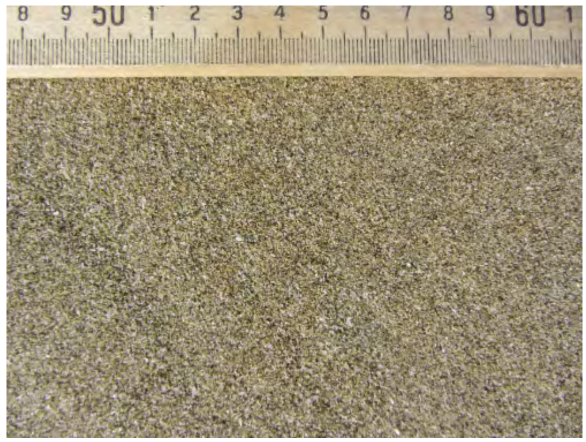

DG-4-4

DG-4-5

Doksuk-ri beach

DK-1-1

DK-1-2

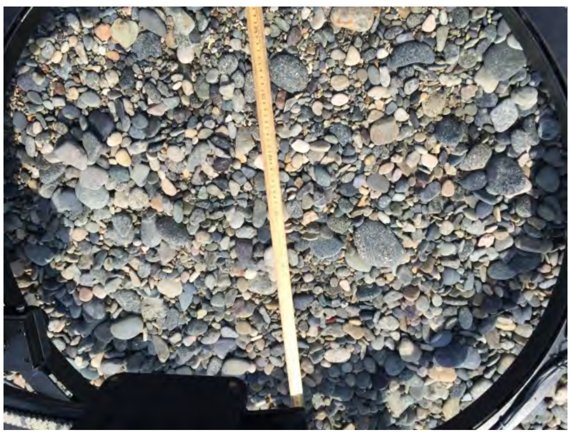

DK-1-3

DK-1-4

DK-1-5

DK-1-6

DK-1-7

DK-1-8

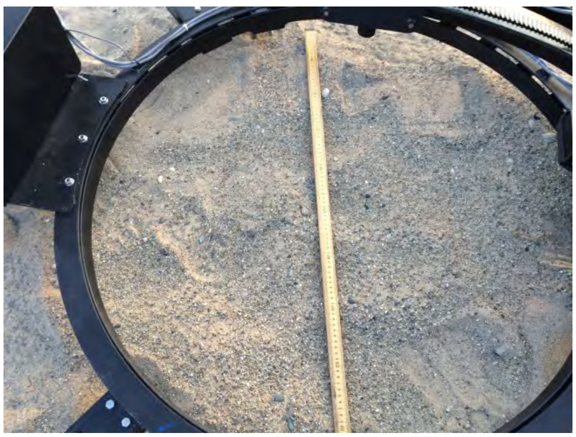

DK-1-11

Hwajin-ri beach


HW-1-1


HW-1-2

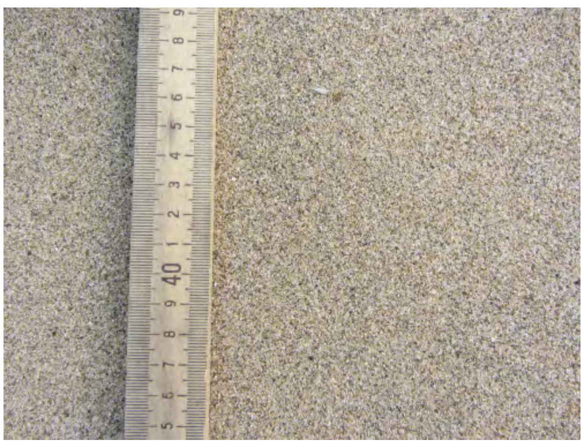

HW-1-3


HW-1-4


HW-1-5

HW-1-6

HW-1-7a


HW-1-8

HW-1-10


HW-1-11


HW-1-12

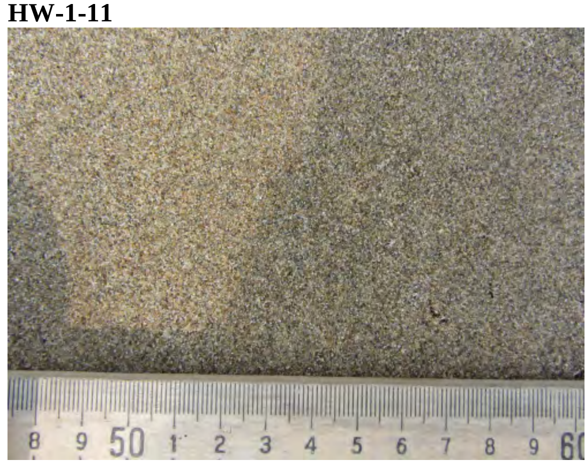
HW-1-13

HW-2-1

HW-2-2

HW-2-3

HW-2-4

HW-2-5

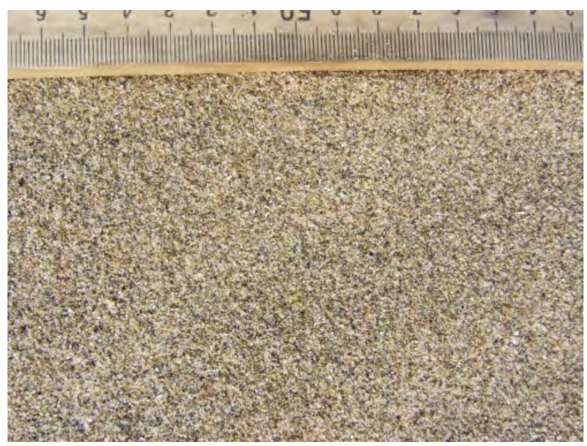

HW-3-1


HW-3-2


HW-3-3


HW-3-4

APPENDIX R

Shear Strength

1. Introduction

A Static Cone Penetrometer (SCP) is a common geotechnical tool that provides a measure of the shear strength of soils *in situ.* The instrument consists of a straight shaft of 18” in length, marked every 3 to 6” for measurements at fixed depth of penetration, a 60 degree cone tip, and a calibrated proving ring (or other measuring device, e.g. a load cell) with a dial indicator or digital display, calibrated to indicate the penetration stress (force of penetration divided by the projected cross-sectional area of the cone). The cone is manually pressed into the soil at a slow and steady rate, and measurements (stress, i.e. Cone Index) are taken, typically every 3” until 18” of the shaft or until the penetration is arrested by the increased soil resistance with depth or an obstruction such as a larger cobble is encountered.

Two different configurations of the SCP exist, both outlined in the US Army Mobility estimation manual (FM5-430-00). These include 0.5 in^2 and 0.2 in^2 cones. Each proving ring is calibrated accordingly to represent the actual stress values (in psi) indicating Cone Index (CI). Each has certain advantages, e.g. the larger cone provides for a finer resolution of force measurements, important in soft soils especially near the surface, where the values could be very low. The smaller cone, on the other hand, requires less force to push and allows reaching deeper strata, especially practical in somewhat harder soils, where the larger cone does not penetrate deep enough. During this experiment, both cones were used at all stations, providing the benefits of both types of measurements. Normally, two or more trials for each cone were performed for each station, allowing for examination of potential subsurface irregularities or homogeneities in strength.

California Bearing Ratio (CBR) is used as an empirical estimate of shear strength of soils. Shear strength is a measure of the ability of a substance to resist shear stresses (induced in soil as a result of surface or volumetric loading), before failure occurs. Failure is defined as a continual rapid deformation after initial (persistent, or not) load application. Combat engineers from Marine Wing Support Squadrons determine soil strength or bearing capacity values for expeditionary airfields before the beginning of aircraft operations. Marine reconnaissance units and Army combat engineers conduct similar measurements in a variety of terrain types. At bases and stations, physical scientists or specially trained civil engineer personnel may conduct these evaluations for monitoring of the quality of constructed fill, or estimates of the in-situ material strength. Engineers conduct Dynamic Cone Penetrometer (DCP) tests that are then related to empirical estimates of the CBR, which in turn, may be used to describe shear strength parameters of sediments.

The DCP is the current USMC and USAF standard for measurement of shear strength for airfield construction. The use of the DCP is described in ASTM D 6951-09 (American Society for Testing and Materials 2009). The dual-mass DCP used in THEMAS'12 and THEMAS’13 testing consisted of a 5/8-in.-diameter steel rod with a steel cone attached to one end, which was driven into the soil by means of a sliding dual-mass hammer. The angle of the cone was 60°, and the diameter of the base of the cone was 0.79 in. The DCP was driven into the ground by dropping a 10.1-lb sliding hammer from a height of 22.6 in. The depth of cone penetration is

measured at selected penetration or hammer-drop intervals and the soil shear strength is reported as the DCP index in millimeters/blow.

In accordance with the ASTM, CBR is computed using the following empirical equations:

For all soils, except CH and CL with CBR < 10: $CBR = \frac{292}{PR^{1.12}}$

For soils classified as CL with CBR < 10: $CBR = \frac{1}{(0.017019 \times PR)^2}$

For CH soils: $CBR = \frac{1}{(0.002871 \times PR)}$

PR = DCP penetration rate (mm/blow)

CL soils = clays of low plasticity

CH soils = highly plastic clays

2. SY14 Data

a. Static Cone Penetrometer

The following chart shows the full assembly of all the Cone Penetration Tests, where each curve is an average of all the individual cone tests for the station, including cones of both sizes ($0.2in^2$, and $0.5in^2$):

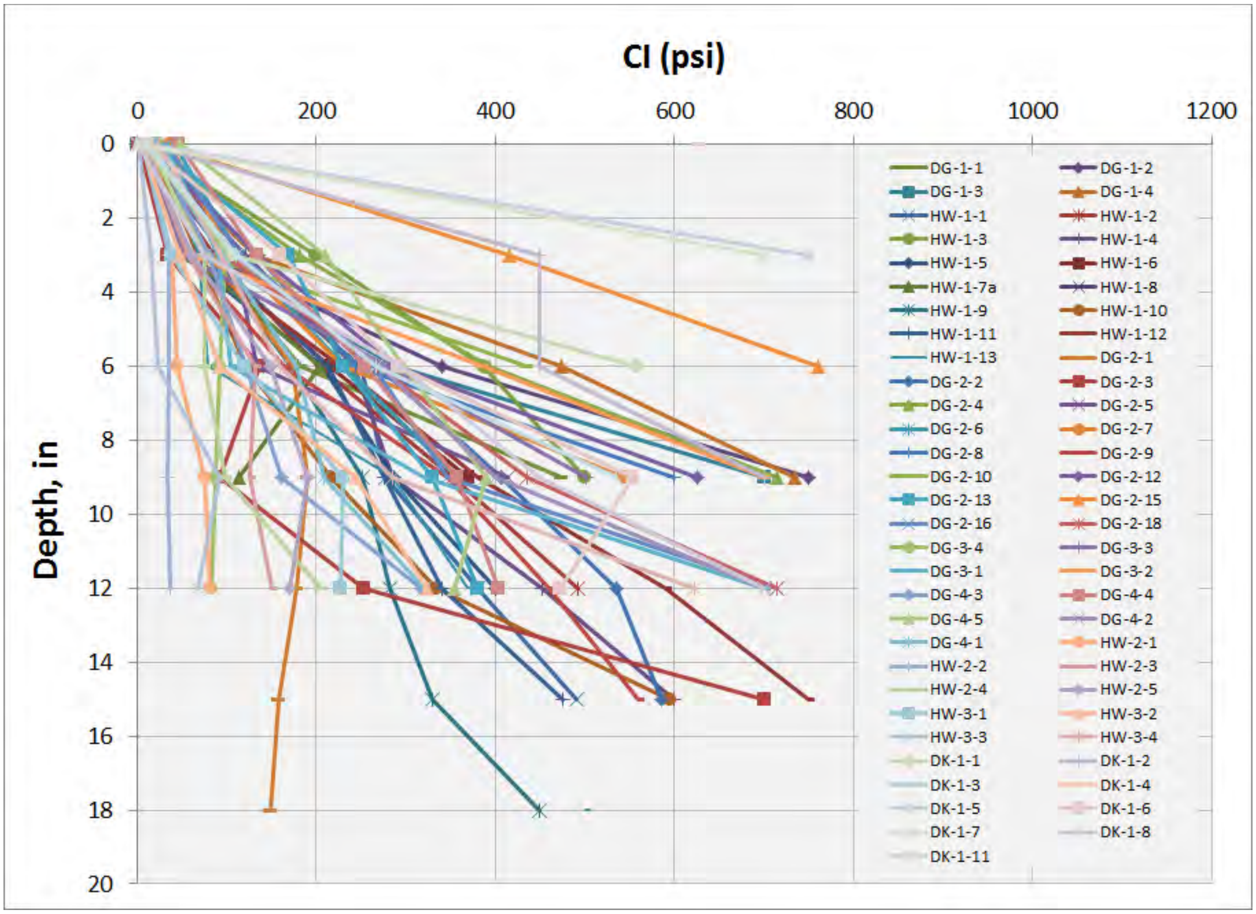

Doksuk-ri Beach only:

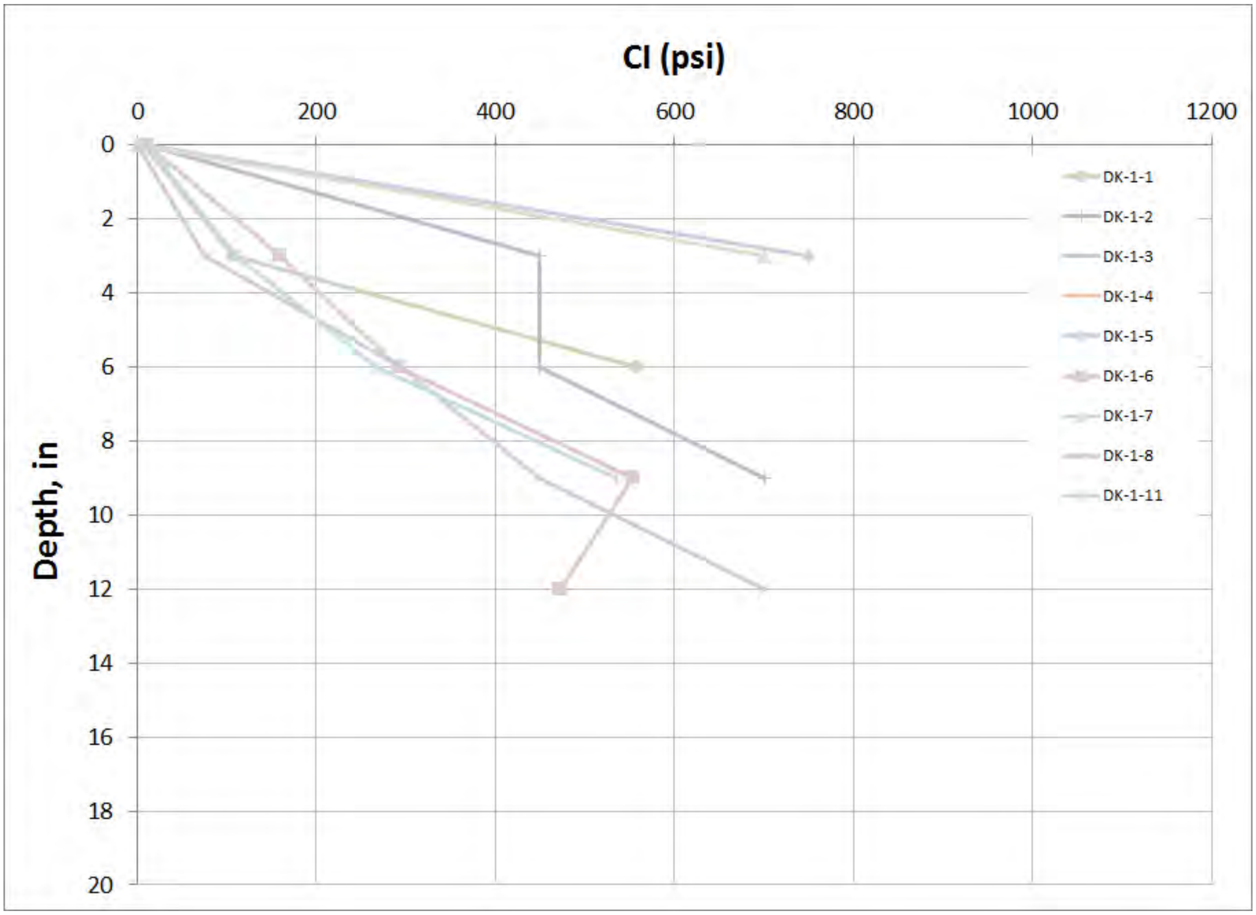

Hwajin-ri Beach only:

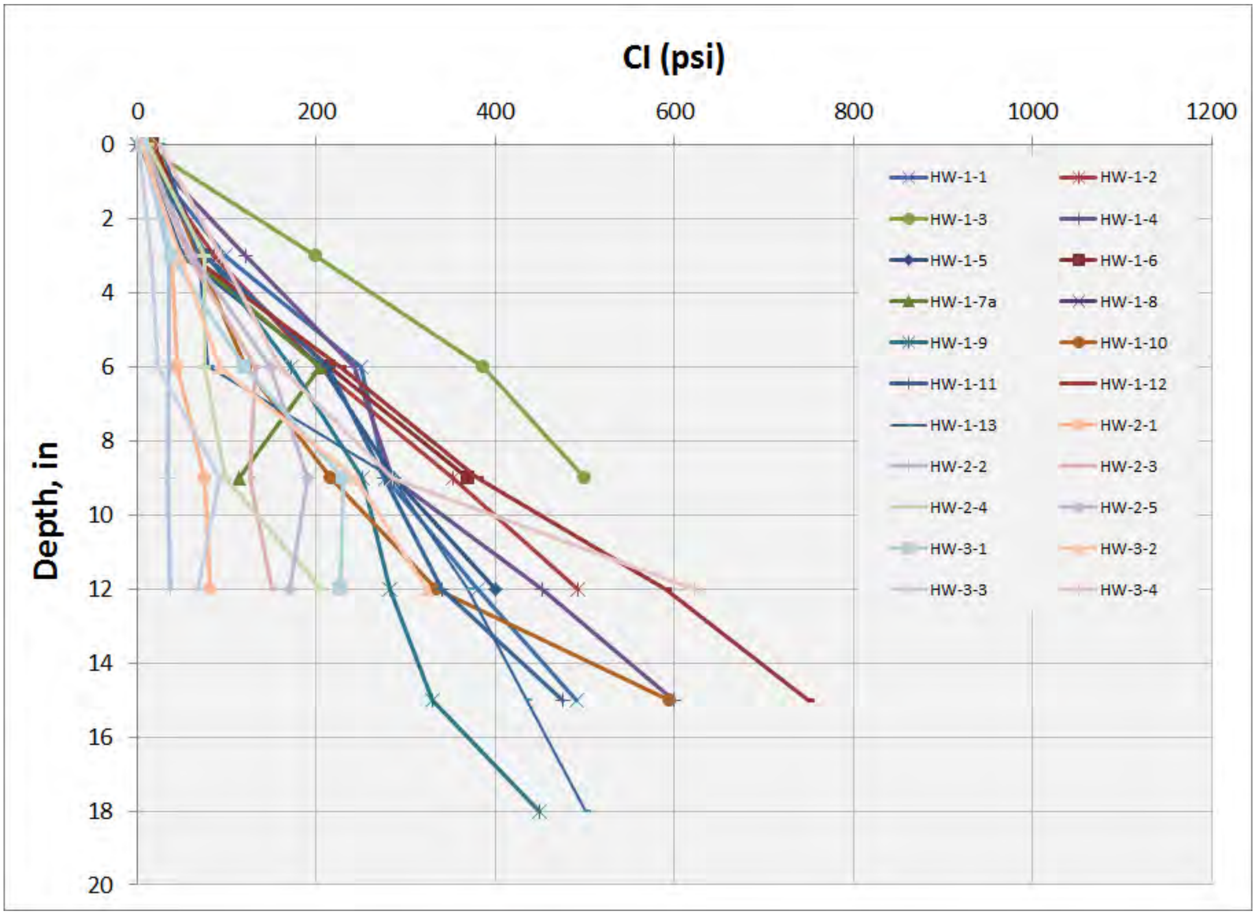

Dogu Beach only

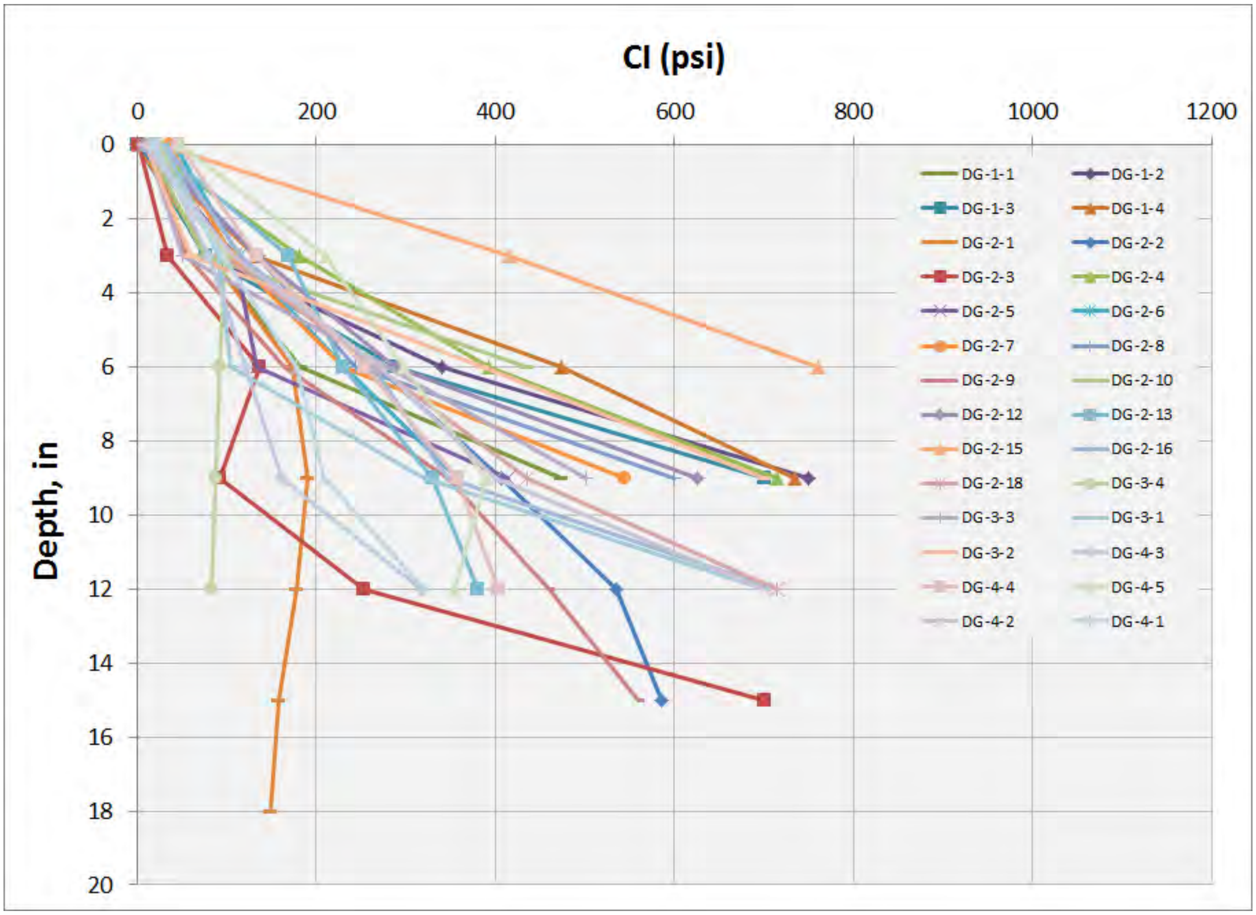

b. Dynamic Cone Penetrometer

All beaches, all stations:

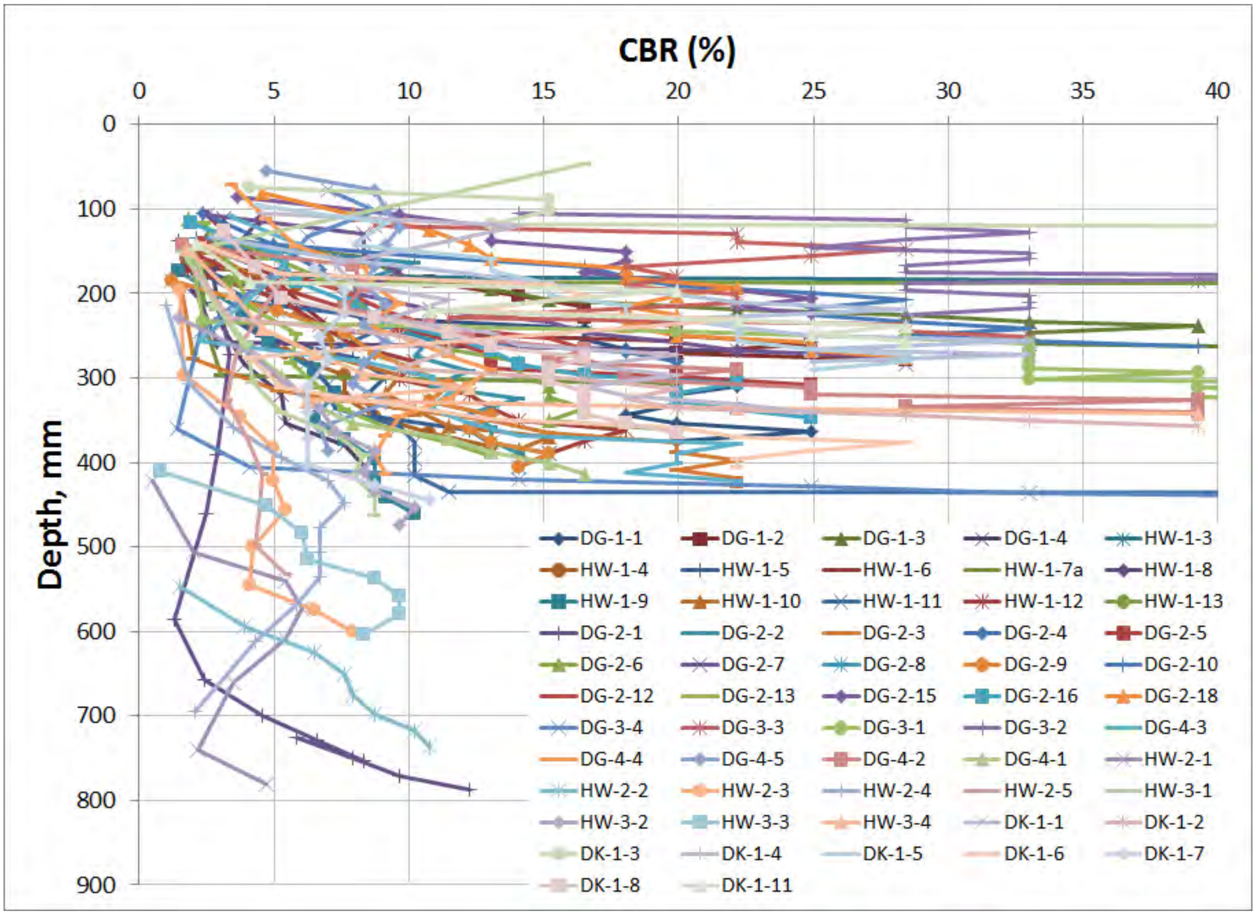

Doksuk-ri beach:

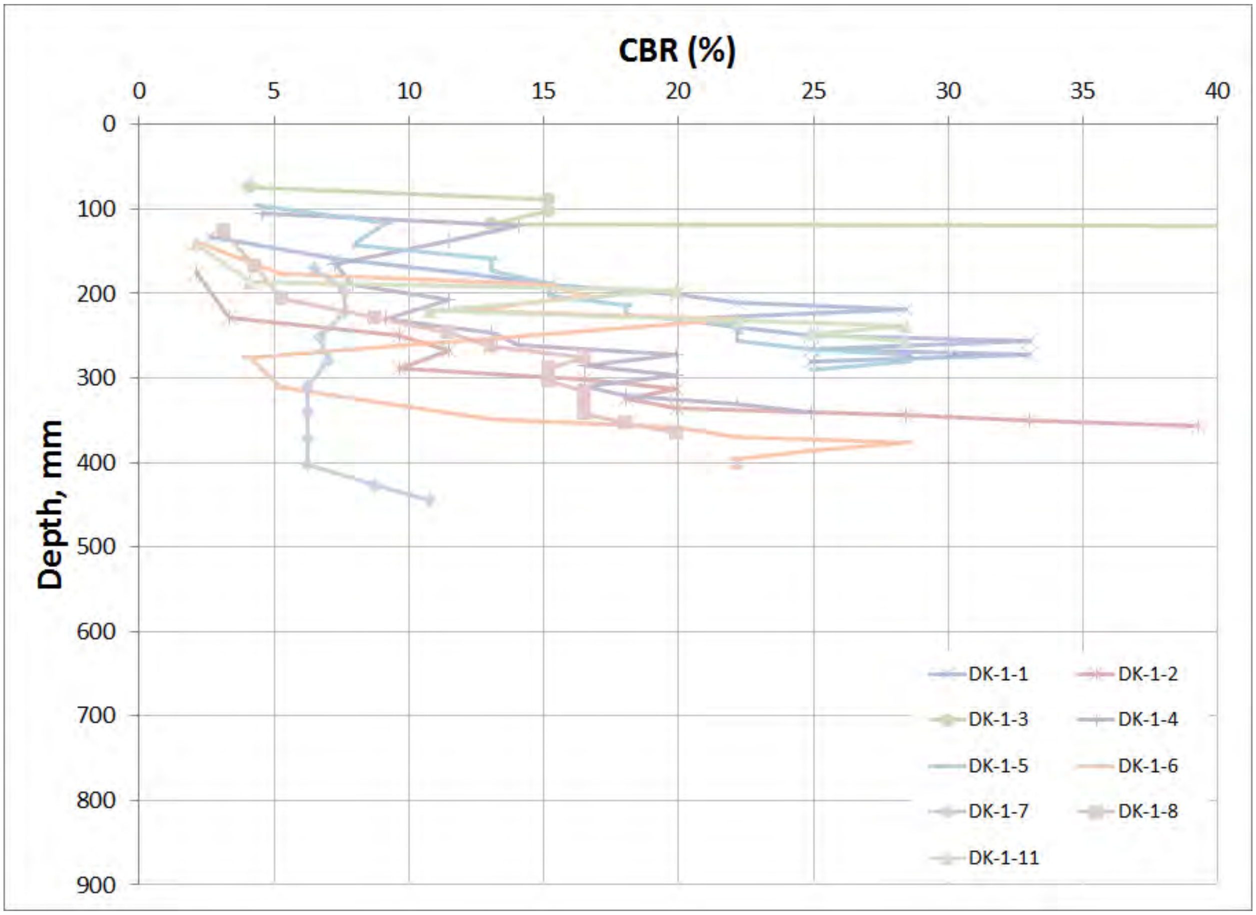

Hwajin-ri beach:

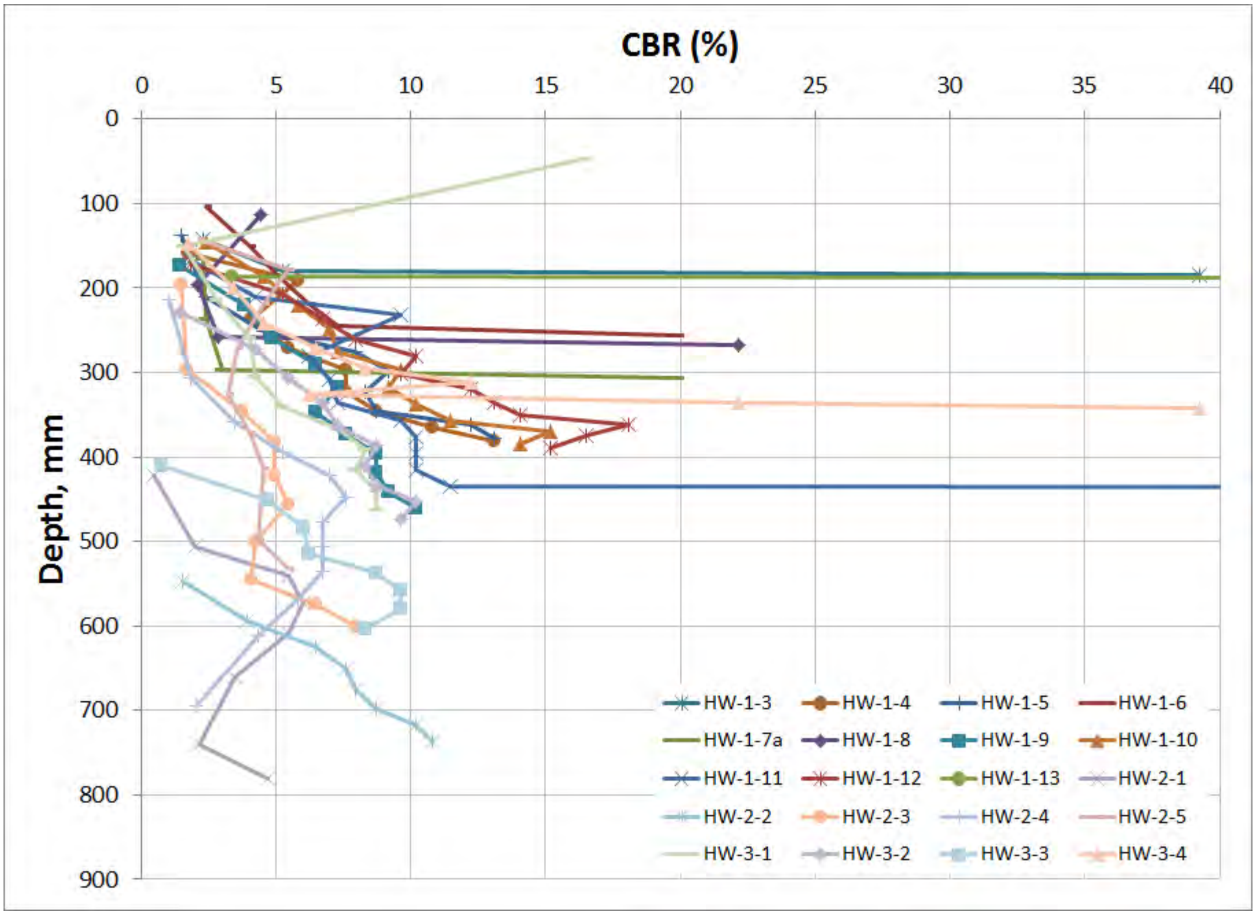

Dogu beach:

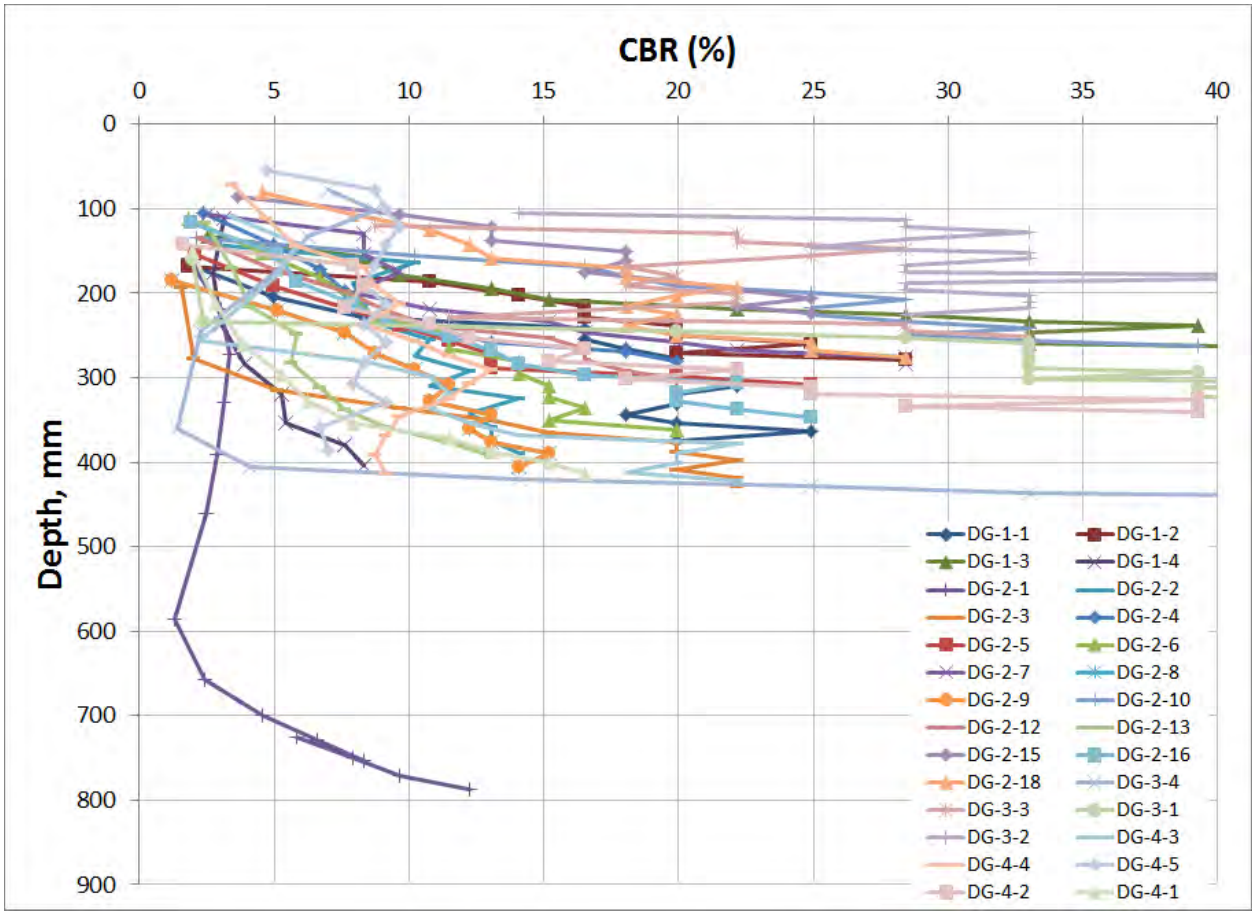

CBR (%)
0
5
10
15
20
25
30
35
40
0
100
200
300
400
500
600
700
800
900
Depth, mm
DG-1-1
DG-1-2
DG-1-3
DG-1-4
DG-2-1
DG-2-2
DG-2-3
DG-2-4
DG-2-5
DG-2-6
DG-2-7
DG-2-8
DG-2-9
DG-2-10
DG-2-12
DG-2-13
DG-2-15
DG-2-16
DG-2-18
DG-3-4
DG-3-3
DG-3-1
DG-3-2
DG-4-3
DG-4-4
DG-4-5
DG-4-2
DG-4-1

APPENDIX S

Dynamic Deflection Modulus – LWD tests

1. Introduction

Light Weight Deflectometer (LWD) is an instrument that includes a weight release mechanism, a guide rod, a falling weight, and a base plate with an embedded accelerometer and a spring. Once the weight drops from the fixed height, the spring provides the buffer system that transmits the load pulse to the plate, and consequently to the soil, resting in a calibrated dynamic load on the soil strata. After the weight has recoiled from the base plate, the resulting vertical plate displacement (and thus, soil deformation) is measured from the acceleration record. All these calculations occur automatically within the device's measurement and recording system. The device is calibrated for the particular weight and plate displacement range and calculates the force of impact as well as an estimate of the soil subgrade (or elastic) modulus.

The Zorn ZFG 2000 thus provides a simple way of estimating the elastic modulus of the material under dynamic loading, which in turn allows for estimation of the soil bearing capacity and trafficability potential.

LWD data are presented below in tabular and graphical format.

2. SY14 Data

Instrument Deployment ID	UTC Date/Time	Mean Displacement, mm	Evd [MN/m²]
2	4/15/2014 00:42	2.872	**7.8**
3	4/15/2014 00:47	3.519	**6.4**
4	4/15/2014 01:10	2.716	**8.3**
6	4/15/2014 01:47	4.768	**4.7**
8	4/16/2014 00:28	2.642	**8.5**
10	4/16/2014 00:48	3.685	**6.1**
12	4/16/2014 01:11	1.361	**16.5**
14	4/16/2014 01:35	1.146	**19.6**
16	4/16/2014 01:55	0.572	**39.3**
18	4/16/2014 02:17	1.596	**14.1**
20	4/16/2014 22:10	1.791	**12.6**
22	4/16/2014 22:42	3.351	**6.7**
24	4/16/2014 23:00	2.810	**8.0**
26	4/16/2014 23:55	0.797	**28.2**
28	4/17/2014 00:21	2.199	**10.2**
30	4/17/2014 00:45	4.914	**4.6**
32	4/17/2014 01:35	3.592	**6.3**
34	4/17/2014 23:18	3.798	**5.9**
36	4/17/2014 23:39	2.992	**7.5**
38	4/17/2014 23:59	4.645	**4.8**
40	4/19/2014 19:43	3.698	**6.1**

Instrument Deployment ID	UTC Date/Time	Mean Displacement, mm	Evd [MN/m²]
42	4/19/2014 20:02	3.515	**6.4**
44	4/19/2014 20:30	1.310	**17.2**
46	4/19/2014 20:52	2.932	**7.7**
48	4/19/2014 21:16	2.199	**10.2**
50	4/19/2014 22:27	2.669	**8.4**
52	4/19/2014 22:50	4.762	**4.7**
54	4/19/2014 23:21	2.933	**7.7**
56	4/20/2014 01:02	3.337	**6.7**
58	4/20/2014 01:26	2.272	**9.9**
60	4/20/2014 01:50	3.136	**7.2**
62	4/20/2014 02:29	3.125	**7.2**
64	4/21/2014 20:35	2.035	**11.1**
66	4/21/2014 21:07	1.912	**11.8**
68	4/21/2014 21:43	2.454	**9.2**
70	4/21/2014 22:05	2.709	**8.3**
72	4/21/2014 22:30	2.933	**7.7**
74	4/21/2014 23:14	3.447	**6.5**
76	4/21/2014 23:57	3.199	**7.0**
78	4/22/2014 00:21	2.956	**7.6**
80	4/22/2014 01:40	2.683	**8.4**
82	4/23/2014 20:17	2.383	**9.4**
84	4/23/2014 20:41	2.111	**10.7**
86	4/24/2014 00:01	1.839	**12.2**
88	4/24/2014 00:05	1.643	**13.7**
90	4/24/2014 01:32	2.172	**10.4**
92	4/24/2014 01:53	1.847	**12.2**
94	4/24/2014 02:12	1.740	**12.9**
96	4/24/2014 02:44	3.031	**7.4**
98	4/24/2014 03:35	4.070	**5.5**
100	4/24/2014 21:23	1.965	**11.5**
102	4/24/2014 22:15	5.196	**4.3**
104	4/24/2014 22:51	4.783	**4.7**
106	4/24/2014 23:27	5.061	**4.4**
108	4/25/2014 00:03	6.706	**3.4**
110	4/25/2014 00:47	5.364	**4.2**
112	4/25/2014 02:30	6.253	**3.6**
114	4/25/2014 02:33	4.883	**4.6**
116	4/25/2014 02:36	5.844	**3.9**

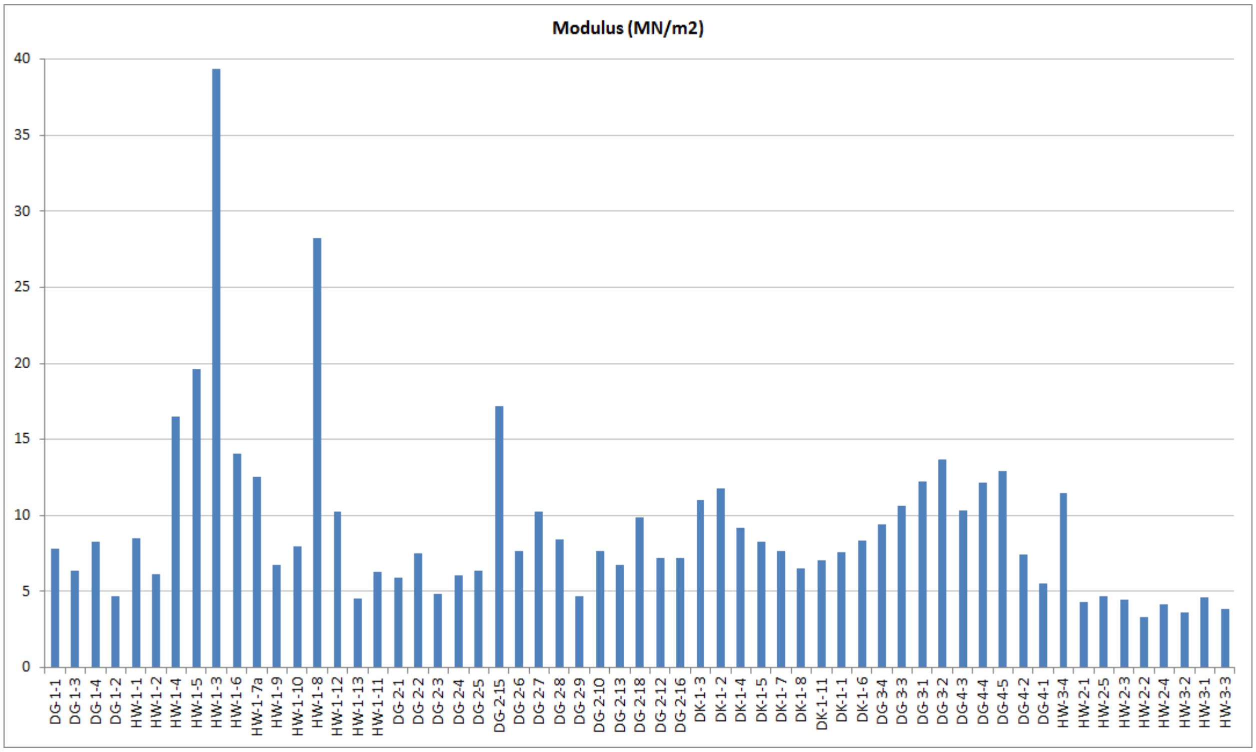
Modulus (MN/m2)
0
5
10
15
20
25
30
35
40
DG-1-1
DG-1-3
DG-1-4
DG-1-2
HW-1-1
HW-1-2
HW-1-4
HW-1-5
HW-1-3
HW-1-6
HW-1-7a
HW-1-9
HW-1-10
HW-1-8
HW-1-12
HW-1-13
HW-1-11
DG-2-1
DG-2-2
DG-2-3
DG-2-4
DG-2-5
DG-2-15
DG-2-6
DG-2-7
DG-2-8
DG-2-9
DG-2-10
DG-2-13
DG-2-18
DG-2-12
DG-2-16
DK-1-3
DK-1-2
DK-1-4
DK-1-5
DK-1-7
DK-1-8
DK-1-11
DK-1-1
DK-1-6
DG-3-4
DG-3-3
DG-3-1
DG-3-2
DG-4-3
DG-4-4
DG-4-5
DG-4-2
DG-4-1
HW-3-4
HW-2-1
HW-2-5
HW-2-3
HW-2-2
HW-2-4
HW-3-2
HW-3-1
HW-3-3

APPENDIX T

Soil Field Density

1. Introduction

Field density of soils may be determined in several ways, including such advanced methods as nuclear density gauges. The latter offer speedy results and are often of acceptable quality for many applications, especially in geotechnical engineering, including backfills, berm and road construction and similar. These devices are fast but are not best suited to characterizing the surface characteristics of sediments, as measurement involves averaging over a large volume of soil (in depth). Trafficability analysis from remote sensing platforms dictates the ability to characterize the surface of the sediment, minimizing the volume averaging of the field density test. Thus, a slower but more accurate and depth-selective method of sand replacement (sand-cone) field density measurement was performed. In this method (ASTM 1556-07) a standard plate is placed on the ground, and a hole is excavated with all the material saved for subsequent weighing and oven drying. This procedure established the wet and the dry weight of soil excavated as well as the moisture content. The excavated hole is then filled using a special canister (see Fig. 3-4b of the main report) with a dry calibrated sand, thus allowing calculation of the volume of the excavated hole. These data allow for computation of the wet and dry field density values.

Station ID	Field Dry Density, g/cm^3	Field Wet Density, g/cm^3
DG-1-1	1.618	1.623
DG-1-2	1.278	1.283
DG-1-3	1.542	1.551
DG-1-4	1.528	1.533
DG-2-1	1.569	1.574
DG-2-2	1.564	1.577
DG-2-3	1.472	1.476
DG-2-4	1.274	1.326
DG-2-5	1.216	1.274
DG-2-6	1.350	1.525
DG-2-7	1.515	1.792
DG-2-8	1.252	1.310
DG-2-9	1.413	1.473
DG-2-10	1.276	1.332

Station ID	Field Dry Density, g/cm^3	Field Wet Density, g/cm^3
DG-2-12	1.341	1.377
DG-2-13	1.472	1.535
DG-2-15	1.392	1.485
DG-2-16	1.317	1.433
DG-2-18	1.383	1.831
DG-3-1	1.326	1.749
DG-3-2	1.365	1.837
DG-3-3	1.350	1.828
DG-3-4	1.460	1.902
DG-4-1	1.279	1.270
DG-4-2	1.458	1.464
DG-4-3	1.337	1.809
DG-4-4	1.312	1.691
DG-4-5	1.387	1.691
HW-1-1	1.648	1.651
HW-1-2	1.552	1.554
HW-1-3	1.562	1.564
HW-1-4	1.466	1.469
HW-1-5	1.544	1.547
HW-1-6	1.385	1.659
HW-1-7a	1.434	1.886
HW-1-8	1.399	1.775
HW-1-9	1.261	1.289
HW-1-10	1.365	1.659
HW-1-11	1.478	1.482
HW-1-12	1.628	1.632
HW-1-13	1.464	1.838
HW-2-1	1.523	1.526

Station ID	Field Dry Density, g/cm^3	Field Wet Density, g/cm^3
HW-2-2	1.417	1.421
HW-2-3	1.568	1.571
HW-2-4	1.531	1.539
HW-2-5	1.571	1.574
HW-3-1	1.586	1.589
HW-3-2	1.537	1.540
HW-3-3	1.525	1.529
HW-3-4	1.403	1.532
DK-1-1	1.321	1.334
DK-1-2	1.557	1.578
DK-1-3	not possible[1]	not possible[1]
DK-1-4	1.364	1.373
DK-1-5	1.267	1.305
DK-1-6	1.615	1.633
DK-1-7	1.443	1.446
DK-1-8	1.468	1.474
DK-1-11	1.500	1.507

[1] – test not possible due to the prevalence of cobbles on the surface.

APPENDIX U

Soil Moisture, Grain Size, and Soil Classification

1. Introduction

All bulk samples collected at all the testing sites were processed according to the ASTM soil preparation standards. Grain size analysis was then conducted using dry sieving technique, according to ASTM D6913. After the complete grain size distribution curve has been established, several important descriptors may be calculated (ASTM D2487), including the coefficient of uniformity, is defined as:

$Cu=(D60/D10)$,

and the coefficient of curvature:

$Cc=(D30)^2 /(D10*D60)$.

Sediment classification was conducted using the ASTM procedure, yielding labels, e.g. SP (poorly-graded sand), SW (well-graded sand), SM (silty-sand) etc.

Soil samples, collected for field soil moisture determination, were stored in two sealed bags to prevent any loss of moisture to evaporation prior to lab measurements. After soil samples were taken to the lab, standard ASTM oven drying procedure was followed to determine the soil moisture content. The moisture content is expressed as a percentage: the mass of water divided by the dry mass of soil (expressed as percentage).

The moisture content was then calculated as follows:

$$w = [(M_{cms} - M_{cds})/(M_{cds} - M_c)]*100$$

where:

w = water content, %
M_{cms} = mass of container and moist specimen, g
M_{cds} = mass of container and dry specimen, g
M_c = mass of container, g

2. Data

Moisture Content:

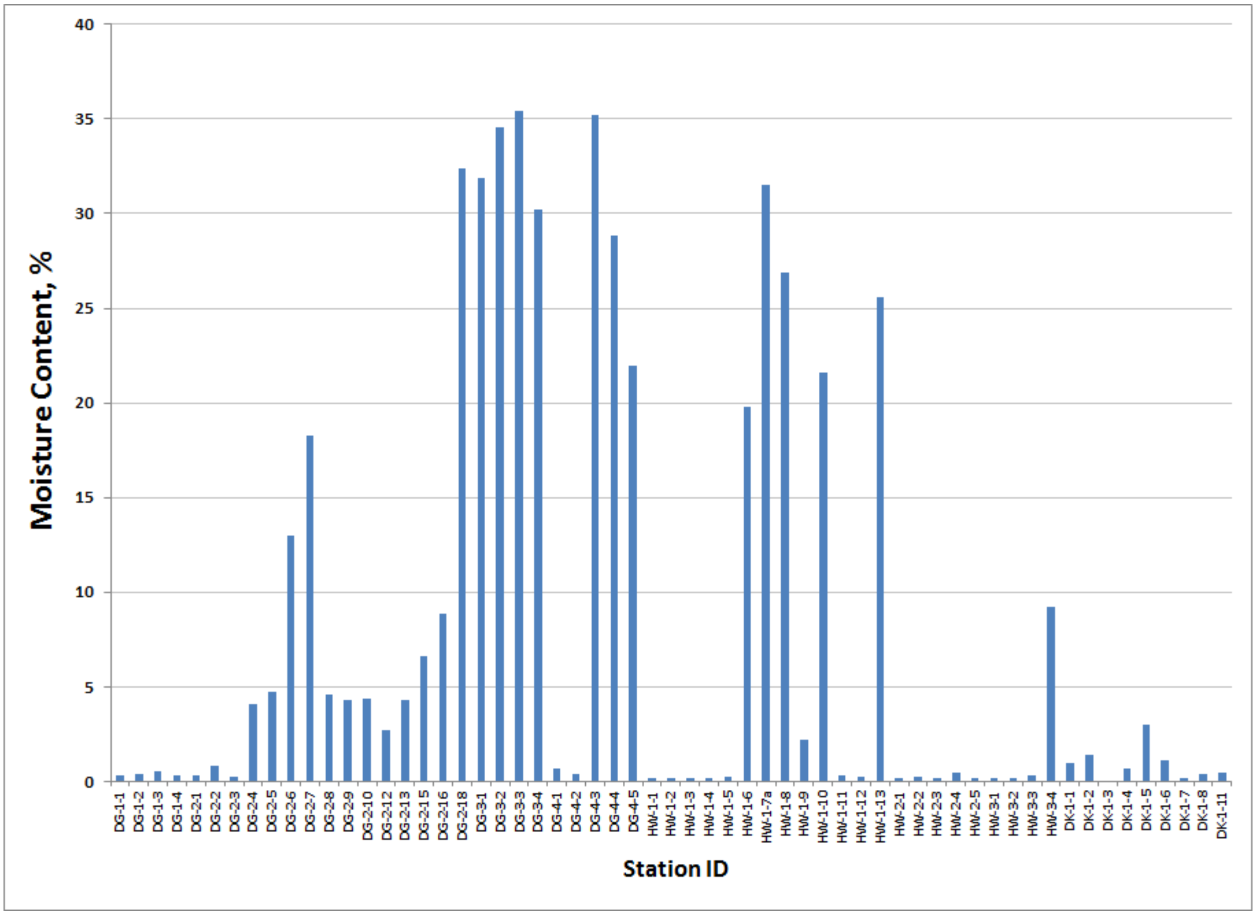

Grain Size Analysis:

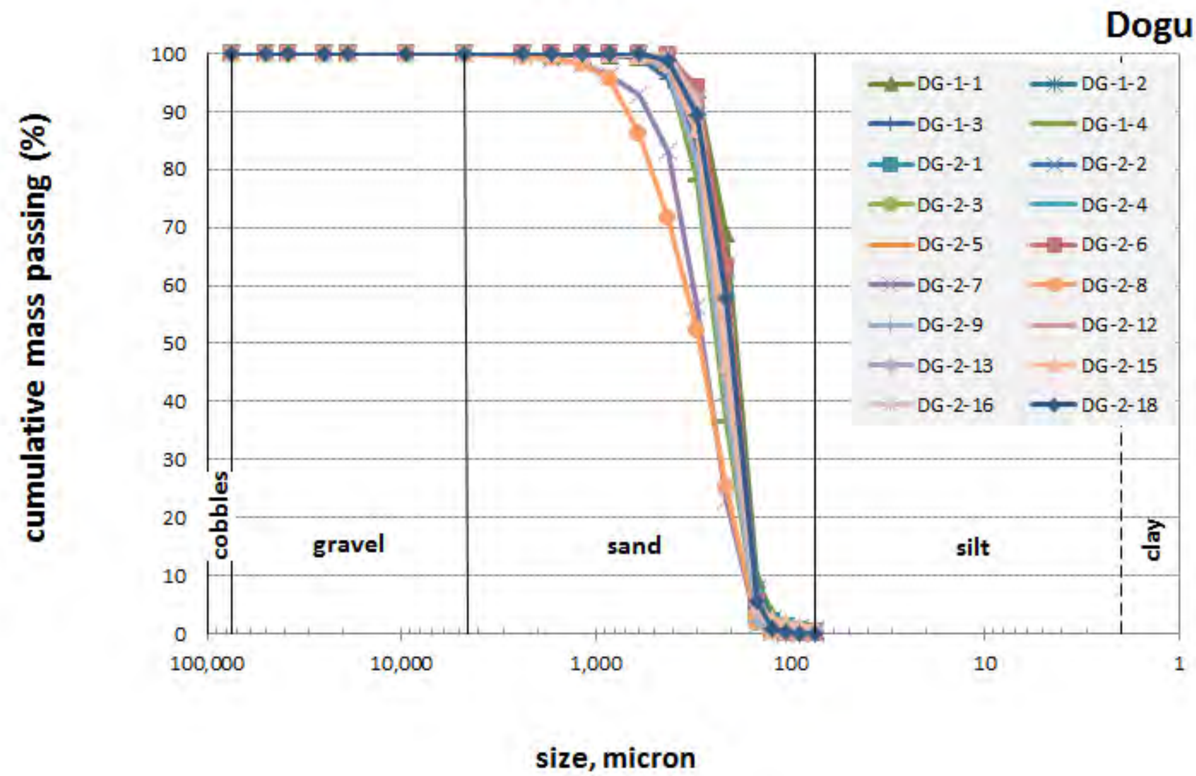

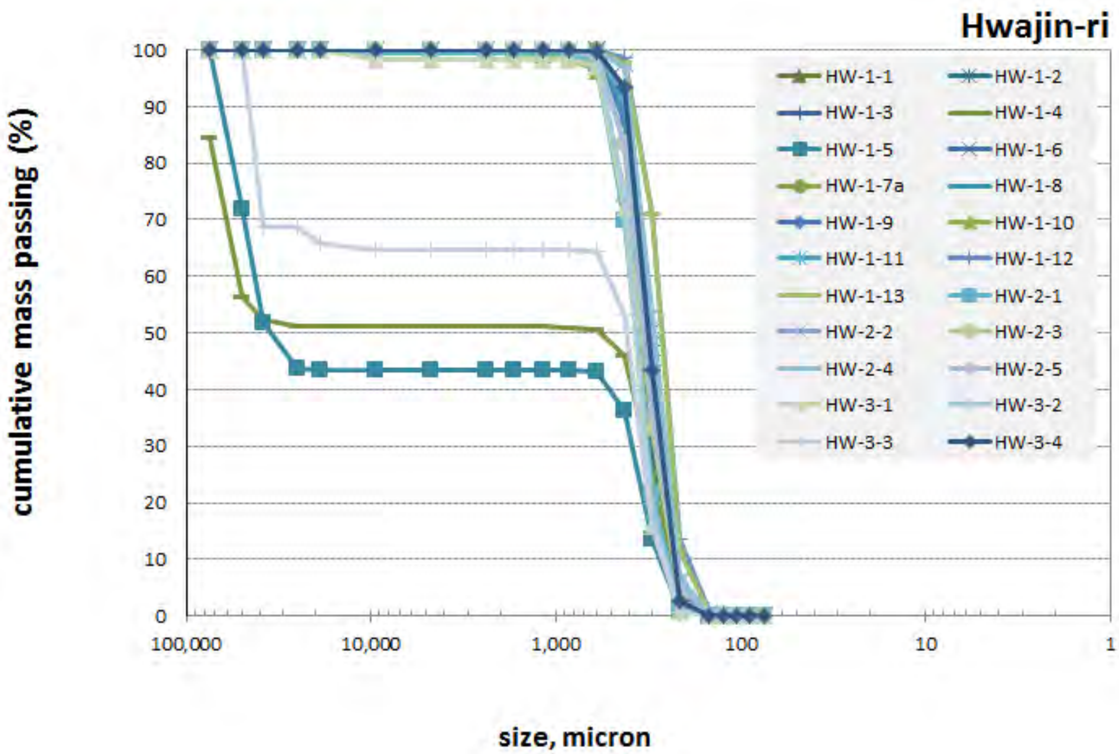
Hwajin-ri
cumulative mass passing (%)
size, micron
100
90
80
70
60
50
40
30
20
10
0
100,000
10,000
1,000
100
10
1
HW-1-1
HW-1-2
HW-1-3
HW-1-4
HW-1-5
HW-1-6
HW-1-7a
HW-1-8
HW-1-9
HW-1-10
HW-1-11
HW-1-12
HW-1-13
HW-2-1
HW-2-2
HW-2-3
HW-2-4
HW-2-5
HW-3-1
HW-3-2
HW-3-3
HW-3-4

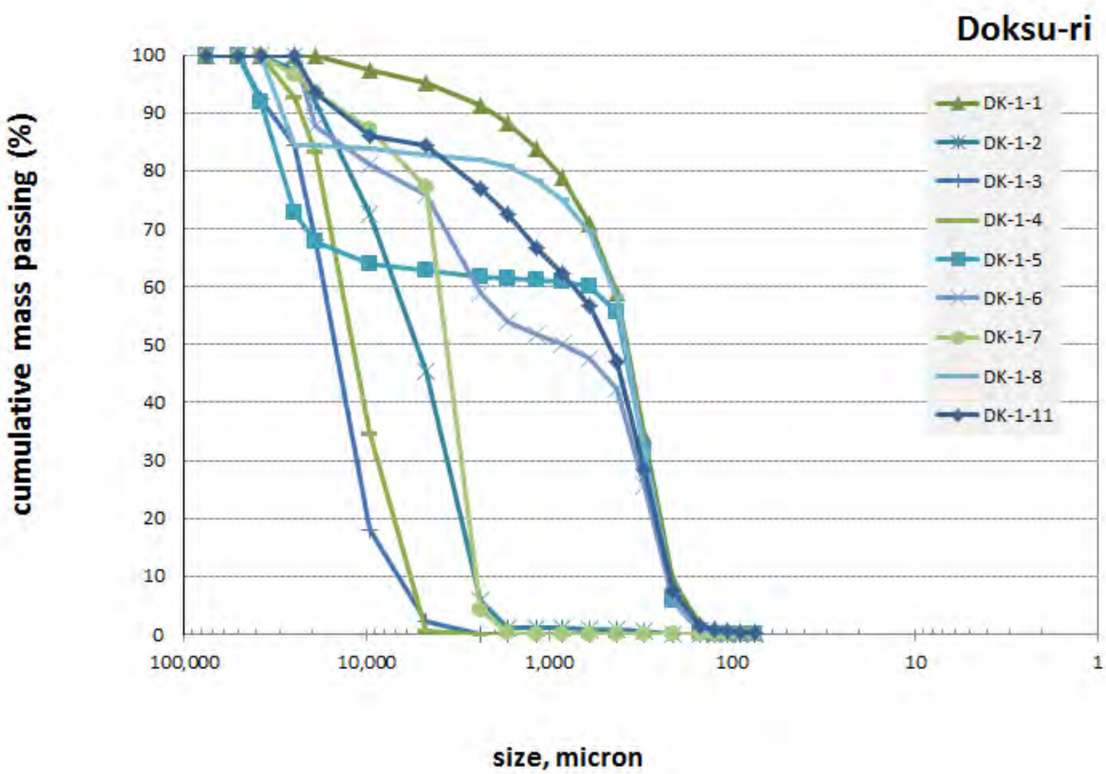
Doksu-ri
cumulative mass passing (%)
size, micron
100
90
80
70
60
50
40
30
20
10
0
100,000
10,000
1,000
100
10
1
DK-1-1
DK-1-2
DK-1-3
DK-1-4
DK-1-5
DK-1-6
DK-1-7
DK-1-8
DK-1-11

Soil Classification according to USCS:

Sample ID	final classification	classification, abbreviated
DG-1-1	SP	SP
DG-1-2	SP	SP
DG-1-3	SP	SP
DG-1-4	SP	SP
DG-2-1	SP	SP
DG-2-2	SP	SP
DG-2-3	SP	SP
DG-2-4	SP	SP
DG-2-5	SP	SP
DG-2-6	SP	SP
DG-2-7	SP	SP
DG-2-8	SP	SP
DG-2-9	SP	SP
DG-2-10	SP	SP
DG-2-12	SP	SP
DG-2-13	SP	SP
DG-2-15	SP	SP
DG-2-16	SP	SP
DG-2-18	SP	SP
DG-3-1	SP	SP
DG-3-2	SP	SP
DG-3-3	SP	SP
DG-3-4	SP	SP
DG-4-1	SP	SP
DG-4-2	SP	SP
DG-4-3	SP	SP
DG-4-4	SP	SP
DG-4-5	SP	SP
HW-1-1	SP	SP
HW-1-2	SP	SP
HW-1-3	SP	SP
HW-1-4	SP, with gravel and cobbles	SPgc
HW-1-5	GP, with sand	GPs
HW-1-6	SP	SP
HW-1-7a	SP	SP

Sample ID	final classification	classification, abbreviated
HW-1-8	SP	SP
HW-1-9	SP	SP
HW-1-10	SP	SP
HW-1-11	SP	SP
HW-1-12	SP	SP
HW-1-13	SP	SP
HW-2-1	SP	SP
HW-2-2	SP	SP
HW-2-3	SP	SP
HW-2-4	SP	SP
HW-2-5	SP	SP
HW-3-1	SP	SP
HW-3-2	SP	SP
HW-3-3	SP, with gravel	SPg
HW-3-4	SP	SP
DK-1-1	SP	SP
DK-1-2	GP, with sand	GPs
DK-1-3	GP	GP
DK-1-4	GP	GP
DK-1-5	SP, with gravel	SPg
DK-1-6	SP, with gravel	SPg
DK-1-7	SP, with gravel	SPg
DK-1-8	SP, with gravel	SPg
DK-1-11	SP, with gravel	SPg

APPENDIX V

Specific Gravity of Soils

1. Introduction

Specific gravity of soils is defined as the density of solid material only, not including any pore spaces and is useful in many fundamental soil relations and equations describing soil state. The specific gravity was determined using a standard ASTM procedure (ASTM D854) using a water pycnometer, a vacuum pump, and a precision scale for weight measurements. Vacuum pump is used to evacuate all dissolved air in the de-ionized water used to fill a calibrated flask (water pycnometer) to a specified volume or level. The flasks are calibrated to ensure the weight and volume measurements. The volume of solids placed inside the water-filled flask is used in calculating the volume of the solid fraction of known dry weight, thus allowing for the density calculation. Specific gravity is then computed relative to the density of water at a standard temperature (with proper temperature adjustments).

The results for all the samples collected are given below:

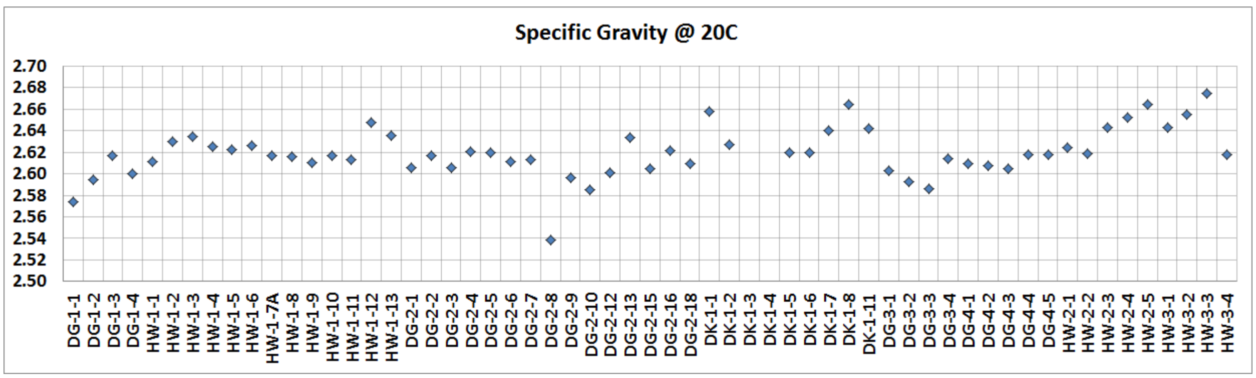

Sample ID	specific gravity at 20degC
DG-1-1	2.574
DG-1-2	2.595
DG-1-3	2.617
DG-1-4	2.600
HW-1-1	2.612
HW-1-2	2.629
HW-1-3	2.635
HW-1-4	2.625
HW-1-5	2.622
HW-1-6	2.626
HW-1-7A	2.617
HW-1-8	2.616
HW-1-9	2.610
HW-1-10	2.617
HW-1-11	2.613
HW-1-12	2.648

Sample ID	specific gravity at 20degC
HW-1-13	2.636
DG-2-1	2.606
DG-2-2	2.617
DG-2-3	2.605
DG-2-4	2.621
DG-2-5	2.620
DG-2-6	2.611
DG-2-7	2.613
DG-2-8	2.539
DG-2-9	2.596
DG-2-10	2.585
DG-2-12	2.601
DG-2-13	2.634
DG-2-15	2.604
DG-2-16	2.622
DG-2-18	2.609
DK-1-1	2.658
DK-1-2	2.627
DK-1-3	not tested[1]
DK-1-4	not tested[1]
DK-1-5	2.620
DK-1-6	2.620
DK-1-7	2.640
DK-1-8	2.665
DK-1-11	2.642
DG-3-1	2.603
DG-3-2	2.592
DG-3-3	2.586
DG-3-4	2.615
DG-4-1	2.610
DG-4-2	2.608
DG-4-3	2.604
DG-4-4	2.618
DG-4-5	2.618
HW-2-1	2.624
HW-2-2	2.618
HW-2-3	2.643
HW-2-4	2.652
HW-2-5	2.664
HW-3-1	2.643
HW-3-2	2.655
HW-3-3	2.674
HW-3-4	2.618

[1] – test not possible due to the prevalence of cobbles.

APPENDIX W

Soil Minimum, Maximum, and Relative Density

1. Introduction

Relative density of sediments was determined using the standard and widely accepted procedures for granular media (ASTM D7481-09, D4254-83, and Creswell et al., 1999). Values of Minimum and Maximum density, combined with the values of the field density discussed earlier, yielded the relative density, expressed in percent. Thus, relative density values of 0% indicate the loosest possible configuration for the soil in question, and the 100% values – the densest possible. Relative density can be used to establish a relationship between the relative packing of grains and soil trafficability and strength. Field density test results are also given for reference.

Station ID	Min density, gr/cm^3	Max density, gr/cm^3	Field density, gr/cm^3	Relative density, %
DG-1-1	1.33	1.62	1.62	100
DG-1-2	1.28	1.52	1.28	0
DG-1-3	1.33	1.56	1.54	95
DG-1-4	1.30	1.55	1.53	93
DG-2-1	1.33	1.57	1.57	100
DG-2-2	1.33	1.56	1.56	100
DG-2-3	1.33	1.47	1.47	99
DG-2-4	1.27	1.52	1.27	0
DG-2-5	1.22	1.54	1.22	0
DG-2-6	1.32	1.54	1.35	15
DG-2-7	1.30	1.51	1.51	100
DG-2-8	1.25	1.53	1.25	0
DG-2-9	1.31	1.57	1.41	44
DG-2-10	1.28	1.52	1.28	0
DG-2-12	1.33	1.56	1.34	7
DG-2-13	1.33	1.52	1.47	76
DG-2-15	1.29	1.44	1.39	72
DG-2-16	1.30	1.49	1.32	8
DG-2-18	1.26	1.52	1.38	54
DG-3-1	1.27	1.50	1.33	28
DG-3-2	1.27	1.50	1.36	47
DG-3-3	1.25	1.46	1.35	51
DG-3-4	1.26	1.48	1.46	91
DG-4-1	1.27	1.47	1.27	0
DG-4-2	1.24	1.46	1.46	99

Station ID	Min density, gr/cm^3	Max density, gr/cm^3	Field density, gr/cm^3	Relative density, %
DG-4-3	1.23	1.46	1.34	52
DG-4-4	1.13	1.39	1.31	75
DG-4-5	1.26	1.50	1.39	57
HW-1-1	1.35	1.65	1.65	100
HW-1-2	1.37	1.63	1.55	74
HW-1-3	1.37	1.66	1.56	71
HW-1-4	1.35	1.64	1.47	45
HW-1-5	1.34	1.63	1.54	75
HW-1-6	1.31	1.61	1.39	28
HW-1-7a	1.29	1.61	1.43	51
HW-1-8	1.29	1.57	1.40	44
HW-1-9	1.26	1.62	1.26	0
HW-1-10	1.32	1.59	1.36	18
HW-1-11	1.34	1.60	1.48	57
HW-1-12	1.35	1.63	1.63	100
HW-1-13	1.33	1.57	1.46	59
HW-2-1	1.38	1.67	1.52	53
HW-2-2	1.32	1.63	1.42	35
HW-2-3	1.37	1.66	1.57	72
HW-2-4	1.39	1.68	1.53	53
HW-3-1	1.39	1.69	1.59	70
DK-1-1	1.32	1.71	1.32	0
DK-1-2	1.51	1.76	1.56	22
DK-1-3	not tested	not tested	not tested	not tested
DK-1-4	not tested	not tested	not tested	not tested
DK-1-5	1.27	1.63	1.27	0
DK-1-6	1.61	1.87	1.61	0
DK-1-7	1.44	1.71	1.44	0
DK-1-8	1.42	1.66	1.47	23